

# **Mechanisms of energy transfer and conversion in plant Light-Harvesting Complex II**

Dissertation

zur Erlangung des Doktorgrades

der Naturwissenschaften

vorgelegt beim Fachbereich 14

Biochemie, Chemie und Pharmazie

der Johann Wolfgang Goethe - Universität

in Frankfurt am Main

von

**Tiago Ferreira de Barros**

aus Porto, Portugal

Frankfurt 2009

Vom Fachbereich Biochemie, Chemie und Pharmazie der Johann Wolfgang  
Goethe-Universität als Dissertation angenommen.

Dekan: Prof. Dr. Dieter Steinhilber

1. Gutachter: Prof. Dr. B. Ludwig

2. Gutachter: Prof. Dr. W. Kühlbrandt

Datum der Disputation:





To my grandfather F. A. de Barros.



# ZUSAMMENFASSUNG

Der Lichtsammelkomplex des Photosystems II (*light-harvesting complex II*, LHC-II) stellt den Hauptantennenkomplex in der pflanzlichen Photosynthese dar. Dieser macht ungefähr 30% des gesamten Proteingehalts in pflanzlichen Chloroplasten aus, weshalb er das quantitativ meist verbreitete Membranprotein auf der Erde sein dürfte. Etwa die Hälfte des pflanzlichen Chlorophylls (Chl) wird durch ihn gebunden. Der Komplex liegt als Trimer in der Thylakoidmembran vor und bindet insgesamt 54 Pigmentmoleküle: 24 Chl *a*, 18 Chl *b*, 6 Luteine (Lut), 3 Neoxanthin- (Neo) und 3 Violaxanthinmoleküle (Vio).

LHC-II fallen fünf Schlüsselrollen in der pflanzlichen Photosynthese zu: (1) Sammeln von Sonnenlicht und Weiterleitung der Anregungsenergie an die Reaktionszentren der Photosysteme I und II, (2) Regulierung der Menge an Anregungsenergie, welche beide Photosysteme erreicht, (3) Stabilisierung der Architektur der photosynthetischen Superkomplexe, (4) Beitrag zur dichten Packung der Grana-Thylakoidstapel in Chloroplasten und (5) Schutz des Photosyntheseapparates vor Lichtschäden durch die nicht-photochemische Löschung der Anregungsenergie (*non-photochemical quenching*, NPQ).

Einen großen Anteil am NPQ besitzt die energieabhängige Komponente qE. Obwohl ihre Notwendigkeit für das Überleben der Pflanze bekannt ist und die zugrunde liegenden Prozesse jahrzehntelang erforscht wurden, sind die exakten Mechanismen des Abführens von absorbierte Lichtenergie unter qE-Bedingungen weitgehend unbekannt. Es gilt als gesichert, dass qE durch den pH-Gradienten über die Thylakoidmembran reguliert wird. Weiterhin ist bekannt, dass infolge des pH-Abfalls im Thylakoidlumen unter Starklichtbedingungen das Enzym Violaxanthin-De-epoxidase (VDE) aktiviert wird, welches im Xanthophyllzyklus das Carotinoid Vio in Zeaxanthin (Zea) umwandelt. Desweiteren zeigten Studien an *Arabidopsis* Mutanten, dass PsbS, eine Untereinheit des Photosystems II, essentiell für qE ist. Inwiefern diese physiologischen Prozesse jedoch dazu beitragen, dass LHC-II von einem aktiven, Energie transferierenden, in einen Energie abführenden Zustand versetzt wird, in welchem Sonnenenergie nicht an die Photosysteme weitergeleitet, sondern in Wärme umgewandelt wird, ist ungeklärt und Gegenstand dieser Arbeit.

Das Abführen überschüssiger Anregungsenergie *in vivo* steht mit einer Fluoreszenzlöschung von LHC-II *in vitro* im Zusammenhang. Deshalb ist es möglich, den qE zugrunde liegenden Mechanismus anhand der Prozesse zu untersuchen, die eine Änderung der Fluoreszenzeigenschaften von LHC-II bewirken. Dementsprechend war ein Großteil der experimentellen Arbeit der spektroskopischen Charakterisierung von LHC-II-Präparationen mit veränderter Pigmentkomposition gewidmet. Die Rolle spezieller Chl-Paare in der Fluoreszenzlöschung wurde mittels stationärer Fluoreszenzspektroskopie von rückgefalteten LHC-II-Mutanten analysiert. Um die Funktion von Zea aufzuklären, wurden drei Methoden zur Gewinnung von Zea-angereichertem LHC-II entwickelt: (1) die Isolierung von LHC-II aus der *Arabidopsis*-Mutante *npq2*, welche in der Synthese von Vio blockiert ist und Zea akkumuliert, (2) die Isolierung von LHC-II aus Spinat- und Erbsenthylakoidmembranen, deren vorausgehende Behandlung einen *in vitro* Xanthophyllzyklus auslöste und (3) die Inkubation von rückgefaltetem LHC-II mit solubilisiertem Zea. Aus der *Arabidopsis*-Mutante *npq2* gereinigtem LHC-II fehlte Neo und der Komplex wurde hauptsächlich als Monomer isoliert. Der Fortschritt in der Etablierung von Wachstumsbedingungen für *Arabidopsis* Pflanzen in Hydrokulturen erlaubte jedoch die Reinigung von sehr reinem, trimeren LHC-II aus WT Pflanzen. Mit Hilfe der anderen beiden Strategien wurden Zea-angereicherte LHC-II Proben gewonnen, welche per transienter Absorptionsspektroskopie, sowie zeitaufgelöster Fluoreszenz- und Zweiphotonenanregungsspektroskopie, analysiert wurden. Innerhalb des Themengebiets „Xanthophyllzyklus“ wurde zusätzlich ein Expressions- und Reinigungsprotokoll für VDE aus *Arabidopsis* etabliert, welches künftige Arbeiten zur Strukturbestimmung dieses Enzyms ermöglicht.

Nach dem Erhalt der hochaufgelösten Röntgenstrukturen von LHC-II aus Erbse und Spinat wurde die kritische Frage aufgeworfen, ob diese Strukturen den Energie transferierenden oder den Energie abführenden Zustand des Komplexes zeigen. Um diese Frage zu beantworten, ist ein Großteil dieser Arbeit der ersten detaillierten spektroskopischen Einzelkristallanalyse von LHC-II gewidmet. Dies erforderte nicht nur ein hochmodernes System zur Spektroskopie von Einzelkristallen, welches an der *Cryobench* der Europäischen Synchrotron Strahlungsanlage (ESRF, Grenoble, Frankreich) zur Verfügung stand, sondern



auch zahlreiche Kristallisationsansätze zur Reproduktion der Kristalle, die für die Strukturbestimmungen verwendet worden waren.

Aus den Ergebnissen, die im Laufe dieser Doktorarbeit erhalten wurden, lassen sich fünf wesentliche Schlussfolgerungen in Bezug auf qE ableiten:

1. ***Der Austausch von Vio gegen Zea in LHC-II ist für ein effizientes Abführen von überschüssiger Anregungsenergie nicht ausreichend.*** Gemäß dem Modell des “Schaltungsmechanismus” (*gear-shift mechanism*) für qE induziert ein Austausch von Vio gegen Zea in LHC-II ein Umschalten in den Energie löschenden Zustand. LHC-II Proben mit oder ohne Zea wurden mittels einer Reihe spektroskopischer Methoden verglichen. Der Austausch von Vio gegen Zea zeigte keine signifikante Auswirkung auf die Lebensdauer des angeregten Zustands von LHC-II, was sowohl anhand transienter Absorptionskinetiken des angeregten Chl-Zustands, als auch anhand zeitaufgelöster Fluoreszenz, gezeigt werden konnte. Dies impliziert, dass der einfache Austausch dieser beiden Carotinoide gegeneinander nicht ausreicht, um ein effizientes Abführen überschüssiger Anregungsenergie in der Thylakoidmembran unter Starklichtbedingungen zu gewährleisten.

2. ***Energielöschung infolge von LHC-II Aggregation benötigt weder Vio und Neo, noch ein spezielles Chl-Paar.*** Es ist bekannt, dass die Energielöschung infolge der Aggregation von LHC-II einige spektroskopische Ähnlichkeiten mit qE aufweist, weshalb ein mechanistischer Zusammenhang vermutet wird. Die Aggregation von rückgefalteten LHC-II-Mutanten, welchen einzelne Chlorophylle fehlen, resultierte in derselben ~100-fachen Reduktion der Fluoreszenzausbeute, welche für den WT beobachtet wurde. Hierdurch wurde nachgewiesen, dass keines der vier potentiell energielöschenden Chl-Dimere im LHC-II-Monomer zur Energielöschung benötigt wird. Der  $\Delta$ Chl 13 Mutante fehlten zusätzlich Neo und Vio. Dennoch zeigte sie nach Aggregation eine vom WT ununterscheidbare Energielöschung, wodurch ausgeschlossen werden kann, dass diesen beiden Carotinoiden in der Energielöschung durch Aggregation eine Bedeutung zukommt.

3. ***Mit einer Ausnahme ist die Pigmentstruktur in LHC-II starr.*** Seit langem hält sich die Hypothese einer Konformationsänderung von LHC-II als mechanistische Erklärung für qE, obwohl bislang kein überzeugender struktureller

Beweis erbracht wurde. Spektroskopische Daten suggerieren, dass mit dieser hypothetischen Konformationsänderung ein *Twist* in der Neo-Konfiguration unter qE-Bedingungen einhergeht. Eine Analyse der B-Faktorverteilung beider Röntgenstrukturen von LHC-II ist in dieser Arbeit dargelegt. Sie zeigt, dass das Innere des Komplexes, in welchem sich die mit der Energielöschung in Zusammenhang gebrachten Pigmente befinden, starr und nur der in die Lipidphase der Thylakoidmembran ragende Teil von Neo flexibel ist. Der *Twist* von Neo scheint daher nicht die Folge einer Konformationsänderung zu sein, sondern auf eine Interaktion zwischen LHC-II und einem anderen Makromolekül hinzuweisen.

**4. Beide Röntgenstrukturen von LHC-II zeigen denselben Energie abführenden Zustand des Komplexes.** Aufgrund einer offensichtlichen Rotverschiebung des Fluoreszenz-Emissionsmaximums und einer Verkürzung der Fluoreszenzlebensdauer in LHC-II nach der Kristallisation wurde von anderen Autoren geschlussfolgert, dass sich der Komplex in Einzelkristallen im Energie löschenden Zustand befindet. Im Gegensatz hierzu konnte mittels stationärer und zeitaufgelöster Fluoreszenzspektroskopie gezeigt werden, dass kristalliner LHC-II, ähnlich wie solubilisierter Komplex, Anregungsenergie weiterleitet und mit einem bei 680 nm gelegenen Emissionsmaximum fluoresziert. Es wurde außerdem eindeutig nachgewiesen, dass die beobachtete Rotverschiebung des Emissionsmaximums durch Eigenabsorption verursacht wird. Gleichmaßen sind die gemessenen Fluoreszenzlebensdauern für eine kristalline Wiederholung von Energie löschenden LHC-II-Trimeren zu lang. Der Vergleich zwischen beiden Röntgenstrukturen ergab, dass beide innerhalb des experimentellen Fehlers gleich sind und deshalb denselben, Energie transferierenden Zustand von LHC-II darstellen.

**5. Kristalliner LHC-II ähnelt dem Komplex in der Thylakoidmembran.** Die Schlussfolgerung, dass LHC-II in Einzelkristallen den Energie löschenden Zustand zeigt, basierte zusätzlich auch auf der (inkorrekten) Annahme, dass die Trimere im Kristallgitter funktionell unabhängig sind, wodurch kein Anregungsenergie transfer zwischen ihnen erfolgt. Im Gegensatz dazu wird in dieser Arbeit nachgewiesen, dass LHC-II-Trimere in Einzelkristallen Anregungsenergie austauschen, und zwar mit vergleichbaren Energietransferraten, welche für Komplexe in der

Thylakoidmembran abgeschätzt wurden. Die ähnlichen Fluoreszenzlebensdauern, welche *in vivo* und in Einzelkristallen beobachtet wurden, spiegeln deshalb die Tatsache wider, dass die Anregungsenergie zu zufällig verteilten, Energie löschenden Zentren innerhalb der Kristalle fließt - auf dieselbe Weise wie zu den Reaktionszentren in der Thylakoidmembran.

Als Korollar aus dieser Doktorarbeit folgen Erklärungsmodelle sowohl für die Aggregations-verursachte Energielöschung *in vitro*, als auch für den qE-Mechanismus *in vivo*. Die infolge der Aggregation von LHC-II *in vitro* beobachtete Energielöschung wird der Bildung von Energiesenken in der Peripherie von LHC-II zugeschrieben, welche durch Interaktion mit anderen Trimeren, freien Pigmenten oder Unreinheiten hervorgerufen werden. Ein ähnlicher, jedoch nicht verwandter, Prozess wird für die Abführung überschüssiger Anregungsenergie in der Thylakoidmembran vorgeschlagen. Dieser beruht auf der spezifischen Interaktion zwischen LHC-II und einem PsbS-Monomer, welches Zea bindet.

Am Ende dieser Arbeit wird ein innovatives experimentelles Modell zur Analyse aller wichtigen Aspekte von qE aufgestellt, um endlich Licht in das Dunkel des qE-Mechanismus zu bringen - einem der letzten ungelösten Probleme in der Photosyntheseforschung.

## SUMMARY

The light-harvesting complex of photosystem II (LHC-II) is the major antenna complex in plant photosynthesis. It accounts for roughly 30% of the total protein in plant chloroplasts, which makes it arguably the most abundant membrane protein on Earth, and binds about half of plant chlorophyll (Chl). The complex assembles as a trimer in the thylakoid membrane and binds a total of 54 pigment molecules, including 24 Chl *a*, 18 Chl *b*, 6 lutein (Lut), 3 neoxanthin (Neo) and 3 violaxanthin (Vio).

LHC-II has five key roles in plant photosynthesis. It: (1) harvests sunlight and transmits excitation energy to the reaction centres of photosystems II and I, (2) regulates the amount of excitation energy reaching each of the two photosystems, (3) has a structural role in the architecture of the photosynthetic supercomplexes, (4) contributes to the tight appression of thylakoid membranes in chloroplast grana, and (5) protects the photosynthetic apparatus from photo-damage by non-photochemical quenching (NPQ).

A major fraction of NPQ is accounted for its energy-dependent component qE. Despite being critical for plant survival and having been studied for decades, the exact details of how excess absorbed light energy is dissipated under qE conditions remain enigmatic. Today it is accepted that qE is regulated by the magnitude of the pH gradient ( $\Delta\text{pH}$ ) across the thylakoid membrane. It is also well documented that the drop in pH in the thylakoid lumen during high-light conditions activates the enzyme violaxanthin de-epoxidase (VDE), which converts the carotenoid Vio into zeaxanthin (Zea) as part of the xanthophyll cycle. Additionally, studies with *Arabidopsis* mutants revealed that the photosystem II subunit PsbS is necessary for qE. How these physiological responses switch LHC-II from the active, energy-transmitting to the quenched, energy-dissipating state, in which the solar energy is not transmitted to the photosystems but instead dissipated as heat, remains unclear and is the subject of this thesis.

Excess excitation energy dissipation *in vivo* is related to LHC-II fluorescence quenching *in vitro*. It is therefore possible to study the mechanism of qE by analysing the processes that lead to changes in LHC-II fluorescence properties.

Accordingly, a large part of the experimental work reported here dealt with spectroscopic characterisation of LHC-II preparations having altered pigment compositions. Refolded LHC-II mutants were used to investigate the role of particular Chl pairs in fluorescence quenching, using steady-state fluorescence spectroscopy. To elucidate the role of Zea, three strategies were developed to obtain Zea-enriched LHC-II samples: (1) LHC-II isolation from the *Arabidopsis* mutant *npq2*, which lacks Vio and accumulates Zea, (2) LHC-II isolation from spinach and pea thylakoid membranes that were treated to trigger the xanthophyll cycle *in vitro* and (3) incubation of refolded LHC-II with solubilised Zea. LHC-II purified from the *Arabidopsis* mutant *npq2* was deficient in Neo and mostly monomeric, but the progress made on the establishment of hydroponic growth conditions for *Arabidopsis* plants enabled large-scale purification of highly pure trimeric LHC-II from WT plants. The other two strategies yielded Zea-enriched LHC-II samples that were analysed by pump-probe, time-resolved fluorescence and two-photon excitation spectroscopy. Also, within the theme of the xanthophyll cycle, an expression and purification protocol for *Arabidopsis* VDE was established, setting the stage for future work aimed at structure determination of this enzyme.

As the high-resolution X-ray structures of pea and spinach LHC-II became available, the critical question was to know whether they show the energy-transmitting or an energy-dissipating state of the complex. To answer this question, the major part of this thesis is devoted to the first detailed spectroscopic characterisation of LHC-II in single crystals. This required not only a state-of-the-art single-crystal spectroscopy system, which was available at the Cryobench of the European Synchrotron Radiation Facility (Grenoble, France), but also extensive crystallisation trials to reproduce the crystals from which the structures were determined.

From the results obtained during this doctoral work, five main conclusions can be drawn concerning the mechanism of qE:

1. ***Substitution of Vio by Zea in LHC-II is not sufficient for efficient dissipation of excess excitation energy.*** According to the gear-shift mechanism of qE, the Vio by Zea substitution in LHC-II induces the switch to the quenched state. LHC-II samples with or without Zea were compared using a wide range of

spectroscopic techniques. Vio by Zea substitution had no significant effect on the lifetime of the LHC-II excited state, as observed by both transient absorption kinetics of the Chl excited state and time-resolved fluorescence, implying that the simple exchange of these two carotenoids is not sufficient for efficient dissipation of excess excitation energy in the thylakoid membrane under high-light conditions.

**2. *Aggregation quenching of LHC-II does not require Vio, Neo nor a specific Chl pair.*** LHC-II aggregation quenching is known to have some spectroscopic similarities with qE and their mechanisms are thought to be related. Aggregation of refolded LHC-II mutants lacking particular Chls resulted in the same ~100-fold reduction in fluorescence yield observed for WT, demonstrating that none of the four potential Chl quenching dimers in the LHC-II monomer is required for quenching. The  $\Delta$ Chl 13 mutant was also deficient in both Neo and Vio, but was quenched in aggregates indistinguishably from WT, showing that also neither of those two carotenoids is required for aggregation quenching.

**3. *With one exception, the pigment structure in LHC-II is rigid.*** An LHC-II conformational switch is a well-held hypothesis for the mechanism of qE, although no conclusive structural evidence has ever been produced. Spectroscopic data suggested that this hypothetical conformational change involves a twist in Neo configuration under qE conditions. An analysis of the B-factor distribution in the two X-ray structures of LHC-II presented in this thesis reveals that the core of the complex, where the pigments implicated in quenching are located, is rigid and that only the portion of Neo that protrudes into the lipid phase of the thylakoid membrane is flexible. Instead of being a consequence of a larger conformational change, the Neo twisting more likely reports a specific interaction between LHC-II and another macromolecule.

**4. *The two X-ray structures of LHC-II show the same energy-transmitting state of the complex.*** Based on an apparent red-shift of the fluorescence emission peak and the shortening of the fluorescence lifetime of LHC-II upon crystallisation, it has been concluded by others that the complex is in the quenched, energy-dissipating state in single crystals. Using steady-state and time-resolved fluorescence spectroscopy, it was found that, on the contrary, crystalline LHC-II is capable of transmitting excitation energy and fluoresces with an emission peak centred at

680 nm, similar to solubilised complexes. The observed red-shift of the emission peak was unambiguously demonstrated to be caused by self-absorption. Likewise, the measured fluorescence lifetimes are too long for a crystalline repeat of quenched LHC-II trimers. Comparison of the two X-ray structures revealed that they are identical within experimental error, and therefore both show the same active, energy-transmitting state of LHC-II.

**5. *Crystalline LHC-II resembles the complex in the thylakoid membrane.***

The conclusion that LHC-II is quenched in single-crystals was additionally based on the (incorrect) assumption that the trimers in the crystalline lattice are functionally independent, so that no excitation energy transfer occurs between them. In contrast, it is shown here that the LHC-II trimers in single crystals do exchange excitation energy, with energy transfer rates that are comparable to those estimated for complexes in the thylakoid membrane. The similar fluorescence lifetimes observed *in vivo* and in single crystals therefore reflect the fact that the excitation energy flow to randomly distributed quenchers in crystals is analogous to the flow to reaction centres in the thylakoid membrane.

Models of the aggregation quenching mechanism *in vitro* and the qE mechanism *in vivo* are presented as a corollary of this doctoral work. LHC-II aggregation quenching *in vitro* is attributed to the formation of energy sinks on the periphery of LHC-II through random interaction with other trimers, free pigments or impurities. A similar but unrelated process is proposed to occur in the thylakoid membrane, by which excess excitation energy is dissipated upon specific interaction between LHC-II and a PsbS monomer carrying Zea.

At the end of this thesis, an innovative experimental model for the analysis of all key aspects of qE is proposed in order to finally solve the qE enigma, one of the last unresolved problems in photosynthesis research.

# TABLE OF CONTENTS

	Page
ZUSAMMENFASSUNG .....	I
SUMMARY .....	VI
TABLE OF CONTENTS .....	X
LIST OF FIGURES .....	XVI
LIST OF TABLES .....	XXI
SYMBOLS AND ABBREVIATIONS .....	XXIII
<b>1 INTRODUCTION .....</b>	<b>1</b>
<b>1.1 Oxygenic photosynthesis.....</b>	<b>1</b>
1.1.1 Light-harvesting systems in plant photosynthesis.....	3
<b>1.2 Plant light-harvesting complex of photosystem II .....</b>	<b>5</b>
1.2.1 The Lhc family .....	5
1.2.2 Biochemistry.....	9
1.2.3 Function.....	11
1.2.4 Crystallisation.....	14
1.2.5 Structure.....	17
1.2.5.1 The LHC-II polypeptide.....	18
1.2.5.2 Chl binding sites .....	19
1.2.5.3 Carotenoid binding sites .....	21
1.2.5.4 Pigment structure.....	22
1.2.5.5 Bound lipids .....	24
1.2.6 Conserved structure of plant LHCs.....	25
<b>1.3 Non-photochemical quenching .....</b>	<b>28</b>
1.3.1 The xanthophyll cycle .....	30
1.3.1.1 Violaxanthin de-epoxidase .....	30
1.3.2 PsbS .....	32
1.3.3 Current models of the qE mechanism .....	33
1.3.3.1 Aggregation quenching .....	33
1.3.3.2 The conformational change hypothesis .....	33
1.3.3.3 Gear-shift and carotenoid radical cation hypothesis .....	34
<b>1.4 Aims of this work.....</b>	<b>36</b>



<b>2</b>	<b>A NOTE ON SPECTROSCOPIC METHODS AND CALCULATIONS .....</b>	<b>37</b>
<b>2.1</b>	<b>Absorption and fluorescence in LHC-II .....</b>	<b>38</b>
<b>2.2</b>	<b>Steady-state and time-resolved spectroscopy .....</b>	<b>40</b>
2.2.1	Time-resolved fluorescence spectroscopy .....	40
2.2.1.1	Decay-associated spectra .....	42
2.2.2	Pump-probe spectroscopy .....	43
2.2.3	Resonant two photon two colour ionisation .....	44
2.2.4	Two-photon excitation spectroscopy .....	45
<b>2.3</b>	<b>Single-crystal spectroscopy.....</b>	<b>47</b>
<b>2.4</b>	<b>Theoretical calculations .....</b>	<b>49</b>
2.4.1	Coupling strength.....	49
2.4.2	Förster energy transfer rates.....	49
<b>3</b>	<b>MATERIALS AND METHODS .....</b>	<b>50</b>
<b>3.1</b>	<b>Biological material .....</b>	<b>50</b>
3.1.1	Pea plant growth.....	50
3.1.2	<i>Arabidopsis</i> plant growth.....	50
3.1.3	<i>Escherichia coli</i> cell growth.....	52
<b>3.2</b>	<b>Basic molecular biology procedures.....</b>	<b>54</b>
3.2.1	Cloning .....	54
3.2.2	Transformation and selection of clones .....	55
<b>3.3</b>	<b>Basic biochemistry procedures .....</b>	<b>56</b>
3.3.1	Protein concentration determination.....	56
3.3.2	SDS gel electrophoresis and staining.....	56
3.3.3	Western blotting .....	58
<b>3.4</b>	<b>Protein and pigment purification from native source .....</b>	<b>59</b>
3.4.1	Thylakoid membrane isolation .....	59
3.4.2	Pigment isolation .....	60
3.4.3	Pigment concentration determination .....	61
3.4.4	Pigment analysis by HPLC.....	61
3.4.5	<i>In vitro</i> xanthophyll cycle .....	62
3.4.6	Purification of native LHC-II.....	63
3.4.7	Purification of native Zea-LHC-II.....	64
<b>3.5</b>	<b>Heterologous expression and purification of recombinant protein .....</b>	<b>65</b>
3.5.1	Production of recombinant LHC-II.....	65
3.5.2	Purification of recombinant LHC-II.....	65

3.5.3 Refolding of recombinant LHC-II.....	66
3.5.4 Purification and refolding of recombinant Zea-LHC-II .....	67
3.5.5 Production of recombinant VDE in <i>Escherichia coli</i> cells in inclusion bodies .....	68
3.5.6 Production of recombinant VDE in <i>Escherichia coli</i> cells in soluble form.....	68
3.5.7 Purification of recombinant VDE purification under denaturing conditions.....	68
3.5.8 Purification of recombinant VDE under native conditions .....	69
<b>3.6 Protein characterization.....</b>	<b>71</b>
3.6.1 Size exclusion chromatography .....	71
3.6.2 VDE activity assay.....	71
3.6.3 Preparation of LHC-II aggregates .....	72
<b>3.7 X-ray crystallography.....</b>	<b>73</b>
3.7.1 LHC-II crystallisation .....	73
3.7.2 Cryoprotection and freezing of LHC-II crystals .....	74
3.7.3 Diffraction experiments.....	74
3.7.4 Data processing .....	74
<b>3.8 Structure analysis and modelling.....</b>	<b>75</b>
3.8.1 Comparison of structures.....	75
3.8.2 Modelling LHC-II – LHC-II interaction <i>in vivo</i> .....	75
<b>3.9 Electron microscopy procedures.....</b>	<b>76</b>
3.9.1 Freeze-fracture of LHC-II crystals.....	76
<b>3.10 Solutions spectroscopy.....</b>	<b>77</b>
3.10.1 Absorption spectra .....	77
3.10.2 Fluorescence spectra at room temperature.....	77
<b>3.11 Single-crystal spectroscopy .....</b>	<b>78</b>
3.11.1 Fluorescence spectra of single LHC-II crystals.....	81
3.11.2 Absorption spectra of single LHC-II crystals.....	82
3.11.3 Time-correlated single photon counting .....	83
<b>4 LHC-II BIOCHEMISTRY .....</b>	<b>84</b>
<b>4.1 Results.....</b>	<b>85</b>
4.1.1 LHC-II purification from pea plants.....	85
4.1.2 <i>Arabidopsis</i> plant growth.....	86
4.1.2.1 Plants grown in soil.....	86
4.1.2.2 Plants grown hydroponically .....	89
4.1.3 LHC-II purification from <i>Arabidopsis</i> WT plants .....	92
4.1.4 Preparation of Zea-LHC-II .....	93
4.1.4.1 Thylakoid isolation from <i>Arabidopsis</i> mutant <i>npq2</i> .....	93

4.1.4.2	LHC-II purification from <i>Arabidopsis</i> mutant <i>npq2</i> .....	94
4.1.4.3	Refolding of recombinant Zea-LHC-II .....	95
4.1.4.4	<i>In vitro</i> de-epoxidation .....	100
4.1.5	Refolding of LHC-II mutants.....	102
4.1.6	Size exclusion chromatography .....	106
<b>4.2</b>	<b>Discussion .....</b>	<b>107</b>
4.2.1	Large scale purification of <i>Arabidopsis</i> LHC-II .....	107
4.2.1.1	Limitations of the <i>Arabidopsis</i> mutant <i>npq2</i> .....	108
4.2.2	Producing Zea-LHC-II .....	111
4.2.3	LHC-II mutants .....	112
4.2.4	LHC-II aggregates at low pH.....	113
<b>5</b>	<b>VDE BIOCHEMISTRY .....</b>	<b>114</b>
<b>5.1</b>	<b>Results .....</b>	<b>115</b>
5.1.1	VDE and VDE-Thrx fusion constructs .....	115
5.1.2	Transformation of <i>E. coli</i> cells with VDE constructs .....	117
5.1.3	VDE expression .....	118
5.1.4	Optimisation of VDE expression .....	120
5.1.5	VDE production in inclusion bodies .....	122
5.1.6	VDE production in soluble form .....	123
5.1.7	VDE purification under denaturing conditions .....	125
5.1.8	VDE purification under native conditions .....	126
5.1.9	Expression and purification of Thrx-VDE fusion .....	127
5.1.10	VDE expression in HEK cells .....	129
5.1.11	Preliminary activity assays.....	130
<b>5.2</b>	<b>Discussion .....</b>	<b>132</b>
5.2.1	VDE production in bacteria.....	132
5.2.1.1	Soluble expression or refolding?.....	133
5.2.2	VDE production in eukaryotic cells .....	135
<b>6</b>	<b>LHC-II CRYSTALLISATION.....</b>	<b>136</b>
<b>6.1</b>	<b>Results .....</b>	<b>137</b>
6.1.1	Reproduction of type-I pea LHC-II crystals.....	137
6.1.2	New crystallisation conditions .....	138
6.1.3	Freeze-fracture of type-I LHC-II crystals .....	144
6.1.4	Diffraction of crystals used for spectroscopic measurements.....	147
6.1.5	A peculiar diffraction pattern – the diffraction flower.....	150
<b>6.2</b>	<b>Discussion .....</b>	<b>151</b>

6.2.1	Type-I LHC-II crystals .....	151
6.2.1.1	Defects in the LHC-II type-I crystal lattice .....	152
6.2.2	Improving the LHC-II structure .....	152
6.2.3	New crystallisation conditions .....	153
<b>7</b>	<b>LHC-II STRUCTURE ANALYSIS, MODELLING AND CALCULATIONS...</b>	<b>155</b>
<b>7.1</b>	<b>Results.....</b>	<b>156</b>
7.1.1	Comparison of LHC-II X-ray structures .....	156
7.1.2	Crystallographic B-factor analysis .....	160
7.1.3	Interaction between LHC-II trimers in crystals and <i>in vivo</i> .....	162
7.1.4	Coupling strength.....	165
7.1.5	Förster energy transfer rates.....	166
<b>7.2</b>	<b>Discussion .....</b>	<b>167</b>
7.2.1	The two X-ray structures of LHC-II are identical within error .....	167
7.2.2	With one exception, the LHC-II pigments are rigid .....	168
7.2.3	Energy transfer between LHC-II trimers .....	171
<b>8</b>	<b>LHC-II SPECTROSCOPY IN SOLUTION .....</b>	<b>172</b>
<b>8.1</b>	<b>Results.....</b>	<b>173</b>
8.1.1	Fluorescence spectrum of native LHC-II in solution .....	173
8.1.2	Aggregation quenching in LHC-II mutants .....	174
8.1.3	Ultrafast transient absorption spectroscopy .....	177
8.1.3.1	Two-photon excitation spectroscopy .....	180
<b>8.2</b>	<b>Discussion .....</b>	<b>182</b>
8.2.1	Quenching does not require a specific Chl pair, Vio or Neo .....	182
8.2.2	Zea binding to LHC-II is not sufficient for efficient quenching .....	183
8.2.3	Zea radical cation in LHC-II .....	185
<b>9</b>	<b>LHC-II SINGLE CRYSTAL SPECTROSCOPY.....</b>	<b>186</b>
<b>9.1</b>	<b>Results.....</b>	<b>187</b>
9.1.1	Absorption spectra of LHC-II crystals .....	187
9.1.2	Emission spectra of LHC-II crystals .....	188
9.1.3	Geometry dependence of LHC-II crystal emission spectra .....	189
9.1.4	Temperature dependence of LHC-II crystal emission spectra .....	193
9.1.5	Fluorescence lifetimes at low temperature .....	194
9.1.6	Fluorescence lifetimes at room temperature .....	198
9.1.7	Wavelength-dependence of LHC-II fluorescence lifetimes .....	198

9.1.8 Concentration-dependence of LHC-II fluorescence decay in solution .....	201
<b>9.2 Discussion .....</b>	<b>203</b>
9.2.1 Self-absorption distorts emission spectra of LHC-II crystals .....	203
9.2.2 Low-temperature 700 nm fluorescence .....	206
9.2.3 Fluorescence lifetimes in crystals, aggregates and solutions .....	207
9.2.4 Crystal structures show the active, energy-transmitting state .....	208
<b>10 GENERAL DISCUSSION .....</b>	<b>210</b>
<b>10.1 Implications for the mechanism of LHC-II aggregation quenching .....</b>	<b>211</b>
10.1.1 Proposed mechanism of LHC-II aggregation quenching .....	211
<b>10.2 Implications for the mechanism of qE .....</b>	<b>214</b>
10.2.1 Crystalline LHC-II resembles the complex in thylakoids .....	214
10.2.2 Structure of Zea-bound LHC-II .....	215
10.2.3 qE is independent from Zea binding to the L2 site .....	216
10.2.4 Proposed mechanism of qE .....	217
<b>10.3 Experiment proposal .....</b>	<b>220</b>
<b>10.4 Concluding remarks and outlook .....</b>	<b>221</b>
<b>REFERENCES .....</b>	<b>222</b>
<b>APPENDIX .....</b>	<b>241</b>
<b>ACKNOWLEDGEMENTS .....</b>	<b>247</b>
<b>CURRICULUM VITAE .....</b>	<b>250</b>

# LIST OF FIGURES

	Page
Figure 1-1 - Oxygenic photosynthesis.....	1
Figure 1-2 - Light-harvesting in plant photosynthesis. ....	3
Figure 1-3 – Core light-harvesting complexes of the photosystems.....	4
Figure 1-4 - The Lhc family. ....	6
Figure 1-5 - Bacterial light-harvesting complex II.....	9
Figure 1-6 - Model of the LHC-II - PS-II supercomplex. ....	12
Figure 1-7 - <i>In vitro</i> LHC-II assemblies. ....	15
Figure 1-8 - LHC-II structure.....	17
Figure 1-9 - Pigment configuration in the LHC-II monomer. ....	23
Figure 1-10 - Lipid and detergent molecules in the LHC-II X-ray structures.....	25
Figure 1-11 - Comparison of LHC-II and Lhcas. ....	27
Figure 1-12 - Schematic representation of the qE component of NPQ.....	29
Figure 1-13 - The xanthophyll cycle. ....	30
Figure 1-14 - The lipocalin fold.....	31
Figure 1-15 - VDE gene structure.....	32
Figure 2-1 - LHC-II absorption spectrum. ....	38
Figure 2-2 – Electronic states of a molecule and transitions between them. ....	39
Figure 2-3 – Schematic diagram of a pump-pump-probe experiment on carotenoids. ....	45
Figure 2-4 – Two-photon excitation spectroscopy in LHC-II.....	46
Figure 3-1 - <i>Arabidopsis</i> plants growth in hydroponic medium.....	51
Figure 3-2 - <i>Arabidopsis</i> plants growth using a hybrid method. ....	51
Figure 3-3 - Overview of the Cryobench laboratory at the ESRF. ....	78
Figure 3-4 - Close-up of the Cryobench optical system. ....	79

Figure 3-5 - Sample holder for room temperature experiments at the Cryobench.....	81
Figure 3-6 - Geometry of fluorescence measurements with single crystals. ....	82
Figure 4-1 - SDS-PAGE of purified native LHC-II .....	85
Figure 4-2 - <i>Arabidopsis</i> plant grown in soil at the MPI for Plant Breeding Research. ....	87
Figure 4-3 - <i>Arabidopsis</i> plant grown in soil at the JW Goethe University. ....	88
Figure 4-4 - Two week old <i>Arabidopsis</i> WT plants. ....	90
Figure 4-5 - One month old <i>Arabidopsis</i> plants.....	91
Figure 4-6 – Two month old <i>Arabidopsis</i> plants grown hydroponically. ....	91
Figure 4-7 - SDS-PAGE gel and Western blot of <i>Arabidopsis</i> LHC-II samples. ....	92
Figure 4-8 - HPLC analysis of <i>Arabidopsis</i> variant thylakoids. ....	94
Figure 4-9 - SDS-PAGE gel and Western blot of thylakoids from <i>Arabidopsis npq2</i> mutant plants fractionated by sucrose gradient centrifugation. ....	95
Figure 4-10 - Sucrose gradients of refolded Zea-LHC-II samples. ....	96
Figure 4-11 - HPLC chromatograms of recombinant LHC-II refolded with a pigment mixture supplemented with Zea.....	96
Figure 4-12 - HPLC chromatograms of refolded LHC-II incubated with Zea.....	98
Figure 4-13 - <i>In vitro</i> de-epoxidation under different experimental conditions.....	100
Figure 4-14 - Time course of the <i>in vitro</i> de-epoxidation reaction in pea thylakoids.....	101
Figure 4-15 - Long term time course of the <i>in vitro</i> de-epoxidation reaction.....	102
Figure 4-16 - Sucrose gradients of refolded LHC-II variants.....	103
Figure 4-17 - HPLC analysis of refolded LHC-II variants.....	104
Figure 4-18 – Size-exclusion chromatography of LHC-II in NG or DDM at neutral or acidic pH.	106
Figure 4-19 – Carotenoids and abscisic acid biosynthetic pathways.....	110
Figure 5-1 - VDE constructs for expression in <i>E. coli</i> .....	115
Figure 5-2 - Agarose gel with PCR products of <i>Arabidopsis</i> VDE cDNA amplification and introduction of 3C/LIC specific sequences.....	116

Figure 5-3 - Agarose gel with PCR products of <i>Arabidopsis</i> cDNA amplification and introduction of Ek/LIC specific sequences.....	116
Figure 5-4 - Agarose gel with VDE cDNA amplified by PCR from plasmid DNA of transformed <i>E. coli</i> strains.....	118
Figure 5-5 - SDS-PAGE gel of recombinant VDE expression tests in <i>E. coli</i> .....	119
Figure 5-6 - Expression tests of Thrx-VDE fusion.....	120
Figure 5-7 - SDS-PAGE gel of recombinant VDE expression in <i>E. coli</i> at different time points after induction.....	121
Figure 5-8 - Western blot from VDE construct expression tests in <i>E. coli</i> strains.....	122
Figure 5-9 - Experimental evidence for ArabVDE expression in inclusion bodies.....	123
Figure 5-10 - Optimisation of soluble VDE expression in <i>E. coli</i> (I).....	124
Figure 5-11 - Optimisation of soluble VDE expression in <i>E. coli</i> (II).....	125
Figure 5-12 - Purification of VDE in denaturing conditions.....	126
Figure 5-13 -Purification of VDE expressed in native conditions.....	127
Figure 5-14 - Expression and purification of Thrx-VDE fusion.....	128
Figure 5-15 - Expression of VDE in HEK cells.....	130
Figure 5-16 - VDE activity assay.....	131
Figure 6-1 - Type-I pea LHC-II crystals.....	137
Figure 6-2 –LHC-II crystals grown from various crystallisation conditions.....	140
Figure 6-3 – Different LHC-II crystal morphologies from the same crystallisation conditions.....	141
Figure 6-4 - Diffraction pattern from a rhomboid LHC-II crystal.....	142
Figure 6-5 - Brick-shaped LHC-II crystals.....	143
Figure 6-6 - Diffraction pattern from small brick shaped LHC-II crystals.....	144
Figure 6-7 - Freeze-fracture image of a type-I LHC-II crystal.....	145
Figure 6-8 – Defects in the crystal lattice of the type-I LHC-II crystals.....	147
Figure 6-9 - Diffraction pattern of a type-I LHC-II crystal used for spectroscopic measurements at the Cryobench.....	149



Figure 6-10 - A peculiar diffraction pattern from a LHC-II crystal. ....	150
Figure 6-11 - Exposed lysine residues in the pea LHC-II structure. ....	153
Figure 7-1 - Superposition of pea and spinach LHC-II polypeptides ....	157
Figure 7-2 - Rms deviation between pea and spinach LHC-II structures. ....	158
Figure 7-3 - Superposition of selected pea and spinach LHC-II pigments. ....	159
Figure 7-4 - B-factor distribution in the pea and spinach LHC-II structures. ....	161
Figure 7-5 - B-factor distribution in the pea and spinach LHC-II carotenoids ....	162
Figure 7-6 - Interactions between neighbouring LHC-II trimers. ....	164
Figure 7-7 - Icosahedral vesicles in LHC-II preparations. ....	169
Figure 8-1 - Fluorescence spectra of solubilised native LHC-II. ....	174
Figure 8-2 - Absorption and fluorescence spectra of refolded LHC-II variants. ....	177
Figure 8-3 - Transient absorption kinetics of the Chl excited state in LHC-II. ....	179
Figure 8-4 - Difference transient absorption spectrum between R2C2PI and pump-probe in LHC-II. .....	179
Figure 8-5 - Relative Car S <sub>1</sub> to Chl energy transfer efficiency ( $\Phi$ ) and Chl fluorescence lifetime ( $\tau$ ) in LHC-II. ....	181
Figure 8-6 - Aggregation quenching of LHC-II mutants. ....	182
Figure 9-1 - Different types of samples used for low temperature spectroscopic measurements at the Cryobench. ....	186
Figure 9-2 - Low temperature absorption spectrum of a type-I LHC-II crystal in the Q <sub>y</sub> region. ...	187
Figure 9-3 - Emission spectra of LHC-II crystals. ....	189
Figure 9-4 - Emission spectra of a type-I LHC-II crystal at different tilt angles. ....	190
Figure 9-5 - Emission spectra of a cubic LHC-II crystal at different tilt angles. ....	190
Figure 9-6 - Normalised emission spectrum of a cubic LHC-II crystal at 0° and 360° ....	192
Figure 9-7 - Emission spectra of a type-I LHC-II crystal in different geometries. ....	192
Figure 9-8 - Room temperature emission spectrum of a type-I LHC-II crystal. ....	194

Figure 9-9 - TCSPC histograms of the fluorescence decay of LHC-II in solution, crystals and aggregates .....	196
Figure 9-10 - Wavelength dependence of the LHC-II fluorescence decay components in crystals at low temperature. ....	200
Figure 9-11 - Concentration dependence of the relative amplitude of a second lifetime component in solubilised LHC-II at low temperature.....	202
Figure 9-12 - Low-temperature fluorescence spectra of a single crystal of pea LHC-II in two different orientations. ....	204
Figure 9-13 – Low temperature LHC-II absorption and fluorescence emission spectra. ....	205
Figure 9-14 - Self-absorption of LHC-II fluorescence in single crystals.....	205
Figure 10-1 - Energy transfer and dissipation by LHC-II <i>in vitro</i> . ....	213
Figure 10-2 – Accessibility of the lutein binding sites in the LHC-II monomer. ....	217
Figure 10-3 - Proposed model for qE in thylakoids. ....	219
Figure 10-4 – Proposed experimental system. ....	220

# LIST OF TABLES

	Page
Table 1-1 - Pigment composition of native LHC monomers of photosystem II.....	20
Table 1-2 - Chl fluorescence quenching processes <i>in vivo</i> .....	29
Table 3-1 - Nutrient solution for <i>Arabidopsis</i> hydroponic growth .....	52
Table 3-2 - List of <i>E. coli</i> strains.....	53
Table 3-3 – Media for <i>E. coli</i> growth.....	53
Table 3-4 – Oligonucleotide primers for PCR .....	54
Table 3-5 – PCR mixture composition .....	55
Table 3-6 - PCR programme .....	55
Table 3-7 - SDS-PAGE gel composition.....	57
Table 3-8 - SDS-PAGE sample buffer (5x stock).....	57
Table 3-9 - SDS-PAGE running buffer .....	57
Table 3-10 - Buffers for thylakoid membrane preparation.....	60
Table 3-11 - HPLC solvent composition.....	62
Table 3-12 - HPLC run programme .....	62
Table 3-13 - De-epoxidation buffer composition .....	63
Table 3-14 - Buffers for LHC-II inclusion body isolation.....	66
Table 3-15 - Buffers for LHC-II refolding .....	67
Table 3-16 - Buffers for VDE purification under denaturing conditions.....	69
Table 3-17 - Buffers for VDE purification under native conditions.....	70
Table 3-18 - Buffers used for SEC with LHC-II .....	71
Table 3-19 - VDE activity assay composition.....	72
Table 3-20 - Type-I pea LHC-II crystallisation conditions .....	74
Table 4-1 - Ratios between pigments in Zea-enriched refolded LHC-II .....	99

Table 4-2 - Pigment composition of refolded LHC-II monomers <sup>a</sup> .....	99
Table 4-3 - Pigment composition of isolated native spinach LHC-II .....	102
Table 4-4 - Pigment composition of LHC-II variants.....	105
Table 5-1 - VDE refolding conditions.....	134
Table 7-1 - Superposition of LHC-II X-ray structures.....	158
Table 7-2 - Coupling strength ( $V$ ) between LHC-II trimers in crystals and <i>in vivo</i> .....	165
Table 7-3 - Förster energy transfer rates ( $K$ ) in crystals and <i>in vivo</i> .....	166
Table 8-1 - Chl pairs in LHC-II and respective mutants.....	175
Table 8-2 – Relative Car S <sub>1</sub> to Chl energy transfer efficiency ( $\Phi$ ) and Chl fluorescence lifetime ( $\tau$ ) in native or refolded LHC-II .....	181
Table 9-1 - Low temperature LHC-II fluorescence lifetimes .....	197
Table 9-2 - Wavelength dependence of the LHC-II fluorescence decay components in crystals at low temperature.....	201

# SYMBOLS AND ABBREVIATIONS

°C, Celsius degrees	HABA, hydroxy-azophenylbenzoic acid
2D, two-dimensional	HEK, human embryonic kidney
3D, three-dimensional	HPLC, high pressure liquid chromatography
Å, angstrom(s)	K, Kelvin degrees
ABRC, Arabidopsis Biological Resource Center	l, liter(s)
Amp, ampicilin	LB, lysogeny broth
A <sub>x</sub> , absorbance at wavelength x	LDS, lithium dodecyl sulfate
BME, β-mercaptoethanol	LHC-II, light-harvesting complex of photosystem II
bp, base pairs	LHC, light-harvesting complex
BSA, bovine serum albumin	LIC, ligation-independent cloning
Cam, chloramphenicol	Lut, lutein
Car <sup>+</sup> (s), carotenoid radical cation(s)	m, meter(s)
Chl(s), chlorophyll(s)	M, moles per liter
Da, Dalton	MGDG, monogalactosyldiacylglycerol
DDM, n-Dodecyl-β-D-maltoside	min, minutes
DGDG, digalactosyldiacylglycerol	MW, molecular weight
dNTP, deoxyribonucleotide triphosphate	MWCO, molecular weight cutoff
DTT, dithiothreitol	Neo, neoxanthin
EDTA, ethylenediaminetetraacetic acid	NG, n-Nonyl-β-D-glucoside
ESRF, European Synchrotron Radiation Facility	NPQ, non-photochemical quenching
g, gram(s)	OG, n-Octyl-β-D-glucoside
h, hours	PAGE, polyacrylamide gel electrophoresis

PCR, polymerase chain reaction

PDB, Protein Data Bank

PG, L-phosphatidyl-D,L-glycerol dipalmitoyl

PS, photosystem

qE, energy-dependent component of NPQ

R2C2PI, resonant 2-colour 2-photon ionisation

rms, root mean square

rpm, rotations per minute

RT, room temperature

s, second(s)

SDS, sodium dodecyl sulfate

SEC, size exclusion chromatography

SLS, Swiss light source

SOC, super optimal broth with catabolite repression

Str, streptomycin

T, temperature

t, time

TCEP, tris(2-carboxyethyl)phosphine

TCSPC, time-correlated single photon counting

Tet, tetracycline

Thrx, thioredoxin

Tris, tris-(hydroxymethyl)-aminomethane

VDE, violaxanthin de-epoxidase

Vio, violaxanthin

Vio-LHC-II, light-harvesting complex of photosystem II containing only violaxanthin

WT, wild type

Zea, zeaxanthin

Zea-LHC-II, zeaxanthin enriched light-harvesting complex of photosystem II

# 1 INTRODUCTION

## 1.1 Oxygenic photosynthesis

Oxygenic photosynthesis is the natural process performed by plants, green algae and cyanobacteria of harvesting, converting and storing solar energy as biologically useful chemical energy. Virtually all higher forms of life on Earth are in one way or another dependent on oxygenic photosynthesis or its end products: molecular oxygen ( $O_2$ ) and carbohydrates.

During the initial, hallmark steps of oxygenic photosynthesis, sunlight is converted into chemical energy in the form of  $O_2$ , reduced nicotinamide adenine dinucleotide phosphate (NADPH) and adenosine-5'-triphosphate (ATP). These so-called light-driven reactions are carried out in the thylakoid membrane by four large integral membrane-protein complexes, known as Photosystems I (PS-I) and II (PS-II), the cytochrome- $b_6f$  complex and the F-type ATP synthase (Figure 1-1; (Nelson & Ben-Shem, 2004) for an excellent review).

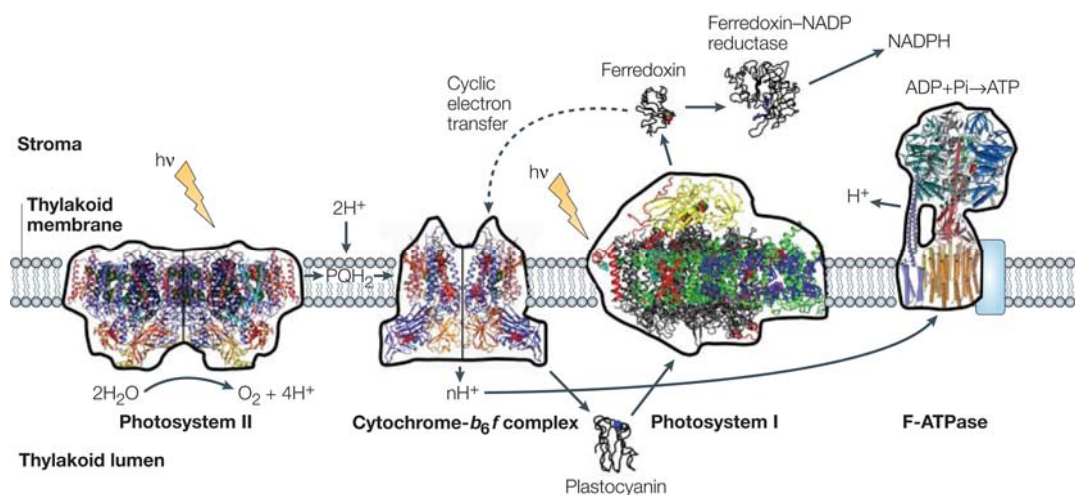


**Figure 1-1 - Oxygenic photosynthesis.**

Four large integral membrane-protein complexes embedded in the thylakoid membrane drive oxygenic photosynthesis. Current structural models of these complexes are shown on the same scale. The figure also shows other soluble enzymes that participate in the light-driven reactions of oxygenic photosynthesis. Adapted from (Nelson & Ben-Shem, 2004).

The chain of events during oxygenic photosynthesis is usually described to start in PS-II, or more precisely in its reaction centre (RC). As excitation energy collected from sunlight reaches a pair of weakly coupled chlorophylls (Chls) known as P680, an electron is ejected from this primary electron donor in PS-II and is passed through a series of electron carriers until it reduces plastoquinone. This process is performed twice, and after uptake of two protons from the stroma of the thylakoids, plastoquinone is converted to plastoquinol. Plastoquinol diffuses into the thylakoid membrane and delivers the electron to the cytochrome-*b<sub>6</sub>f* complex. Consequently, the reduced cytochrome-*b<sub>6</sub>f* complex reduces the oxidised PS-I primary donor (P700), via plastocyanin. At this stage, another quantum of light is necessary to drive the electron from the PS-I reaction centre to  $\text{NADP}^+$ , through the intermediate carriers ferredoxin and ferredoxin- $\text{NADP}^+$ -reductase, to form NADPH. Each electron ejected from the PS-II primary donor is replaced by an electron from a cluster of four manganese ions, which together with other co-factors constitute the oxygen evolving complex (OEC). When the OEC is provided with four oxidizing equivalents, two substrate water molecules are split (oxidised) into  $\text{O}_2$ , 4 protons ( $\text{H}^+$ ) and 4 electrons ( $e^-$ ). The 4  $e^-$  reset the manganese cluster to its fully reduced state, and the photosynthetic chain is then ready for another cycle.

A consequence of the light-driven reactions is the establishment of a protonmotive force across the thylakoid membrane, by the accumulation of protons in the lumen as a result of electron transfer through the cytochrome-*b<sub>6</sub>f* complex and the water splitting reaction. F-type ATP synthase, the fourth macromolecular complex of the chain, uses this electrochemical potential to synthesise ATP by photophosphorylation. The energy equivalents produced during the light-driven reactions (ATP and NADPH) fuel the light-independent reactions, by which carbon dioxide is “fixed” from the atmosphere and used to synthesise three-carbon sugars through the Calvin-cycle (Bassham et al, 1950).

In plants, the overall efficiency of this fundamental process, in which water, carbon dioxide and light are converted in  $\text{O}_2$  and biomass that fuels all forms of life, is estimated to be in the order of 4% (Zhu et al, 2008).

---



### 1.1.1 Light-harvesting systems in plant photosynthesis

The primary events in plant photosynthesis are the absorption of photons from sunlight (light-harvesting) and the transmission of that energy to the reaction centres of the photosystems (Figure 1-2).

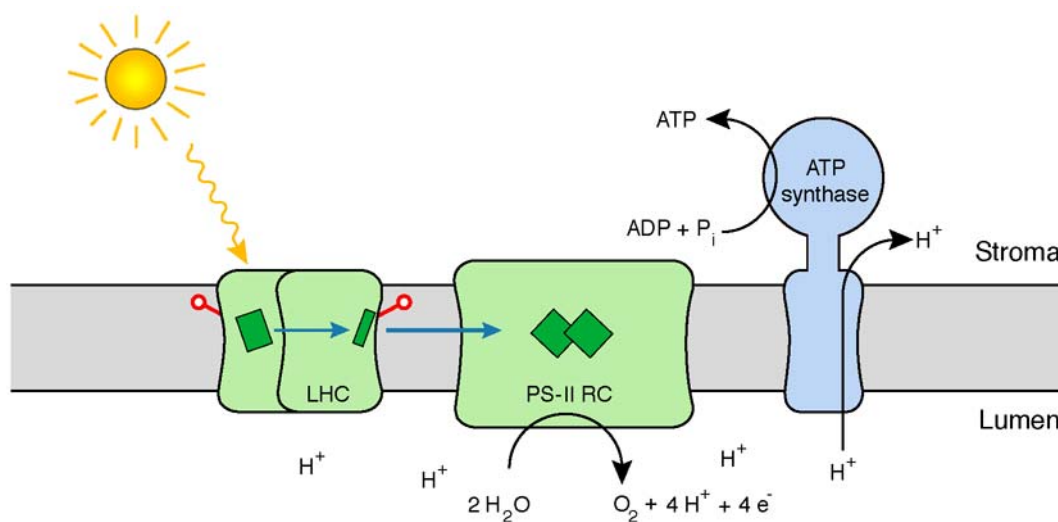


**Figure 1-2 - Light-harvesting in plant photosynthesis.**

The light-harvesting complexes (LHCs), rather than the photosystems themselves, are the major sunlight collectors that fuel plant photosynthesis.

Light is absorbed by photosynthetic pigments, which in plants belong to two major classes: chlorophylls (Chls) and carotenoids. In spite of having such pigments in the reaction centres of both photosystems, the light that is captured by them is not sufficient to drive photosynthesis; additional pigment-protein complexes are required to harvest sunlight and transmit the energy to the reaction centres in order to meet the energetic demands of the photochemical reactions. The light-harvesting complexes in plant photosynthesis (LHCs) can be divided into two major classes, depending on how they associate with the photosystems. The core LHCs (or core antenna; Figure 1-3), are integral components of the photosystems, while the peripheral LHCs (or peripheral antenna) form supercomplexes with the photosystems.

The peripheral antenna of the two plant photosystems consists of macromolecular complexes of pigments (Chls and carotenoids) and polypeptides of the Lhc super-gene family. The prototype of these antenna complexes is the major

light-harvesting complex of photosystem II (LHC-II). The structure and function of LHC-II, as well as its photoprotective role under high light conditions, are the main subject of this work.

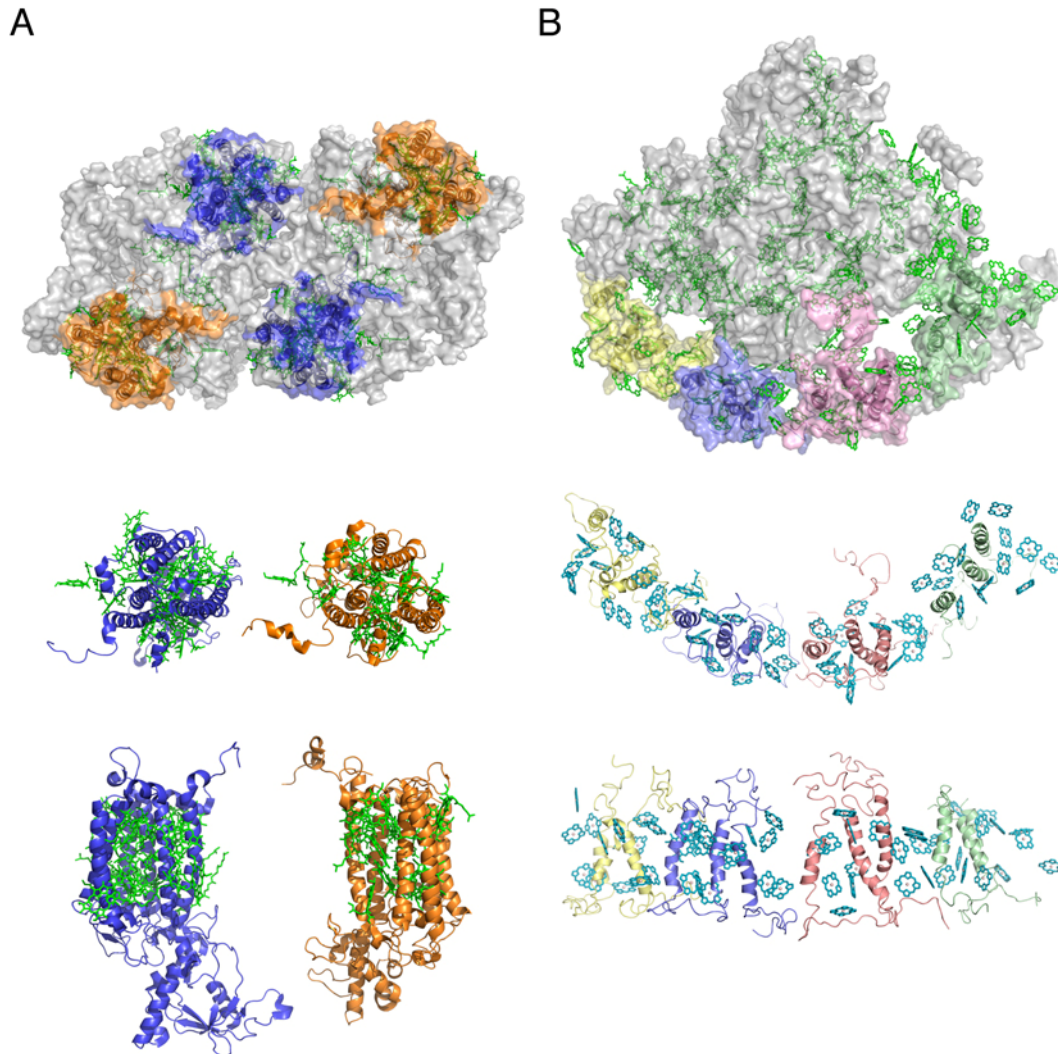


**Figure 1-3 – Core light-harvesting complexes of the photosystems.**

Both photosystems have a set of core LHCs that increase their absorption cross-section and provide the necessary excitation energy to fuel photochemistry. (A) CP43 (orange) and CP47 (blue) are two Chl *a* binding integral membrane-complexes that flank the reaction centres of a PS-II dimer (PDBid: 2axt; (Loll et al, 2005)); (B) The core LHCs of PS-I have a very distinct architecture, forming a belt that embraces the monomeric reaction centre (PDBid: 2oO1; (Amunts et al, 2007)). Green, chlorophyll.

---

---

## 1.2 Plant light-harvesting complex of photosystem II

The plant light-harvesting complex of photosystem II (LHC-II) is arguably the most abundant membrane protein on Earth. The complex was discovered by Philip Thornber in 1965, then at the Twyford Laboratories Ltd., London, a basic research unit subsidiary of the Arthur Guinness Brewery (Thornber, 1995). Thornber was washing up centrifuge tubes he had used to fractionate plant leaf extracts. He noticed that the detergent he used to dissolve the green pellet produced a clear green solution. Out of curiosity, he examined this solution by polyacrylamide gel electrophoresis, then a new technique, and found that it produced two prominent green bands, which he referred as Complex I and Complex II (Ogawa et al, 1966; Thornber et al, 1967). First it was thought that the bands represented the two photosystems I and II. Later it was discovered that Complex I was photosynthetically active, and indeed corresponded to PS-I, whereas Complex II had no photosynthetic activity. It was subsequently identified as a light-harvesting complex that served as an antenna for the photosystems, and first referred to as LHC (Thornber & Highkin, 1974).

### 1.2.1 The Lhc family

LHC-II accounts for roughly 30% of all protein in plant thylakoid membranes, and binds roughly half of the total Chl in chloroplasts (Peter & Thornber, 1991). It is the prototype of a large and abundant class of chloroplast membrane proteins. The LHC apoproteins are the product of the Lhc super-gene family, which comprises at least 30 homologous genes in *Arabidopsis* (Jansson, 1999). The family contains not only the three main polypeptide components of the major LHC-II, Lhcb1, Lhcb2 and Lhcb3, but also the so-called “minor” antenna complexes of photosystem II, referred to as CP24, CP26 and CP29 (Camm & Green, 2004), which originate from the gene products Lhcb6, Lhcb5 and Lhcb4, respectively (Jansson et al, 1992). Other members are the antenna complexes of photosystem I Lhca1, Lhca2, Lhca3 and Lhca4 and the related and more recently identified Lhca5 and Lhca6 (Jansson, 1999).



```

Pea Lhcb1 126 AIWATQVILMGAVEGYRIAG-GPLGE-----VVDPlyPgg-SFDP LGLAD-----DPEAFaelKvKELkNGR 185
Lhcb1.1 125 AIWATQVILMGAVEGYRVAGNGPLGE-----AEDLLyPggS-FDP LGLAT-----DPEAFaelKvKELkNGR 185
Lhcb1.4 124 AIWATQVILMGAVEGYRVAGDGPLGE-----AEDLLyPggS-FDP LGLAT-----DPEAFaelKvKELkNGR 184
Lhcb2 122 AIWAVQVILMGFIeGYRIgG-GPLGE-----GLDPLyPggA-FDP LNLAE-----DPEAFselKvKELkNGR 181
Lhcb3 116 AVLGFQVILMGVFRINGLDGVE-----GNDLYPggQYFP LGLAD-----DPVTFaelKvKElkNGR 176
Lhcb5 133 LAVVAEVLLGGAEYRIITNGLD-----FEDKLHPgg-PFP LGLA-----KDPEQallKvKElkNGR 190
Lhcb4.2 156 TLIWIEVLVIGYIEFORNAELDS-----EKRLyPggKFFP LGLA-----SDPVKkaQlQlAEIkHAR 213
Lhcb4.1 158 TLIWIEVLVIGYIEFORNAELDS-----EKRLyPggKFFP LGLA-----ADPEKTAQlQlAEIkHAR 215
Lhcb4.3 162 TLIWIEVLVVGyIEFORNSLDP-----EKRIyPgg-YFP LGLA-----ADPEKLDlQlQlAEIkHAR 218
Lhca1 96 TILAIeFAIAfVehQRMEKD-----PEKKyPggA-FDP LgYS-----KDPKkleELkVKEIkNGR 152
Lhca3 113 TLFVLEMALMGFAeHRRLQDWNyPgsMGKQYfLGL-----EKLAGSgnPaYPggPFFN LgFG-----KDEKslKELkLkEVKNGR 189
Lhca2 94 TLFVVEILLIGWAeGRRWADIIKPGSVNTDPVFNKLT-----GTDVgYPggLWFP LgWGSg-----SPAKlKELRtKEIkNGR 169
Lhca6 102 TLFVAQVILMGWAEGRWADLIKPGSVDIePKYP-----HKVnEPdVgYPggLWfFmWGSg-----SPEFvMVLrTKEIkNGR 177
Lhca5 101 TLIvVQVILMGFAeTKRyMDfVSPGSQAKeGSFF-----GLEAAleGlePYpGGlln LGLA-----KDVQnAHdWkLkElkNGR 178
Lhcb6 97 SLLGTQLLLMGWESKRWDFFNPDSQSVeWATPWSKTAENFANTGDQYpGGRFFP LGLAGKnRDGYePDEKLERLkLAEIkHAR 186
Lhca4 89 TLFVIEFLFHVYIEIRRWODIKNPGSVNQDPiFKQ-----YSLPKeGVgYPGGI-FN LNFa-----PTOEAkEKELANGR 158
PsbS 67 -IYEAEPLLLFFILFTLlGAlGALGD-----RGKFVDDPPTGLEKAVIppKNvRSALGLKE-----QGPLFGFTTKANELFVGR 139
. : ..... : * : ..... : PG* : ..... : E.....R

Pea Lhcb1 186 LAMFSMFGFFVQA-IVTGKGFLENLADHLSDPvNnNAwSYATnFvPGK----- 232
Lhcb1.1 186 LAMFSMFGFFVQA-IVTGKGFLENLADHLSDPvNnNAwAFATnFvPGK----- 232
Lhcb1.4 185 LAMFSMFGFFVQA-IVTGKGFLENLADHLSDPvNnNAwAFATnFvPGK----- 231
Lhcb2 182 LAMFSMFGFFVQA-IVTGKGFLENLADHLSDPvNnNAwSYATnFvPGK----- 228
Lhcb3 177 LAMFSMFGFFVQA-IVTGKGFLENLADHLSDPvNnNAwAFATnFvPGK----- 223
Lhcb5 191 LAMFAMLGFFIQA-YVTGEGFVENLAKHLSDPFGNLLTVIAGTAERAPTL----- 240
Lhcb4.2 214 LAMVGFGLFAVQA-AATGKGFLENLADHLSDPvNnNAwSYATnFvPGK----- 256
Lhcb4.1 216 LAMVAFGLFAVQA-AATGKGFLENLADHLSDPvNnNAwSYATnFvPGK----- 258
Lhcb4.3 219 LAMVAFGLFAVQA-AATGKGFLENLADHLSDPvNnNAwSYATnFvPGK----- 247
Lhca1 153 LALLAFVGFVQQAAYPTGTFLENLADHLSDPvNnNAwSYATnFvPGK----- 197
Lhca3 190 LAMLAIFLGYFIQG-LVTGVPYQNLADHLSDPvNnNAwSYATnFvPGK----- 232
Lhca2 170 LAMLAVMGAWFQH-IYTGTFIDNLFALHADPGHATIFAATPK----- 212
Lhca6 178 LAMLAFLGFCFQA-TYTSQDP IENLMAHADPGHCNVFSATSH----- 220
Lhca5 179 LAMMAMLGFFVQA-SVHTTGF IDNLVEHLSNPWHKTIQTFTSTS----- 223
Lhcb6 187 LAMVAMLIFFYFEA-GQGTFPLGALGL----- 211
Lhca4 159 LAMLAFLGFWVQH-NVTGKGFLENLADHLSDPvNnNAwSYATnFvPGK----- 199
PsbS 140 LAQLG-TAFSLIGELITGKALAQNLNIETGIPIQDIEPLVLLNVAFVFFFAINPGNKFIITDDGEES 205
LA.....

```

Pigment-binding residues in the sequence are colour coded: light blue, Chl *a* ligands via side chain; dark blue, Chl *a* ligands via backbone and water; light green, Chl *b* Mg and formyl ligands via side chain; dark green, Chl *b* Mg and formyl ligands via backbone and water; pink, carotenoids. (\*) indicates strict conservation except for PsbS. Note that Chls 7 and 10 do not have polypeptide ligands but are held in place by coordination of the central Mg to PG and Chl 13 (via water), respectively. The program MUSCLE (Edgar, 2004) was used for the alignment.

More distantly related family members are the photoprotective early light-induced stress-response proteins (ELIPS)(Meyer & Kloppstech, 1984; Adamska, 1997), and the photosystem II component PsbS (Kim et al, 1992; Wedel et al, 1992), which in its mature form shares a sequence identity of only 15% with Lhcb1. LHC-II is nuclear-encoded (Kung et al, 1972), as are all Lhc family members.

The LHC-II cDNA was first isolated (Broglie et al, 1981) and sequenced (Coruzzi et al, 1983) in the early 1980s by Cashmore and co-workers. Members of the LHC-II protein family are distinguished by an extreme degree of sequence conservation, with 58% sequence identity and 77% sequence similarity between Lhcb1, Lhcb2 and Lhcb3, suggesting that the three-dimensional (3D) structures of the three subtypes are virtually the same. The similarity of the mature minor LHCs to Lhcb1 is less pronounced, with sequence identities of 29% for CP24, 45% for CP26 and 32% for CP29, suggesting differences in their 3D structures that may be functionally significant.

LHC-II and its relatives are found only in plants, and are thus a later addition to the arsenal of photosynthetic pigment-protein complexes than the core antenna chlorophyll proteins CP43 and CP47 of photosystem II (Figure 1-3). In contrast to the LHC family, the CP43/47 class of antenna proteins, which also contains the iron stress protein IsiA from marine phytoplankton (Straus, 1994), are encoded by genes in the plant chloroplast genome (Bricker, 1990). CP43/47 show no obvious sequence or structural similarity to the LHC family (Ferreira et al, 2004; Loll et al, 2005; Murray et al, 2006). In terms of structure and sequence, both classes are different from one another and from the bacteriochlorophyll (bChl) *a*-containing light-harvesting complexes of the photosynthetic purple bacteria, often referred to as LH1, LH2 and LH3 (Brunisholz & Zuber, 1992; McDermott et al, 1995; Cogdell et al, 2006)(Figure 1-5). Photosynthetic light-harvesting complexes that also include non-membrane proteins such as the bChl *a*-containing antenna complex from the green photosynthetic bacteria such as *Chlorobium* (Fenna & Matthews, 1975), or the phycocyanins and phycoerythrins of phycobilisomes (for a review see (Samsonoff & MacColl, 2001)), are thus much more varied than the photosynthetically active reaction centre complexes, which are always integral membrane proteins. Reaction centres obey the same basic building plan in all

---

photosynthetic organisms, and were thus invented only once. This reflects the fact that light-induced charge separation, the hallmark of photosynthetic reaction centres, requires a special geometry of a pair of Chl or bChl molecules which ultimately withdraws an electron from a substrate. By contrast, efficient excitation energy transfer in the photosynthetic antenna is clearly possible with many different arrangements of the light-harvesting pigments.

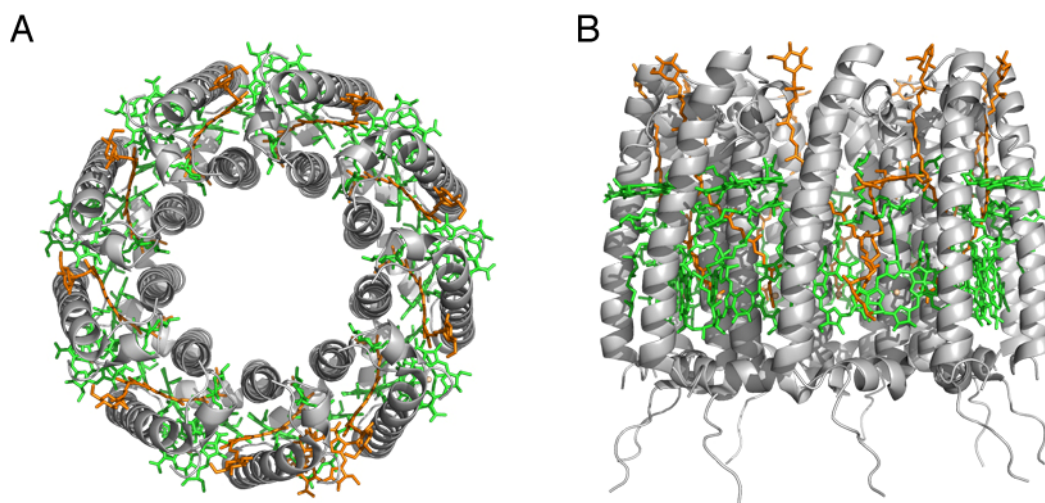


**Figure 1-5 - Bacterial light-harvesting complex II.**

The figure shows the circular arrangement of the bacterial light-harvesting complex 2 (PDB code: 2FKW)(Cherezov et al, 2006) from (A) the top and (B) within the membrane. Each of the nine subunits that form the ring are composed of a single copy of the  $\alpha$  and the  $\beta$ -apoprotein, one rhodopin glucoside carotenoid and three bacteriochlorophyll *a* molecules. Green, bacteriochlorophyll *a*; orange, rhodopin glucoside; grey, polypeptide.

### 1.2.2 Biochemistry

The characteristic dark green colour of the LHC-type antenna complexes is due to their high Chl content, comprising both Chl *a* and Chl *b* (see Appendix for molecular structures) in proportions that are, within certain limits, predefined and minimally variable for each complex under native conditions. In addition, the LHCs bind yellow or orange carotenoids, in particular lutein (Lut), neoxanthin (Neo), violaxanthin (Vio), zeaxanthin (Zea) and  $\beta$ -carotene. The three subtypes of the major LHC-II have the same pigment content and spectroscopic properties (Palacios et al, 2006). Because they contain comparatively large amounts of Chl *b* (in fact the entirety of Chl *b* in plants), the members of the LHC family have often been referred to as Chl *a/b* proteins. By comparison, CP43 and 47

contain only Chl *a*, whereas some of the prochlorophyte members of the IsiA class also contain Chl *b* (La Roche et al, 1996).

The LHC-II apoprotein is synthesized in the cytoplasm and passes through the chloroplast outer and inner envelope, before being inserted into the thylakoid membrane, a process mediated by the chloroplast signal recognition particle (Cline, 1986). Both cpSRP54 and cpSRP43 are required for membrane targeting (Schuenemann et al, 1998). Apparently, the cpSRP recognises and forms a complex with the DPLG sequence motif at the stromal end of trans-membrane helix 3 that later provides a binding site for Lut1 (Stengel et al, 2008).

LHC-II and related Chl *a/b* binding proteins are able to self-assemble *in vitro*, yielding complexes biochemically and spectroscopically very similar to the native complexes isolated from thylakoid membranes. The first LHC-II reconstitution experiments used polypeptides and pigments that were both extracted from thylakoids (Plumley & Schmidt, 1987). A few years later a method was developed to refold LHC-II from isolated pigments and recombinant polypeptide expressed in *E. coli* (Paulsen et al, 1990). The recombinant minor LHCs CP29 (Giuffra et al, 1996), CP26 (Ros et al, 1998) and CP24 (Pagano et al, 1998) were similarly refolded from their components, as were the three different sub-types of LHC-II (Lhcb1, Lhcb2 and Lhcb3 (Standfuss & Kühlbrandt, 2004), which cannot be isolated in pure form, and the members of the Lhca sub-family (Schmid et al, 1997; Castelletti et al, 2003; Storf et al, 2005). With the publication of the first atomic model of LHC-II (Kühlbrandt et al, 1994), it became possible to devise and refold mutants that lacked individual Chl binding side chains. In this way, the specific roles of particular pigments in LHC-II could be directly investigated. Soon this strategy was used not only for LHC-II (Remelli et al, 1999; Rogl & Kühlbrandt, 1999) but also for the monomeric CP29 (Bassi et al, 1999), and later for Lhca1 (Morosinotto et al, 2002b), Lhca2 (Croce et al, 2004), Lhca3 (Mozzo et al, 2006) and Lhca4 (Corbet et al, 2007). The capacity of the complex to self-assemble *in vitro* is no less remarkable than its assembly *in vivo*. Based on the dynamics of excitation energy transfer in the process of refolding, it has been suggested that Chl binding during *in vitro* assembly of LHC-II happens in two kinetic phases (Booth & Paulsen, 1996), such that Chl *a* binds predominantly during the first phase, whereas Chl *b*

---



binds during the second, slow phase (Horn et al, 2007). However, the assembly of the mature pigment-protein complex in the membrane, and whether or not it follows the same pathway is not well understood (for a review of recent progress see (Schmid, 2008)). Free Chl that is not in van-der-Waals contact with a carotenoid would invariably form triplet states in the light, which in turn give rise to highly reactive and damaging singlet oxygen. It is therefore thought that Chl must be bound to a molecular chaperone, most likely a protein such as ELIP, in complex with a protective carotenoid before being incorporated into LHC-II.

In the membrane, the assembled LHC-II invariably assembles into trimers, whereby the three main subtypes Lhcb1, 2 and 3 evidently form trimers of all possible permutations promiscuously, although they have varying propensities to do so (Standfuss & Kühlbrandt, 2004). It has been shown (Hobe et al, 1995) that the WYGPDR motif present in LHC-II and CP26, but not in CP24, CP29 or the Lhca proteins (Green & Pichersky, 1994), is required for trimer formation. The assembly of the LHC-II trimer from monomers most likely occurs spontaneously, as the trimer also assembles readily from monomers in detergent solution (Hobe et al, 1994). Apparently the monomer-trimer equilibrium is shifted far towards the trimer. Consequently the concentration of free LHC-II monomers in the thylakoid membrane is negligible, whereas the situation is less clear-cut for the minor LHCs, For example, when Lhcb1 and Lhcb2 are absent, trimers of CP26 appear to substitute for the major LHC-II, and the macro-organisation of the PS-II supercomplex is preserved (Ruban et al, 2003).

### 1.2.3 Function

As its name suggests, the primary function of LHC-II is to make the photosynthetic process in green plants more effective by intercepting solar photons and delivering their excitation energy to the reaction centres. Without such an antenna, the plant photosystems would be hopelessly inefficient. Whereas PS-II contains only 6 reaction centre chlorophylls (and two pheophytins), it is estimated that there are between 130 and 250 antenna chlorophylls per PS-II core dimer (Jansson et al, 1997), or up to 8 LHC-II trimers (Peter & Thornber, 1991). LHC-II trimers and PS-II reaction centres form supercomplexes of various stoichiometries in the membrane, which can be isolated by mild detergent treatment and visualised

in the electron microscope (Boekema et al, 1995; Boekema et al, 1999), in which LHC-II trimers and the PS-II dimer are visible. The assignment of other regions to individual minor LHCs is however largely speculative.

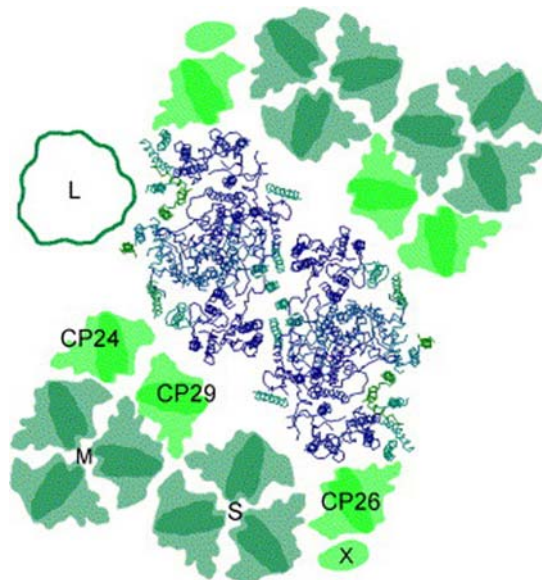


**Figure 1-6 - Model of the LHC-II - PS-II supercomplex.**

Electron microscopy of negatively stained particles was used to generate this structural model of the PS-II supercomplex (Dekker & Boekema, 2005). LHC-II trimers are thought to adopt three different positions within the supercomplex, known as “S” (strongly bound), “M” (moderately bound) and “L” (loosely bound). The three minor LHCs (CP24, CP26 and CP29) form a barrier between the trimeric LHC-IIs and the PS-II core.

The dynamics of light-harvesting and excitation energy transfer within LHC-II have been thoroughly investigated over the years, using a wide variety of spectroscopic techniques (see (van Amerongen & van Grondelle, 2001) for review). Besides their structural and photoprotective roles, the LHC-II carotenoids complement the light-harvesting function of the Chls, thereby increasing the regions of the visible spectrum that can be harvested. The overall Car to Chl excitation energy transfer efficiency is estimated to be  $\sim 70\text{--}90\%$ , with time constants between 50 and 200 ps (see (Polivka & Sundstrom, 2004) for review). The high-resolution structures, which unambiguously identified the position and identity of all pigments in the complex, have greatly assisted the interpretation of the accumulated spectroscopic data. A model for the excitation energy dynamics has recently been presented (Novoderezhkin et al, 2005). A hallmark of these processes is the efficient and fast energy transfer from Chl *b* to Chl *a*, which typically occurs

---

---

on the sub-ps time scale. Spatial equilibration of the excitation energy is estimated to be reached within ~48 ps (Barzda et al, 2001b), after which it resides predominantly in the Chl *a* cluster comprising Chl 1, Chl 2 and Chl 7 (van Grondelle & Novoderezhkin, 2006). This cluster is situated at the periphery of the trimer, which is the obvious site for efficient energy transfer to photosystems, either directly or via the minor LHCs.

More than 30 years ago it was discovered that LHC-II is phosphorylated (Bennett, 1977) by a specific kinase (Bennett, 1979) at a threonine residue near the N-terminus (Mullet, 1983) which is conserved in Lhcb1 and Lhcb2, but not in Lhcb3. This provides the plant with the potential adaptation to light conditions changing on the timescale of minutes. The main effect of LHC-II phosphorylation appears to be a partial dissociation of the complex from PS-II, and a closer association with PS-I (Bennett et al, 1980). This correlates with state transitions, whereby the antenna funnels more energy into PS-I than into PS-II in state 2, and vice versa in state 1 (reviewed by (Allen, 1992; Allen & Forsberg, 2001; Wollman, 2001)). State transitions enable the plant to balance photosynthetic activity between cyclic electron flow around PS-I and vectorial electron flow through PS-II. Consistent with this, the redox state of the plastoquinone pool controls LHC-II kinase activity, and therefore the state transitions (Allen et al, 1981). As Lhcb3 lacks the phosphorylation site, this component, or indeed LHC-II trimers containing it, do not move from PS-II to PS-I, and hence do not participate in state transitions (Jansson, 1994). The LHC-II kinase is required for state transitions and light adaptation (Bellafiore et al, 2005), proving that LHC-II phosphorylation is the key factor in this process. Accordingly, plants without Lhcb1 and Lhcb2 that lack the phosphorylation site do not undergo state transitions (Andersson et al, 2003).

Mild proteolytic treatment of isolated photosynthetic membranes removes the N-terminal segment of LHC-II carrying the phosphorylation site and 3 or 4 Arg and Lys residues, which make it highly positively charged at physiological pH. LHC-II is mainly responsible for membrane appression and grana formation in chloroplast thylakoids. The charged N-terminal segment mediates membrane appression by electrostatic interaction (Ryrie & Fuad, 1982). The electrostatic repulsion between the charged membrane surfaces is reduced by mono- or divalent

cations, whereby  $Mg^{2+}$  is roughly 10 times more effective than  $Na^+$  or  $K^+$  in charge screening and thus in inducing membrane stacking (Barber, 1980). *Arabidopsis* mutants lacking both Lhcb1 and Lhcb2 still have chloroplast grana (Andersson et al, 2003), implying that Lhcb3 and other proteins, most likely PS-II, also contribute to grana formation.

### 1.2.4 Crystallisation

The extraordinary propensity of LHC-II for forming crystalline arrays has been noticed from the early days of investigating cation-induced precipitates of the complex in the electron microscope. Freeze-fracture replicas of such *in vitro* aggregates showed that they were stacks of crystalline sheets (McDonnell & Staehelin, 1980; Mullet & Arntzen, 1980), which in some ways resemble stacked thylakoid membranes of chloroplast grana. It was later shown that these sheets were two-dimensional crystals of LHC-II trimers alternating in an up/down orientation relative to the membrane plane (Kühlbrandt et al, 1983). Such arrangement does not exist in native thylakoids, where all complexes naturally face the same way, although the complex does crystallise *in situ* (Lyon & Miller, 1985) when sufficient detergent is added to membrane preparations to enable a proportion of the complexes to invert their native orientation. A first three-dimensional map of such crystalline membranes showed that LHC-II in the 2D crystals is a trimer, and indicated its dimensions and symmetry (Kühlbrandt, 1984). Later it was shown by analytical ultracentrifugation that the complex is also a trimer in detergent solution (Butler & Kühlbrandt, 1988).

2D crystallisation conditions were optimised by introducing n-nonylglucoside (NG) as a second detergent, and by adopting a carefully controlled temperature regime. In this way it was possible to avoid stacking and to grow single 2D crystals that measured up to 10  $\mu m$  across, diffracting electrons to 3.2 Å or better when cooled with liquid nitrogen (Wang & Kühlbrandt, 1992). At this time, Henderson and colleagues were developing their new method for determining the structures of bacteriorhodopsin by electron diffraction and cryo-EM of 2D crystals at near-atomic resolution (Henderson et al, 1986; Grigorieff et al, 1996). The stage was therefore set for using the 2D crystals of LHC-II to work

---

out the structure of this complex by electron diffraction (Wang & Kühlbrandt, 1992), high-resolution cryo-EM and image-processing (Kühlbrandt et al, 1994).

Early attempts to grow 3D crystals of pea LHC-II yielded two different crystal forms (Kühlbrandt, 1987). One form grew in the shape of octahedra with cubic symmetry and a large unit cell. The octahedral crystals are most likely of the same type used by Liu et al to determine the 2.7 Å structure spinach LHC-II (Liu et al, 2004), which consist of icosahedral vesicles of 20 LHC-II trimers packed on a cubic lattice. Indeed, such small vesicles can be seen by negative-stain electron microscopy in preparations of crystalline aggregates. Most likely, the “heptameric assemblies” of LHC-II reported by Dekker et al (Dekker et al, 1999) are nothing other than these icosahedral vesicles as their appearance and dimensions are identical (Figure 1-7).

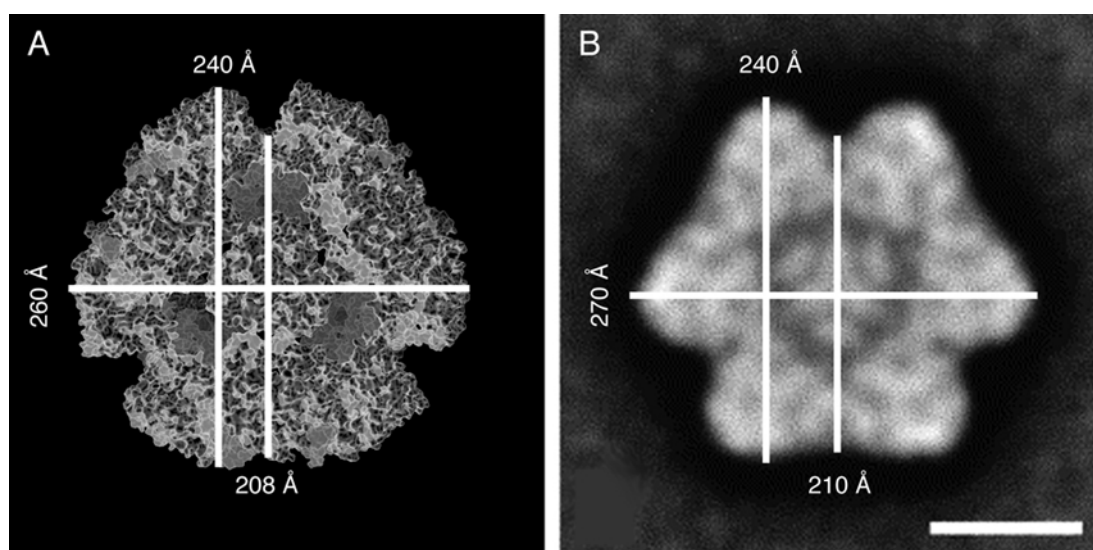


**Figure 1-7 - *In vitro* LHC-II assemblies.**

(A) Representation of the 20 trimers in one complete icosahedral vesicle, as in the cubic spinach LHC-II crystals (Liu et al, 2004). (B) The dimensions of the LHC-II assemblies described by Dekker et al (Dekker et al, 1999) are almost identical. Scale bar: 100 Å.

The other crystal form of LHC-II obtained in the mid-1980s grew in the shape of hexagonal plates. Electron diffraction of thin specimens indicated the same unit cell and apparent symmetry as the 2D crystals (Kühlbrandt, 1987). This form evidently was of Michel’s type-I (Michel, 1983), consisting of stacked 2D crystals..

These crystals were too small for the X-ray sources available at the time, and structure determination by electron crystallography of the well-ordered 2D crystals seemed the more promising alternative. More than 15 years later, the hexagonal plates yielded the 2.5 Å X-ray structure of pea LHC-II (Standfuss et al, 2005)(Figure 1-8).

It is interesting to note that the two crystal types of LHC-II are due to two different, fortuitous properties of the LHC-II trimer: one to its unique propensity to form planar 2D lattices in the membrane by surface complementarity, and the other to its unrelated ability to form small icosahedral lipid-protein vesicles that resemble virus capsids and pack like spheres into a cubic lattice.

### 1.2.5 Structure

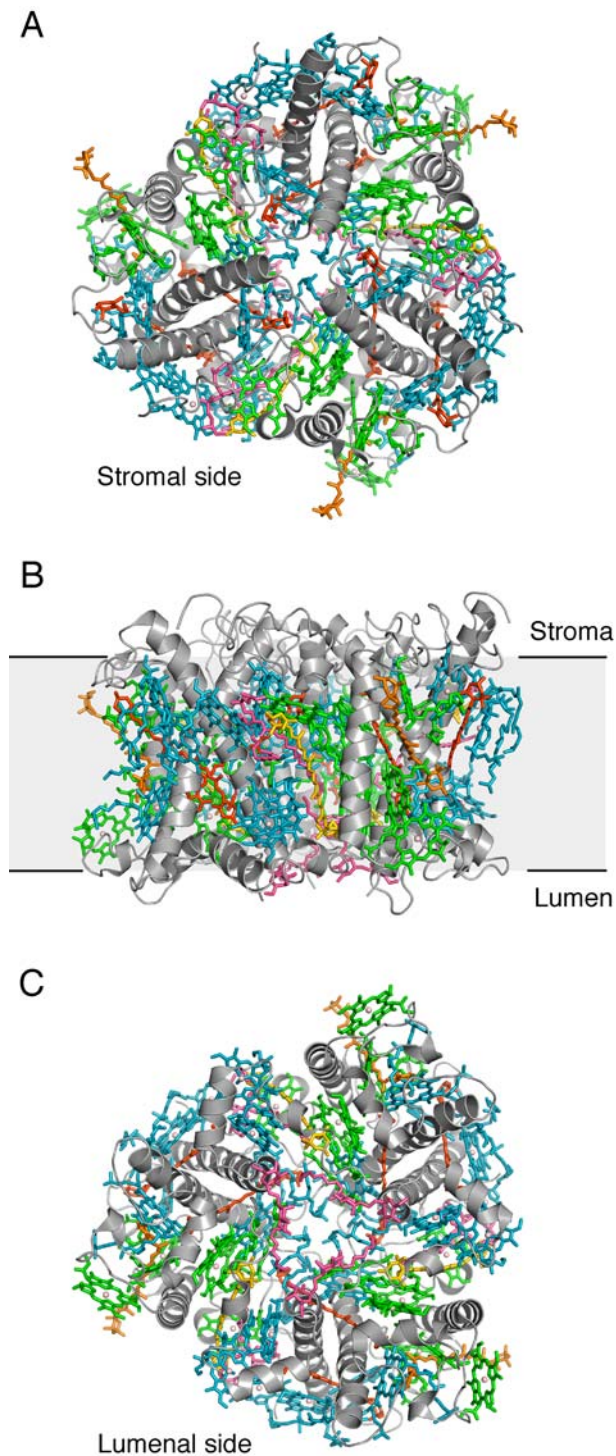


**Figure 1-8 - LHC-II structure.**

The trimeric complex is shown (A) from the stromal side, (B) from within the membrane and (C) from the luminal side. Grey, polypeptide; cyan, Chl *a*; green, Chl *b*; dark orange, lutein; light orange, neoxanthin; yellow, violaxanthin; pink, lipids.

### 1.2.5.1 The LHC-II polypeptide

The chain trace of the LHC-II polypeptide was essentially complete in the 3.4 Å EM structure, apart from an unresolved stretch between helices B and C, which comprises a short amphipathic helix on the luminal surface, and the first 25 residues at the N-terminus. As had already been obvious from the earlier 6Å map (Kühlbrandt & Wang, 1991) there were three membrane-spanning helices, two of them (helices 1 and 4 in the X-ray structure; B and A in the EM maps, respectively) unusually long and tilted, and related by local near-twofold symmetry. This symmetrical arrangement reflects an internal repeat in the polypeptide (Hoffman et al, 1987) that indicates a gene duplication event in the early evolution of the complex. Many of the more recently reported membrane proteins show evidence for internal repeats, although in most cases the repeats are inverted, as e.g. in the aquaporins (Murata et al, 2000) and Na-coupled solute transporters (Yamashita et al, 2005; Faham et al, 2008), whereas this is not the case in LHC-II. The two long helices are linked by a third, shorter and slightly curved helix (helix 3 in the X-ray structure; C in the EM maps). The two short amphipathic helices on the luminal side (helices 2 and 5), related by the same local near-twofold symmetry, link helix 1 to helix 3, and helix 4 to the C-terminus.

The two central helices 1 and 4 are interlocked by a symmetrical pair of salt bridges, making this part of the complex particularly rigid. The Arg and Glu residues forming these salt bridges are a signature motif of the family (Figure 1-4). The assembly of the two long tilted helices plus the two Luts that sit in the grooves at either side of the helix pair, and the 6 Chls *a* closest to them form the central structural motif of LHC-II and is highly conserved. The interlocking salt bridges are found even in the single-helix ELIPs, which are thus likely to form dimers in the membrane and may be the early ancestors of LHC-II (Green & Kühlbrandt, 1995). The salt-bridge forming residues are also present in PsbS, which is therefore likely to have the same central coiled-coil helix motif found in LHC-II (Figure 1-4). Since the glutamate oxygens of both salt bridges each serve as a Chl *a* ligand in LHC-II, PsbS has at least the potential to bind two Chls in these positions. A third salt bridge in helix 3, which provides the Mg ligand for Chl 12, is fully conserved except in PsbS.

---



The segment also includes the WYGPDR “trimerisation motif” common to those LHCs that are known to form trimers *in vivo*; i.e. the major LHC-II itself and CP26 (Lhcb5; Figure 1-4). It has been shown that a tryptophan 11 residues from the C-terminus (Trp 222 in pea Lhcb1) is also critical for trimer formation (Kuttkat et al, 1996), and that a hydrophobic residue is required in this position for stable trimers. Inspection of the LHC-II structure reveals that Trp222 is sandwiched between Vio and Chl 10 of the neighbouring trimer, obviously a sensitive site for trimer stability. This finding demonstrates nicely that the presence or absence of a single hydrophobic contact, equivalent to 3 kcal/mol (Tanford, 1962), can decide whether or not an oligomeric complex forms in the membrane.

It was suggested early on that membrane appression *in vitro* and thylakoid stacking seen in normal chloroplasts are brought about by the same mechanism and involve LHC-II polypeptides directly (Day et al, 1984). More than 20 years later, the LHC-II structure showed that the positively charged N-terminal segment and the otherwise negatively charged stromal surface of the complex complement one another, and may give rise to a velcro-like interaction between parallel grana membrane surfaces (Standfuss et al, 2005). This would explain why phosphorylation, which effectively neutralizes one positive charge at the N-terminus, reduces this interaction, making it easier for LHC-II to move out of the granal membranes towards PS-I.

#### 1.2.5.2 Chl binding sites

The central Mg in the Chl chlorin ring requires an extra ligand with a free electron pair, such as an N or carbonyl O for stable binding. In a protein, these ligands are usually amino acid side chains, or water molecules H-bonded to a main-chain carbonyl. Many of the residues involved in Chl binding are conserved throughout the family. These include the side chains that coordinate Chls 1-5, 8 (except in Lhcb4.3 and Lhcb6), 12 and 13, suggesting that these residues bind Chls also in the corresponding family members. Chls 6, 9, 11 and 14 are coordinated by main chain carbonyls *via* a water molecule. The central Mg of Chls 7 and 10 do not have a protein ligand but are coordinated by the PG head group (Chl 7) or a Chl 13 oxygen. For Chls without side chain ligands it is difficult to tell whether their

binding sites are conserved or not, although this is likely for Chl 6 which is part of the central set of 6 Chls *a*.

The specificity of a binding site for Chl *a* or *b* is determined by the presence of a hydrogen bonding partner for the Chl *b* formyl group. Although Chl *a* sites can be forced to accept Chl *b* and *vice versa* under artificial *in vitro* reconstitution conditions (Giuffra et al, 1996; Pagano et al, 1998; Croce et al, 2002), there is no evidence for mixed occupancy of any Chl site in either X-ray structure. Each binding site therefore seems to be specific for its proper pigment under *in vivo* equilibrium conditions.

In the sequence alignment of Figure 1-4, hydrogen bonding donors are fully or partly conserved for the Chl *b* formyls of Chls 10, 11, 12 and 14, so that these are probably also Chl *b* in the corresponding complexes. Chl 7 is likely to be confined to the trimer-forming species, which contain the PG coordinating this pigment. Chl *b* molecules 11 and 14 are most likely present only in the major LHC-II, i.e. Lhcb1-3. A minimum set of Chls common to most LHCs thus includes Chl *a* molecules 1-6 and 8, plus Chl *b* molecules 12 and 13. This is broadly consistent with the experimentally determined Chl content and *a/b* ratios of the minor LHCs.

**Table 1-1 - Pigment composition of native LHC monomers of photosystem II**

LHC	Chl <i>a</i>	Chl <i>b</i>	Chl <i>a/b</i>	Lut	Neo	Vio	Chl / Car	Ref.
<i>CP29</i>	6	2	3	1	0.35	0.65	4	(Crimi et al, 2001)
	6.8	2.0	3.4	0.9	0.6	1.2	3.3	(Ruban et al, 1999)
<i>CP26</i>	6.2	2.8	2.2	1.02	0.61	0.38	4.5	(Croce et al, 2002)
	7.5	3.0	2.5	1.2	1.0	0.9	3.4	(Ruban et al, 1999)
<i>CP24*</i> ( <i>n</i> )	2.7	2.3	1.17	0.54	-	0.47	5	(Pagano et al, 1998)
<i>CP24*</i> ( <i>r</i> )	5	5	1	1.5	-	0.5	5	(Pagano et al, 1998)

\* - Values for (*n*) native and (*r*) recombinant CP24 are given.

### 1.2.5.3 Carotenoid binding sites

Unlike the Chls, carotenoids do not require electron-rich side-chain ligands that are easy to spot in a sequence alignment. The LHC-II carotenoids do however have an hydroxyl group at each end, and thus the potential to form specific hydrogen bonds to the polypeptide. Close inspection of the LHC-II sequence alignment reveals that the binding sites of the Lut head groups in LHC-II are even more highly conserved than most of the Chl binding sites. The characteristic Lut binding motif is the DPLG sequence in the hook-like extension (Kühlbrandt & Wang, 1991) at the stromal end of trans-membrane helix 4, which is part of the internal repeat and also occurs in the equivalent extension at the stromal end of helix 1. Whereas in this position the motif has mutated to DTAG in LHC-II, it is repeated without modification in Lhca1, Lhca2 and Lhcb6, which suggests that these proteins are evolutionarily the oldest members of the LHC family. The hook-like shape of this motif provides the stereoselective binding pocket for the Lut head groups, which make two hydrogen bonds each, one to the Asp and the other to the main chain nitrogen before the Gly in this sequence. At the opposite end of Lut 1 and 2, two highly conserved residues accommodate the other head group and provide a hydrogen bonding partner. Neither of the two Lut-binding DPLG motifs are conserved in PsbS, which is thus unlikely to bind Lut but may bind other carotenoids transiently.

Neo is similarly held in place by a single hydrogen bond to Tyr 112, which is conserved in the Lhcbs, and an otherwise hydrophobic binding pocket that is highly specific for this carotenoid (Paulsen et al, 1993). The Lut and Neo binding sites are thus specific for their respective carotenoid, although they can be forced to accept other carotenoids by *in vitro* refolding. Even though all LHC-II carotenoids are of the same length, their stereochemistry is different and therefore they can only be accommodated in the wrong binding site at the expense of the integrity and stability of the whole complex. Vio is the only LHC-II carotenoid that is not held in place by direct polar contacts with the polypeptide scaffold, but rather by hydrogen bonds of its hydroxyl groups to a glycerol hydroxyl group of PG, and to the phytyl carbonyl of Chl 10. Probably on account of this, and its position at the monomer interface, Vio has a low binding affinity and is easily lost during LHC-II purification (Ruban

et al, 1999), probably as a result of partial dissociation and reassociation of the LHC-II trimer in the presence of detergent. The location of Vio at the monomer-monomer interface would make it easy to exchange this carotenoid for Zea in the xanthophyll cycle (Yamamoto et al, 1962; Yamamoto, 1985).

#### 1.2.5.4 Pigment structure

Perhaps the most remarkable property of LHC-II is its ability to bind a total of 54 pigments of 5 different kinds in one trimer, and orient them precisely relative to one another. On average, LHC-II uses only 13 amino acids per pigment to achieve this, which makes it almost twice as effective in terms of polypeptide economy compared to bacterial antenna complexes. Within the trimer, the Chls are located in two layers near the stromal and luminal membrane surface, respectively. Five Chl *a* and three Chl *b* are found in the stromal layer; the other three Chl *a* and three Chl *b* are located in the luminal layer. The centre-to-centre distances between neighbouring Chls fall within a narrow range of 10Å to 13Å. As expected of an efficient solar energy collector, the orientation of the 42 Chl  $Q_y$  dipole moments in the trimer sample all directions in space about evenly, maximising light-harvesting efficiency.

The X-ray structures ended the long-standing uncertainty on the exact number and type of Chls and carotenoids bound per LHC-II monomer. A total of 18 pigments are bound, comprising 8 Chl *a*, 6 Chl *b*, 2 Lut, 1 Neo and 1 Vio (Liu et al, 2004; Standfuss et al, 2005). In the LHC-II trimer, the 6 Chl *b* molecules (Chls 9 to 14) form a cluster around the Neo binding pocket near the monomer interface, suggesting that they may be a later addition compared to the central set of 6 Chls *a* surrounding the Luts. The contact surfaces of Chl 11 and Chl 13 with Neo are especially extensive. Accordingly, a recombinant, refolded LHC-II mutant lacking Chl 13 binds either almost no Neo (this work), or only half of the amount compared to WT (Remelli et al, 1999; Rogl & Kühlbrandt, 1999), depending on the exact refolding conditions. Even so, the complex is still stable and functional, although its ability to form trimers is diminished.

The same local twofold symmetry that relates the two long alpha helices linked by the pair of ion bridges within the LHC-II monomer also applies to the

---

two Luts and the 6 Chls *a* closest to them, and indeed to all Chls in the stromal layer. When superposing the two Luts, Chl 1, Chl 2 and Chl 3 overlap almost perfectly with their symmetry mates Chl 4, Chl 5 and Chl 6 (Figure 1-9). This pigment/protein arrangement seems to be an ancient feature that is highly conserved, most likely because it is optimal for light-harvesting, energy transmission and photoprotection. The high conservation of key residues in the LHC fold and on the binding pockets of many pigments throughout the LHC family further suggests that the same basic arrangement is also shared by the minor LHCs.

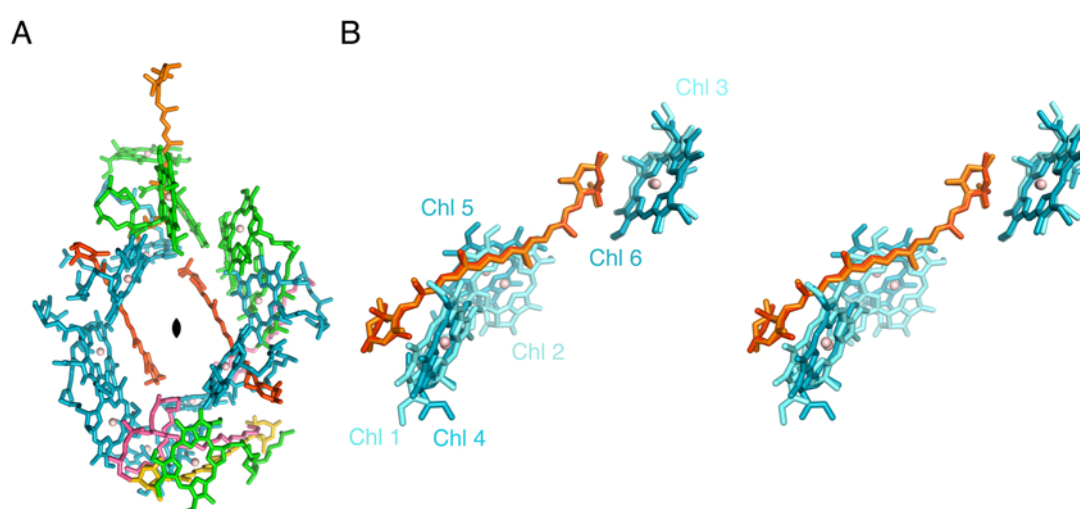


**Figure 1-9 - Pigment configuration in the LHC-II monomer.**

(A) All pigments bound to one LHC-II monomer are shown, in the same colour code as in Figure 1-8. (B) Stereo diagram highlighting the local two-fold symmetry of key pigments.

In the superposition of Figure 1-9, the conformation of the  $\pi$ -system in the two Luts is essentially the same, in contrast to a previous suggestion (Yan et al, 2007). Yan et al arrived to the conclusion that the two Luts in LHC-II have different conformations after superposing the Lut 1–Chl 2 and Lut 2–Chl 5 pairs. However, in such superposition the two Lut molecules do not overlap, as the distance between Lut 1 and Chl 2 is shorter than the corresponding distance in the Lut 2–Chl 5 pair. When only the coordinates of the Lut molecules are used for the superposition, as in Figure 1-9, it is clear that the conformation of the two pigments is identical. Whereas the pair of Lut molecules occupies a central location in the interior of the LHC-II monomer, Vio and Neo assume more peripheral positions.

Neo is distinct from the other carotenoids in the complex in that roughly half of its length protrudes into the lipid phase of the membrane. The significance of this striking feature is still unknown. Its exposed position would make this pigment predestined for functionally important interactions with other membrane proteins in the photosynthetic apparatus of green plants.

#### 1.2.5.5 Bound lipids

In addition to the polypeptide and pigments, two different lipids complete the LHC-II structure. Of these, PG is known to be required for trimer formation (Trémolières et al, 1981). Hydrolysis of PG by phospholipase A2 causes the trimer to break up into monomers, highlighting the structural role of this lipid as a hydrophobic glue between subunits (Nussberger et al, 1993). Dissociation of the trimer into monomers also occurs when the first 49 residues are proteolytically cleaved off the LHC-II polypeptide (Nussberger et al, 1993). This segment includes Tyr44, which makes a polar contact with the PG head group. The segment also includes the WYGPDR “trimerisation motif” common to those LHC-IIs that are known to form trimers *in vivo*; i.e. the major LHC-II itself and CP26. This motif is structurally close to the PG lipid, although no direct contacts are evident. Probably its absence disrupts the PG binding site, so that trimer formation is prevented. PG also coordinates the central Mg of Chl 7, indicating that PG has more than one role in the assembly of the complex

Like PG, DGDG is required for the formation of both 2D and 3D crystals of LHC-II (Nussberger et al, 1993). While PG is present in one copy per monomer, several molecules of DGDG per monomer co-purify with the trimeric complex. Biochemical experiments had indicated that PG must bind at the monomer interface and has a direct structural role in the trimer, whereas DGDG binds more peripherally (Nussberger et al, 1993). This is indeed borne out by the two high-resolution structures, which show DGDG either in a central hydrophobic cavity on the luminal surface in the higher-resolution structure of the pea complex (Standfuss et al, 2005), or at the periphery, bridging the gap between two adjacent trimers on the stromal side of the spinach complex (Liu et al, 2004). In fact, the DGDG position is the most apparent difference between the two LHC-II structures (Figure 1-10). The lipid in the hydrophobic cavity on the threefold axis is no doubt present

---

in both, but was not resolved by Liu et al. In the structure of the pea complex, DGDG is most likely also present in the large cavities between trimers in the 2D lattice (along with detergent and other lipids) but not resolved, as it may not occupy a unique binding site. On the other hand, two ordered molecules of peripherally bound DGDG per monomer are resolved in the structure of the spinach complex, where they mediate contacts between trimers in adjacent trimers forming the icosahedral vesicles, and are thus immobilized. Note however that this particular trimer interaction is not physiological, as it would impose an extreme membrane curvature which cannot occur in the planar grana thylakoids.

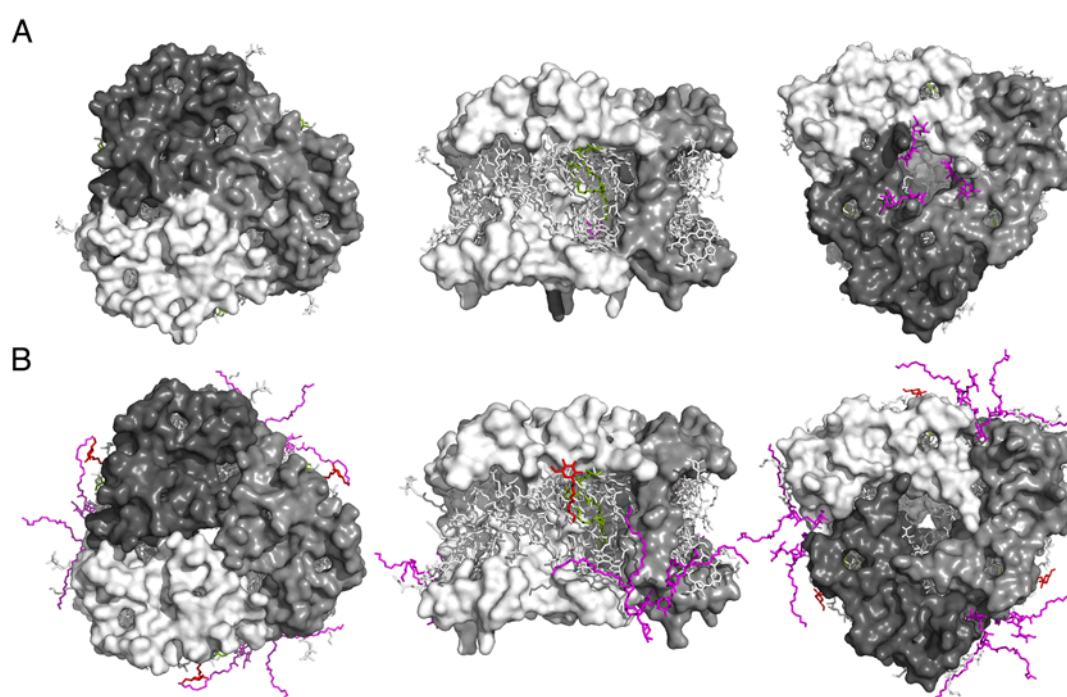


**Figure 1-10 - Lipid and detergent molecules in the LHC-II X-ray structures.**

The most evident difference between the pea (A) and the spinach (B) LHC-II structure is the location of lipid and detergent molecules. Green, PG; magenta, DGDG; red, NG detergent.

### 1.2.6 Conserved structure of plant LHCs

The recent 3.4 Å structure of pea PS-I confirmed that the four Lhca proteins attached to PS-I have the same fold as LHC-II (Amunts et al, 2007). The characteristic 2 central, intertwined transmembrane helices, and the third helix that runs roughly perpendicular to the membrane, superpose almost perfectly with those of LHC-II (Figure 1-11). The only exception is helix 4 (A) of Lhca3, which appears

much less tilted and almost parallel to helix 1 (B). In fact, in the superposition of the polypeptide backbones, this helix of Lhca3 would cut through Lut2 in the LHC-II structure. As the Luts are amongst the most highly conserved features in the LHC family, and the signature residues that form polar contacts to Lut 1 and 2 are conserved in the Lhca3 sequence, the apparent orientation of helix 4 in Lhca3 may perhaps reflect the comparatively ill-defined map density in this region.

When the Chl positions are compared in this superposition, it is interesting to note that the arrangement of each Lut in close contact with 3 Chls *a*, as observed in LHC-II, is also found in the Lhcas. The only apparent difference is in the orientation of Chl 1 in Lhca1 and Lhca2. This is surprising because Glu180, which coordinates the Chl 1 Mg in the pea structure, is strictly conserved in all LHCS and is also involved in the ion bridge with Arg70, which is equally conserved. The position of Chl 3 in the 5 structures is remarkably similar. Gln197, which coordinates the Mg of Chl 3 also makes polar contacts to the head group of Lut1 and to the conserved Asn208. This might explain why the position and orientation of Chl 3 is so similar in LHC-II and the Lhcas. Note that only the polypeptide backbones were used for alignment, so the superposition is not biased by the pigment geometry.

The two prolines at the beginning and end of the short amphipatic helix 5 on the luminal surface are conserved in most family members except PsbS. In this protein, the predicted unique fourth transmembrane helix is supposed to be located in this region, so the lack of sequence conservation is not surprising. It is more surprising that the Lhca proteins resolved in the 3.4 Å structure of pea PS-I seem to lack this amphipatic helix (Amunts et al, 2007) even though the sequence alignment indicates that it should be there, including the Chl 8 binding site. Poorly defined electron density in this region of the map might explain this discrepancy. The 33 C-terminal residues of PsbS, which have no equivalence in any other LHC, show a striking, but probably coincidental similarity to a sequence in SO4266, a protein of the FIC (Filamentation Induced by cAMP) family from *Shewanella oneidensis* MR-1. The crystal structure of SO4266 reveals that this stretch forms an  $\alpha$ -helix (PDB code: 3EQX) (Das et al, 2009). It can therefore be safely assumed that this region of

---



PsbS likewise forms an  $\alpha$ -helix, as has been suggested on the basis of its hydrophobicity (Haripal et al, 2006).

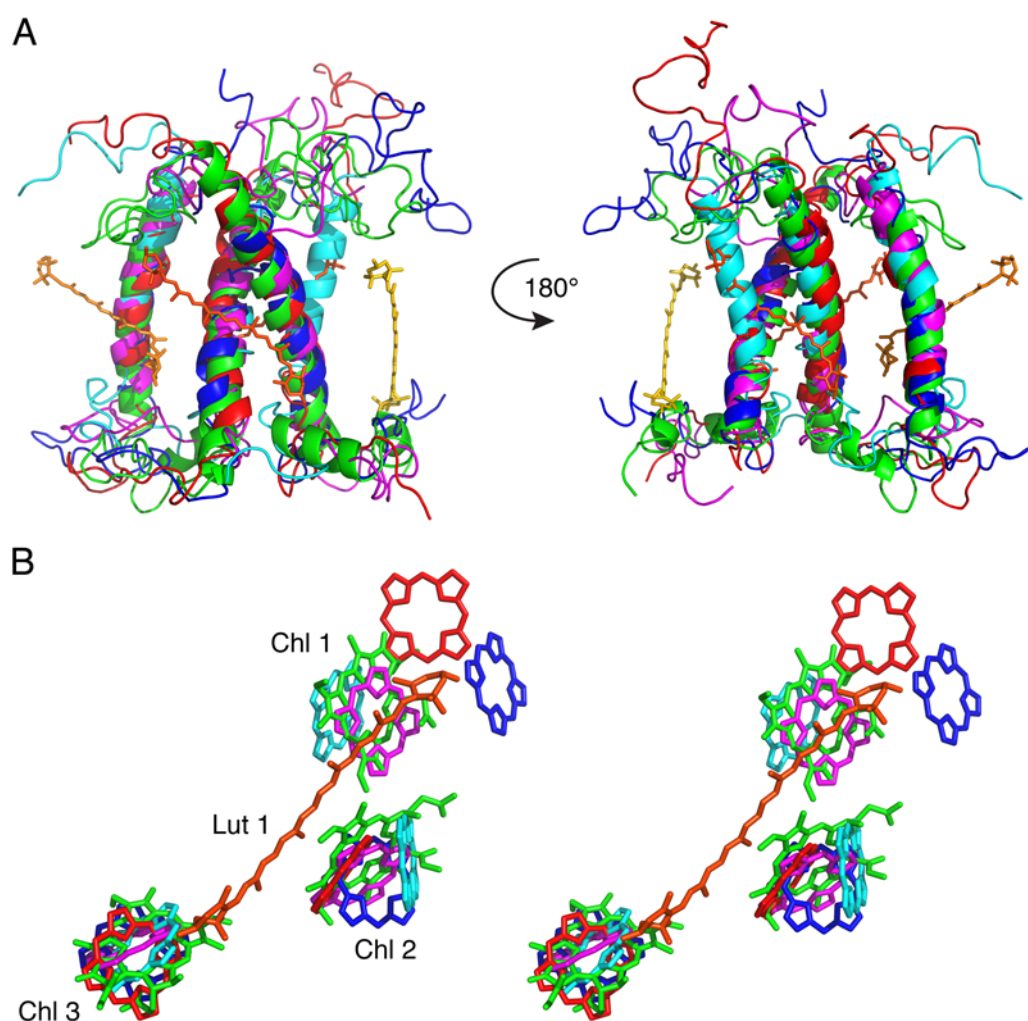


**Figure 1-11 - Comparison of LHC-II and Lhcas.**

(A) Lhca1, Lhca2 and Lhca4 superpose almost perfectly with LHC-II. One of the central helices of Lhca3 deviates from the others and clashes with Lut 2 in LHC-II. (B) Stereo view of conserved Chl positions in LHC-II and the Lhcas. Differences in chlorin ring orientation may reflect map quality or interpretation. Green, LHC-II; blue Lhca1; red, Lhca2; cyan, Lhca3; magenta, Lhca4; dark orange, Lut; light orange, Neo; yellow, Vio.

### 1.3 Non-photochemical quenching

Apart from their main light-harvesting function, members of the LHC family also have an essential role in the dissipation of excess solar energy under high-light conditions. The thylakoid membranes of land plants experience frequent and drastic changes in light intensity. Under steady-state conditions, the photosynthetic efficiency of the thylakoid membrane is optimal for a given light level. This level can change in the time frame of minutes or seconds, be it through changes in cloud cover, or the sudden exposure of a shade leaf to bright sunlight. The resulting potential over-excitation of the photosynthetic system can lead not only to an excessive proton gradient across the thylakoid membrane, but also to photodamage to the photosystems themselves, due to singlet oxygen formation upon interaction of molecular oxygen with Chl triplets. To guard against this, plants have developed a set of photo-protective mechanisms collectively referred to as non-photochemical quenching (NPQ), by which excess excitation energy is safely dissipated as heat.

The assumed, and in some cases well-substantiated roles of plant LHCs in NPQ have been the subject of numerous studies and debates for now more than 2 decades. NPQ has three components ( $q_E$ ,  $q_T$ , and  $q_I$ ; Table 1-2), each of them characterised by their relaxation kinetics (Müller et al, 2001). Most of the recent investigations have focussed on  $q_E$ , the rapidly inducible and reversible component of NPQ, which is governed by lumenal pH (Figure 1-12). Under high-light conditions, protons accumulate in the thylakoid lumen, due to the high activity of the photosynthetic electron transport chain, and the resulting imbalance between proton accumulation in the lumen and the consumption of the proton gradient ( $\Delta pH$ ) for  $CO_2$  fixation and ATP production by the ATP synthase. The increase in  $\Delta pH$  across the thylakoid membrane triggers a series of physiological responses, which ultimately result in  $q_E$ . The ability to activate  $q_E$  to cope with a sudden increase in light intensity is crucial for plant fitness in the field (Külheim et al, 2002). In an effort to identify the main players in  $q_E$ , it has been shown that *Arabidopsis* plants lacking *Lhcb1* and *Lhcb2* have reduced  $q_E$  (Andersson et al, 2003), confirming previous suggestions that LHC-II itself plays an important role in this photoprotective mechanism (Ruban & Horton, 1994). However, despite the efforts of several groups over many years of research and an admirable number of

---

publications devoted to the topic, the exact details of the qE mechanism and the role of LHC-II and the other members of the Lhc family remain obscure.

**Table 1-2 - Chl fluorescence quenching processes *in vivo***

Name and abbreviation	Definition
Photochemical quenching;	qP Fluorescence yield is lowered because of use of excitation energy for photochemical reactions
Non-photochemical quenching	NPQ All mechanisms that lower the fluorescence yield apart from photochemistry, divided into qE, qT, and qI according to their relaxation kinetics
Energy-dependent quenching;	qE Requires the build-up of a proton gradient; relaxes within seconds to minutes
State-transition quenching;	qT The major light-harvesting complex separates from PS-II, thereby reducing the amount of excitation energy in PS-II that can de-excite to fluorescence; relaxes within tens of minutes
Photoinhibitory quenching;	qI This quenching is caused by photoinhibition and shows very slow relaxation kinetics in the range of hours

From (Müller et al, 2001).

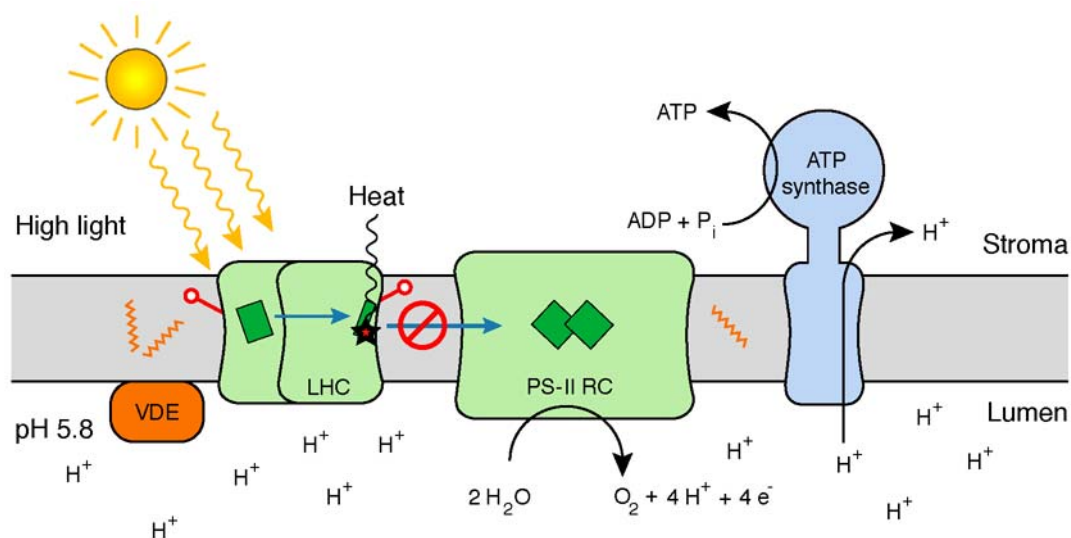


**Figure 1-12 - Schematic representation of the qE component of NPQ.**

Under high light conditions, protons accumulate in the lumen of the thylakoids, triggering activation of violaxanthin de-epoxidase (VDE) and switch of the LHCs to a quenched state. Energy transfer from the antenna LHCs of photosystem II (PS-II) is thus blocked and excess energy is safely dissipated as heat.

### 1.3.1 The xanthophyll cycle

A well-known consequence of the pH drop in the lumen of the thylakoids is the activation of the xanthophyll cycle (Yamamoto et al, 1962; Yamamoto, 1985; Figure 1-13). In this enzymatic cycle Vio, one of the carotenoids bound to LHC-II under normal light conditions, is converted to Zea by the luminal enzyme violaxanthin de-epoxidase (VDE). Presumably, the increase in Zea and the concomitant reduction of Vio results in an exchange of Vio by Zea in the LHCs. Once the light stress is over, the stromal enzyme zeaxanthin epoxidase (ZE) catalyses the reverse reaction, so that the LHCs return to their initial pigment composition. The xanthophyll cycle and its regulation have recently been reviewed (Jahns et al, 2009).

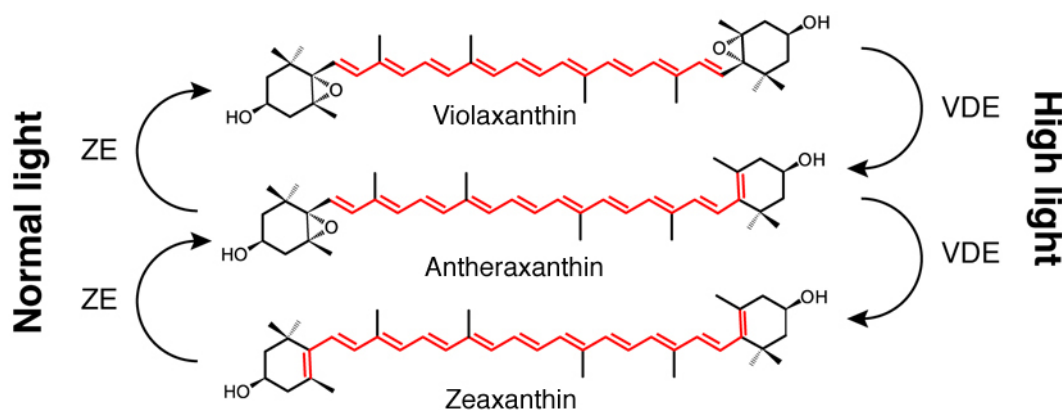


**Figure 1-13 - The xanthophyll cycle.**

Vio and Zea are interconverted via the xanthophyll cycle. Under high light conditions the drop of the lumen pH activates VDE, which removes the two epoxy groups from Vio, converting it into Zea and extending the  $\pi$ -system of the carotenoid by two conjugated double bonds. As soon as the pH in the lumen of the thylakoids returns to normal and VDE is inactivated, the constitutively active ZE converts Zea back to Vio. The  $\pi$ -system of the xanthophylls is shown in red.

#### 1.3.1.1 Violaxanthin de-epoxidase

VDE belongs to the lipocalin protein family, which is widespread not only in plants but also animals and bacteria (Flower, 1996; Barker & Manning, 1997). The members of the family share a common tertiary structure characterised by an 8 stranded anti-parallel  $\beta$ -barrel with a repeated +1 topology (Figure 1-14). An additional structural feature of the family is a short  $3_{10}$   $\alpha$ -helix formed by a

conserved sequence motif. Most frequently, the lipocalins transport small hydrophobic compounds, such as retinol (by the retinol binding protein). Only very few lipocalins, of which VDE and ZE are the chief examples, have been shown to have enzymatic activity (Jahns et al, 2009).

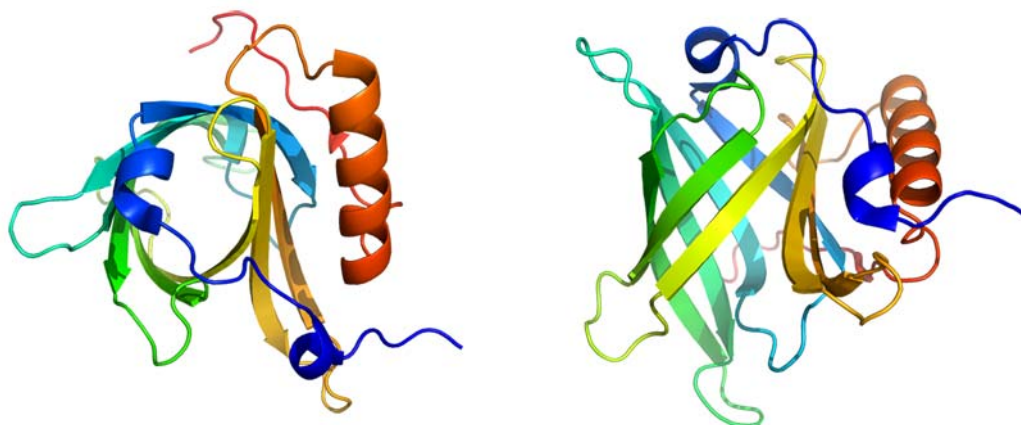


**Figure 1-14 - The lipocalin fold.**

The figure shows two views of the structure of a variant of the human retinol binding protein (Greene et al, 2001)(PDB code: 1JYJ), a member of the lipocalin family of proteins that has 21% identity with the lipocalin domain of VDE from *Arabidopsis thaliana*.

The VDE cDNA from romaine lettuce was first cloned and expressed in *E. coli* in 1996 by the Yamamoto group in Hawaii (Bugos & Yamamoto, 1996). The gene structure comprises 4 regions (Figure 1-15). The first region corresponds to the signal peptide, which targets the expression product of the nuclear gene to the lumen of the thylakoids. After cleavage of this signal peptide, the mature enzyme has a molecular weight of approximately 40 kDa. The catalytic site of VDE is located in the N-terminal region of the mature enzyme, which has an unusually high cysteine content (11 cysteines in the first 80 residues). It has been shown that disulphide bridge reduction by dithiothreitol (DTT) reversibly inhibits the enzymatic activity (Bugos & Yamamoto, 1996). Interestingly, incubation of the protein with DTT at pH 7.2 does not affect the enzyme activity, suggesting that low pH activates the enzyme by exposing the catalytic site to the solvent. VDE activity requires not only low pH (optimum pH is around 5.5) but also ascorbate and the lipid MGDG. Ascorbate is the electron donor, while MGDG is probably required to mediate the access of the membrane-embedded Vio to the catalytic site of the enzyme. The central lipocalin domain provides the hydrophobic cavity for the

enzymatic reaction, and dictates the enzyme selectivity for 3-OH, 5,6-epoxycarotenoids in configuration 3R, 5S, 6R (Grotz et al, 1999). The third and final domain is rich in glutamate residues. The function of this domain is unclear, as 71 residues can be deleted from the C-terminus of VDE without significantly affecting its activity (Hieber et al, 2002).



**Figure 1-15 - VDE gene structure.**

The VDE gene comprises 4 regions: a signal peptide that targets the protein to the lumen of the thylakoids, a cysteine-rich domain where the catalytic site is located, the lipocalin domain that provides the hydrophobic cavity accommodating the substrate during catalysis and a C-terminal domain rich in glutamate residues of unknown function.

Despite its essential role in NPQ, the mechanisms of VDE activation and Vio de-epoxidation are largely unknown. Also interestingly, of all the main players in NPQ (Figure 1-12), VDE is the only one for which there is essentially no structural information. Clearly, a structure of VDE would constitute a major contribution to our understanding of the xanthophyll cycle and, more importantly, NPQ.

### 1.3.2 PsbS

Random mutagenesis studies of *Arabidopsis* led to the discovery that PsbS is required for qE (Li et al, 2000). In some ways this was a surprise, as the protein had already by that time been shown to be stable in the absence of pigments (Funk et al, 1995). Pigment binding by PsbS is still a matter of controversy (Aspinall-O'Dea et al, 2002; Bonente et al, 2008). Depending on whether or not PsbS binds pigments, two scenarios are possible. Either PsbS participates directly in the quenching event, and in this case it must bind pigments, even if transiently, or it is an effector of qE by interaction with one or several of the LHCS.

The sensitivity of PsbS to lumenal pH is well-established (Bergantino et al, 2003) and is conferred by two pH-sensing glutamate residues (Li et al, 2002): Glu62 and Glu166 according to the predicted sequence of the mature protein (Jansson, 1999) and in our alignment in Figure 1-4. Low pH-sensing by PsbS leads to the formation of monomers (Bergantino et al, 2003). Interestingly, when thylakoids

---

---

were incubated at low pH, PsbS monomers were predominantly found together with LHC-II, while dimers were preferentially associated with the PS-II core (Bergantino et al, 2003). Two additional lines of evidence support PsbS interaction with the LHCs. Immunoaffinity experiments have shown interaction between PsbS and both LHC-II and CP29 (Teardo et al, 2007). Resonance Raman measurements *in vivo* under qE conditions have correlated the distortion of the Neo configuration with the PsbS content of the thylakoid membrane (Ruban et al, 2007).

### **1.3.3 Current models of the qE mechanism**

#### **1.3.3.1 Aggregation quenching**

The pronounced dependence of the fluorescence properties of LHC-II on its aggregation state has intrigued researchers for more than two decades (Ide et al, 1987; Ruban & Horton, 1992; Mullineaux et al, 1993; Ruban et al, 1995a; Vasil'ev et al, 1997; Barzda et al, 2001a; Kirchhoff et al, 2003; Lambrev et al, 2007; van Oort et al, 2007a). The bright 680 nm fluorescence and long lifetimes of the detergent-solubilized complex contrast strongly with the quenched fluorescence and very short lifetimes of LHC-II aggregates (Mullineaux et al, 1993; Ruban et al, 1995a; Vasil'ev et al, 1997; van Oort et al, 2007a). Another spectroscopic marker of LHC-II aggregates is the appearance of an emission peak centred around 700 nm at cryogenic temperatures. Likewise, a drop in Chl fluorescence yield, shorter fluorescence lifetimes at ambient temperature and concomitant increase in 700 nm fluorescence at liquid nitrogen temperature (77 K) were also observed in isolated thylakoids (Ruban et al, 1991; Gilmore et al, 1995) and plant leaves (Ruban & Horton, 1994) under qE conditions. These similarities lead to the proposal of the aggregation quenching model by Horton (Horton et al, 1991; Horton et al, 2005), whereby a pH induced conformational change in LHC-II results in its aggregation in the thylakoid membrane, and ultimately in the enhancement of excitation energy dissipation as heat. This model assumes that (a) LHC-II aggregation occurs *in vivo* and (b) LHC-II can switch between alternative conformations.

#### **1.3.3.2 The conformational change hypothesis**

The local Chl concentration in LHC-II is roughly 300 mM, yet the complex is able to transmit energy to the reaction centres in the thylakoid membrane, or, in

the isolated complex, to re-emit it in the form of fluorescence. By comparison, solutions of free Chl at a similar concentration emit no fluorescence at all, due to concentration quenching (Beddard & Porter, 1976), so that all the absorbed light energy is converted into heat. It would therefore only take a small change in the pigment geometry to turn LHC-II from a complex that collects and transmits excitation energy into one that instead dissipates it in the form of heat. It is then tempting to postulate a conformational switch mechanism that would convert LHC-II from an active antenna into a quenching centre under high-light conditions, to protect the photosynthetic apparatus from damage. Such a mechanism has often been proposed (Gilmore & Yamamoto, 1992; Horton et al, 2000; Moya et al, 2001; Dall'Osto et al, 2005; Horton et al, 2005; Pascal et al, 2005; Ruban et al, 2007; Yan et al, 2007; Ahn et al, 2008), but so far no conclusive structural evidence of an actual conformational change in LHC-II or the minor LHCs has been forthcoming.

### **1.3.3.3 Gear-shift and carotenoid radical cation hypothesis**

The effect of the substitution of Vio by Zea on the function of the LHCs is a matter of debate. Some early publications reported quenching induced by Zea (Wentworth et al, 2000). More recently, an 11% reduction in fluorescence quantum yield upon Zea binding to refolded LHC-II has been reported (Avenson et al, 2008b). Other studies have shown no significant reduction on the Chl excited state lifetimes in Zea-LHC-II (Mullineaux et al, 1993). This is in line with recent calculations, which indicate that the excited state energies of Vio and Zea in LHC-II are virtually identical, and that therefore the simple exchange of xanthophylls is not sufficient for effective dissipation of excess excitation energy (Dreuw & Wormit, 2008). Other effects such as pH sensing by PsbS are likely to play a role.

Although Zea formation is correlated with qE (Demmig et al, 1987), it is still not clear whether or not Zea binding is necessary for switching the antenna into the quenched state. Some recent studies have conjectured that Zea acts as an allosteric effector of quenching, rather than being directly involved in the quenching mechanism (Horton et al, 2000; Dall'Osto et al, 2005; Horton et al, 2005; Crouchman et al, 2006; Avenson et al, 2008a; Perez-Bueno et al, 2008). If quenching were to be brought about by bound Zea, it is however not clear by which mechanism the excitation energy would be dissipated. It could either be excitation

---



energy transfer from Chl to Zea (the gear-shift model; (Frank et al, 1994)) or through electron transfer from Zea to Chl (the carotenoid radical cation model; (Dreuw et al, 2003)). Current opinion leans towards the latter hypothesis. Indeed, the spectroscopic signature of a carotenoid radical cation has been detected in thylakoids under qE conditions (Holt et al, 2005) but its identity or origin within the photosynthetic apparatus was not resolved. Recent experiments have suggested that the minor LHCs, rather than LHC-II itself are the location of the carotenoid radical cation (Avenson et al, 2008b), although even in this model, Zea binding is thought to be a necessary, but not sufficient step towards quenching (Ahn et al, 2008). It has been proposed that a conformational change in the minor LHCs is necessary to bring a Chl pair into close contact with a Zea molecule occupying the binding site of lutein 2, so that they form a quenching charge-transfer state (Ahn et al, 2008).

## 1.4 Aims of this work

The mechanism governing the functional switch of LHC-II between the energy-transmitting and the energy-dissipating state is unknown. The aim of this thesis is to ascertain this mechanism by answering three specific questions:

**1. What is effect of the Vio by Zea substitution on LHC-II function?**

To address this question it is necessary to establish a protocol for obtaining Zea-enriched LHC-II for spectroscopic studies and possibly crystallisation of Zea-LHC-II. Our understanding of the relationship between the xanthophyll cycle and LHC-II would also benefit from establishing an *in vitro* system integrating the complex and VDE.

**2. Which functional state of LHC-II is represented by the structures?**

Answering this question requires a detailed spectroscopic analysis of LHC-II single crystals. In addition, obtaining a new crystal structure of LHC-II at higher resolution would assist the computational analyses of LHC-II function.

**3. Are the mechanisms of LHC-II aggregation quenching and qE related?** The strategy for addressing this question is to target the function of particular pigments using aggregates of LHC-II mutants. Additionally, the spectroscopic characterisation of LHC-II single crystals, which are a particular case of aggregation that resembles the complex in the thylakoid membrane, can be used to compare the quenching mechanisms *in vitro* and *in vivo*.

---

## **2 A NOTE ON SPECTROSCOPIC METHODS AND CALCULATIONS**

The photosynthetic membrane is arguably the best-understood membrane system in Biology. This undoubtedly results from the synergy between the structure elucidation of the key macromolecular complexes (photosystems, light-harvesting complex, ATP synthases and others) and the development of ever more sophisticated spectroscopic techniques.

With roughly one third of its mass coming from carotenoids and Chls, LHC-II is an object of choice for spectroscopy. Relatively simple spectroscopic techniques such as steady-state absorption and fluorescence spectroscopy in the visible range can be used to investigate the LHC-II function. However, state-of-the-art spectroscopic techniques like ultrafast transient absorption and two-photon excitation are required to gain more detailed insights onto the mechanisms of energy transfer and conversion in LHC-II.

## 2.1 Absorption and fluorescence in LHC-II

Absorption of a photon by a pigment molecule (for example, a carotenoid or a Chl in LHC-II) causes the transition from the lowest electronic energy level, the ground state, to an electronically excited state ( $S_i$ ). For a macromolecular complex like LHC-II, which is composed of different colourful pigment molecules with characteristic electronic structures, an absorption spectrum can be recorded, which reflects the electronic transitions occurring in carotenoids and Chls after excitation with light in the visible range (Figure 2-1). Upon absorption of a photon, the pigment molecule usually undergoes a transition to a high vibrational state of the higher electronic state (Figure 2-2), which contributes to broadening of the absorption bands; decay to the lowest vibrational state is usually reached within  $10^{12}$  s or less by internal conversion.

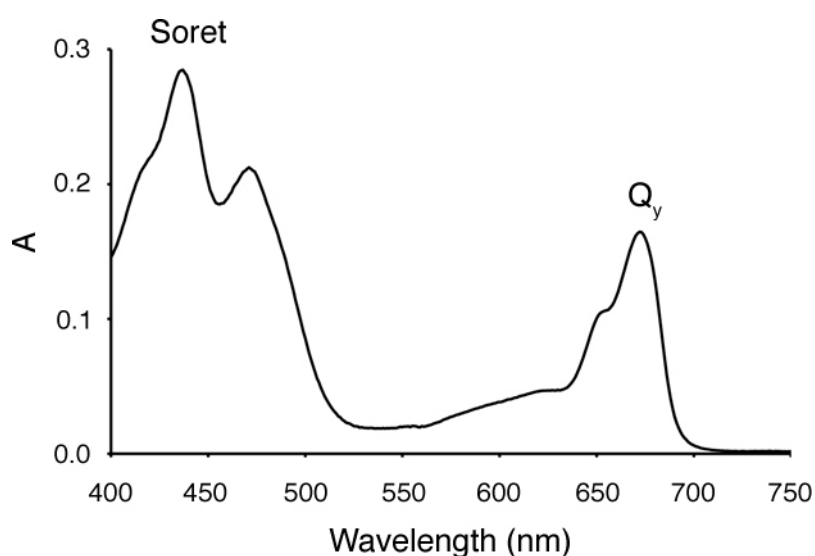


**Figure 2-1 - LHC-II absorption spectrum.**

A typical absorption spectrum of LHC-II in detergent solution is shown. The Soret and  $Q_y$  bands of Chl *a* are indicated.

Several processes can then occur that return the pigment molecule to its ground state (Figure 2-2). Among these is the emission of a photon with a longer wavelength (lower energy) than that of the absorbed photon, by fluorescence. The fluorescence emission spectrum of a pigment is determined by the energy levels of the emitting states. In isolated LHC-II, the emission spectrum is characterised by a

---

single strong peak at 680 nm, indicating that all the excitation energy absorbed by the complex is funnelled to a particular set of Chls (the final emitter) that emit a photon at that particular wavelength. About 25% of the visible light absorbed by isolated LHC-II leads to this very characteristic emission at 680 nm (Palacios et al, 2002). In the thylakoid membrane energy transfer to other pigment-protein complexes, such as the minor LHCS and the photosystems, competes with the fluorescent decay, so that only residual fluorescence is observed.

The absorption and fluorescence spectra of a complex system like LHC-II reflect not only the energy levels of the individual constituent pigments but also the coupling between them. The absence of particular pigments or a change in pigment configuration will alter the electronic structure of the coupled system of pigments, which will be translated into changes in the overall spectroscopic properties of the entire complex. For this reason, absorption and fluorescence spectra can be used to examine the functional state of LHC-II.

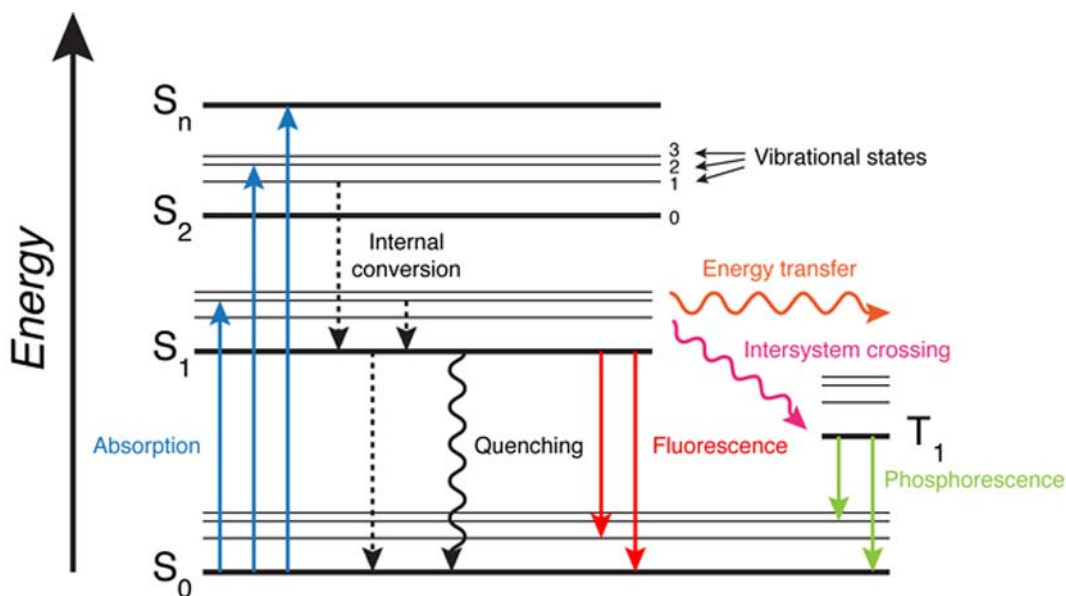


**Figure 2-2 – Electronic states of a molecule and transitions between them.**

The figure shows one form of a Jablonski diagram (Jablonski, 1935; Lakowicz, 2006). Absorption of a photon by a pigment molecule corresponds to the transition from the ground state ( $S_0$ ) to an electronically excited state ( $S_1$ ,  $S_2$ , ...  $S_n$ ). The pigment molecule can return to the ground state via a variety of processes. Straight lines indicate absorption or emission of a photon, while dashed or wavy lines indicate non-radiative processes.

## 2.2 Steady-state and time-resolved spectroscopy

Absorption and fluorescence measurements can be broadly categorised into two types: steady-state and time-resolved measurements. Steady-state measurements allow determination of the energy levels of the different electronic states, so that the energy of the excited states in Figure 2-2 can be determined. In fact, the excited states of a molecule are characterised not only by their energy levels but also by their lifetime. In a steady-state experiment, an average signal over time is measured, and the information regarding the lifetimes is lost. Time-resolved measurements, on the other hand, give information about the lifetime of the excited states and the rates at which the different decay processes occur. A complete description of the energy transfer and conversion within a complex system of pigments like in LHC-II requires both steady-state and time-resolved measurements.

### 2.2.1 Time-resolved fluorescence spectroscopy

Fluorescence lifetimes are measured by time-resolved fluorescence spectroscopy and reflect the time a fluorophore spends in the excited state before returning to the ground state (Lakowicz, 2006). In the absence of non-radiative processes, the measured lifetime corresponds to the intrinsic or natural fluorescence lifetime of the fluorophore. However, most often the emission of a photon is only one of several processes by which the molecule returns to the ground state. The fluorescence lifetime is then the reciprocal of the sum of emissive and non-radiative (which include internal conversion and quenching) energy dissipation rates

#### Equation 2-1

$$\tau = \frac{1}{k_r + k_{nr}}$$

where  $\tau$  is the fluorescence lifetime and  $k_r$  and  $k_{nr}$  are the emissive and non-radiative decay rates, respectively.

If only one radiative process is observed, the fluorescence decay is described as a single exponential. In a more complex system, like LHC-II, several radiative

---

processes may occur simultaneously, so that the fluorescence decay is multiexponential. Each of the radiative processes is associated with a decay component, so that the measured fluorescence intensity varies with time according to

**Equation 2-2**

$$I(t) = \sum_{i=1}^n \alpha_i \exp\left(-\frac{t}{\tau_i}\right)$$

with  $\sum \alpha_i$  normalised to unity.

In this expression  $\tau_i$  and  $\alpha_i$  are the lifetime and the amplitude (or pre-exponential factor) of the decay component  $i$  at  $t = 0$ , respectively.  $n$  is the number of decay components. The different decay components may originate from different fluorophores in a mixture or from a complex decay from a single fluorophore, as is the case in LHC-II. For example, LHC-II populations with different pigment content, conformations or interactions with other complexes or external pigments may lead to different components in the fluorescence decay. It can be assumed that  $\alpha_i$  values represent the fraction of the molecules in each population at  $t = 0$ , which corresponds to the ground-state equilibrium.

Irrespective of whether the multiexponential decay originates from a single fluorophore or multiple fluorophores, the values of  $\alpha_i$  and  $\tau_i$  can be used to determine the fractional contribution  $f_i$  of each decay time to the steady-state intensity. These values are given by

**Equation 2-3**

$$f_i = \frac{\alpha_i \tau_i}{\sum_j \alpha_j \tau_j}$$

$f_i$  are called fractional steady-state intensities in a multiexponential intensity decay. They do not correspond to the fraction of that population at  $t = 0$ .

The term  $f_i$  is proportional to the area under the decay curve for each decay time. In a steady-state measurement, one measures the total emission irrespective of

when the photon is emitted. This is why the intensity is usually weaker for a short decay time: the  $\alpha_i\tau_i$  product is smaller.

When the multiexponential decay law is used, it is often useful to determine the average lifetime  $\bar{\tau}$ , which is given by

**Equation 2-4**

$$\bar{\tau} = \frac{\int_0^{\infty} t \cdot I(t) \cdot dt}{\int_0^{\infty} I(t) \cdot dt}$$

It can be derived that for a n-exponential decay  $\bar{\tau}$  is given by

**Equation 2-5**

$$\bar{\tau} = \frac{\int_0^{\infty} t \sum_{i=1}^n \alpha_i \exp\left(-\frac{t}{\tau_i}\right) \cdot dt}{\int_0^{\infty} \sum_{i=1}^n \alpha_i \exp\left(-\frac{t}{\tau_i}\right) \cdot dt} = \frac{\sum_{i=1}^n \alpha_i \tau_i^2}{\sum_{i=1}^n \alpha_i \tau_i} = \sum_{i=1}^n f_i \tau_i$$

In practice, fluorescence lifetimes are most often used to evaluate the quenched or unquenched state of LHC-II in different experimental scenarios. Typically, isolated LHC-II in detergent solution has an average fluorescence lifetime of about 4 ns at room temperature. A drop in the average lifetime signifies an increase of the non-radiative processes, and in particular an increase of quenching.

### 2.2.1.1 Decay-associated spectra

A common way of characterising the radiative processes by which an excited molecule returns to the ground state is to determine how the amplitude of the respective decay component varies within the emission spectrum. In practical terms, the emission spectrum is probed by measuring the fluorescence decay of the molecule at certain emission wavelengths using a monochromator. A sophisticated fitting routine known as global analysis is then used to find the minimum set of variables (a certain number decay components and their characteristic lifetime) that

---



best describe the data. The variation of the amplitude of each decay component with wavelength illustrates the emission spectrum of the corresponding radiative process. Such representation of the time-resolved data is known as decay-associated spectra.

### **2.2.2 Pump-probe spectroscopy**

As discussed above, absorption of a photon (the pump) by a pigment molecule leads to transient population of an excited state. This excited state has its own particular spectroscopic characteristics, i.e. it will absorb another photon with a certain energy (the probe, which corresponds to another transition to an even higher energy level) and is only populated for a certain period of time (its lifetime). It is then possible to sample the evolution of the excited state by probing the absorption of photons by the excited molecule over time. This constitutes the principle behind the so-called pump-probe or transient absorption experiments. Essentially, for as long as the excited state is populated the molecule will absorb light of the probe flash. After decay to the ground state (or another excited state) the probe photons will no longer be absorbed. The data recorded contains information about the energy level of the different states that are populated and also the rates at which transitions between them occur.

As an example, transient absorption experiments with LHC-II are used to follow the dynamics of excitation energy transfer within the complex, based on the fact that upon excitation of a Chl, the excitation energy will “hop” downhill through the coupled network of Chls towards the final emitter (Novoderezhkin et al, 2005). Each Chl or set of coupled Chls has characteristic absorption signatures, which can be probed with time to trace the energy flow dynamics.

Transient absorption can also be used as an alternative to time-resolved fluorescence. To determine the lifetime of the LHC-II fluorescence emitters' excited state, it is equivalent to measure the fluorescence lifetime of the LHC-II final emitters by means of time-resolved spectroscopy or to determine their excited state lifetime by transient absorption spectroscopy. An advantage of the latter is that LHC-II in the ground state does not absorb the probe pulses and only the molecules in the excited state will give rise to a signal. On the other hand, LHC-II absorbs

quite significantly at its emission peak (680 nm) so that in concentrated samples like crystals or aggregates some of the emitted photons will be reabsorbed which will tend to increase the measured fluorescence lifetime.

### **2.2.3 Resonant two photon two colour ionisation**

According to the carotenoid radical cation ( $\text{Car}^{\bullet+}$ ) model of qE, excitation energy dissipation occurs via a charge transfer state of a carotenoid-Chl heterodimer (Dreuw et al, 2003; Dreuw et al, 2005). If quenching occurs through this mechanism, it should be possible to detect the transient formation of  $\text{Car}^{\bullet+}$  within the pigment-protein complexes. An elegant way to generate  $\text{Car}^{\bullet+}$  artificially is to use resonant two photon two colour ionisation (R2P2CI; Figure 2-3).

R2P2CI is essentially a pump-pump-probe experiment. The first pump laser pulse is used to excite a particular pigment (usually a carotenoid in LHC-II) to an intermediate excited state, the second laser pulse is resonant with the transition between that excited state  $S_n$ , which promotes ionisation of the molecule, and the third pulse is used to probe absorption by the generated radical cation. In the case of the carotenoids in LHC-II, a higher vibrational state of Car  $S_2$  is populated after the first excitation pulse. From this state, the Car will then decay very rapidly to the lowest vibrational state of  $S_2$ , and then more slowly to the  $S_1$  state. For this reason, it is necessary to adjust the delay between the two pump pulses, so that the molecule absorbs the second pulse while it is still in the  $S_2$  state, and the amount of  $\text{Car}^{\bullet+}$  that is created is maximised. The probe pulse uses a white light continuum so that an absorption spectrum of  $\text{Car}^{\bullet+}$  can be determined. Also, the delay between the pump and probe pulses can be used to follow the dynamics of  $\text{Car}^{\bullet+}$ .

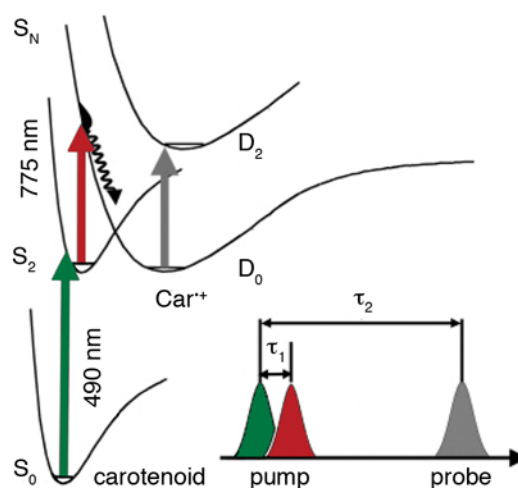


**Figure 2-3 – Schematic diagram of a pump-pump-probe experiment on carotenoids.**

A typical resonant two photon two colour ionisation experiment with carotenoids is essentially a pump-pump-probe experiment, in which the first pump pulse excites the carotenoid to the  $S_2$  state, and the second pulse is resonant with the  $S_2$ - $S_N$  transition. The absorption spectrum of the generated carotenoid radical cation can be analysed by applying a white light continuum as a probe pulse. The lifetime of the radical can be determined by varying the delay between the pump and the probe pulses.

### 2.2.4 Two-photon excitation spectroscopy

Both the ground state ( $S_0$ ) and first excited state ( $S_1$ ) of the carotenoids in LHC-II have  $A_g^-$  symmetry. Fundamental optical selection rules dictate that transitions between these two states are forbidden so they neither show a significant absorption nor fluorescence (Tavan & Schulten, 1987). Only the second excited state, carotenoid  $S_2$ , contributes to the absorption of carotenoids and shows a rapid decay to the  $S_1$  state by internal conversion. This comes as a drawback to the investigation of the carotenoids role in NPQ, as both the gear-shift and the carotenoid radical cation models implicate the  $S_1$  state of Zea in the quenching mechanism, yet conventional spectroscopy cannot be used to access this state. However, this problem can be bypassed by using two-photon excitation (TPE) because transitions between states of  $A_g$  symmetry, like the carotenoids  $S_0 \leftrightarrow S_1$  transitions are, in general, two-photon allowed.

One of the functions of the carotenoids in LHC-II is to complement the absorption range of the Chls, therefore extending the action spectrum of the complex. The energy of the excited carotenoids is efficiently transferred to nearby Chls (Polivka & Sundstrom, 2004). In isolated complexes, a portion of the

transferred excitation energy is ultimately dissipated as Chl fluorescence. The intensity of the Chl fluorescence upon carotenoid excitation is dependent on the quantum efficiency of the carotenoid  $\rightarrow$  Chl excitation energy transfer. In particular, when TPE is applied, the measured Chl fluorescence reflects carotenoid  $S_1$  - Chl coupling leading to energy transfer from carotenoid to Chl. On the other hand, the measured Chl fluorescence is additionally dependent on their fluorescence quantum yield. The extent of carotenoid  $S_1$  - Chl coupling ( $\Phi_{\text{coupling}}$ ; Figure 2-4) is thus directly proportional to the ratio between the Chl fluorescence upon one photon excitation (OPE) and TPE, and is given by

**Equation 2-6**

$$\Phi_{\text{coupling}}^{\text{Car } S_1 - \text{Chl}} \propto \frac{F^{\text{TPE}}}{F^{\text{OPE}}}$$

These measurements are particularly useful for the study of the role of carotenoids in the LHC-II quenching mechanisms, as they give direct evidence for enhanced or decreased energy transfer between carotenoids and Chls, due to alterations in the pigments composition or configuration.

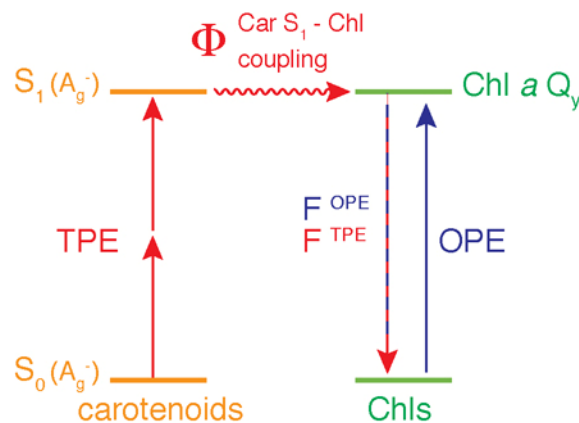


**Figure 2-4 – Two-photon excitation spectroscopy in LHC-II.**

Due to symmetry reasons and optical selection rules, the carotenoid  $S_1$  state cannot be populated by conventional one photon excitation (OPE). However the carotenoid  $S_0 \rightarrow S_1$  transition is two photon allowed, and two-photon excitation (TPE) can therefore be used to circumvent that problem. Coupling between carotenoid (Car)  $S_1$  and Chl in LHC-II will lead to Chl fluorescence after excitation energy transfer. The ratio between Chl fluorescence upon one photon and two photon excitation ( $F^{\text{OPE}}$  and  $F^{\text{TPE}}$ , respectively) is directly proportional to the coupling between carotenoid  $S_1$  and the Chls.

## 2.3 Single-crystal spectroscopy

Combining X-ray crystallography with single crystal spectroscopy is a relatively new technique and becomes increasingly popular in structural biology (De la Mora-Rey & Wilmot, 2007). The three main applications of this approach are: (1) identification of the chemical composition of the crystals (for example by determining the redox state of a bound ligand), (2) monitoring X-ray induced radiation damage and (3) kinetic crystallography (Hajdu et al, 2000; Bourgeois & Royant, 2005), by which the structure of different intermediates along the reaction coordinate is determined. Signal achievements of this last application include a three-dimensional movie of the X-ray driven catalytic reduction of a bound O<sub>2</sub> molecule in horseradish peroxidase (Berglund et al, 2002) and studies on conformational changes and intermediates during the bacteriorhodopsin photocycle (Edman et al, 1999; Royant et al, 2000; Sass et al, 2000).

Traditionally, single crystal studies with biological samples made use of absorption spectroscopy in the visible and UV range. More recently, other techniques such as fluorescence (Royant et al, 2007), Raman (Katona et al, 2007), Fourier-transformed infrared (Moukhametzianov et al, 2006) and X-ray absorption (Yano et al, 2006) spectroscopy have also been introduced. The paper from Yano et al addressed the highly controversial debate regarding the structure of the oxygen-evolving complex (OEC) in PS-II. Supposedly, the geometry of the OEC is artificially disrupted during traditional X-ray diffraction experiments, due to the prolonged exposure to highly intense X-ray beams. Yano et al used much lower X-ray doses in their polarised EXAFS experiments and in combination with X-ray diffraction proposed a novel geometry of the Mn<sub>4</sub>Ca cluster of the OEC.

Spectroscopic methods on crystals of macromolecules suffer from a number of limitations. Most single-crystal spectra are anisotropic and therefore the isotropic solution spectrum cannot be obtained with a single crystal orientation. Prisma effects and variable path lengths also contribute significantly to spectral distortion. For these reasons, changes in absorbance are generally analysed in a qualitative rather than quantitative manner. The same goes for fluorescence measurements. In

some cases, the extremely high fluorophore concentration in crystals inevitably leads to distortion in the emission spectra, due to self-absorption.

Time-resolved fluorescence spectroscopy has also been applied to a number of macromolecular crystals. Naturally fluorescent proteins such as the Green Fluorescent Protein (GFP)(Perozzo et al, 1988) and Enhanced Cyan Fluorescent Protein (ECFP)(Royant et al, 2007) are unsurprisingly among those that were first studied. Nevertheless, application of time-resolved fluorescence spectroscopy can in principle be extended to almost all protein crystals, using the intrinsic fluorescence of tryptophan residues.

Prior to this work, two studies have investigated the fluorescence properties of spinach LHC-II in cubic crystals (Liu et al, 2004), both using unconventional experimental approaches. Pascal et al (Pascal et al, 2005) used Fluorescence Lifetime Imaging Microscopy (FLIM) to measure LHC-II fluorescence lifetime in single crystals and concluded that the complex is quenched in the crystalline state. This was supposedly corroborated by the emission spectrum of 10 individual crystals that were closely positioned in the centre of the excitation beam. Yan et al (Yan et al, 2007) arrived to the same conclusion, based on the fluorescence emission spectrum of crystalline LHC-II. These authors used a conventional fluorometer at liquid nitrogen temperature to measure the spectrum of LHC-II crystals that had presumably been placed in a cuvette. It is then safe to assume that neither one of these studies can be truly classified as a single-crystal study. A large part of the work presented in this thesis was devoted to the first real single-crystal spectroscopic analysis of LHC-II.

---

## 2.4 Theoretical calculations

### 2.4.1 Coupling strength

The coupling strength ( $V$ ) between individual Chls in LHC-II can be estimated (van Amerongen & van Grondelle, 2001) by

Equation 2-7

$$V = \frac{\alpha\kappa}{R^3}$$

in which  $\langle \rangle$  corresponds to 90 or 75 nm<sup>3</sup>cm<sup>-1</sup> for Chl *a*:Chl *a* or Chl *a*:Chl *b* pairs, respectively.  $\kappa$  is the orientation factor given by

Equation 2-8

$$\kappa = \vec{\mu}_1 \cdot \vec{\mu}_2 - 3(\vec{\mu}_1 \cdot \vec{r})(\vec{\mu}_2 \cdot \vec{r})$$

with  $\vec{\mu}_1$ ,  $\vec{\mu}_2$  and  $\vec{r}$  being the normalised vectors of the transition dipole moments of the individual Chls and of the centre-to-centre distance.

### 2.4.2 Förster energy transfer rates

Förster energy transfer rates were estimated from (van Amerongen & van Grondelle, 2001) by

Equation 2-9

$$K_{ET} = \frac{\beta\kappa^2}{\eta^4 R^6}$$

where  $\eta$  is the refractive index ( $\sim 1.55$ ) and  $\beta$  is 32.26 or 9.61 nm<sup>6</sup>ps<sup>-1</sup> for Chl *a*:Chl *a* or Chl *a*:Chl *b* pairs, respectively.

## **3 MATERIALS AND METHODS**

All protein and sample preparation procedures described in this thesis were performed with the technical assistance of H. Betz.

### **3.1 Biological material**

#### **3.1.1 Pea plant growth**

Pea (*Pisum sativum*; Feltham First variety) seeds purchased from Treppens, Berlin, were pre-soaked in water overnight and sown in trays between two layers of vermiculite. Pea plants grew for 3 weeks under a light intensity of 10000 to 15000 lux at 20°C and 50% humidity. The daily photoperiod was 10 hours of light and 14 hours of darkness.

#### **3.1.2 *Arabidopsis* plant growth**

*Arabidopsis thaliana* seeds (wild-type, and *npq1* and *npq2* mutants) were purchased from the Nottingham Arabidopsis Stock Centre, Loughborough, UK. Plants were grown in 3 different ways: in soil, hydroponically according to Tocquin et al (Figure 3-1)(Tocquin et al, 2003), or using a hybrid method (Figure 3-2), in which they were initially grown in soil for 2 to 3 weeks and then transferred to hydroponic growth until harvesting (roughly after 2 months). The chemical composition of the nutrient solution for hydroponics is given in Table 3-1. The same light, temperature and humidity conditions described for pea plants growth were used.

---



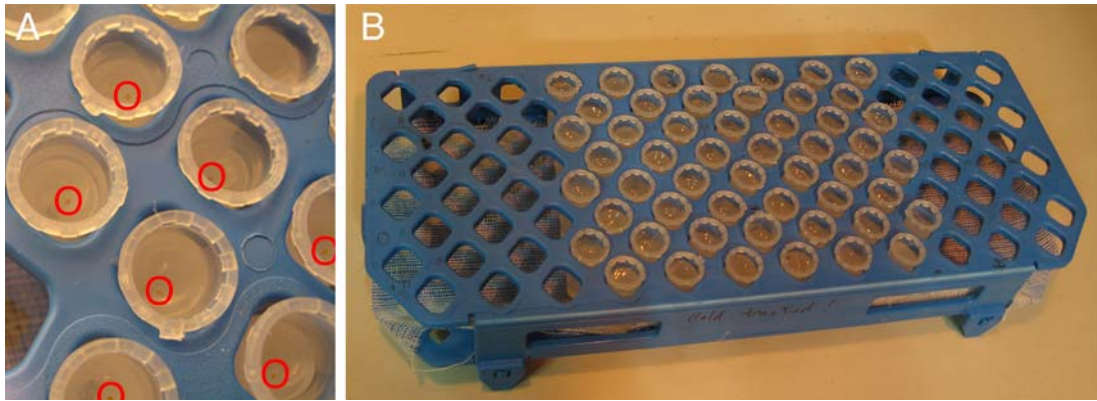


**Figure 3-1 - *Arabidopsis* plants growth in hydroponic medium.**

(A) *Arabidopsis* seeds (within red circles) were suspended in 0.2% agar and placed individually in eppendorf tubes filled with 0.65% agar. (B) The rack with the eppendorf tubes was placed in a container with the hydroponic solution. The bottom of the tubes was cut to allow diffusion of the hydroponic solution.

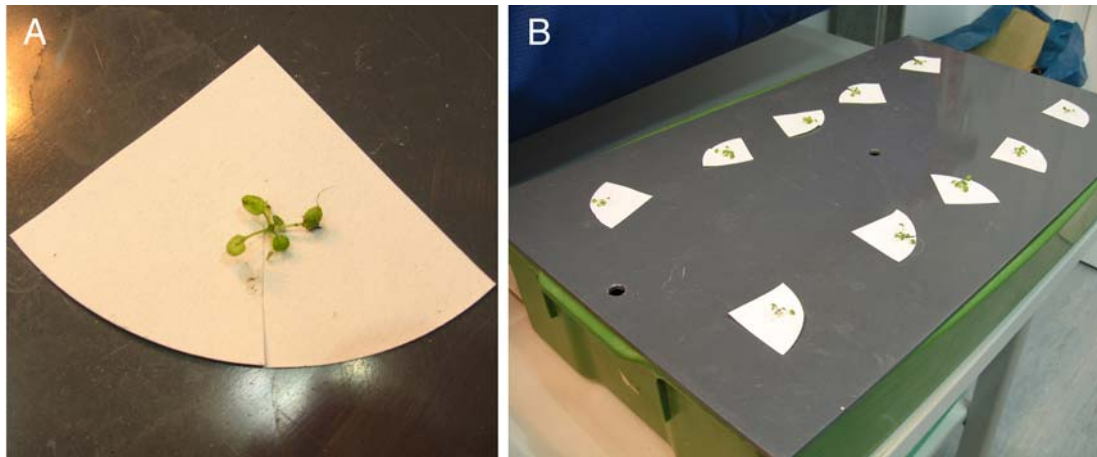


**Figure 3-2 - *Arabidopsis* plants growth using a hybrid method.**

(A) After 2 to 3 weeks of growth in soil, individual plants were supported in a piece of filter paper, so that the roots of the plants passed through the holes on the grey plastic board. (B) The plastic board, with the suspended plants, was placed on top of the container with the hydroponics solution.

**Table 3-1 - Nutrient solution for *Arabidopsis* hydroponic growth**

Chemical component	Final concentration (M)	Mass for 1 l of 100x stock (g)
Ca(NO <sub>3</sub> ) <sub>2</sub> ·4H <sub>2</sub> O	1.01E-03	23.851
FeSO <sub>4</sub> ·7H <sub>2</sub> O	2.24E-05	0.623
EDTA Na	2.23E-05	0.830
KNO <sub>3</sub>	5.10E-03	51.566
NH <sub>4</sub> H <sub>2</sub> PO <sub>4</sub>	1.30E-04	1.495
NH <sub>4</sub> NO <sub>3</sub>	2.93E-05	0.235
MgSO <sub>4</sub>	4.98E-04	12.275
H <sub>3</sub> BO <sub>3</sub>	9.68E-06	0.060
MnCl <sub>2</sub> ·4H <sub>2</sub> O	2.03E-06	0.040
ZnSO <sub>4</sub> ·7H <sub>2</sub> O	3.14E-07	0.009
CuSO <sub>4</sub> ·5H <sub>2</sub> O	2.10E-07	0.005
NaMoO <sub>4</sub> ·H <sub>2</sub> O	1.39E-07	0.003
Co(NO <sub>3</sub> ) <sub>2</sub> ·6H <sub>2</sub> O	8.59E-08	0.003
NaOH	3.13E-05	0.125

### 3.1.3 *Escherichia coli* cell growth

*E. coli* cultures for DNA isolation were inoculated from agar slabs (PIR1 strain; Table 3-2) or single colonies from agar plates (NovaBlue, RosettaBlue and Rosetta-gami; Table 3-2) and grown overnight at 37°C in 15 or 100 ml LB medium (Table 3-3) with the appropriate antibiotics for selection (50 µg/ml Amp; 34 µg/ml Cam; 15 µg/ml Kan; 12.5 µg/ml Tet). Glycerol stocks from positive clones, checked by sequencing of the plasmid insert, were prepared (500 µl of overnight culture plus 500 µl of 50% glycerol), plunged in liquid nitrogen and stored at -80°C.

**Table 3-2 - List of *E. coli* strains**

Strain	Antibiotic resistances	Comments
PIR1	Kan <sup>R</sup>	Clones carried full VDE cDNA from <i>Arabidopsis thaliana</i> ; obtained from ABRC
NovaBlue	Tet <sup>R</sup>	Use for DNA amplification
RosettaBlue	Cam <sup>R</sup> , Tet <sup>R</sup>	Used for expression
Rosetta-gami	Cam <sup>R</sup> , Tet <sup>R</sup> , Kan <sup>R</sup> , Str <sup>R</sup>	Used for expression

**Table 3-3 – Media for *E. coli* growth**

Medium	Component	Medium	Component
<i>LB (Luria)</i>	(g/l)	<i>TB</i>	(g/l)
	Tryptone		Tryptone
	10		12
	Yeast extract		Yeast extract
	5		24
	NaCl		Glycerol
	10		5
			KH <sub>2</sub> PO <sub>4</sub> * 2.3
			K <sub>2</sub> HPO <sub>4</sub> * 12.5
			* - autoclaved separately
<i>SOC</i>	(g/l)		
	Tryptone		20
	Yeast extract		5
	NaCl		0.5
			(mM)
	KCl		2.5
	Mg <sup>2+</sup>		20
	Glucose		20
	NaOH		to pH 7.0

## 3.2 Basic molecular biology procedures

### 3.2.1 Cloning

All cloning procedures to obtain VDE constructs followed the LIC cloning method (Aslanidis & de Jong, 1990; Haun et al, 1992), using kits from Novagen. In brief, plasmid DNA extracted (mini- or maxi-prep using Qiagen kits) from *E. coli* PIR1 cells grown overnight carrying the pUNI51 vector with the *Arabidopsis thaliana* VDE full cDNA was used to produce and amplify VDE constructs (Table 3-4) by PCR (Mullis et al, 1986). Details are listed in Table 3-5 and Table 3-6. The amplified product was analysed by agarose gel (1% agarose in Tris-acetate-EDTA buffer) electrophoresis and the DNA bands were excised from the gel for DNA extraction (using a Qiagen kit). The purified DNA was then treated with T4 DNA polymerase to produce “sticky” overhangs. The processed product was annealed with the linear vectors pET52b(+)<sub>3C</sub>/LIC and pET32 Ek/LIC (both from Novagen and conferring ampicillin resistance; Appendix) for the *E. coli* expression system and pTriEX-6 <sub>3C</sub>/LIC (Novagen; Appendix) for HEK cells expression system. All reagent quantities and reaction volumes were strictly followed as described by the manufacturer’s protocol.

**Table 3-4 – Oligonucleotide primers for PCR**

Vector	Construct	Primer sequence
pET 52b	ArabVDE	fwd 5' CAGGGACCCGGTGTGATGCACTTAAAACCTTGTGC 3'
and	ArabVDE-Long	fwd 5' CAGGGACCCGGTGAGCTGAAAGAGCTGACCGC 3'
pTriEX-6	(for both)	rev 5' GGCACCAGAGCGTTCCTGACCTTCCTGATTGGC 3'
	Thrx- ArabVDE	fwd 5' GACGACGACAAGATAGTTGATGCACTTAAAACCTTGTGC 3'
pET32	C-term His tag	rev 5' GAGGAGAAGCCCGGTACCTGACCTTCCTGATTGGC 3'
	No C-term His tag	rev 5' GAGGAGAAGCCCGGTCTGACCTTCCTGATTGGC 3'

**Table 3-5 – PCR mixture composition**

<b>Component</b>	<b>Volume (µl)</b>
10x Pfu Turbo reaction buffer (Stratagene)	5
dNTP mix (2 mM each)	5
fwd primer (10 µM)	1
rev primer (10 µM)	1
DNA template	to 20 ng
Pfu Turbo DNA polymerase (Stratagene; 2.5 U /µl)	1
H <sub>2</sub> O (MiliQ)	to 50 µl

**Table 3-6 - PCR programme**

<b>Step</b>	<b>Cycles</b>	<b>T (°C)</b>	<b>t (s)</b>
Initiation	1	96	180
Denaturation	30	96	45
Annealing	30	55	45
Elongation	30	68	150
Cooling	1	4	-

### 3.2.2 Transformation and selection of clones

Chemically competent cells (prepared by J. Zeelen or H. Betz, MPI of Biophysics) stored at -80°C were slowly thawed on ice before transformation. Roughly 10 ng of plasmid DNA were added to 200 µl of competent cells and incubated on ice for 30 min. A heat shock at 42°C for 120 s was then applied to the cells, after which the tubes were returned to ice and 1 ml of SOC medium (Hanahan, 1983);Table 3-3) was added. Finally, the cultures were incubated at 37°C for 30 min and then plated in a dilution series (undiluted, 10-fold and 100-fold dilution) on agar plates supplemented with ampicilin. Individual colonies grown overnight on agar plates were picked for sequencing (provided by Scientific Research and Development GmbH, Bad Homburg).

### **3.3 Basic biochemistry procedures**

#### **3.3.1 Protein concentration determination**

The concentration of LHC-II inclusion bodies was determined using 1:200 dilutions of sample in  $A_{280}$  buffer (Table 3-14), which were incubated for 5 min at 95°C. Protein concentration was determined measuring  $A_{280}$ , so that  $A_{280}=1$  corresponds to 525  $\mu\text{g/ml}$ . VDE concentration was determined by the Bradford method (Bradford, 1976) or using the 660 nm Protein Assay from Pierce, using a microplate reader. In both cases BSA solutions of known concentration were used as standards for a calibration curve.

#### **3.3.2 SDS gel electrophoresis and staining**

Polyacrylamide gel electrophoresis under denaturing conditions was performed according to (Fling & Gregerson, 1986). Gels were either prepared from stock solutions (Table 3-7) or purchased from Biorad. Samples were pre-diluted in Laemmli sample buffer (Laemmli, 1970); Table 3-8) and heated to 95°C for 5 min, unless otherwise indicated. All runs were performed at constant voltage (100V; Table 3-9). Coomassie gel staining followed the protocol by Studier (Studier, 2005). In brief, gels were transferred just after electrophoresis to 50 ml of solution I (50% ethanol, 10% acetic acid) and heated in a microwave oven. After cooling for ~10 min on a rocker, the gels were transferred to solution II (5% ethanol, 7.5% acetic acid) and 200  $\mu\text{l}$  of Coomassie stock solution (0.25% Coomassie brilliant blue R250 in 95% ethanol) were added. The solution with the gels was heated once again and finally left to cool on a rocker. For silver staining SDS-PAGE gels the protocol described by (Nesterenko et al, 1994) was followed.

---

**Table 3-7 - SDS-PAGE gel composition**

<b>Stacking gel</b>	<b>5%</b>	<b>Separating gel</b>	<b>10%</b>	<b>12%</b>	<b>15%</b>
<i>Component</i>	<i>(ml)</i>	<i>Component</i>	<i>(ml)</i>	<i>(ml)</i>	<i>(ml)</i>
40% Polyacrylamide	3.75	40% Polyacrylamide	12.50	15.00	18.75
0.5 M Tris-HCl, pH6.8	7.50	1.5M Tris-HCl ,pH8.8	12.50	12.50	12.50
10% SDS	0.30	10% SDS	0.50	0.50	0.50
1% Bromophenol blue	0.05				
H <sub>2</sub> O	18.10	H <sub>2</sub> O	26.50	21.50	17.75
<i>For each 5 mL add:</i>	<i>(<math>\mu</math>l)</i>		<i>(<math>\mu</math>l)</i>	<i>(<math>\mu</math>l)</i>	<i>(<math>\mu</math>l)</i>
10% Ammonium Persulfate	50		50	50	50
TEMED	5		3	3	3

**Table 3-8 - SDS-PAGE sample buffer (5x stock)**

<b>Component</b>	<b>For 10 ml</b>
0.5 M Tris-HCl, pH 6.8	6.25 ml
Glycerol	5 g
10% SDS	1 g
BME	100 $\mu$ l
1% Bromophenol blue	125 $\mu$ l
H <sub>2</sub> O	to 10 ml

**Table 3-9 - SDS-PAGE running buffer**

<b>Component</b>	<b>Concentration</b>	<b>Mass for 5 l (g)</b>
Tris	25 mM	15
Glycine	192 mM	72
SDS	0.1%	5

### 3.3.3 Western blotting

Transfer of proteins from SDS-PAGE gels to methanol-activated PVDF membranes (Millipore) was performed using a semi-dry system from Biorad. The gel and the membrane were sandwiched between layers of filter paper pre-soaked in transfer buffer (20 mM Tris, 150 mM glycine, 0.02% SDS, 20% methanol). To ensure complete transfer of proteins to the membrane, blotting was carried out for 45 min at ~15 V and 3 mA/cm<sup>2</sup>. After transfer, the membranes were immediately transferred to blocking buffer (5% milk powder (His-tag and Lhcb1 detection) or 3% BSA (for Strep-tag detection) in 10 mM Tris-HCl pH 7.5, 150 mM NaCl). After ~1 h the membranes were briefly washed with TBS buffer (10 mM Tris-HCl, 150 mM NaCl, pH 7.5). Binding of monoclonal  $\alpha$ -His-tag antibody conjugated with alkaline phosphatase (from Sigma; 1:3000 dilution), Strep-Tactin conjugate with alkaline phosphatase conjugate (from IBA; 1:4000 dilution) or  $\alpha$ -Lhcb1 antibody (from rabbit, purchased from Agrisera) was performed overnight at 4 °C. After two washing steps in TBS buffer, binding of  $\alpha$ -rabbit secondary antibody coupled with alkaline phosphatase for Lhcb1 detection (from Sigma) or  $\alpha$ -mouse secondary antibody coupled with horseradish peroxidase for His-tag detection via chemiluminescence (from GE Healthcare) was performed for 1 h at room temperature. After two additional brief washes with TBS buffer, the blots using antibodies conjugated with alkaline phosphatase were developed using BCIP/NBT tablets from Sigma and let to dry in the dark. For chemiluminescent detection the ECL system from GE Healthcare was used, following the instructions of the manufacturer.

---



## 3.4 Protein and pigment purification from native source

### 3.4.1 Thylakoid membrane isolation

Thylakoid membranes from pea, spinach or *Arabidopsis* leaves were isolated as described (Burke et al, 1978; Kühlbrandt et al, 1983). In summary, leaves (washed and briefly dried with paper towels for spinach samples) were homogenised in ST buffer (Table 3-10; 100 ml per 35 g of leaves) using a blender. The slurry (typically 500-750 ml) was filtered through a cheesecloth-cotton filter (8 layers of cheesecloth, one layer of cotton, 2 layers of cheesecloth) and then centrifuged for 15 min at 7000 rpm in a Sorvall GSA rotor. Starch coating the centrifuge tube was removed with a brush. The pellet was washed in 250 ml of NT buffer and centrifuged for 15 min at 10000 rpm with the same rotor. Additional starch coating the centrifuge tubes was removed and the dark green pellet containing the chloroplasts was resuspended and homogenised in 250 ml of NT buffer. The suspension was incubated at RT for ~30 min, to break the chloroplasts by osmotic shock. Broken chloroplasts were centrifuged for 15 min at 14000 rpm with the same rotor, washed in NT buffer and centrifuged as in the previous centrifugation step. Pellets were resuspended in ~240 ml of SE buffer and the pH was adjusted to 6.0 with dilute HCl. After 15 min of stirring at room temperature to de-stack the thylakoid membranes, the suspension was centrifuged as in the two previous centrifugation steps. Finally, the unstacked thylakoids were suspended in 100 ml of S buffer and the Chl concentration was measured. Samples were then either used or immediately stored at -20 °C.

**Table 3-10 - Buffers for thylakoid membrane preparation**

Buffer	Composition	Mass	Volume	pH
ST	0.33M Sorbitol	60,12 g	1 l	7,8 with KOH
	0.10M Tricine	17,96 g		
NT	10mM NaCl	0,29 g	500 ml	7,8 with KOH
	1mM Tricine	0,10g		
NET	10mM NaCl	0,58 g	1 l	7,8 with KOH
	1mM Tricine	0,18 g		
	5mM EDTA	1,86 g		
SE	100mM Sorbitol	9,11 g	500 ml	7,8 with KOH
	5mM EDTA	0,93 g		
S	100mM Sorbitol	3,64 g	200 ml	Not adjusted

### 3.4.2 Pigment isolation

About 1 kg of spinach leaves bought the day before from a local market were washed, dried with paper towels and kept in the dark at 4°C overnight. Leaves were homogenized in ~4 l acetone using a blender and the slurry was filtered through filter paper. Acetone was evaporated using a rotatory evaporator cooled with dry-ice and ethanol and the aqueous phase containing “wet” pigments was stored. All organic solvent evaporation steps were performed in a fumehood. Pigments were extracted from the “wet” material by two washes with diethyl ether, using a separatory funnel to separate the aqueous from the organic (pigment containing) phase. At this stage it was important to saturate the aqueous phase with solid NaCl to help the phase separation. Typically, ~5 l of diethyl ether were need to extract all pigments. The organic solvent was then removed using a rotatory evaporator, so that the pigments (Chls and carotenoids) coat the round-bottom flask. These were dissolved in 100 ml acetone with sonication and 10 ml water and 10 ml dioxane were added. The mix was first stirred for 15 min at RT and then stored for 2 hr at -20 °C. During this time Chls precipitated and were separated from the carotenoids by filtration with filter paper. Carotenoids containing traces of lipids and Chls were immediately dried and stored at -20°C under nitrogen. Chls were retrieved from the filter paper by washing with diethyl ether. In order to remove the dioxane, the ether

solution was washed 4 times with water (without shaking). After removing the diethyl ether using the rotatory evaporator, the “wet” Chls were dried with Sephadex G-25 (GE Healthcare) resin powder. Chls were finally washed free of the resin with diethyl ether, filtered through filter paper, dried in the rotatory evaporator and stored under nitrogen at -20 °C.

### 3.4.3 Pigment concentration determination

Chl concentration was determined according to (Porra et al, 1989). Chl-containing samples were diluted in 80% acetone and  $A_{646.8}$ ,  $A_{663.6}$  and  $A_{750}$  were measured. The following equations were used to calculate [Chl *a*] and [Chl *b*] in µg/ml:

#### Equation 3-1

$$[\text{Chl } a] = 12.25 \cdot A_{663.6} - 2.55 \cdot A_{646.6}$$

#### Equation 3-2

$$[\text{Chl } b] = 20.31 \cdot A_{646.6} - 4.91 \cdot A_{663.6}$$

#### Equation 3-3

$$[\text{Chl } a + b] = 17.76 \cdot A_{646.6} + 7.34 \cdot A_{663.6}$$

The total carotenoid (xanthophylls and carotenes) concentration in 100% acetone in µg/ml was determined using the following equation (Lichtenthaler, 1987):

#### Equation 3-4

$$[\text{carotenoids}] = (1000 \cdot A_{470} - 1.82 \cdot [\text{Chl } a] - 85.02 \cdot [\text{Chl } b]) / 198$$

### 3.4.4 Pigment analysis by HPLC

A modified version of the protocol by (Gilmore & Yamamoto, 1991) was used for the analysis of pigment composition by reversed-phase HPLC. Pigments were extracted from samples with 2-butanol in a 1:1 ratio (typically 100 µl total volume) and centrifuged at maximum speed in a tabletop centrifuge for 3 min at 4 °C. ~20 µl of the organic phase containing the pigments were injected per

chromatographic analysis. The non-polar stationary phase consisted of a Synergi Hydro-RP column (Phenomenex; 4  $\mu$ m particle size; 250 mm  $\times$  4.6 mm), which was protected by a guard column (Phenomenex; SecurityGuard Cartridge C18 4x3.0 mm). A dual solvent system was used for each run (Table 3-11; Table 3-12). All solvents were HPLC grade and thoroughly degassed. All chromatograms were recorded at 440 nm. Quantification of each pigment was achieved by integration of chromatogram peaks and comparison of the respective areas with standard values for Lut, Neo, Vio, Zea, Chl *a* and Chl *b* (determined by L. Wilk, MPI of Biophysics). All runs were performed at RT.

**Table 3-11 - HPLC solvent composition**

Solvent A		Solvent B	
<i>Component</i>	<i>Volume ratio</i>	<i>Component</i>	<i>Volume ratio</i>
Acetonitrile	75	Methanol	4
Methanol	15	n-Hexane	1
0.1 M Tris-HCl, pH 8	4		

**Table 3-12 - HPLC run programme**

Time (min) <sup>a</sup>	Solvent A (%)	Solvent B (%)
0 to 2	100	0
3 to 18	100 to 50 <sup>b</sup>	0 to 50 <sup>b</sup>
18 to 20	50	50
20 to 26	0	100
26 until next run	100	0

<sup>a</sup> – constant flow rate at 1.5 ml/min

<sup>b</sup> - linear gradient

### 3.4.5 *In vitro* xanthophyll cycle

Thylakoid membranes in S-buffer from spinach or pea plants were resuspended in de-epoxidation buffer (Table 3-1) to a Chl concentration of

~0.5 mg/ml with (40 mM) or without ascorbate and incubated at room temperature with stirring. Reaction mixtures containing ascorbate were exposed to light during incubation, while samples without ascorbate were kept in the dark. The de-epoxidation reaction was followed by HPLC analysis of samples collected at different time points. This protocol is partially based on that described by (Ruban et al, 1999) and was optimised by varying ascorbate concentration, pH and temperature.

**Table 3-13 - De-epoxidation buffer composition**

Compound	Concentration (mM)
Sorbitol	350
MES, pH 5.5	25
MgCl <sub>2</sub>	5
D(+) - isoascorbic acid	40 or 0

### 3.4.6 Purification of native LHC-II

The procedure described below for LHC-II purification is based on previously published protocols (Burke et al, 1978; Kühlbrandt et al, 1983; Standfuss et al, 2005). In summary, thylakoid membranes in S buffer were centrifuged for 20 min at 18000 rpm on a Sorvall SS34 rotor. The pellet was homogenised in water to a Chl concentration of 0.5 mg/ml with a glass potter and Triton X-100 was added dropwise from a 10% stock solution to a final concentration of 0.5%. After 30 min of incubation at RT, samples were centrifuged for 30 min at 18000 rpm in the same rotor to pellet non-solubilised membranes. Linear sucrose gradients with a total volume of 50 ml per tube were prepared between 0.1 and 1.0 M sucrose with 0.05% Triton X-100 in Beckman Ti45 ultracentrifuge tubes using a gradient mixer and a peristaltic pump. ~10 ml of solubilised material were carefully loaded on each gradient. Gradients with loaded samples were then centrifuged overnight (~15 hours) at 38000 rpm on a Beckman Ti45 rotor. The red fluorescent, dark green band corresponding to trimeric LHC- II was harvested from the sucrose gradient and incubated with 300 mM KCl added as a solid for 30 min at 4 °C. This suspension was centrifuged for 15 min at 18000 rpm on a Sorvall SS34 rotor. The

pellets were washed twice with 100 mM KCl, and once with distilled water, repeating the same centrifugation step between washes. Finally, purified LHC-II pellets were solubilised in 1% NG to a Chl concentration around 5.5 mg/ml. When the Chl concentration was below 5.5 mg/ml, samples were concentrated using an Amicon device (Millipore, 100 kDa molecular weight cutoff). Samples were immediately stored at -20 °C.

### **3.4.7 Purification of native Zea-LHC-II**

For purification of native Zea-LHC-II, thylakoid membranes subject to de-epoxidation reaction (described above) were used. The same steps described in the previous section were followed. For spectroscopic studies, thylakoids incubated with the de-epoxidation buffer in the presence or absence of ascorbate were used to obtain Zea-LHC-II or Vio-LHC-II samples, respectively.

## **3.5 Heterologous expression and purification of recombinant protein**

### **3.5.1 Production of recombinant LHC-II**

The experimental procedures described in this and the two following sections follow the protocol established by Dr. H. Rogl in this department (Rogl et al, 1998; Rogl & Kühlbrandt, 1999; Rogl et al, 2002) and the modifications introduced by Dr. J. Standfuss, MPI of Biophysics (Standfuss & Kühlbrandt, 2004).

Frozen glycerol stocks of *E. coli* cells transformed with expression vectors carrying WT or mutant LHC-II DNA sequences were used to inoculate 100 ml of LB medium supplemented with the appropriate antibiotic. After overnight growth at 37°C with vigorous (250 rpm) shaking, 25 ml of the culture were used to inoculate 2 l of LB medium supplemented with the appropriate antibiotic in a 5 l culture flask. This culture was grown at 37°C with shaking until OD<sub>600</sub> was reached. At this point, IPTG was added to a final concentration of 1 mM to induce the recombinant protein expression. After 4 additional hours of growth, the cells were harvested by centrifugation (Beckmann JS 4.2 rotor, 4200 rpm for 20 min at 4°C) and either frozen at -20°C or immediately used for inclusion bodies purification.

### **3.5.2 Purification of recombinant LHC-II**

Cells pellet was resuspended in ~100 ml of water and a spatula tip of DTT and some DNase I crystals (Roche) were added. This suspension was first filtered through a nylon mesh (20 µm exclusion size) before cells were disrupted by several passages through a microfluidizer. Crude inclusion bodies were harvested as a pellet by centrifugation (Sorvall SS34 rotor, 19000 rpm for 10 min at 4°C). Inclusion bodies were then homogenised with a glass potter in 120 ml of detergent buffer (Table 3-14) and centrifuged as previously. The same procedure was repeated with Triton buffer. Finally, the washed inclusion bodies were resuspended in 40 ml Tris buffer and the protein concentration was determined as described above. Samples were then stored at -20°C.

**Table 3-14 - Buffers for LHC-II inclusion body isolation**

<b>Buffer</b>	<b>Component</b>	<b>Concentration</b>
<i>Detergent</i>	Tris-HCl, pH 7.5	20 mM
	NaCl	200 mM
	BME	10 mM
	EDTA	2 mM
	Deoxycholate	1%
	Nonidet P-40	1%
<i>Triton</i>	Tris-HCl, pH 7.5	20 mM
	EDTA	1 mM
	Triton X-100	5%
	BME	10 mM
<i>Tris</i>	Tris-HCl, pH 8.0	50 mM
	EDTA	1 mM
	BME	10 mM
<i>A<sub>280</sub></i>	Tris-HCl, pH 6.8	10 mM
	SDS	2%
	BME	1 mM

### 3.5.3 Refolding of recombinant LHC-II

For small scale refolding experiments, 0.7 mg of LHC-II inclusion bodies (WT or any of the variants) were solubilised in 1.4 ml of reconstitution buffer (Table 3-15), heating the mix for 5 min at 95 °C. When the mix had cooled to room temperature 150 µl of 100 mM BME were added and then cooled on ice. In the meantime, pigments (0.5 mg of Chl with Chl *a*/Chl *b* ratio ~3, and 0.15 mg of total thylakoid carotenoids) were dissolved in 150 µl ethanol and then added to the apoprotein mix. Samples were returned to ice for 20 min and then 15 µl of OG stock solution (10%) were added. Finally, dodecylsulphate was removed by precipitation by addition of 200 µl of 3 M KCl. The refolded LHC-II monomers were retrieved after 5 min centrifugation in a tabletop centrifuge at maximum speed. Samples were either stored at -20 °C or immediately used for further purification and in-column trimerisation.



Trimerisation of refolded LHC-II monomers was induced on the column, after binding LHC-II monomers to immobilised Ni<sup>2+</sup> on a chromatographic matrix (Chelating Sepharose from GE Healthcare). Refolded monomers were loaded onto the column (pre-washed with 2 column volumes of 50 mM Tris-HCl buffer, pH 7.5 to remove leaky Ni<sup>2+</sup> ions) and the bound monomers were washed with 1 column volume each of OG buffer and TX buffer. Elution from column was then initiated with elution buffer and all green material was collected. Sucrose gradients (20.5% sucrose, 50 mM Tris 7.5, 0.05% DDM) prepared by one single freeze-thaw step were used to separate free-pigments, refolded monomers and refolded trimers. Ultracentrifugation was run at 40000 rpm for 20 hr at 4 °C on a Beckmann SW40 swing-out rotor. Samples harvested from sucrose gradients were stored at -20 °C.

**Table 3-15 - Buffers for LHC-II refolding**

Buffer	Component	Concentration
Reconstitution	Tris-HCl, pH 9.0	100 mM
	LDS	2 %
	Sucrose	12.5%
OG	Tris-HCl, pH 9.0	100 mM
	OG	1%
	Sucrose	12.5 %
TX	Tris-HCl, pH 7.5	100 mM
	Triton X-100	0.05%
	PG	0.1 mg/ml
Elution	Imidazole, pH 7.5	300 mM
	DDM	0.1 %

#### 3.5.4 Purification and refolding of recombinant Zea-LHC-II

Refolded Zea-LHC-II was obtained by the protocol described above. In addition, Zea-enrichment was promoted by incubation of refolded monomers with Zea dissolved in a small volume (100 µl) of ethanol. The mix was kept on ice for 20 min before being applied to the Ni<sup>2+</sup> affinity column as described above.

### **3.5.5 Production of recombinant VDE in *Escherichia coli* cells in inclusion bodies**

For expressing VDE as inclusion bodies, 100 ml of LB medium supplemented with Amp and Cam were inoculated with a glycerol stock of RosettaBlue cells containing a VDE expression plasmid. These cultures were grown overnight at 37 °C with vigorous shaking. 50 ml from these cultures were used to inoculate 2 l of LB medium with the same antibiotics. The cultures were grown at 37 °C until  $A_{600} \sim 0.6$  and IPTG was added to a final concentration of 1 mM. The culture was further grown for 2-3 hours and harvested by centrifugation (Beckmann JS 4.2 rotor, 4200 rpm for 20 min at 4°C). Cells were stored at -20 °C for later use.

### **3.5.6 Production of recombinant VDE in *Escherichia coli* cells in soluble form**

For expressing VDE in soluble form, 100 ml of LB medium supplemented with Amp and Cam were inoculated with a glycerol stock of Rosetta-gami cells containing a VDE expression plasmid. These cultures were grown overnight at 37 °C with vigorous shaking. 50 ml from these cultures were then used to inoculate 2 l of TB medium with the same antibiotics (typically, 12 l of culture were used in each large-scale expression experiment). The cultures were grown at 37 °C until  $A_{600} \sim 1$  and the temperature was reduced to 25 °C. After cooling, IPTG was added to a final concentration of 0.1 mM. The culture was further grown overnight and harvested by centrifugation (Beckmann JS 4.2 rotor, 4200 rpm for 20 min at 4°C). Cells were stored at -20 °C for later use.

### **3.5.7 Purification of recombinant VDE purification under denaturing conditions**

VDE inclusion bodies were isolated as described for LHC-II (Section 3.5.2). The inclusion bodies were solubilised for 1 h at room temperature in unfolding buffer (Table 3-16) containing 8 M urea or 6 M guanidinium chloride. The protein concentration during unfolding was typically around 0.5 mg/ml. Samples were centrifuged (Beckmann Ti45 rotor, 30000 rpm for 50 min at 4 °C) and the supernatant was incubated at room temperature with Sigma His-Select Nickel Affinity gel in a Falcon tube with gentle mixing. The suspension was loaded onto an empty column and the flow-through was collected. The column material with

---

bound proteins was washed with washing buffer. Specifically bound proteins were eluted with elution buffer. To completely elute strongly bound proteins, additional elution steps were performed with elution buffer supplemented with imidazole (250 and 500 mM).

**Table 3-16 - Buffers for VDE purification under denaturing conditions**

Component	Unfolding buffer	Washing buffer	Elution buffer
Urea / Guanidinium chloride	8 M / 6 M	8 M / 6 M	8 M / 6 M
NaCl	200 mM	200 mM	200 mM
Phosphate buffer	100 mM, pH 8.0	100 mM, pH 6.3	100 mM, pH 4.5
TCEP	2 mM	2 mM	2 mM

### 3.5.8 Purification of recombinant VDE under native conditions

Frozen cells were suspended in 100 ml of buffer W (Table 3-17) supplemented with protease inhibitors cocktail and a DNase I from Roche and filtered through a nylon mesh to remove large aggregates. Cells were broken by 6 passages through a microfluidizer (Microfluidics Corporation). The suspension of broken cells was first centrifuged at low speed (Sorvall SS-34 rotor, 19000 rpm for 30 min at 4 °C) to remove debris and then at high speed (Beckmann Ti40 rotor, 40000 rpm for 1 h at 4 °C). The supernatant was split in 10 ml aliquots and each aliquot was loaded onto a Strep-tactin column (1 ml of column material) pre-equilibrated in buffer W. The column was then washed with 5 column volumes of buffer W without EDTA. Elution was initiated by adding 6 times half a column volume of buffer E. The column was finally regenerated with buffer R and stored in the same buffer at 4 °C.

Recombinant VDE eluted from the Strep-tag affinity purification was further purified by His-tag affinity chromatography. The eluted fractions from the Strep-tag affinity purification containing VDE were incubated for ~30 min with 1 ml of Sigma His-Select Nickel Affinity gel, which was pre-equilibrated with buffer W (Table 3-17). This suspension was loaded onto an empty column and the

flow-through was collected. The column was then washed with 6 column volumes of buffer W. Elution of bound VDE was initiated using a set-gradient of increasing imidazole concentration (typically 15, 25, 50, 100, 250 mM on in buffer W without EDTA). Purified VDE was then concentrated on a spin column with a molecular weight cut-off of 30 kDa. Imidazole was removed by washing the concentrated samples on the spin column with imidazole-free buffer.

**Table 3-17 - Buffers for VDE purification under native conditions**

<b>Component</b>	<b>Buffer W</b>	<b>Buffer E</b>	<b>Buffer R</b>
NaCl	150 mM	150 mM	150 mM
Tris-HCl, pH 8.0	100 mM	100 mM	100 mM
EDTA	0 or 1 mM	-	1 mM
TCEP	2 mM	2 mM	2 mM
Desthiobiotin	-	2.5 mM	-
HABA	-	-	1 mM

The Thrx-ArabVDE fusion was purified by Ni-affinity chromatography using the same protocol described above on the second purification step of ArabVDE.

---

## 3.6 Protein characterization

### 3.6.1 Size exclusion chromatography

Analytical size exclusion chromatography (SEC) was performed at room temperature on an Ettan chromatography system (GE Healthcare) using a Superdex 200 or Superose 6 column (both from GE Healthcare). The flow rate was kept constant at 50  $\mu$ l/min. All buffers were filtered (0.2  $\mu$ m exclusion size) and degassed before runs. The buffers used to determine the dependence of the LHC-II aggregation state on pH and detergent are described in Table 3-18.

**Table 3-18 - Buffers used for SEC with LHC-II**

Buffer	Composition
1	0.3% NG, 50 mM Tris-HCl, pH 7.5
2	0.05% DDM, 50 mM Tris-HCl, pH 7.5
3	0.3% NG, 50 mM MES, pH 5.3
4	0.05% DDM, 50 mM MES, pH 5.4

### 3.6.2 VDE activity assay

The classical dual-wavelength method developed by Yamamoto (Yamamoto, 1985) was optimised to make use of 96-well microplates. The de-epoxidation reaction was monitored spectrophotometrically by following  $A_{502}-A_{540}$  with time.  $A_{502}-A_{540}$  is proportional to the amount of Zea present in the reaction mixture. The original protocol with a reaction volume of 3 ml was scaled down to 200  $\mu$ l. The compositions of the reaction mixture in the 96-well plate format and in the original protocol are given in Table 3-19. Vio (CaroteNature) and MGDG (Lipid Products) were dissolved in methanol. All reagents except sodium ascorbate were mixed and pipetted into the 96-well plate.  $A_{502}-A_{540}$  was then measured until a stable baseline was obtained. The reaction was initiated by adding sodium ascorbate to the reaction mixture. All assays were performed at room temperature.

**Table 3-19 - VDE activity assay composition**

Reagent	Stock concentration	Volume ( $\mu$ l)	
		96 wells plate	Cuvette
Vio	10 $\mu$ M	10	50
MGDG	270 $\mu$ M	10	50
Sodium citrate, pH 5.1	0.2 M	100	500
VDE	variable	0 - 10	0-50
Water	-	to 200	to 1000
Sodium ascorbate	3 M	4	20

### 3.6.3 Preparation of LHC-II aggregates

The general strategy to obtain LHC-II aggregates of native or refolded complex was to decrease the detergent concentration well below its CMC, most often by dilution. When the relative fluorescence yield of solubilised and aggregated samples was to be compared, the original samples were diluted equally in buffer with and without detergent. To enhance aggregation, KCl or MgCl<sub>2</sub> were added to the aggregation buffers. Aggregates of native LHC-II from pea were prepared by 100-fold dilution of highly concentrated samples in 50 mM MgCl<sub>2</sub>. Precipitated protein was collected by centrifugation, washed twice in 50 mM MgCl<sub>2</sub> and finally resuspended in buffer (50 mM Tris-HCl, pH 7.5; 10 mM MgCl<sub>2</sub>). The same protocol was used to obtain aggregates of refolded LHC-II (WT and mutants). In addition, refolded LHC-II aggregates were also prepared by overnight incubation of the samples with BioBeads (BioRad).

## 3.7 X-ray crystallography

### 3.7.1 LHC-II crystallisation

The work described in this thesis includes experiments aiming at finding new LHC-II crystallisation conditions and other experiments aiming at reproducing previously established crystallisation conditions for spectroscopic measurements. For the first aim, commercial crystallisation screens were used, notably the MemStart, MemSys and MemGold screens from Molecular Dimensions and the MbClass and MbClass II screens from Qiagen. All crystallisation trials were performed in 96-well plates in hanging drop or sitting drop using the Mosquito crystallisation robot. Typically, the crystallisation droplets were prepared using 400 nl of protein solution plus 400 nl of crystallisation solution, while the crystallisation well contained 100  $\mu$ l of crystallisation solution. Promising conditions were scaled up to 24-well plates. Different temperatures were tested.

The type-I LHC-II crystals that were used to solve the X-ray structure of the pea complex (Standfuss et al, 2005), were reproduced for spectroscopic measurements. The crystallisation solution composition is given in Table 3-20. The Chl concentration of the samples used in these crystallisation experiments was adjusted immediately prior to setting the crystallisation drops to 4.25-4.75 mg/ml, while the detergent (NG) concentration was screened around 1.85% in 0.05% steps. Crystallisation droplets were prepared by mixing 1  $\mu$ l of protein stock solution with 1  $\mu$ l of crystallisation solution and equilibrated in hanging drop against 1 ml of crystallisation solution. Cubic crystals of pea LHC-II for spectroscopic measurements were grown by Prof. W. Kühlbrandt (MPI of Biophysics), as described (Kühlbrandt, 1987).

**Table 3-20 - Type-I pea LHC-II crystallisation conditions**

<b>Component</b>	<b>Concentration</b>
PEG 350 MME	12 – 18%
Glycerol	10 – 20%
MES, pH 5.4 – 5.6	50 mM
NaCl	20 mM

---

### **3.7.2 Cryoprotection and freezing of LHC-II crystals**

LHC-II crystals handling, cryo-protection and freezing were critical steps prior to the spectroscopic measurements at the Cryobench. The type-I crystals appeared after 2 weeks and grew to a final size of around  $150 \times 150 \times 15 \mu\text{m}^3$  within 4 weeks. These thin hexagonal plates were harvested within 2-4 weeks. The cryo-protectant had a similar composition to the mother liquor of the crystallisation experiments (Table 3-20) but both the glycerol and PEG 350 concentrations were increased to 20%. Each crystal was washed at least twice in pigment-free droplets of cryo-protectant, after which they were flash frozen in liquid nitrogen or immediately used for room-temperature measurements.

### **3.7.3 Diffraction experiments**

LHC-II crystals were tested for X-ray diffraction at the PXII beamline of the Swiss Light Source (Villigen, Switzerland) and beamlines BM16 and ID14-eh3 of the ESRF (Grenoble, France). The diffraction quality was judged from 2 or 3 images  $30^\circ$  or  $45^\circ$  apart from one another. On a very few occasion, data sets covering  $180^\circ$  rotation of the crystal in  $0.5^\circ$  steps were recorded. All experiments were performed at 100 K on pre-frozen crystals.

### **3.7.4 Data processing**

X-ray diffraction data were analysed and processed using the programs XDS (Kabsch, 1993) and MOSFLM (Leslie, 1992).

---



## 3.8 Structure analysis and modelling

### 3.8.1 Comparison of structures

The atomic coordinates of the spinach (Liu et al, 2004) and pea (Standfuss et al, 2005) LHC-II X-ray structures were obtained from the PDB (PDB codes 1RWT and 2BHW, respectively). The LHC-II trimer constituted by chains C, E and H in the asymmetric unit of the spinach crystal structure was used for comparison with the pea LHC-II structure. Superposition of the two structures was performed using SUPERPOSE (Krissinel & Henrick, 2004), from the CCP4 suite of programs (Collaborative, 1994). The rms deviations between all atoms, the protein main chain, all pigments or the aromatic rings of the Chls from the two superposed structures were calculated separately, matching corresponding atoms from each structure to perform the superposition. All figures showing the superposed spinach and pea LHC-II structures were prepared with PyMOL.

### 3.8.2 Modelling LHC-II – LHC-II interaction *in vivo*

The packing of the type-I pea LHC-II crystal structure was used as a starting point to model the interaction between two LHC-II trimers in the thylakoid membrane. The program COOT (Emsley & Cowtan, 2004) was used to create the model. Two trimers were generated using a symmetry operator of the C2 space group, so that they were side by side in an up and down arrangement. The distances between closest atoms from each trimer were measured. One of the trimers was then turned by 180° in an axis parallel to the hypothetical membrane, so that both trimers were then in the same orientation relatively to the membrane. This trimer was then first translated in Z direction to have both trimers at the same height in the hypothetical membrane, and then in X and Y directions so that the distance between closest atoms from each trimer were roughly similar to the original crystal packing and no major clashes between trimers were observed. Figures from the final model were prepared with PyMOL.

## **3.9 Electron microscopy procedures**

### **3.9.1 Freeze-fracture of LHC-II crystals**

Single LHC-II crystals were harvested from the crystallisation droplets, washed in cryoprotectant and placed between two small copper plates serving as sample holders. This crystal sandwich was then rapidly plunged in liquid ethane. Freeze-fracturing was carried out with a BAF 060 machine (Bal-Tec, Principality of Liechtenstein) at a temperature of  $-140\text{ }^{\circ}\text{C}$  and a pressure of  $2 \times 10^{-7}$  mbar. After the fracture, the sample was shadowed with platinum/carbon followed by pure carbon shadowing for reinforcing the replica which then after cleaning was analyzed in an EM208S electron microscope (FEI Company). Images were collected on a 1K x 1K slow scan CCD camera (TVIPS, Gauting, Germany). The author performed the crystal preparation and handling steps and Dr. W. Haase (MPI of Biophysics) performed all subsequent freeze fracturing and imaging steps.

---

## **3.10 Solutions spectroscopy**

### **3.10.1 Absorption spectra**

Room temperature absorption spectra of LHC-II (native or refolded) were recorded on a Lambda Bio 40 spectrophotometer (Perkin Elmer) with 1 cm pathlength quartz cuvettes. Absorption spectra were measured typically between 400 to 700 nm with a 1 nm bandwidth. All spectra were corrected for solvent absorption using blank samples.

### **3.10.2 Fluorescence spectra at room temperature**

All room temperature fluorescence spectra were performed using a Hitachi F-4500 fluorometer and quartz cuvettes with 1 cm pathlength for excitation light and 0.5 cm pathlength for emission light. Excitation and emission slits were set at 5 and 2.5 nm, respectively, and the scan speed was 60 nm/min. Typically, the excitation light was set at 420, 470 or 441 nm, in order to preferentially excite Chl *a*, Chl *b* or both, respectively. Emitted fluorescence was recorded between 640 and 740 nm. All spectra were measured in replicate (usually in duplicate) and averaged to reduce noise in the data. When the relative fluorescence yield was to be compared, the samples were diluted so that they had the same optical density at the excitation wavelength.

### 3.11 Single-crystal spectroscopy

All single crystal spectroscopic measurements were performed at the Cryobench of the European Synchrotron Radiation Facility (ESRF), Grenoble, France (Figure 3-3)(Royant et al, 2007). The description of the system here presented is only meant to highlight the main features that were critical to obtain the results included in this thesis. A computer script was written to assist the visualization of the recorded absorbance and fluorescence spectra and fluorescence decays (see Appendix).



**Figure 3-3 - Overview of the Cryobench laboratory at the ESRF.**

The Cryobench system can be seen as an adapted X-ray diffractometer, including a computerised goniometer head with a magnetic pin holder, a cryostream system to keep the measured crystal in cryogenic conditions and a video camera used to align the crystal (Figure 3-4). In addition to this, 3 microscope objectives are used to focus the incoming light onto the crystal and the light leaving the crystal (fluorescent or non-absorbed photons) onto the detection device. Optical

---

fibers are used to lead the light to and from the objective lenses (Figure 3-4). The size of the focal spot depends on the width of the optical fibers. Typically, 100  $\mu\text{m}$  optical fibers were used, which gave a focal spot of  $\sim 15 \mu\text{m}$  at the sample position. Obtaining such a small focal spot, comparable to the thickness of the thicker crystals, was critical for the fluorescence measurements. Fine-tuning of the micrometric screws of the goniometer head enabled precise positioning of the crystals in all 3 directions. The computerised motor of the goniometer head was used for precise rotation of the crystals relative to the direction of the light rays.

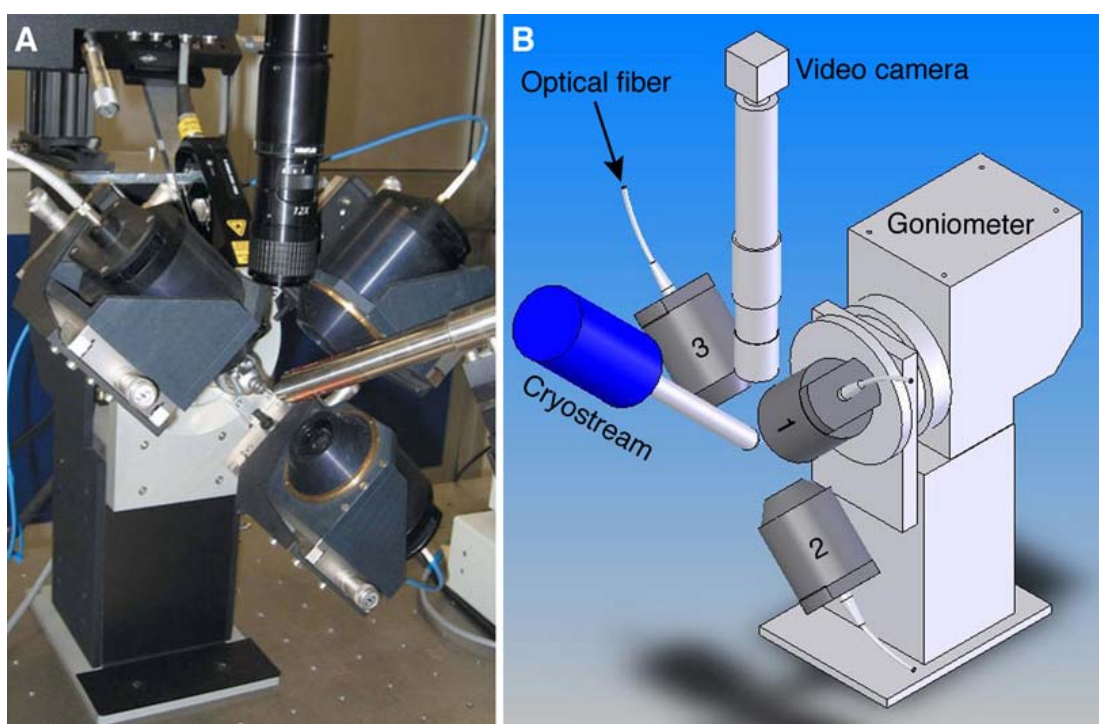


**Figure 3-4 - Close-up of the Cryobench optical system.**

The optical system of the Cryobench resembles a common X-ray diffractometer, in which the X-ray source is substituted by a UV/VIS light source and a set of objective lenses is used to focus the light. (A) Photo of the optical system; (B) Schematic representation of the system. 1, 2 and 3 indicate the objective lenses. Adapted from (Royant et al, 2007).

For measurements at 100 K, pre-frozen crystals were quickly transferred from the cryo-vials to the magnetic holder on the goniometer head. Alternatively, fresh crystals harvested from the crystallization plate and washed in cryo-protectant solution to remove free pigments were transferred directly to the goniometer head, where they were rapidly frozen in the cryo-stream. Some crystals were recovered from the optical system with liquid nitrogen filled cryo-vials for further X-ray diffraction experiments. To measure LHC-II samples in solution under the same

experimental conditions as the crystals, cryo-loops thoroughly washed in ethanol and water were dipped in 1  $\mu$ l droplets of protein sample diluted in cryo-protectant. To prevent unwanted aggregation, these cryo-protectant solutions were similar to those used to cryo-protect the crystals but PEG 350 was removed and the glycerol concentration was increased to 40%. The small volume suspended in the cryo-loop was then flash frozen directly at the goniometer head or plunged in liquid nitrogen and then transferred to the goniometer head. The thickness of the solution film was roughly controlled by removing the cryo-loop from the droplet at different angles (thicker when removed flat, thinner when removed sideways). Ice formation was evaluated by visual inspection of the frozen solution on the cryo-loop with the video camera.

Room temperature measurements at the Cryobench required the use of a special sample holder to place the samples (protein solution or crystal in buffer solution) and to prevent dehydration (Figure 3-5; (Royant et al, 2007)). In brief, a small ( $\sim 0.5$   $\mu$ l) droplet of protein solution or cryo-protectant, in which a single crystal was placed, was pipetted onto the centre of a glass cover slide. A ring of silicone grease was spread around the sample and another cover slide was placed on top of the ring, avoiding direct contact with the droplet, so that a small hermetic chamber was created containing the sample. This sample-cover slide sandwich was placed on an adapted magnetic pin holder, which was attached to the goniometer head. The sample was aligned in the optical system with the help of the video camera. A disadvantage of this apparatus was that crystals could not be rotated to optimise their orientation or to compensate for drift in the droplet.

---

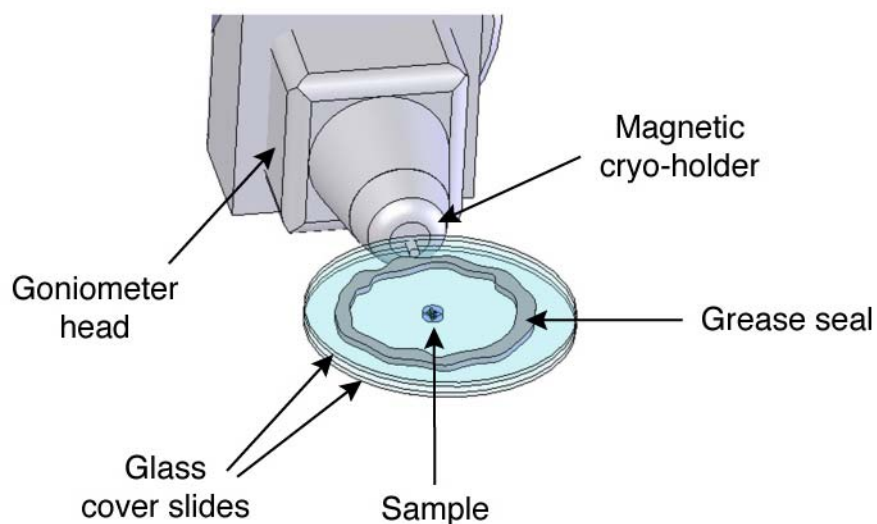


**Figure 3-5 - Sample holder for room temperature experiments at the Cryobench.**

A crystal in a droplet of mother liquor or a small droplet of sample in solution is placed at the centre of the glass cover slide. A hermetic chamber is created by a ring of silicon that holds the two cover slides. Adapted from (Royant et al, 2007).

### 3.11.1 Fluorescence spectra of single LHC-II crystals

The three objective lenses of the Cryobench system allowed fluorescence measurements in two alternative geometries (Figure 3-6). This was critical to identify and characterise self-absorption artefacts. In practical terms, measurements with detection at  $90^\circ$  and  $270^\circ$  were set up by connecting the detector of the spectrophotometer to either objective 2 or 3 (Figure 3-4), while the excitation laser was focussed onto the crystal through objective 1.

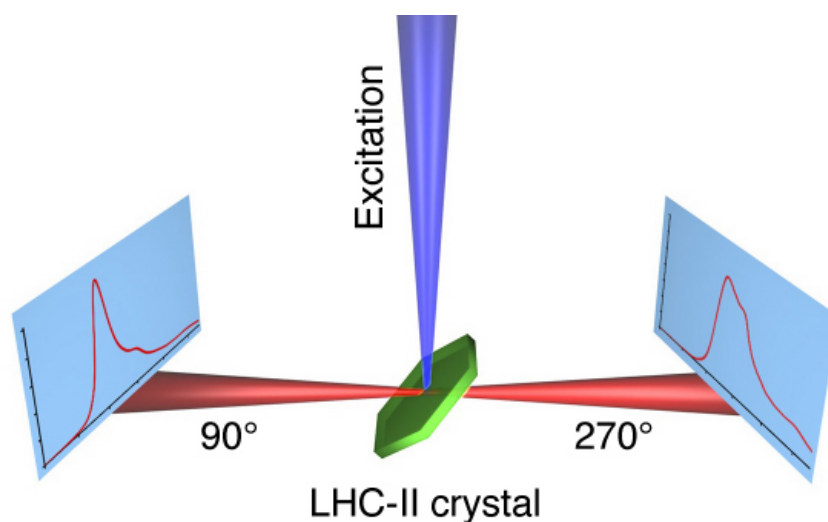


**Figure 3-6 - Geometry of fluorescence measurements with single crystals.**

Fluorescence measurements at the Cryobench can be performed with detection at 90° or 270°, with respect to the excitation laser.

In all fluorescence measurements a 440 nm laser beam focused to  $\sim 15 \mu\text{m}$  was used for excitation. A long pass filter, which blocks all light at wavelengths shorter than 550 nm, was inserted in the objective connected to the spectrophotometer detector. This was important to prevent scattered excitation light from reaching the detector. The variation of the fluorescence spectra with the precise geometry of the measurement, including detection geometry, crystal rotation and position of the focussed laser on the crystal, were monitored in real time. The acquisition time was adjusted in each individual measurement, ranging roughly between 5 and 200 ms per read. The entire spectral range between  $\sim 200$  and  $\sim 1100$  nm was recorded. Final fluorescence spectra are averages over 10 to 20 individual reads.

### **3.11.2 Absorption spectra of single LHC-II crystals**

A deuterium-tungsten white light source was used to measure absorption spectra of LHC-II crystals and solutions. Initially, the photons detected by the spectrophotometer in the absence of sample were used to set the spectrum corresponding to 100% of transmission (no absorption). This spectrum reflects the spectral shape of the light source, and serves as a blank for the absorption spectra of samples. The crystals or solutions were then placed in the optical system and irradiated with the white light. Absorption spectra were recorded from the



difference between the spectra with and without sample. Due to the very high optical density of the LHC-II crystals, the acquisition time of the measurement with the crystal had to be increased in order to improve the signal-to-noise ratio of the data. For this reason, the baseline of the crystals absorption spectra had to be offset and, therefore, the determined absorbance values are not on an absolute scale. Similarly to the fluorescence emission spectra, the final absorption spectra are averages of 10 to 20 individual reads.

### 3.11.3 Time-correlated single photon counting

Fluorescence lifetime measurements were performed using time-correlated single-photon counting (TCSPC). As for the fluorescence spectra measurements, a 440 nm laser with a  $\sim 15 \mu\text{m}$  focal spot was used for excitation. Histograms were recorded until at least  $10^4$  photons had accumulated on the channel of highest intensity. While recording the fluorescence spectra, neutral filters of various optical densities were inserted in addition to the long pass filter used, to adjust the amount of photons detected by the photomultiplier during the TCSPC measurements. In the absence of a monochromator, the wavelength dependence of the fluorescence lifetimes was analysed by placing band-pass filters with 10 nm bandwidth in front of the detector, sampling the 670 nm to 750 nm range in 10 nm intervals. 10 histograms were recorded in each experiment. TCSPC data were individually fitted to exponential decays by Dr. A. Royant using either FluoTimeFit (Royant et al, 2007) or PeakFit (Seasoft Software Inc., San Jose CA). The number of exponentials used and the quality of the fit to the fluorescence decays was monitored by  $\chi^2$  statistics. A global analysis procedure was not available to determine accurate decay-associated spectra. However, as the number of fitted decay components was limited to 3 and their lifetime was approximately uniform throughout the emission spectrum, approximated decay-associated spectra were plotted using the amplitudes of the decay components in each of the 10 nm-wide intervals.

## 4 LHC-II BIOCHEMISTRY

The main goal of the biochemical work with LHC-II was to obtain new preparations, within the scope of NPQ, for spectroscopic and crystallisation studies. Emphasis was placed on the preparation of Zea-LHC-II, using both native and recombinant complexes. In the first case, purifying LHC-II from the *Arabidopsis thaliana* mutant *npq2*, which is deficient in Vio and naturally enriched in Zea-LHC-II, seemed like a very promising approach. For this reason, an effort was made to establish optimal growth conditions for these plants and to adapt the previously described LHC-II purification protocols for the purification of LHC-II from these plants. Alternatively, *in vitro* protocols that yielded Zea-LHC-II have been established or optimised. Another important part of the biochemical work included refolding of LHC-II mutants to target the role of specific pigments in LHC-II fluorescence quenching. Finally, the influence of the pH, another important parameter within NPQ, on the aggregation state of LHC-II was addressed.

---

## 4.1 Results

### 4.1.1 LHC-II purification from pea plants

A reliable protocol for obtaining large amounts of highly pure native LHC-II was essential for the progress of the work here presented. Such a protocol (Section, 3.4.6; Burke et al, 1978; Kühlbrandt et al, 1983; Standfuss et al, 2005) was applied routinely to purify pea LHC-II, mostly for crystallisation trials but also for spectroscopic studies. Figure 4-1 shows a Coomassie stained SDS-PAGE gel with several preparations of purified pea LHC-II. In all lanes, one major band around 25 kDa is observed. Very faint bands are present at higher molecular weights for some preparations. These correspond most likely to LHC-II trimers that have not been disrupted by the SDS-PAGE sample buffer. There is no evidence for the presence of other contaminants, within the resolution of the gel, or the sensitivity of the Coomassie (Figure 4-1) or silver staining (not shown). The only exception is the *Arabidopsis* sample (lane 7 in Figure 4-1), for which a faint band at ~20 kDa can be distinguished. The yield of the purification was somewhat variable, mostly due to the efficiency of the pea thylakoid solubilisation. Typical pea LHC-II purifications used 200 – 300 g of pea leaves, yielding the equivalent of at least 10 mg of Chl. The Chl *a*/Chl *b* (mg/mg) ratio in purified pea LHC-II was  $1.37 \pm 0.06$ .

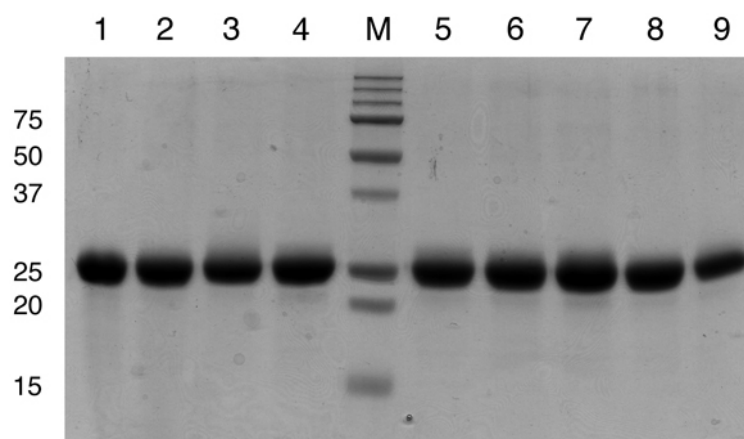


**Figure 4-1 - SDS-PAGE of purified native LHC-II**

Coomassie stained SDS-PAGE gel of purified native LHC-II samples. M, molecular weight standards (in kDa). 1 to 9 correspond to different LHC-II preparations. All samples are pea LHC-II preparations except sample 7, which is purified *Arabidopsis* LHC-II. All pea LHC-II samples were purified from pea leaves, except sample 6, which was deliberately purified from pea leaves and stalks.

### **4.1.2 *Arabidopsis* plant growth**

Plant growth was initiated in dedicated facilities at the MPI for Plant Breeding Research (Cologne) or at the Biocenter of the JW Goethe University (Frankfurt) and then transferred to the plant growth room in-house at the MPI of Biophysics. Plants grown in soil were mainly used to obtain seeds from the different variants. Hydroponic cultures were used to obtain large amounts of plant leaves for LHC-II purification.

#### **4.1.2.1 Plants grown in soil**

Seeds from *Arabidopsis* WT, *npq1* and *npq2* variants, obtained from ABRC, were first sown in soil and grown under a long daylight regime, at the MPI for Plant Breeding Research. This light regime induced flowering of the plants roughly 2 months after sowing the seeds (Figure 4-2). It is evident from the figure that the *npq2* mutant plants grew much less and appear less robust than the other variants. In all three cases, the plant leaves were small, not providing sufficient biological material to be used for purifying LHC-II. Shortly after this stage, the seeds were collected for all three variants. Once again, the *npq2* mutant plants developed a much smaller number of seeds than the other two variants (not shown).

---

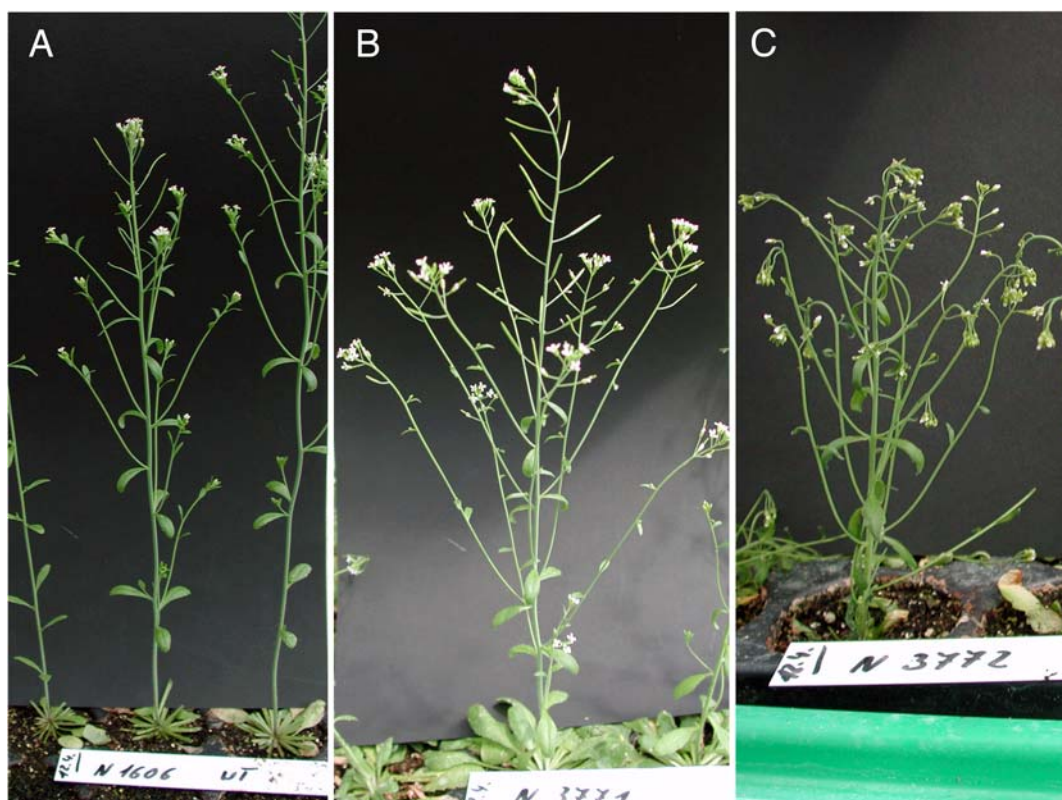


**Figure 4-2 - *Arabidopsis* plant grown in soil at the MPI for Plant Breeding Research.**

~2 month old *Arabidopsis* (A) WT, (B) *npq1* and (C) *npq2* mutant plants growing in soil under a long daylight regime.

In order to increase the amount of leaf material, the next generation of plants was grown under a short daylight regime. These plants were grown in a growth room at the Biocenter of the JW Goethe University. Figure 4-3 shows the three *Arabidopsis* variant plants, at roughly the same age as those shown in Figure 4-2. The size of the plant leaves is noticeably larger when the plants are subjected to the short daylight regime. Furthermore, only a very small number of these plants began flowering, which is another important difference from the long daylight regime plants.

A common observation in both types of light regime was the significantly larger size of the leaves from WT and *npq1* plants compared to *npq2* plants. In fact, Figure 4-3 further shows that not only are the leaves smaller in the *npq2* mutant plants, but the leaf shape is also different. While the other two variants had broad leaves with smooth, round edges, the *npq2* mutant leaves were narrower and their edges were spiny.



**Figure 4-3 - *Arabidopsis* plant grown in soil at the JW Goethe University.**

~2 month old *Arabidopsis* (A) WT, (B) *npq1* and (C) *npq2* mutant plants growing in soil under a short daylight regime. Comparison with the plants in Figure 4-2 shows the remarkable influence of the light regime on plant development.

---

#### 4.1.2.2 Plants grown hydroponically

The first method used to grow *Arabidopsis* hydroponically was described by Tocquin et al (Tocquin et al, 2003). Figure 4-4 shows how the plants developed within the first 2 weeks (see Figure 3-1 for comparison). At this stage, the plants grown in hydroponic medium or in soil show no noticeable difference in their development. However, differences became evident one month after sowing the plants (Figure 4-5). Those that were grown in agar-filled eppendorf tubes were much less developed, constrained by the available space within the tube. This method, in our implementation of its original description, is very convenient but did not yield sufficient leaf material for LHC-II purification.

The hybrid method, beginning growth of *Arabidopsis* plants on soil and then transferring them to hydroponic medium, turned out to be the best solution to obtain large amounts of leaves with a minimum of maintenance. The two week old plants grown in soil were transferred to hydroponics, supported on filter paper so that their roots were immersed in the hydroponic solution (Figure 3-2; Figure 4-4). After one month of growth, the plants growing by this hybrid method presented leaves that were about twice as large as those from plants grown solely on soil (Figure 4-5). This difference in leaf size was even larger when compared to plants grown hydroponically, which had leaves that were smaller by a factor of roughly 5. The plants grown by the hybrid method had already at this stage a size that could be used for LHC-II purification. The leaves of the *npq2* mutant plants grown by this method had the same characteristic spiny edges as seen before in plants grown on soil and were approximately half the size of those from WT plants.

All plants were harvested at an age of roughly 2 months. Figure 4-6 shows that the WT plants have the same large leaves that were observed in plants grown on soil under the short daylight regime (Figure 4-3). Note that the plants grown hydroponically were exposed to 10 hours of light per day, which corresponds to a short daylight regime. On the other hand, the *npq2* mutant plants did not achieve the same size as those grown on soil under the same light conditions. In addition, the *npq2* mutant plants showed indications of Chl bleaching in some leaves. It is not known if this phenomenon was caused by the brighter growth-room light or by some other physiological response to the *npq2* mutation. Nevertheless, this

phenotype was exclusive to the *npq2* mutant, i.e. neither the WT or the *npq1* plants presented the same Chl bleaching.

Overall, the switch from the long daylight regime to the short daylight regime resulted in a 5 to 6-fold increase in biological material usable for LHC-II purification. With the initial growth conditions in soil and long daylight regime, 10 *Arabidopsis thaliana* plants yielded 20 to 30 g of leaf material. After switching to short days and, in the case of WT plants, to growth in hydroponic medium, this yield was increased to ~150 g.

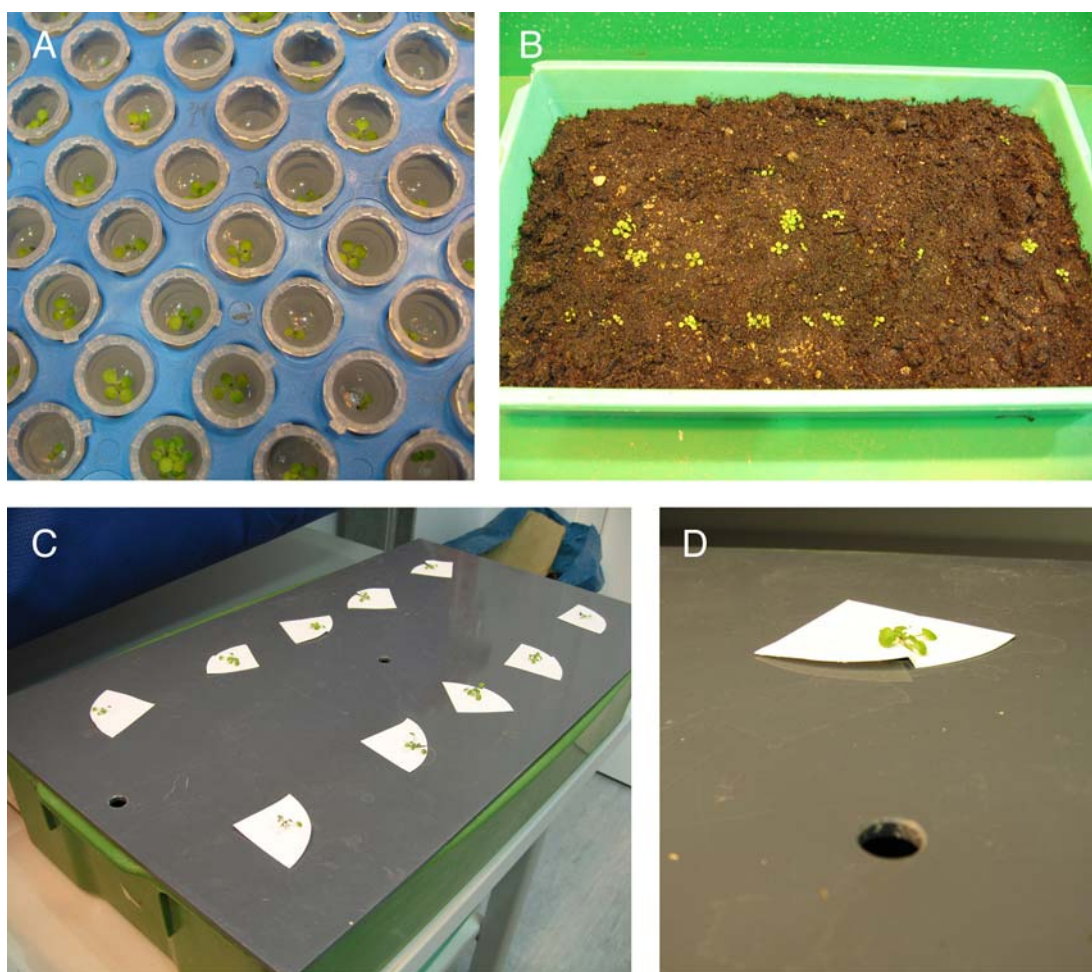


**Figure 4-4 - Two week old *Arabidopsis* WT plants.**

WT plants growing (A) in hydroponics, supported on low percentage agar and (B) in soil, two weeks after sowing the seeds. Plants grown in soil (B) were removed from the tray and transferred to hydroponics, supported on filter paper. (C) Overall view of a hydroponics tray; (D) Close-up of a single plant.

---



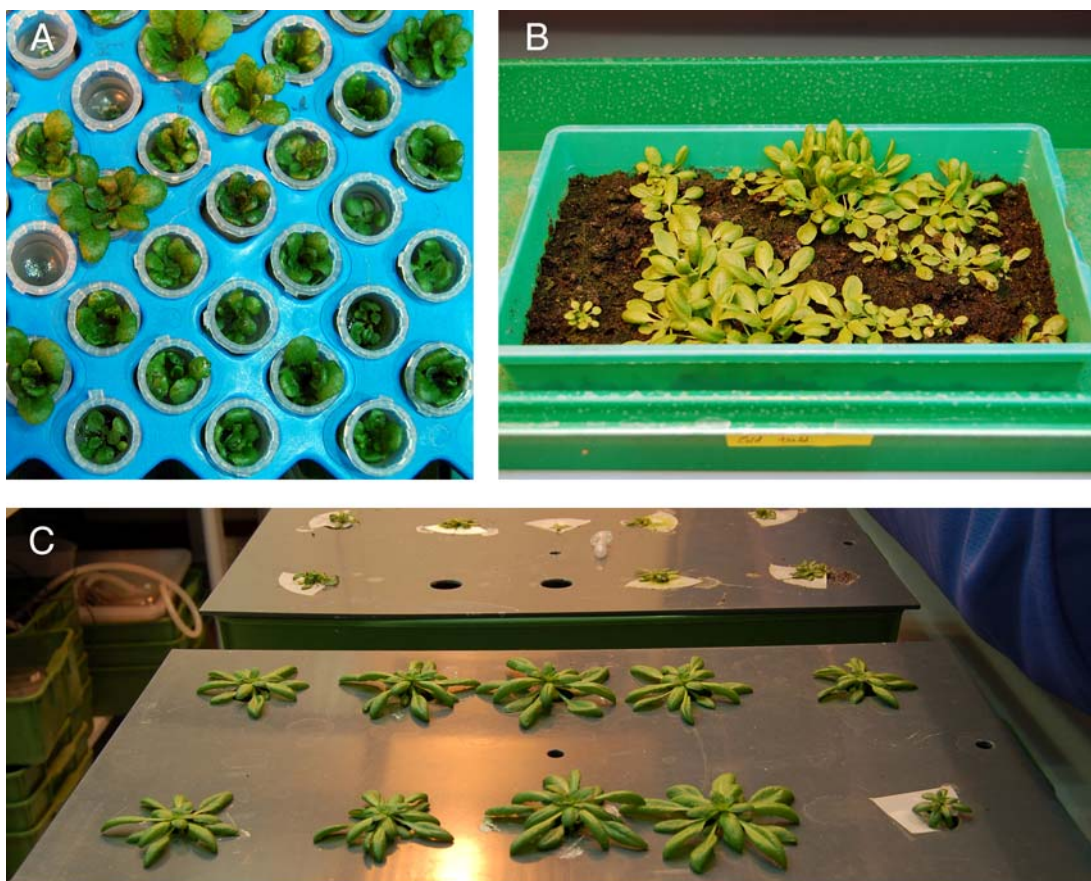


**Figure 4-5 - One month old *Arabidopsis* plants.**

One month old *Arabidopsis* WT plants growing (A) in hydroponics, supported on low percentage agar and (B) in soil and (C) in hydroponics, supported on filter paper. In (C) *npq2* mutant plants are shown in background.

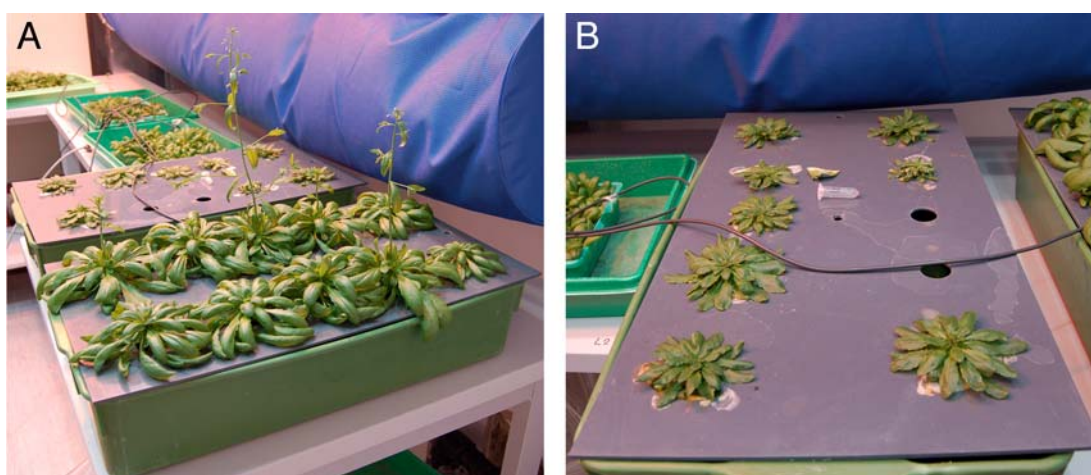


**Figure 4-6 – Two month old *Arabidopsis* plants grown hydroponically.**

The figure shows ~2 month old *Arabidopsis* (A) WT and (B) *npq2* mutant plants grown hydroponically. The WT plants have noticeably larger leaves and already present some flowers, while the *npq2* plants are less developed.

### 4.1.3 LHC-II purification from *Arabidopsis* WT plants

The original motivation for establishing a protocol for LHC-II purification from *Arabidopsis* was to use the *npq2* mutant to obtain sufficient amounts of Vio-less LHC-II to be used for crystallisation trials. As described in the previous section, the *npq2* plants grew to roughly half the size of the WT plants, correspondingly yielding half the amount of biological material for LHC-II purification. For that reason it was necessary to first establish the purification protocol using WT plants and then, if successful, apply it to the *npq2* plant leaves.

The protocol used to purify pea LHC-II for crystallisation (Burke et al, 1978; Kühlbrandt et al, 1983) was also used with WT *Arabidopsis* leaves. This method turned out to be very successful, yielding *Arabidopsis* LHC-II of the same high purity as routinely obtained with pea leaves. Assessment of the purified samples via SDS-PAGE reveals a single band at 25 kDa, with a green smear towards higher molecular weights (Figure 4-7 A). The green colour can only be attributed to the presence of Chls. The smear is therefore due to incomplete denaturation of LHC-II monomers, resulting in populations with different amounts of Chl attached to the protein. Western-blot analysis using an  $\alpha$ -Lhcb1 antibody revealed one single band at 25 kDa, ensuring that the purified product was indeed LHC-II (Figure 4-7 B).

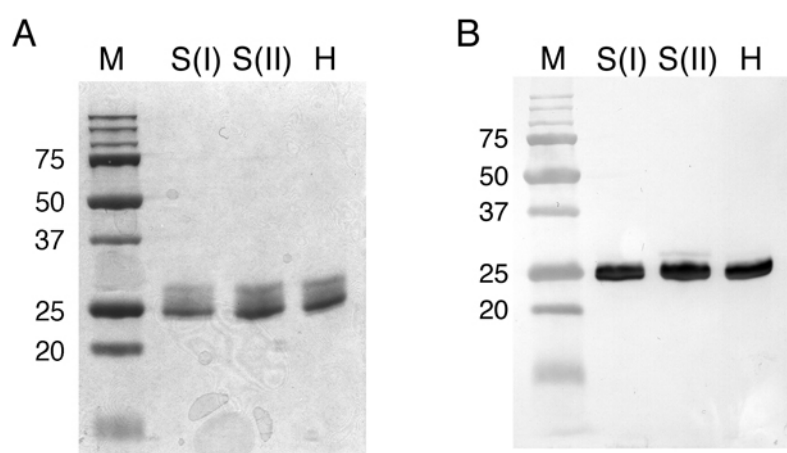


**Figure 4-7 - SDS-PAGE gel and Western blot of *Arabidopsis* LHC-II samples.**

(A) Coomassie stained SDS-PAGE gel of LHC-II samples purified from WT *Arabidopsis* plants grown in soil (S) and in hydroponics (H). I and II correspond to two different preparations. (B) Western blot of the same samples as in (A), using an  $\alpha$ -Lhcb1 (primary) antibody and an  $\alpha$ -rabbit (secondary) antibody coupled to alkaline phosphatase for detection. M, molecular weight standards (mass in kDa).

The Chl *a*/Chl *b* (mg/mg) ratio in purified LHC-II from *Arabidopsis thaliana* thylakoids was  $1.36 \pm 0.04$  as expected (Standfuss et al, 2005), and is identical to that usually obtained with a pea LHC-II purification (Section 4.1.1). A typical purification from 10 individual *Arabidopsis* plants yielded at least 2.5 mg of Chl, corresponding to  $\sim 500 \mu\text{l}$  of LHC-II at 5.0 mg/ml, which is the usual concentration of LHC-II samples used for crystallisation.

#### 4.1.4 Preparation of Zea-LHC-II

One of the main aims of this work was to purify LHC-II enriched in Zea. This is an absolute requirement for studying the role of LHC-II in NPQ and the qE mechanism. Ideally, the Zea-LHC-II preparations should be Vio-free. This is particularly critical if one aims to determine the Zea-LHC-II structure by crystallography. As for spectroscopy, having a mixed population of Vio- and Zea-LHC-II in the samples is acceptable, and should in principle allow study of the effect of the Zea for Vio substitution in the function of LHC-II. Three strategies were applied: (1) LHC-II isolation from the Zea-LHC-II enriched *npq2 Arabidopsis* mutant, (2) refolding of Zea-LHC-II from inclusion bodies and purified pigments, and (3) LHC-II isolation from pea and spinach thylakoids after triggering the xanthophyll cycle *in vitro*.

##### 4.1.4.1 Thylakoid isolation from *Arabidopsis* mutant *npq2*

Thylakoids of the *Arabidopsis* mutant *npq2* were prepared by the same protocol routinely used for the isolation of pea thylakoids (Section 3.4.1). HPLC analysis of these thylakoids shows that indeed they are essentially Vio-free and Zea is the only xanthophyll cycle pigment present (Figure 4-8). The Chl *a* / Chl *b* ratio (mg/mg) in the thylakoids of this mutant was roughly 3, as in the WT. However, the chromatogram shows that Neo is also absent in these thylakoids. This is an undesirable feature, as LHC-II purified from these thylakoids will then be deficient in Neo, and therefore have an abnormal carotenoid content that does not resemble the carotenoid composition under high-light conditions *in vivo*.

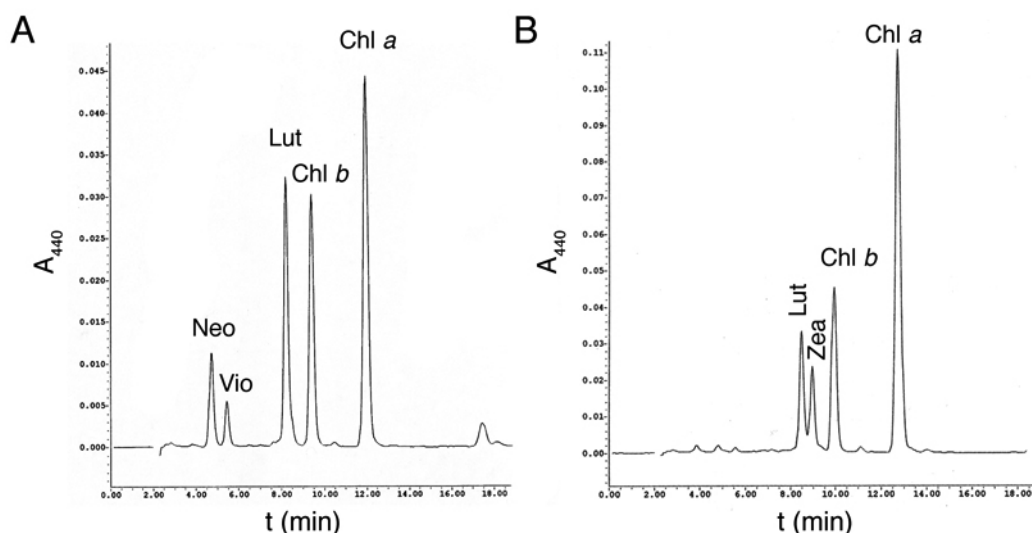


**Figure 4-8 - HPLC analysis of *Arabidopsis* variant thylakoids.**

Pigments were extracted from isolated thylakoids of *Arabidopsis* (A) WT and (B) *npq2* mutant plants and analysed by HPLC.

#### 4.1.4.2 LHC-II purification from *Arabidopsis* mutant *npq2*

Isolated thylakoids from *Arabidopsis* mutant *npq2* were solubilised with Triton X-100 and separated by sucrose gradient centrifugation overnight (Section 3.4.6). Two thicker green bands were observed, roughly at half-height of the centrifuge tube. This was identical to what is observed after the separation of solubilised complexes from *Arabidopsis* WT, pea and spinach thylakoids. Figure 4-9 shows the SDS-PAGE analysis of these two bands and the corresponding Western blot using an antibody against Lhcb1, the most abundant isoform of LHC-II. It can be clearly seen that the upper band, corresponding to complexes of lower molecular weight, has a higher Lhcb1 content than the lower band (which contains complexes of higher molecular weight). In both cases, the observed bands in the Western blot migrate at an apparent molecular weight of  $\sim 25$  kDa, consistent with the molecular weight of the monomeric Lhcb1 polypeptide. In *Arabidopsis* WT, pea and spinach preparations, these upper and lower bands usually correspond to the fraction enriched in minor LHCs, and monomeric LHC-II and trimeric LHC-II, respectively. Thylakoids from plants grown on soil or in hydroponics yielded virtually identical results.

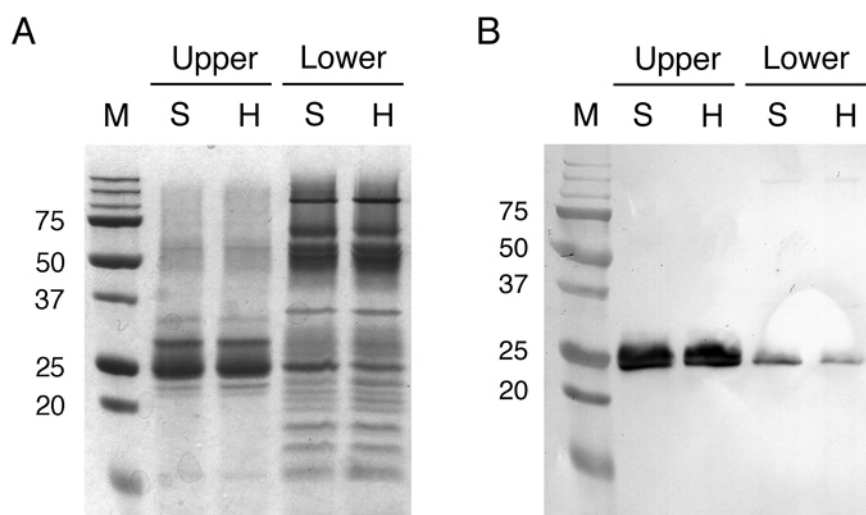


**Figure 4-9 - SDS-PAGE gel and Western blot of thylakoids from *Arabidopsis npq2* mutant plants fractionated by sucrose gradient centrifugation.**

Thylakoid membranes from *Arabidopsis npq2* mutant plants grown in soil (S) or hydroponics (H) were solubilised and loaded onto sucrose gradients. (A) Two main green bands (upper and lower band) were collected, and their protein composition was analysed by SDS-PAGE. (B) In order to verify the presence of LHC-II in each of the two bands, a Western-blot was performed using an  $\alpha$ -Lhcb1 antibody. M, molecular weight standards (in kDa).

#### 4.1.4.3 Refolding of recombinant Zea-LHC-II

The same protocol previously established to refold Vio-LHC-II and its mutants was applied to refold Zea-LHC-II (Figure 4-10; Section 3.5.4). Initially Zea was added to a pigment mixture containing all other pigments (Chl *a*, Chl *b*, Lut, Neo and Vio) so that the LHC-II monomers would incorporate Zea during refolding. However, this approach had a major drawback, revealed by the HPLC pigment analysis of the refolded complexes (Figure 4-11; Table 4-1). While Zea was indeed incorporated into refolded LHC-II, the Lut content of these refolded Zea-LHC-II complexes was much lower than in the control experiment (refolding in the absence of Zea). This can be observed by the dramatic decrease of the Lut / Chl ratio after the presence of Zea in the pigment mixture (Table 4-1). Decreasing the amount of Zea in the mixture only reduced the severity of this problem, but did not solve it, as the Lut content was consistently reduced compared to WT. This may indicate non-specific binding of Zea to at least one of the two Lut binding sites in LHC-II. The Neo and Vio content and the Chl *a*/Chl *b* ratio in these samples were not affected by the incorporation of Zea.

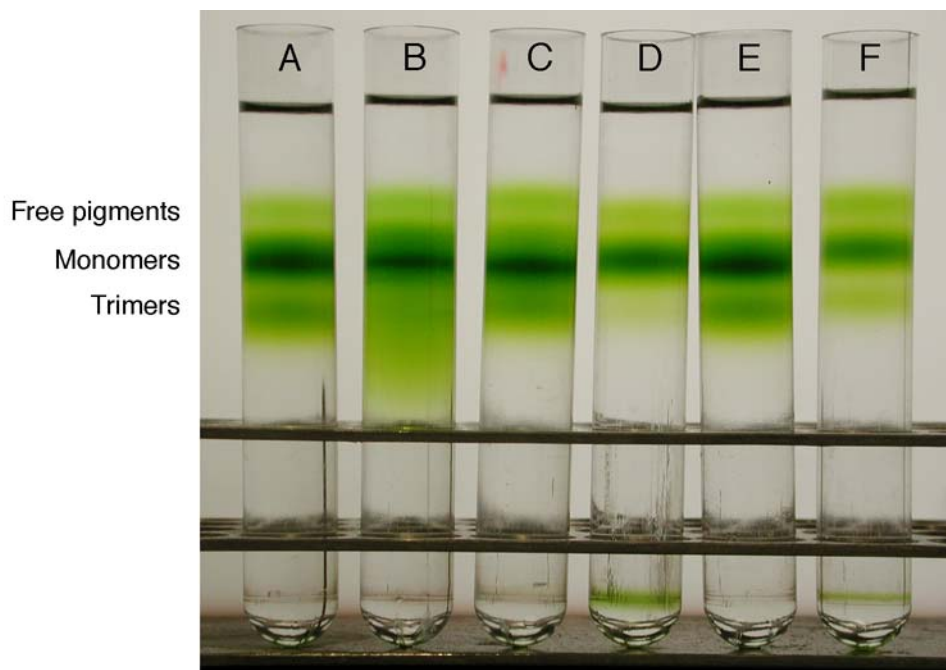


**Figure 4-10 - Sucrose gradients of refolded Zea-LHC-II samples.**

Zea was incorporated into refolded LHC-II by either supplementing the pigment mixture with different quantities (B, C and D) of Zea or by incubation of refolded monomers with different amounts of Zea (E and F). (A) Control experiment without Zea; (B), Zea added to the pigment mixture to a Vio:Zea ratio of 1:0.5; (C), Zea added to the pigment mixture to a Vio:Zea ratio of 1:0.25; (D), Zea added to the pigment mixture to a Vio:Zea ratio of 1:0.1; (E), refolded monomers incubated with Zea with a Vio:Zea ratio of 1:0.5; (F), refolded monomers incubated with Zea with a Vio:Zea ratio of 1:0.25. All ratios are in mg per mg.

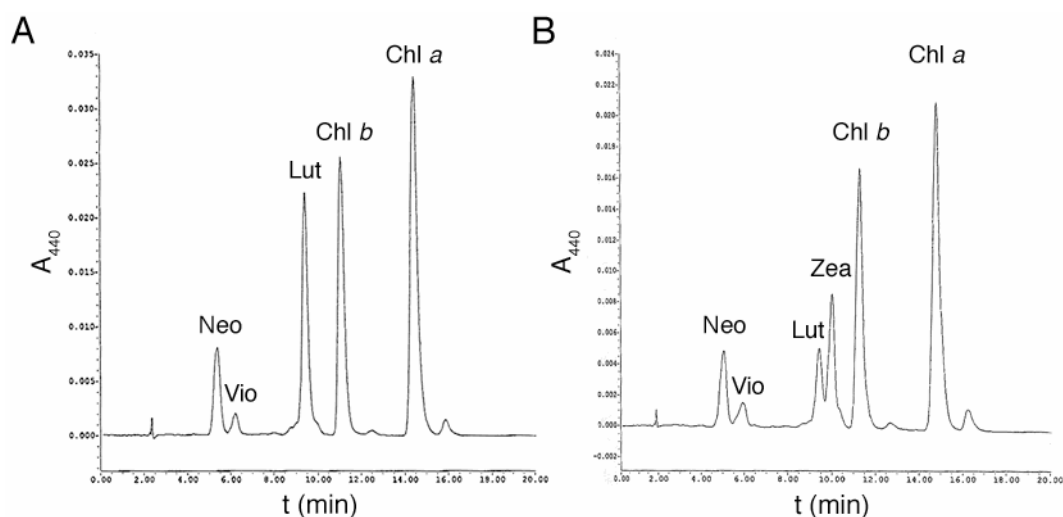


**Figure 4-11 - HPLC chromatograms of recombinant LHC-II refolded with a pigment mixture supplemented with Zea.**

The pigment content of refolded Zea-LHC-II was analysed by HPLC. (A) Control refolding experiment using a normal pigment mixture, as extracted from spinach leaves. (B) Refolding experiment in which the pigment mixture was supplemented with Zea to a final Vio:Zea ratio of 1:3 (mg/mg).

---

To circumvent this problem, another strategy was developed, in which the LHC-II monomers were refolded with the standard pigment mixture (Zea-free) before being incubated with different amounts of Zea (Section 3.5.4). After incubation with Zea, the monomers were then loaded onto an immobilised Ni-affinity column to promote trimerisation and separation from free-pigments and other impurities. As in the previous experiments, the sucrose gradient separation revealed that the refolded samples are mostly composed of monomeric LHC-II (Figure 4-10). The efficiency of the trimerisation was not affected by the incubation of the LHC-II monomers with Zea, as compared to the control experiments. A very thin green band was observed near the bottom of the centrifugation tube when smaller quantities of Zea were used. In fact, such a band was also observed when smaller quantities of Zea were added to the pigment mixture. The composition of this band is unknown. It is likely due to sporadic Chl aggregates.

Figure 4-12 and Table 4-1 summarise the results of the HPLC analysis obtained with this alternative approach of Zea incorporation into refolded LHC-II. The Lut / Chl ratio was relatively uniform in all analysed samples, although with a slight trend towards lower Lut content with the increasing quantities of Zea added to the refolded monomers. Another consistent observation was the increase in the Lut / Vio ratio as a consequence of incubating the monomer with Zea. On the other hand, both the Zea / Vio and the Zea / Lut ratios seem to be more affected by the oligomeric state of the refolded samples than by the quantity of Zea used during incubation. Overall, the HPLC analysis indicates that Zea incorporation is more efficient in LHC-II monomers than trimers. Table 4-2 lists the typical pigment composition of refolded Vio-LHC-II and Zea-LHC-II monomers.

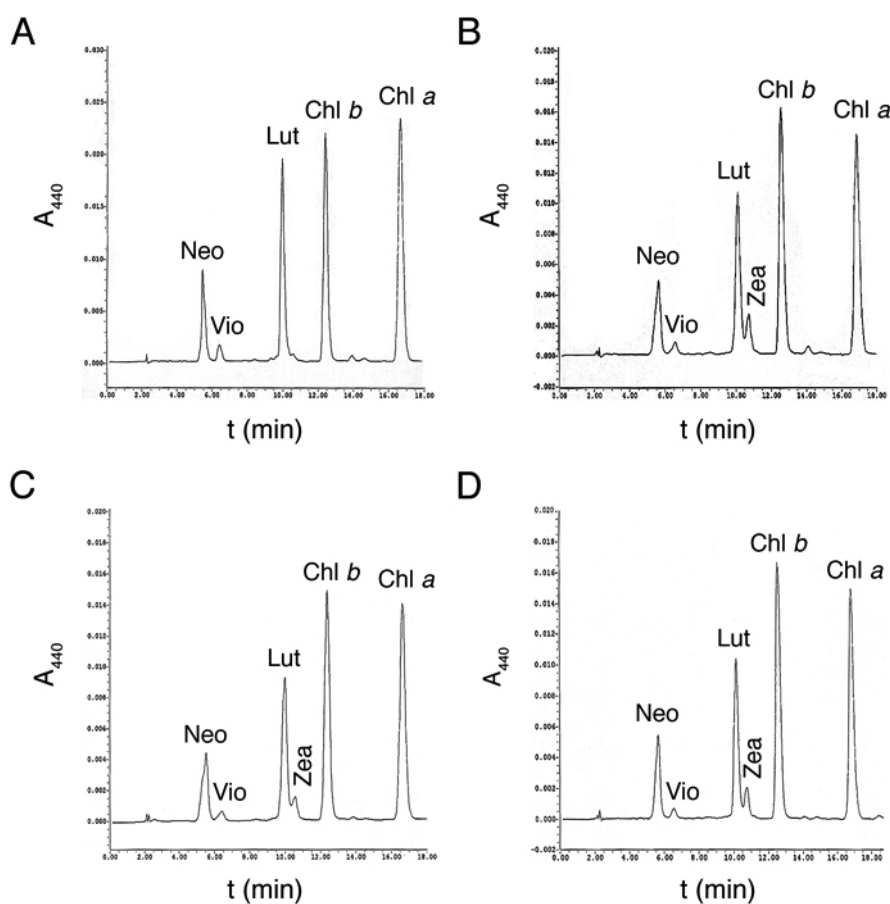


**Figure 4-12 - HPLC chromatograms of refolded LHC-II incubated with Zea.**

Refolded LHC-II monomers were incubated with different amounts of Zea solubilised in ethanol. The amount of Zea used was determined proportionally to the Vio content of the pigment mixture used for refolding. The HPLC analysis was performed after harvesting the refolded samples from the sucrose gradients. (A) Control with no Zea; trimers. (B) Zea added to a Vio:Zea ratio of 1:1; monomers; (C) Zea added to a Vio:Zea ratio of 1:0.5, trimers; (D) Zea added to a Vio:Zea ratio of 1:2, trimers. All ratios are in mg/mg.



**Table 4-1 - Ratios between pigments in Zea-enriched refolded LHC-II**

	<b>Sample</b>	<b>Vio / Zea</b> (used) <sup>b</sup>	<b>Lut / Vio</b>	<b>Lut / Chl<sup>a</sup></b> (final sample) <sup>c</sup>	<b>Zea / Lut</b>	<b>Zea / Vio</b>
<i>Zea in pigment mix</i>						
	Control	1 : 0	10.78	0.29	0	0
	+ Zea	1 : 3	2.11	0.08	1.70	3.55
<i>Refolded monomers</i>						
<i>exposed to Zea</i>						
	Control; trimers	1 : 0	10.56	0.33	0	0
	+Zea; monomers	1 : 1	12.13	0.32	0.25	3.03
	+Zea; trimers	1 : 0.5	11.43	0.30	0.16	1.86
	+Zea; trimers	1 : 2	12.50	0.25	0.16	2.00

<sup>a</sup> – Total Chl (i.e. Chl *a* + Chl *b*)

<sup>b</sup> - Ratio (mg/mg) between Vio and Zea in the pigment mixture used for refolding or during the exposure of refolded monomers to Zea in detergent solution.

<sup>c</sup> - Ratio between the areas under the respective peaks of the chromatogram.

**Table 4-2 - Pigment composition of refolded LHC-II monomers<sup>a</sup>**

	<b>Neo</b>	<b>Vio</b>	<b>Lut</b>	<b>Zea</b>	<b>Chl <i>a</i></b>	<b>Chl <i>b</i></b>
Vio-LHC-II	0.71	0.21	2.21	-	5.37	8.63
Zea-LHC-II	0.75	0.20	1.94	0.36	5.71	8.29

<sup>a</sup> – Values are in number of pigments per monomer, normalised to 14 Chls per monomer.

#### 4.1.4.4 *In vitro* de-epoxidation

The third approach to obtain Zea-LHC-II was to promote the xanthophyll cycle *in vitro* in pea or spinach thylakoids and then purify LHC-II from them. Protocols to promote the xanthophyll cycle *in vitro* have been described in the literature. However, none of them yielded “Vio-LHC-II”-free preparations, which would be a requirement for crystallographic studies and desirable for spectroscopic studies. Efforts were then made to optimise the *in vitro* de-epoxidation protocol.

Key parameters that were optimised include: pH, ascorbate and Chl concentrations, temperature and time. Several combinations of these parameters were tested and the evolution of the xanthophyll cycle was monitored by HPLC. Figure 4-13 shows the Zea / Chl ratios for a representative subset of the tested conditions at two different time points using pea thylakoids.

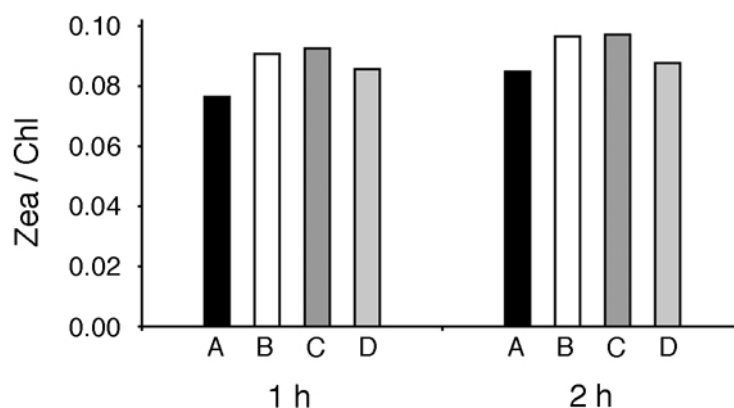


**Figure 4-13 - *In vitro* de-epoxidation under different experimental conditions.**

The yield of the de-epoxidation reaction was measured by determining the Zea/Chl peak areas ratio by HPLC. Different ascorbate concentrations, pH and temperatures were tested. (A) 40 mM ascorbate, pH 5.0, 20°C; (B) 100 mM ascorbate, pH 6.0, 37°C; (C) 40 mM ascorbate, pH 5.0, 30°C; (D) 100 mM ascorbate, pH 5.0, 30°C.

The results were quite similar for all tested conditions. A lower temperature led to a somewhat slower xanthophyll cycle, in particular after the first hour. However, increasing the temperature to 37°C was no better than 30°C. Adjusting the pH of the reaction mixture to 5.0 led to a slightly higher Zea content when compared with reaction mixtures at pH 6.0. On the other hand, increasing the ascorbate concentration by a factor of 2.5 was not translated into a clear difference in the extent of the reaction. From the presented assays, the optimal values for the

three tested parameters were: 40 mM ascorbate, pH 5.0 and 30°C. This condition was then used to trace the kinetics of the *in vitro* de-epoxidation reaction. Pea thylakoids were incubated in the de-epoxidation buffer and aliquots were taken at different time points and analysed by HPLC. Figure 4-14 shows the evolution of the Zea content in the thylakoids with time. There is a rapid increase in Zea content during the first 30 min. At this timepoint roughly half of the final extent of the reaction is reached. The curve also shows that after 2 h the reaction is essentially complete, as the Zea content increases only slightly thereafter. After 2 hours the Zea / Vio ratio was 1.62, and increased to only 1.92 after 3.5 h.

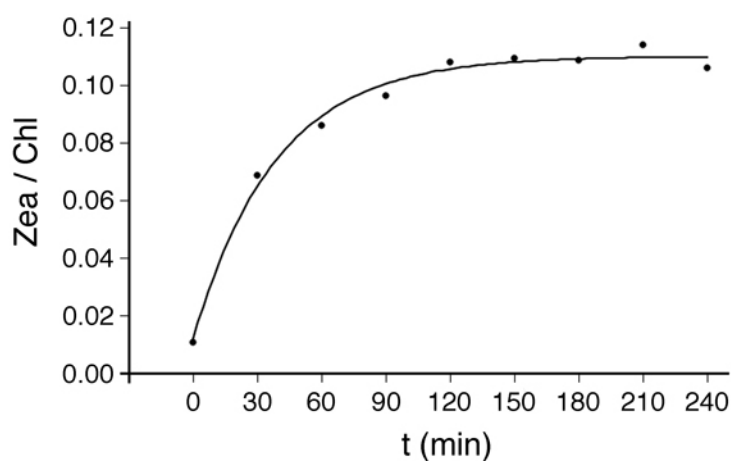


**Figure 4-14 - Time course of the *in vitro* de-epoxidation reaction in pea thylakoids.**

Aliquots of the reaction mixture were analysed by HPLC at different time points after induction of the de-epoxidation reaction. The Zea / Chl peak areas ratio from the HPLC chromatograms is presented.

Although the de-epoxidation reaction seemed to be essentially complete after 4 h, the reaction was monitored for a longer time to ensure that no additional Vio to Zea conversion would take place in the de-epoxidation buffer. Figure 4-15 shows such a time course and confirms that after ~2 h of incubation in the de-epoxidation buffer the reaction reaches a plateau and the Zea content remains basically unchanged from then on. In an attempt to push the de-epoxidation reaction further, the thylakoids were exposed to additional artificial light. The results show that this did not increase the Zea content in the thylakoids and, conversely, a small decrease in the Zea / Chl ratio was observed.

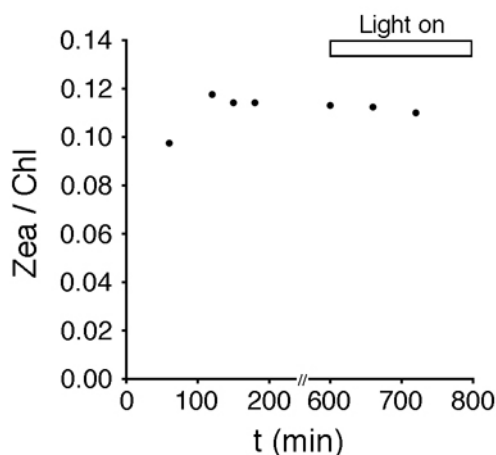


**Figure 4-15 - Long term time course of the *in vitro* de-epoxidation reaction.**

The *in vitro* de-epoxidation reaction was carried out overnight. The “Light on” bar indicates the period in which the thylakoids were exposed to additional light. The Zea / Chl ratio presented is calculated using the areas of the respective peaks in the HPLC chromatogram.

Pea and spinach LHC-II was isolated from these de-epoxidised thylakoids by the standard protocol (Table 4-3). It should be mentioned that the low pH treatment of the thylakoid membranes hindered their complete detergent solubilisation. This was corrected by adjusting the pH of the thylakoid membrane suspension to 6.0 before adding the detergent. When the pH was not adjusted, the Chl concentration of the LHC-II bands in the sucrose gradients after overnight centrifugation was too low to allow cation-specific precipitation of the complex.

**Table 4-3 - Pigment composition of isolated native spinach LHC-II**

	Neo	Vio	Ant	Lut	Zea	Chl <i>a</i>	Chl <i>b</i>
Vio-LHC-II	0.91	0.53	-	2.27	-	6.04	7.96
Zea-LHC-II	0.94	0.28	0.07	2.43	0.14	6.08	7.92

Number of pigments per monomer, normalised to 14 Chls per monomer.

#### 4.1.5 Refolding of LHC-II mutants

The LHC-II mutants are very valuable tools for studying qE, as they give unique insights into the role of specific pigments in the LHC-II fluorescence quenching mechanism. Five mutants ( $\Delta$ Chl 2,  $\Delta$ Chl 5,  $\Delta$ Chl 8,  $\Delta$ Chl 12 and  $\Delta$ Chl 13) were refolded along with the WT complex using the previously established

protocols (Section 3.5.3; (Rogl et al, 1998; Rogl & Kühlbrandt, 1999; Standfuss & Kühlbrandt, 2004). Sucrose gradient separations of the refolded samples showed that the yield of trimerisation was systematically lower for the mutants than for the WT, and was different from mutant to mutant (Figure 4-16). For this reason, the monomeric complexes were used in the subsequent studies in order to facilitate comparison between the results of different mutants.

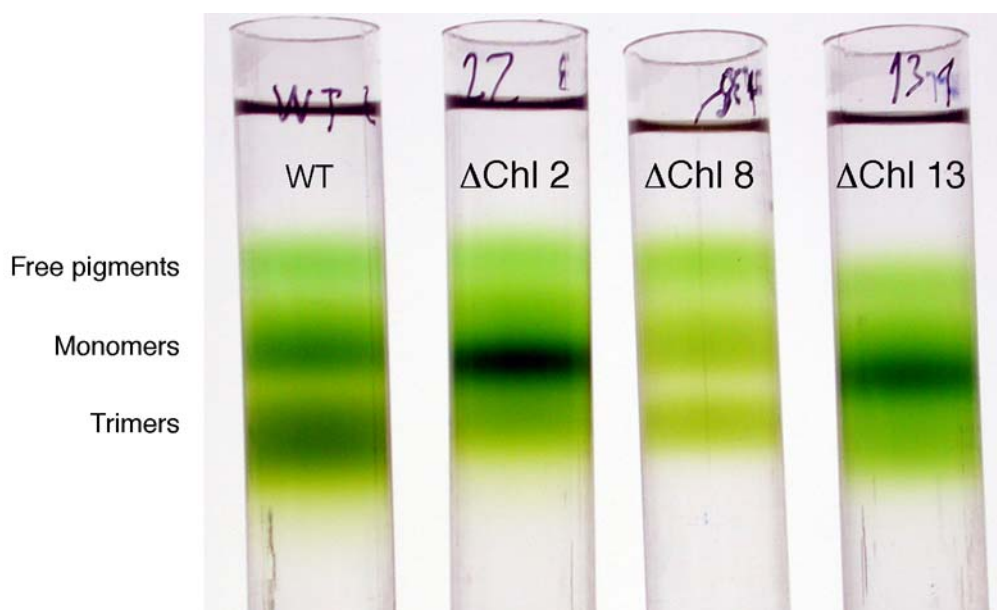


**Figure 4-16 - Sucrose gradients of refolded LHC-II variants.**

Separation of free pigments, monomers and trimers in refolded samples of WT and  $\Delta\text{Chl } 2$ ,  $\Delta\text{Chl } 8$  and  $\Delta\text{Chl } 13$  mutants.

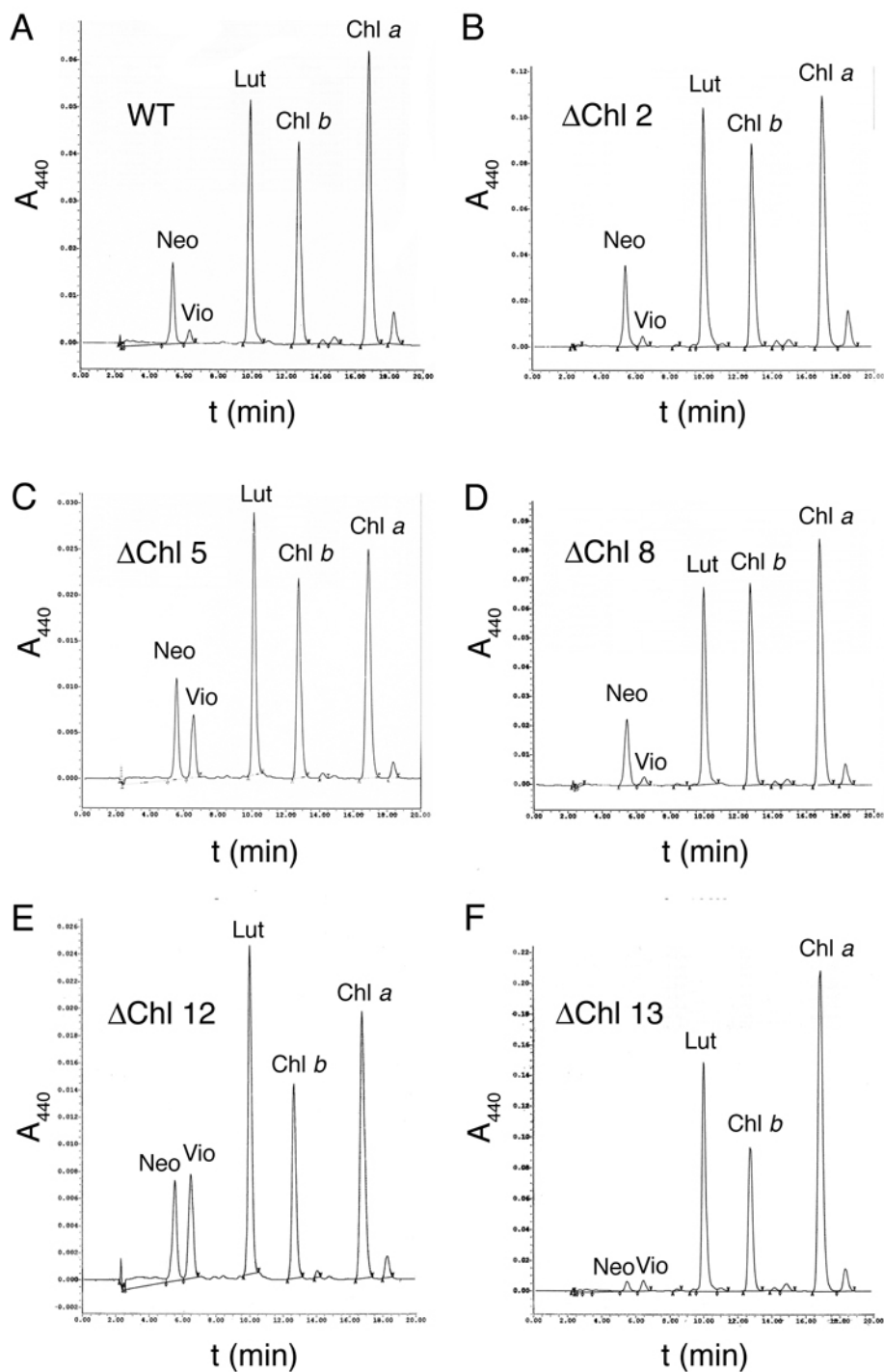


**Figure 4-17 - HPLC analysis of refolded LHC-II variants.**

The pigment composition of LHC-II variants was analysed by HPLC. The monomeric fractions separated by sucrose gradient were used for this analysis. The area of the peaks in each chromatogram was integrated and used to calculate the pigment compositions presented in Table 4-4.

**Table 4-4 - Pigment composition of LHC-II variants**

Pigment	LHC-II variant					
	WT	$\Delta$ Chl 2	$\Delta$ Chl 5	$\Delta$ Chl 8	$\Delta$ Chl 12	$\Delta$ Chl 13
<i>Normalised to 2 Lut per monomer</i>						
Neo	0.90	0.87	1.14	1.00	0.98	0.12
Vio	0.13	0.09	0.62	0.11	0.88	0.11
Lut	2.00	2.00	2.00	2.00	2.00	2.00
Chl <i>b</i>	5.23	5.04	5.13	6.08	3.77	3.79
Chl <i>a</i>	6.96	5.68	5.39	6.70	4.64	7.85
<i>Normalised to 14 or 13 Chls per monomer<sup>a</sup></i>						
	WT	$\Delta$ Chl 2	$\Delta$ Chl 5	$\Delta$ Chl 8	$\Delta$ Chl 12	$\Delta$ Chl 13
Neo	1.03	1.06	1.41	1.02	1.52	0.14
Vio	0.15	0.11	0.76	0.11	1.36	0.13
Lut	2.30	2.42	2.47	2.03	3.09	2.23
Chl <i>b</i>	6.01	6.11	6.34	6.18	5.82	4.24
Chl <i>a</i>	7.99	6.89	6.66	6.82	7.18	8.76

<sup>a</sup> – The number of pigments per monomer was normalised to 14 Chls for LHC-II WT and to 13 Chls for all mutants.

The pigment composition of the refolded monomers was analysed by HPLC (Figure 4-17; Table 4-4). For  $\Delta$ Chl 2 and  $\Delta$ Chl 5 mutants the pigment composition corresponded to the expected values, with both mutants clearly containing one Chl *a* less than the WT, keeping roughly the same carotenoid content. However, some differences were observed with the other three mutants. The Chl *a* / Chl *b* ratio of the  $\Delta$ Chl 13 mutant was higher than expected, due to a higher Chl *a* content than the WT. In addition, this mutant was unique in that it was essentially Neo-free. The carotenoid content of the  $\Delta$ Chl 5 and  $\Delta$ Chl 12 had the converse problem, as they both had higher Neo content than the WT. The  $\Delta$ Chl 12 mutant additionally had increased amounts of both Lut and Vio than the WT. For all variants the amount of monomeric complex obtained from a single sucrose gradient was sufficient to perform fluorescence measurements on solutions and aggregates (Section 8.1.2).

#### 4.1.6 Size exclusion chromatography

The pH drop in the lumen of the thylakoids is one of the first consequences of plant exposure to excessive sunlight and one of the triggers for NPQ. Size exclusion chromatography was used to evaluate the influence of pH on the LHC-II aggregation state. Two different pH values were used, which were close to the extremes of the pH range that LHC-II faces *in vivo*. This study was performed with two different detergents (NG and DDM) to increase the robustness of the results. Figure 4-18 shows the chromatograms obtained. All curves reveal the presence of different aggregation states in both pH values and both detergents. There was however a large shift of the elution peak towards higher aggregation states under acidic conditions. At pH 5.3, most LHC-II eluted at the void volume of the SEC column. This pH effect was much more pronounced than the influence of the detergent. At acidic and neutral pH, the samples solubilised in NG eluted in two close peaks, in which the earlier one, corresponding to the population of larger size, coincided with the main peak obtained with the samples solubilised in DDM.

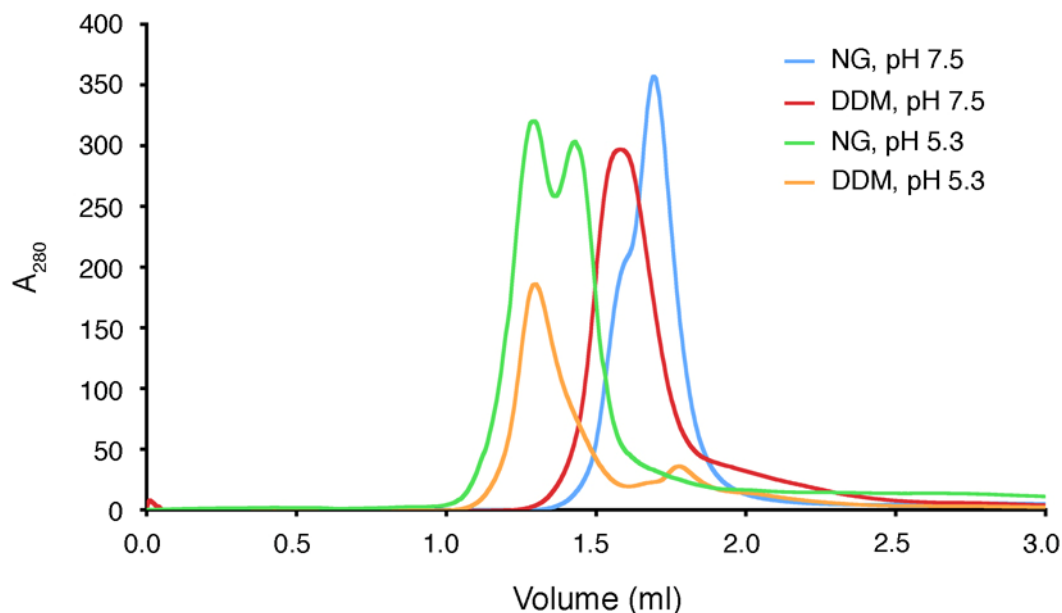


**Figure 4-18 – Size-exclusion chromatography of LHC-II in NG or DDM at neutral or acidic pH.**

The dependence of the LHC-II aggregation on pH and detergent was analysed by SEC. The figure shows the chromatograms obtained after loading LHC-II samples (25  $\mu\text{g}$  of Chl) onto a Sepharose 6 column (GE Healthcare). Further details are described in Section 3.6.1.



---

## 4.2 Discussion

### 4.2.1 Large scale purification of *Arabidopsis* LHC-II

Given the diversity of *Arabidopsis* mutants that have been described in the literature, these plants became key tools in photosynthesis research and in particular for the study of NPQ. Among these mutants, *npq1* and especially *npq2* are particularly interesting with regard to NPQ (Niyogi et al, 1998), as their xanthophyll cycle is impaired in such way that these plants only have Vio-LHC-II or Zea-LHC-II, respectively. Purifying LHC-II from the mutant *npq2* plants therefore seemed a promising approach to obtain the large amounts of homogeneous complexes that would be required to determine its structure. On the other hand, the spectroscopic comparison between Vio-LHC-II and Zea-LHC-II would benefit considerably from having isolated complexes from each of the two mutant plants. For these reasons, it was then necessary to: (a) obtain seeds from all variants to ensure their propagation, (b) establish growth conditions for the production of sufficient biological material for large scale LHC-II purification and (c) devise an LHC-II purification protocol from *Arabidopsis* thylakoid membranes. All three tasks were successfully completed without major difficulties.

The long daylight regime used to grow the first *Arabidopsis* plants (at the MPI for Plant Breeding, Cologne) induced flowering of the three *Arabidopsis* variants after 2 months (Figure 4-2). For WT and mutant *npq1* plants, the number of seeds collected from 10 to 12 plants was enough to ensure several generations of plants. The amount of seed collected from mutant *npq2* plants was substantially reduced, but was nevertheless sufficient to grow all the generations of *npq2* plants used during this work.

Switching the plants to a short daylight regime turned out to be the most important parameter for increasing the amount of biological material that could be harvested from each generation of plants. The ~6-fold increase in the amount of leaf material per plant (Figure 4-2; Figure 4-3) allowed large-scale *Arabidopsis* LHC-II purification, similar to spinach and pea plants which provide a large amount of biological material. Switching from growing the *Arabidopsis* plants in soil to hydroponics did not affect the amount of leaf material produced by each plant (and

was in fact unfavourable for the *npq2* plants; Figure 4-6). However, the hydroponic cultures have two advantages. First, they allow a better synchronisation of the growing plants (Tocquin et al, 2003), which can be important during purification. The thylakoid membrane composition (in terms of both lipids and proteins) of the synchronised plants will presumably be more homogenous. Second, they require essentially no maintenance. This advantage was however slightly compromised, as the hybrid method (Section 3.1.2), which yielded the best results in terms of amount of material (Section 4.1.2.2), requires the plants to be grown in soil for the first 2 to 3 weeks. It is nevertheless clear that *Arabidopsis* plants can indeed provide enough leaf material to make large-scale LHC-II purification feasible.

The last, and perhaps most complicated task was to devise a purification protocol for LHC-II from *Arabidopsis* thylakoid membranes. The starting point was the well established protocol first described by (Burke et al, 1978) with the later modifications by (Kühlbrandt et al, 1983) that yield large amounts of highly pure LHC-II from pea thylakoid membranes (Figure 4-1). This exact same protocol was found to give identical results with *Arabidopsis* thylakoid membranes (Figure 4-7), in terms of both purity and yield. This was true for plants grown in soil and in hydroponics. The ~0.25 mg of Chl per WT *Arabidopsis* plant that were obtained were more than sufficient for spectroscopic studies and crystallisation. This amount of LHC-II purified per plant roughly corresponds to the amount of sample that is used in each 24-well plate of the pea type-I crystal screen.

During his doctoral work in our institute, Dr. J. Standfuss obtained 3D crystals of refolded *Arabidopsis* Lhcb2 complexes, which diffracted up to 3.5 Å resolution. It would be interesting to determine whether the same crystallisation conditions also yield 3D crystals of the native complexes.

#### **4.2.1.1 Limitations of the *Arabidopsis* mutant *npq2***

The original motivation to establish the LHC-II purification protocol from *Arabidopsis* thylakoid membranes was to purify the complex from *npq2* plants, aiming at the structure determination of Zea-LHC-II. However, the biochemical analysis of the thylakoid membranes and LHCS from this mutant revealed some major drawbacks.

---

HPLC analysis of the pigment content in the thylakoid membranes showed that the mutant is not only deficient in Vio but also in Neo (Figure 4-8). This can be easily explained by the sequence of steps in the carotenoid biosynthetic pathway (Figure 4-19)(Niyogi et al, 1998; Pogson et al, 1998; Diretto et al, 2006), in which Zea is the precursor of both Vio and Neo. As a consequence, the LHCs isolated from this mutant will necessarily be deficient in Neo and will therefore have an artificial pigment composition that does not resemble that of the WT plants under high light conditions. The total absence of Vio in LHC-II may also explain the observed severe reduction in trimeric complexes in this mutant (Figure 4-9; previously also reported in (Tardy & Havaux, 1996; Lokstein et al, 2002)). In another *Arabidopsis* mutant (*aba4-1*), which is deficient in Neo but not in Vio, the amount of trimeric LHC-II is not severely affected (Dall'Osto et al, 2007). Pigment analysis of this mutant revealed an increase in the unusual 9-*cis*-Vio. Neo is the only 9-*cis*-carotenoid in LHC-II under normal circumstances, and the increase in 9-*cis*-Vio might be necessary to compensate for the lack of Neo. This compensatory effect is not possible in the *npq2* plants as Vio is also absent, inevitably leading to less stable complexes. On the other hand, the Vio binding site is located directly at the monomer-monomer interface, and any small changes in this region will affect the trimer stability. The two additional conjugated bonds in the  $\pi$ -system of Zea as compared to Vio make the former more rigid. In particular, the head groups of Zea would have to adopt a different configuration, as they cannot rotate to the same geometry observed for Vio in the crystal structures. This could possibly shift the monomer-trimer equilibrium towards monomers.

It is tempting to claim that the differences in growth and robustness of the *npq2* plants compared to WT and *npq1* result from a less efficient light-harvesting system. However, this is most certainly not the case. The *npq2* plants present the same phenotype with respect to light stress (Niyogi et al, 1998) and the same pigment composition (Duckham et al, 1991; Rock & Zeevaart, 1991) as *aba1* mutants (Koornneef et al, 1982). The *aba1* mutation was described to block the abscisic acid biosynthetic pathway (for review see (Nambara & Marion-Poll, 2005). Abscisic acid is an important plant hormone that mediates signalling cascades under different stress conditions and controls plant development (Himmelbach et al, 2003). Interestingly, abscisic acid is synthesised in plants starting from either

Neo or Vio. It is then likely that the deficient growth and robustness of *npq2* plants is primarily caused by this hormone unbalance.

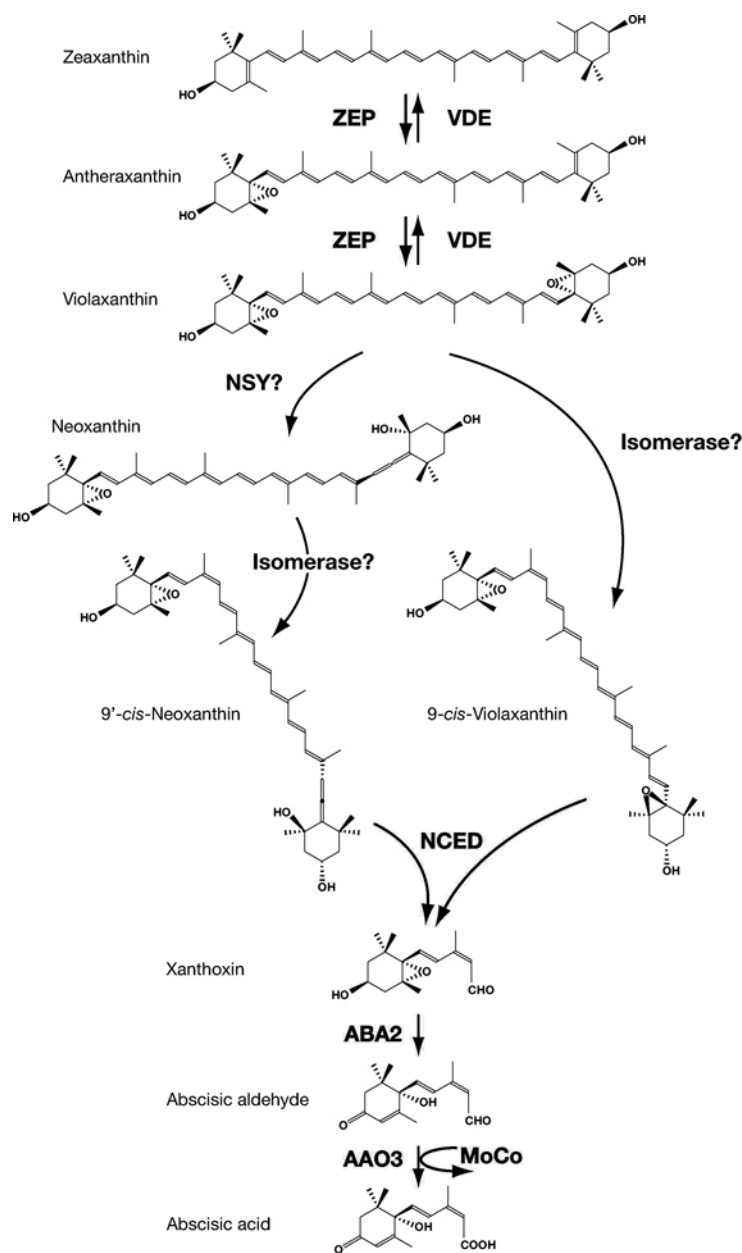


**Figure 4-19 – Carotenoids and abscisic acid biosynthetic pathways.**

It is interesting to note that although the Zea content in the thylakoid membranes is normally low in normal light and only increases under high light conditions, this Car is in fact a precursor of both Vio and Neo and the plant hormone abscisic acid. Adapted from (Nambara & Marion-Poll, 2005).

Lack of Neo, reduced trimer stability and small the amount of leaf material produced by the *npq2* mutant plants make the isolation of LHC-II from these plants a suboptimal option.

### 4.2.2 Producing Zea-LHC-II

Once the purification from *npq2* plants was excluded, Zea-LHC-II production was attempted by two other approaches. *In vitro* de-epoxidation of spinach and pea thylakoids yielded highly pure trimeric Zea-LHC-II in sufficient amounts for spectroscopic studies. However, despite all efforts employed to optimise the de-epoxidation reaction (Section 4.1.4.4), the yield of Vio to Zea conversion was never above 50%. All samples obtained were thus a mixture of Vio-LHC-II and Zea-LHC-II. Complete exchange of Vio by Zea in a LHC has indeed never been reported. It was also clear that not only the Zea content in purified LHC-II was never close to 100% but also the total amount of xanthophyll cycle carotenoids was reduced after the de-epoxidation reaction (Table 4-3). However, the comparison between the spectroscopic characteristics of Vio-LHC-II and Zea-LHC-II should not be affected by the sub-occupancy of the Vio binding site, making this method suitable for preparing samples for that purpose. On the other hand, Zea-LHC-II crystallisation would benefit considerably from a full occupancy of this binding site by Zea. In this case, the conditions used for the *in vitro* de-epoxidation of plant thylakoids were clearly unsatisfactory. Further optimisation of the de-epoxidation conditions may be the key to obtain Zea-LHC-II from natural sources. The relatively small number of conditions tested during this work was largely due to the necessity of analysing a very large number of samples by HPLC for each tested condition, which was impractical with the HPLC system available at the time.

The second approach to obtain Zea-LHC-II was experimentally very different, but yielded similar results. The incubation of refolded LHC-II with ethanol solubilised Zea promoted binding of this Car to empty Vio binding sites in the refolded complexes. This was supported by the observation that the Lut/Vio ratio was only marginally increased after incubation of the refolded complexes with Zea (Table 4-1). Not surprisingly, due to the exposure of the Vio binding site, the amount of Zea incorporated into monomeric LHC-II was higher than for the trimers. Although it is not certain that all incorporated Zea molecules were bound to the Vio binding site, nonspecific binding to other parts of the complex or even to the detergent micelles is very unlikely, as after incubation with Zea the refolded complexes were extensively washed during the subsequent Ni-affinity

chromatography. When Zea was added to the pigment mixture used to refold the LHC-II monomers, the Lut content dropped sharply. This can only be interpreted as evidence for forced binding of Zea to the Lut binding sites. It is possible that the same occurs in the thylakoid membranes of the *Arabidopsis* mutant *npq2*, where the Zea content is artificially high. This can be another cause for the instability of the LHC-II trimers in those plants.

### 4.2.3 LHC-II mutants

The LHC-II mutants used in the present work were selected from a collection of mutants previously designed and produced in this laboratory (Rogl & Kühlbrandt, 1999). The pigment composition of the refolded complexes obtained in the present work (Table 4-4) was very similar to the original description of these mutants (Rogl & Kühlbrandt, 1999), with the exception of mutants  $\Delta$ Chl 12 and  $\Delta$ Chl 13..

According to (Rogl & Kühlbrandt, 1999) the  $\Delta$ Chl 12 mutant binds roughly half the amount of Neo and Vio as the WT. In this work it was found that the refolded monomers of this mutant bound the same amount of Neo as WT, but the Vio content was higher by a factor of 4. Additionally, the Chl content of  $\Delta$ Chl 12 was the lowest of all mutants and indeed suggests that these refolded complexes lack not only Chl 12 but also at least two Chl *a*. On the other hand, the mutant lacking Chl 5, which makes a potential quenching Chl pair with Chl 12, had a Chl *a*/Chl *b* ratio identical to that previously described (Rogl & Kühlbrandt, 1999).

Due to the proximity of Chl 13 and Neo in the LHC-II monomer, it was not surprising that the first  $\Delta$ Chl 13 mutants also had a reduced Neo content (Rogl & Kühlbrandt, 1999). However, the  $\Delta$ Chl 13 here obtained had even less Neo than the originally described mutants. Additionally, these mutants seem to lack not one but two Chl *b*. Looking at the structure of the LHC-II monomer, it can be suggested that the other Chl *b* missing in these refolded mutants is either Chl 11 or Chl 14. The loss of Chl 11 could be justified by the fact that Neo is placed as a barrier between the chlorin ring of this Chl and the exterior of the complex. The Chl 14 is the most isolated of all Chls in the LHC-II monomer and is in close proximity to Chl 13. It is plausible that the lack of the latter would affect the binding affinity of

---

---

Chl 14. In fact, the Chl a/Chl b ratio of the  $\Delta$ Chl 13 monomers obtained here is very similar to that found originally (Rogl & Kühlbrandt, 1999).

It should be noted that the Chl content of refolded WT,  $\Delta$ Chl 2 and  $\Delta$ Chl 8 is not only in good agreement with (Rogl & Kühlbrandt, 1999) but also with the expected values (Standfuss et al, 2005).

#### **4.2.4 LHC-II aggregates at low pH**

Size exclusion chromatography (SEC) was used to evaluate the homogeneity of LHC-II solubilised in two detergents and at neutral (7.5) and acidic (5.3) pH. The detergent used for solubilisation had a much smaller effect on the elution volume than the pH. At neutral pH, the differences between the samples solubilised in DDM and NG can be explained by the larger size of the DDM micelle as compared to the NG micelle. The large shifts in the elution volume of LHC-II solubilised in the two detergents after incubation at low pH (5.3) can only be explained by aggregation of the complex, which indeed masked any influence of the detergent micelle. An increase in aggregation is the only plausible explanation, as it is not expected that a pH-induced conformational change imposes such a large deviation of the elution peaks.

The biological significance of the observed increase in aggregate size is not clear. *In vivo*, only the luminal surface of LHC-II is exposed to low pH under qE conditions. In the SEC experiments, the solubilised complexes in the detergent micelle will be surrounded by the buffer, which implies that also the stromal surface of the complex, in which several aspartate and glutamate residues are located, will be exposed to the low pH. On the other hand, the arrangement of these pH-induced aggregates is not known, so it is unclear if they could also be formed under the constraints imposed by the thylakoid membranes.

## 5 VDE BIOCHEMISTRY

Together with PsbS, violaxanthin de-epoxidase (VDE) is one of the two key players in qE (Figure 1-12) for which no structural information is available. Despite extensive biochemical characterisation of VDE, the de-epoxidation mechanism and in particular the role of the numerous cysteine residues in the N-terminal domain of VDE is still unknown. A crystal structure of VDE would certainly contribute to answering these questions. On the other hand, having recombinant VDE would be useful for studying qE *in vitro*, as it would allow mimicking the Vio by Zea exchange in the LHCs in reconstituted systems. For these purposes, a VDE expression and purification protocol was established. The starting point was the full *Arabidopsis* VDE cDNA, which was used to design and produce several expression constructs. Expression was tested in *E. coli* and a mammalian cell expression system.

---



## 5.1 Results

### 5.1.1 VDE and VDE-Thrx fusion constructs

*E. coli* cells containing the full cDNA of *Arabidopsis* VDE were obtained from ABRC. Initially, two constructs were designed. The first construct comprised the full amino acid sequence of the mature enzyme (ArabVDE; Figure 5-1).

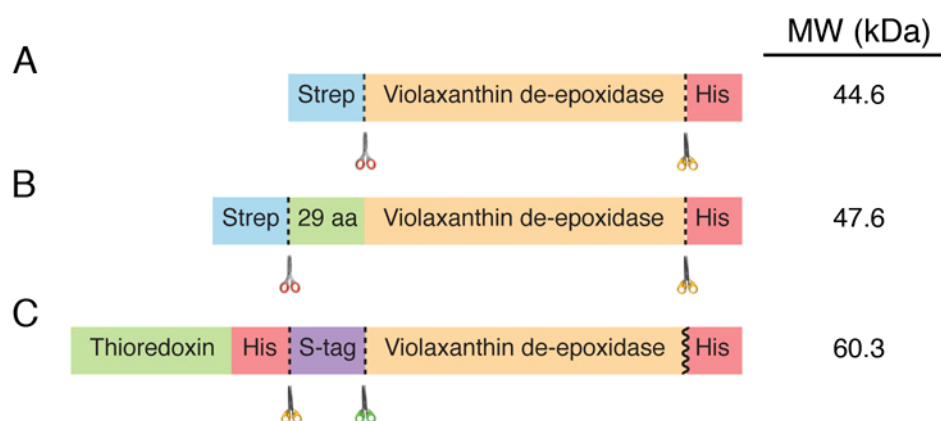


**Figure 5-1 - VDE constructs for expression in *E. coli*.**

Three VDE constructs were designed. The ArabVDE construct (A) comprises the full amino acid sequence of the mature enzyme in between two affinity tags. ArabVDE-Long (B) is identical, but 29 amino acids from the signal peptide were kept in the construct. A thioredoxin-VDE fusion was also designed and produced with a C-terminal His-tag (C). Strep, Strep-II tag; His, His-tag; dashed lines, protease cleavage sites; red scissors, HRV 3C protease; yellow scissors, thrombin; green scissors, enterokinase.

The second construct kept the 29 last amino acids of the signal peptide in addition to the full sequence of the mature enzyme (ArabVDE-Long). A Strep-II-tag and a 10xHis-tag flank these constructs at the N- and the C-termini, respectively. Both tags are encoded by the pET-52b (+) 3C/LIC vector sequence (see Appendix for vector details), and cleavable by HRV 3C protease and thrombin, respectively.

VDE construct DNA was amplified by PCR from the full cDNA introducing 3C/LIC specific sequences. The PCR products were analysed by agarose gel electrophoresis, and were of the expected size (1073 bp for ArabVDE and 1160 bp for ArabVDE-Long; Figure 5-2).

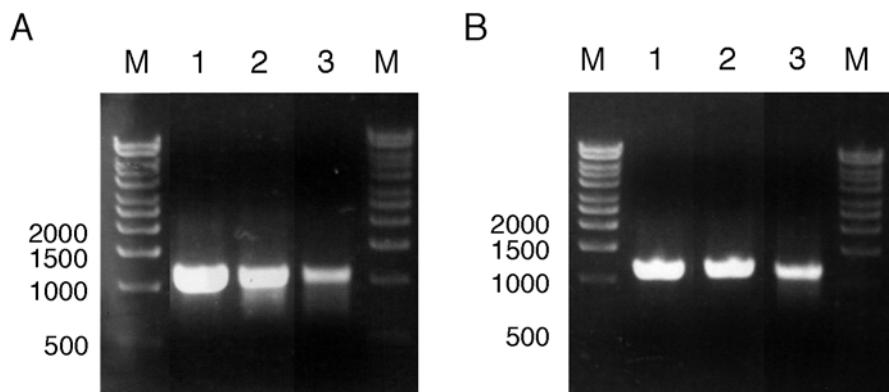


**Figure 5-2 - Agarose gel with PCR products of *Arabidopsis* VDE cDNA amplification and introduction of 3C/LIC specific sequences.**

VDE cDNA was obtained from ABRC and used to generate two constructs by PCR. (A) Amplification of ArabVDE; (B) Amplification of ArabVDE-Long. 1 to 3 correspond to different PCR conditions; M, molecular weight standards (sizes in bp).

Two additional constructs were designed to obtain fusions between VDE and thioredoxin (Figure 5-1) in the pET32 Ek/LIC vector (see Appendix for vector details), with and without a C-terminal His-tag. These constructs contain the full sequence of the mature VDE without the 29 amino acid extension. As before, Ek/LIC specific primers were used to amplify the mature VDE DNA from the full cDNA sequence and to introduce the necessary extensions.

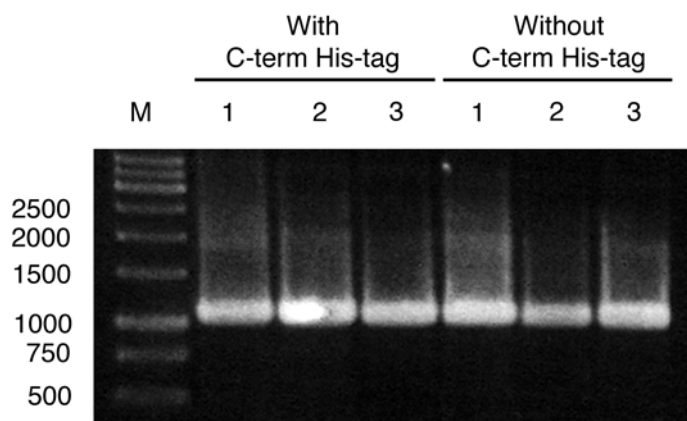


**Figure 5-3 - Agarose gel with PCR products of *Arabidopsis* cDNA amplification and introduction of Ek/LIC specific sequences.**

The amplified products were used to construct the Thrx-ArabVDE fusion with and without a C-terminal His-tag. 1 to 3 correspond to different PCR conditions; M, molecular weight standards (sizes in bp).

---

As the pTriEx6 3C/LIC vector for mammalian cell expression used the same overhangs as the pET-52b(+) vector, the same DNA fragments (ArabVDE and ArabVDE-Long; Figure 5-2) were used to generate these clones. The translation product in the eukaryotic system should therefore have the same sequence as in the bacterial system.

### **5.1.2 Transformation of *E. coli* cells with VDE constructs**

After annealing of the linearised plasmids with the treated PCR products, the obtained circular plasmid containing the VDE construct was used for transformation of *E. coli* strains (NovaBlue, RosettaBlue and Rosetta-gami). Positive clones were identified by selective agar plates and their plasmid DNA was extracted. The presence of the correct VDE DNA sequences was first positively confirmed by PCR (Figure 5-4) and then re-confirmed by sequencing. 48 hours were required to obtain positive clones, starting from the full cDNA in the *E. coli* cells obtained from ABRC. The exact same procedures yielded positive clones for the Thrx-ArabVDE fusions and for the ArabVDE and ArabVDE-Long sequences inserted in the pTriEx6 vector for mammalian cell expression (not shown). The RosettaBlue *E. coli* cells made competent in house by J. Zeelen had a higher transformation efficiency than the commercial competent NovaBlue cells, using exactly the same transformation conditions. In fact, for all transformation experiments with RosettaBlue cells and the pET 52b (+) vectors a 100x dilution of the transformation culture was needed to obtain single colonies on the agar plates.

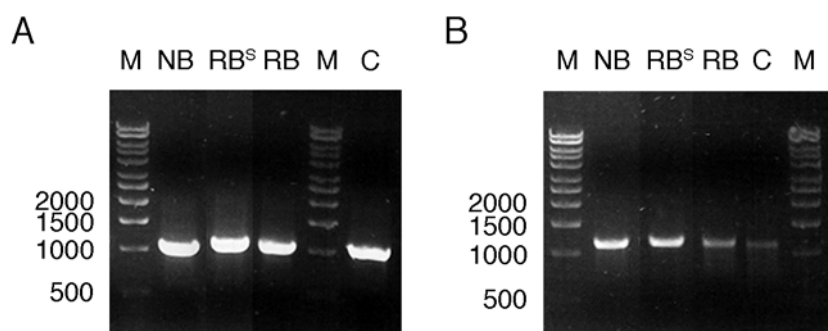


**Figure 5-4 - Agarose gel with VDE cDNA amplified by PCR from plasmid DNA of transformed *E. coli* strains.**

The plasmid DNA of *E. coli* strains transformed with a pET-52 3C/LIC vector carrying the VDE inserts was isolated and used for PCR with the VDE specific primers. (A) PCR reactions with plasmid DNA of cells carrying the short VDE construct; (B) PCR reactions with plasmid DNA of cells carrying the long VDE construct. NB, NovaBlue strain; RB, RosettaBlue strain; RB<sup>S</sup>, RosettaBlue pLys strain; M, molecular weight standards (in bp); C, control reaction using plasmid DNA from the *E. coli* strain obtained from ABRC.

### 5.1.3 VDE expression

After identification of positive clones carrying the VDE DNA constructs, expression tests were performed. Figure 5-5 shows the first expression tests, in which the ArabVDE and ArabVDE-Long constructs and RosettaBlue and RosettaBlue pLysS cells were used. Cells were lysed in sample buffer and analysed by SDS-PAGE. The appearance of a thick band slightly under the 50 kDa marker indicates high expression of the protein. On the other hand, the samples of induced and non-induced cells carrying the ArabVDE-Long DNA do not show any noticeable difference in the SDS-PAGE analysis, suggesting no or little expression of the recombinant protein. The latter was shown to be correct by Western-blotting using an  $\alpha$ -His-tag antibody (not shown).

It is worth mentioning that all the work from amplification of VDE DNA from the ABRC cells until obtaining expressed protein in the expression test was carried out in less than 72 hours.

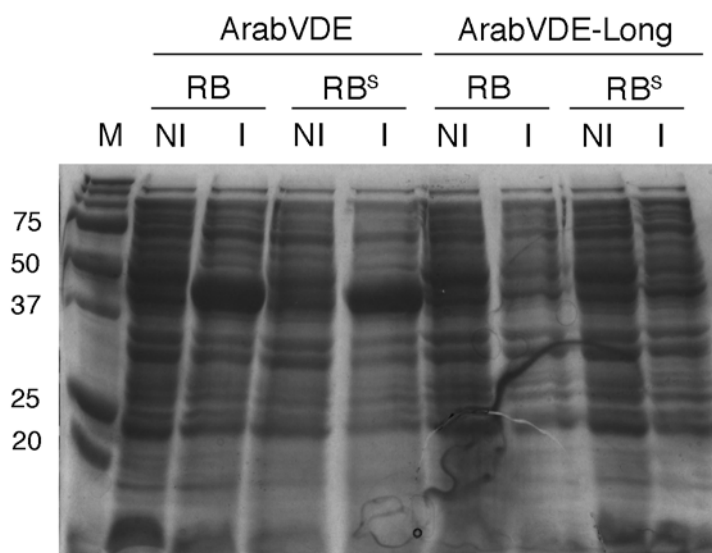


**Figure 5-5 - SDS-PAGE gel of recombinant VDE expression tests in *E. coli*.**

*E. coli* cells transformed with a pET-52-3C/LIC vector carrying the short or the long VDE construct were grown in LB medium at 37°C to  $A_{600} \sim 0.6$  and split into two parts. One half (I; induced) was supplemented with 1 mM IPTG. Cells were harvested 3 hours after induction, centrifuged and lysed in SDS-PAGE sample buffer. M, molecular weight standards (in kDa); NI, not induced; I, induced; RB, RosettaBlue strain; RB<sup>s</sup>, RosettaBlue pLysS strain.

The same procedure described for the expression tests of ArabVDE and ArabVDE-Long were used for the Thr<sub>x</sub>-ArabVDE fusions with and without the C-terminal His-tag. However, in this case cells were first broken by sonication and the soluble and insoluble fractions were separated by ultracentrifugation, prior to the SDS-PAGE and Western-blotting. Using an  $\alpha$ -His-tag antibody, successful expression of both variants of Thr<sub>x</sub>-VDE was confirmed (Figure 5-6). The Western-blot also showed a small number of bands of slightly lower mass than the predicted size of the two variants of the fusions. These presumably correspond to degradation or aborted translation products.

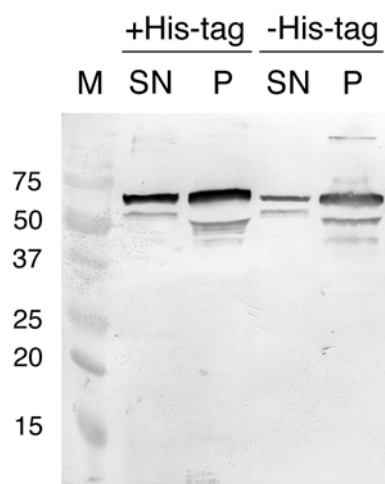


**Figure 5-6 - Expression tests of Thrx-VDE fusion**

Western-blot for His-tag detection in the supernatant (SN) and pellet (P) after cell breakage. M, molecular weight standards (in kDa); +His-tag, a C-terminal His-tag is present in the construct; -His-tag, no C-terminal His-tag. Both constructs have an N-terminal His-tag, therefore the samples on +His-tag have two times the number of epitopes as -His-tag.

In summary, the expression tests revealed that using the ligation-independent cloning method, all positive clones after transformation were indeed capable of expressing the different VDE constructs; requiring a minimum of experimental work in a very short period of time.

#### **5.1.4 Optimisation of VDE expression**

To optimise ArabVDE and ArabVDE-Long expression in *E coli*, two different cells densities at the time of induction were tested. Aliquots of the cultures were taken at different timepoints after induction and were run on SDS-PAGE. Figure 5-7 shows the results for the expression of the ArabVDE construct in RosettaBlue cells. A band just under the 50 kDa marker, corresponding to ArabVDE, increases in size over time, for cells induced at high and low density. In both cases, the intensity of the band does not seem to increase substantially after ~4 hours. Similar experiments using the ArabVDE-Long construct did not result in such a clearly visible gradient of an increasingly thicker band (not shown).

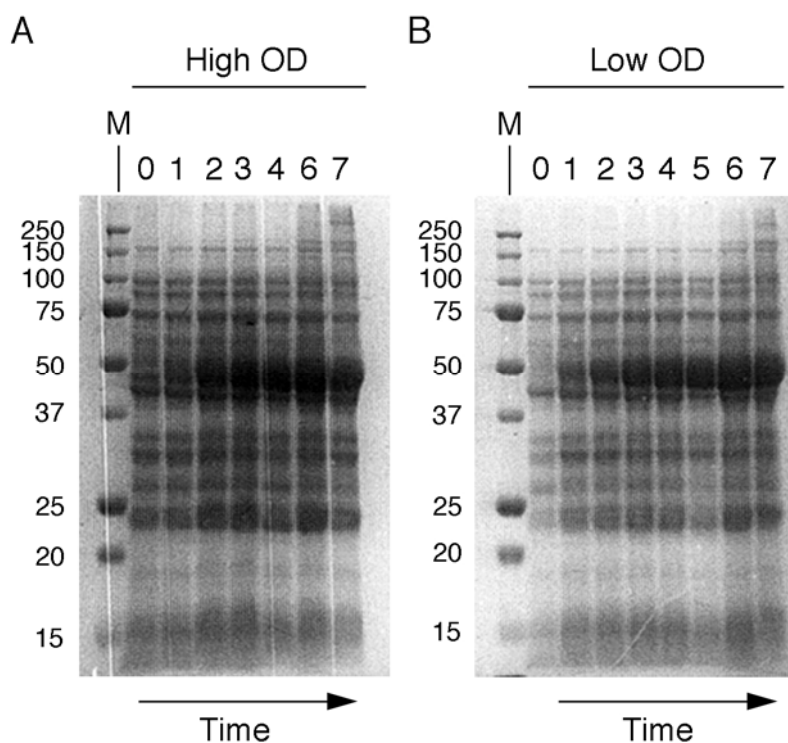


**Figure 5-7 - SDS-PAGE gel of recombinant VDE expression in *E. coli* at different time points after induction.**

RosettaBlue *E. coli* cells transformed with a pET-52-3C/LIC vector carrying the ArabVDE construct were grown in LB medium at 37°C to  $A_{600} \sim 0.5$  (low OD) or  $A_{600} \sim 1.0$  (high OD). Cells were induced (1 mM IPTG), collected at different time points, centrifuged and lysed in SDS-PAGE sample buffer. M, molecular weight standards (in kDa); 0, before induction; 1, ~35 min after induction; 2, ~75 min after induction; 3, ~120 min after induction; 4, ~160 min after induction; 5, ~200 min after induction; 6, ~6 h after induction; 7, overnight after induction.

Western-blot analysis was used to verify the ArabVDE and ArabVDE-Long expression levels (Figure 5-8). As with the SDS-PAGE results, there is a clear difference in the expression level of ArabVDE and ArabVDE-Long. In all tested conditions, the expression tests with ArabVDE yielded a very strong chemiluminescence signal. On the other hand, the ArabVDE-Long only yielded fainter bands, and their intensity varied with time, strain and cell density at the time of induction. It is difficult to identify a pattern in these expression tests with the ArabVDE-Long construct. When using the RosettaBlue pLysS strain, the stronger bands were observed when induction was carried out for longer time with cells at low density. On the other hand, higher expression levels were obtained with RosettaBlue cells that were induced at low density. The differences in intensity of the bands are unlikely to be caused by different amounts of total protein loaded

onto the gel, as care was taken to load the same amount of protein on each lane. Due to the large difference in expression levels between the two constructs, ArabVDE was used for the following experiments.

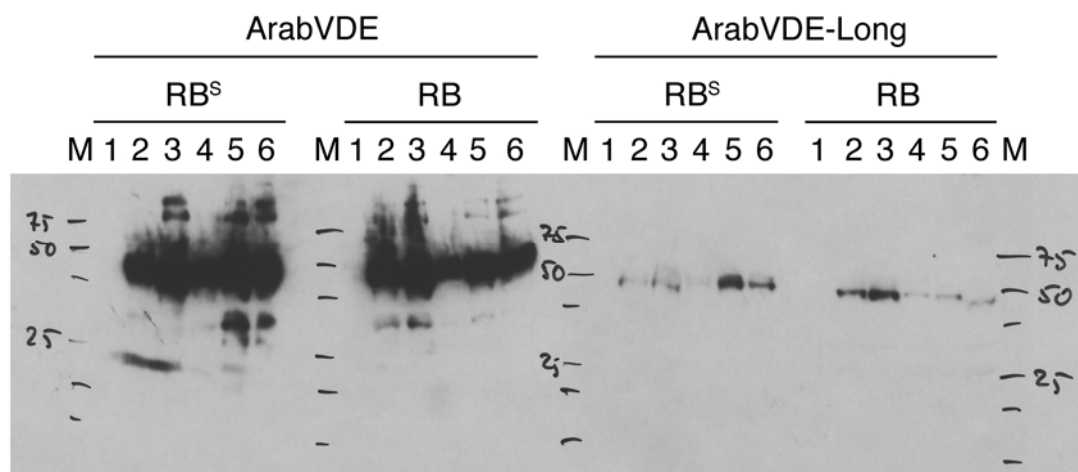


**Figure 5-8 - Western blot from VDE construct expression tests in *E. coli* strains.**

Cells were grown in LB medium at 37°C to  $A_{600} \sim 1.0$  (high OD; samples 1, 2 and 3) or  $A_{600} \sim 0.5$  (low OD; samples 4, 5 and 6) before induction with 1 mM IPTG. Aliquots of the cultures were then harvested at different time points and lysed in SDS-PAGE sample buffer. After SDS-PAGE, the Western Blot was performed using a primary  $\alpha$ -His-tag antibody and a secondary  $\alpha$ -mouse antibody for detection on photographic film via chemiluminescence. RB, *E. coli* RosettaBlue; RB<sup>S</sup>, *E. coli* RosettaBlue pLysS; M, molecular weight standards (in kDa); 1, before induction; 2, 120 min after induction of cells; 3, ~6 h after induction; 4, 1 h after induction; 5, ~6 h after induction; 6, overnight after induction.

### 5.1.5 VDE production in inclusion bodies

From the experiments presented so far it was not possible to know if the ArabVDE was expressed in a fully folded, soluble form or in inclusion bodies. To investigate this, cells were broken and fractionated before performing the SDS-PAGE and Western-blot experiments (Figure 5-9). The strongest bands on the Western-blots with the correct molecular weight were observed in the samples solubilised in 8 M urea. Some faint bands with the correct molecular weight were observed in the soluble and detergent-solubilised fractions when the  $\alpha$ -Strep-tag conjugate was used for detection, but were absent when the  $\alpha$ -His-tag antibody was used. The strong band under 20 kDa on the  $\alpha$ -Strep-tag Western blot in the lane corresponding to the soluble fraction can be assigned to the Biotin Carboxyl Carrier Protein from *E. coli*, which is known to cross-react with the  $\alpha$ -Strep-tag conjugate.



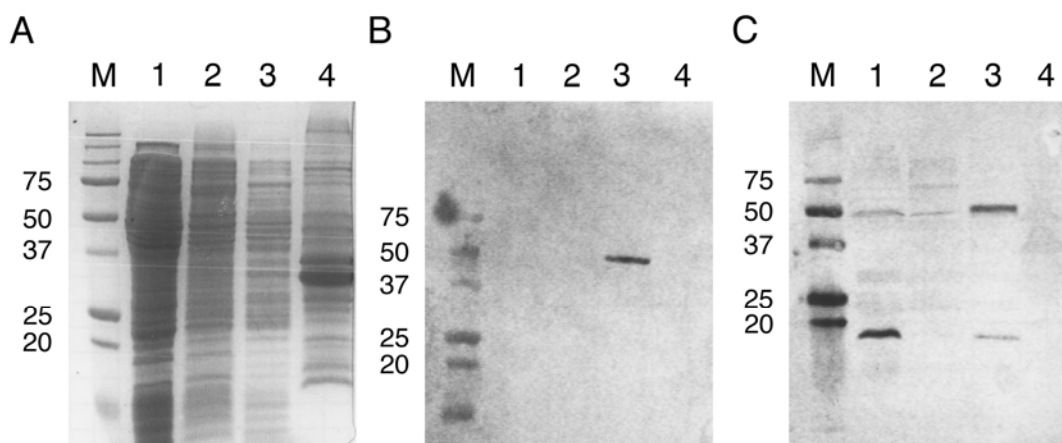


**Figure 5-9 - Experimental evidence for ArabVDE expression in inclusion bodies.**

RosettaBlue cells grown in LB medium at 37°C were induced with 1 mM IPTG for expression of ArabVDE. Cells were harvested and broken. The resulting pellet was solubilised with 5% TX-100. After another centrifugation step, the resulting pellet was solubilised in 8 M urea. A final centrifugation step was then performed. (A) Coomassie stained SDS-PAGE gel. (B) Western blot using an  $\alpha$ -His-tag antibody. (C) Western blot using Strep-Tactin conjugated to alkaline phosphatase (for Strep-tag detection). M, molecular weight standards (in kDa); 1, supernatant after cell breakage; 2, supernatant after detergent solubilisation; 3, supernatant after solubilisation in 8 M urea; 4, pellet after solubilisation in 8 M urea.

### 5.1.6 VDE production in soluble form

Production conditions to obtain ArabVDE in soluble form were optimised by testing different *E. coli* strains, expression temperature, medium composition and IPTG concentrations for induction.

In all the conditions that were tested, ArabVDE was expressed at least partially as inclusion bodies (Figure 5-10). Most conditions did not yield any soluble expression. The exceptions were two very mild induction conditions using substantially lower temperatures and a lower IPTG concentration.

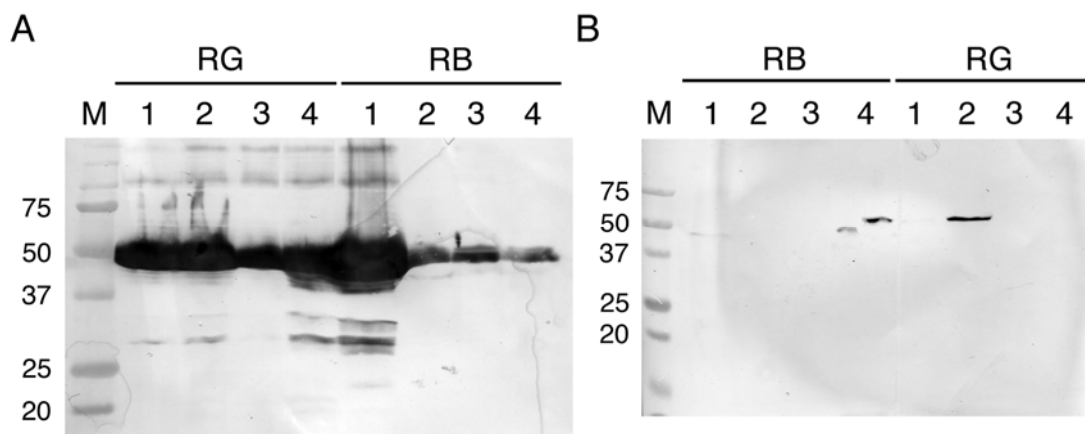


**Figure 5-10 - Optimisation of soluble VDE expression in *E. coli* (I).**

To obtain ArabVDE in a soluble form, different strains and expression conditions were tested. *E. coli* strains used were RosettaBlue (RB) and Rosetta-gami (RG), both growing in TB medium at 37 °C before induction. M, molecular weight standards (in kDa); 1, induction with 1 mM IPTG, expression at 37 °C for 4 hours; 2, induction with 0.1 mM IPTG, expression at 25 °C for 4 hours; 3, induction with 0.1 mM IPTG, expression at 25 °C for 18 hours; 4, induction with 0.4 mM IPTG, expression at 16 °C for 18 hours. (A) Western-blot against His-tag of the pellet after cell breakage (inclusion bodies); (B) Western-blot against His-tag, using the supernatant after cell breakage (soluble proteins).

Further optimisation of the expression conditions that led to the first soluble expression did not increase the protein yield. It was found that Rosetta-gami cells induced with 0.1 mM IPTG at 25 °C produced the most soluble protein.

As the amount of IPTG required to induce the cells for production of ArabVDE in soluble form was low, cultures were grown overnight without IPTG to verify if the protein could be obtained by “leaky” expression. Two temperatures were tested (30 and 37 °C) but neither led to detectable amounts of recombinant protein.

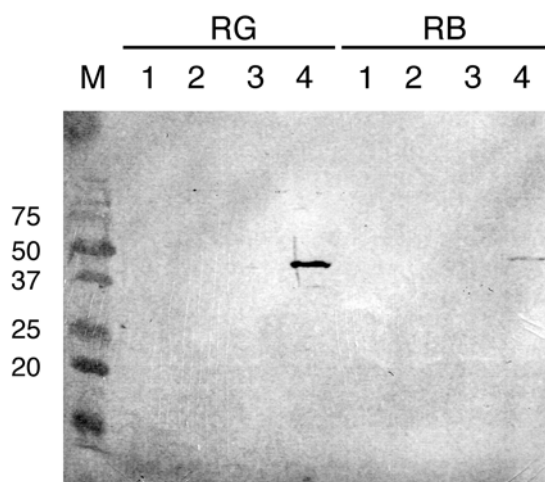


**Figure 5-11 - Optimisation of soluble VDE expression in *E. coli* (II).**

The figure shows a Western-blot using an  $\alpha$ -His-tag antibody. The same amount of protein (supernatant of broken cells) was loaded onto each lane. M, molecular weight standards (in kDa); RG, Rosetta-gami cells; RB, RosettaBlue cells; 1, overnight expression in TB medium at 30 °C; 2, overnight expression in TB medium at 37 °C; 3, expression in LB medium at 25 °C for 4 hours, induced with 0.1 mM IPTG; 4, expression in TB medium at 25 °C for 4 hours, induced with 0.1 mM IPTG.

### 5.1.7 VDE purification under denaturing conditions

ArabVDE is already quite pure in the inclusion body fraction, as determined by SDS-PAGE (Figure 5-12). However, subsequent refolding and crystallisation experiments would benefit from removing the few contaminants and therefore an additional purification step was performed.

The inclusion bodies were solubilised with a denaturing agent (8 M urea or 6 M guanidinium chloride) and centrifuged to remove any unsolubilised material. The supernatant containing the denatured proteins was loaded onto an immobilised Ni column for His-tag affinity chromatography. The choice of the denaturing agent turned out to affect the success of the affinity chromatography (Figure 5-12). When solubilised with guanidinium chloride, the protein did not bind to the column material, and all the protein eluted in the flow-through or during the washing step. On the other hand, protein solubilised in urea was quite strongly bound to the column material. The elution is usually done by pH shift with a buffer at pH ~4. This was not sufficient to completely elute the protein from the column, and 250 mM imidazole was added to retrieve the rest of the protein. ArabVDE was essentially pure after this step.

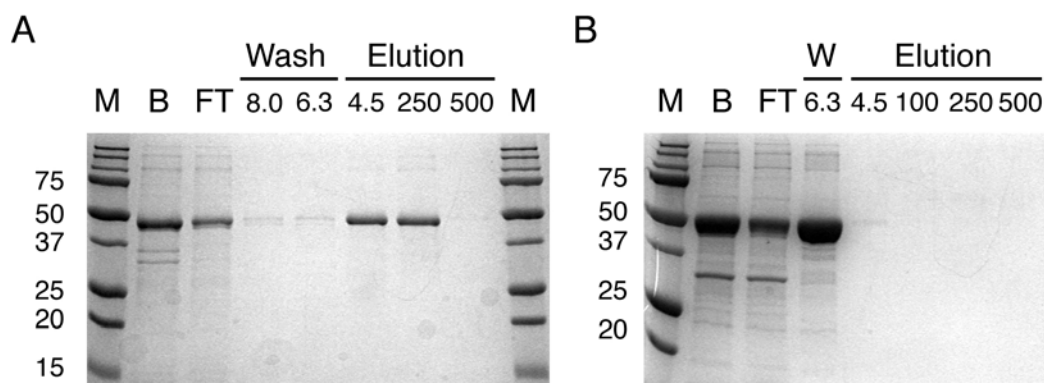


**Figure 5-12 - Purification of VDE in denaturing conditions.**

Coomassie stained SDS-PAGE from different fractions during ArabVDE purification under denaturing conditions. VDE inclusion bodies were unfolded using (A) 8 M urea or (B) 6 M guanidinium chloride. VDE was then further purified using His-tag affinity chromatography under denaturing conditions. M, molecular weight standards (in kDa); B, samples before chromatography; FT, flow-through; W, wash; 8.0, 6.3 and 4.5 indicate the solution pH; 100, 250 and 500 indicate imidazole concentrations.

### 5.1.8 VDE purification under native conditions

The two affinity tags at either end of the ArabVDE construct were used for purification under native conditions.

On the first purification step the complete soluble fraction of the *E. coli* lysate was loaded onto a Strep-tactin column (Figure 5-13 A). Most contaminants were removed by the washing step and the elution fractions contained pure protein corresponding to ArabVDE. Even though the concentration of soluble VDE in the *E. coli* lysate was low, as confirmed by Western-blot, the recombinant protein was highly concentrated and purified in this single purification step. One of the contaminants present in the elution fractions runs on the SDS-PAGE just below the 20 kDa marker, analogous to the cross-reaction band in the  $\alpha$ -Strep-tag Western blot (Figure 5-9). This suggested that this band was due to specific binding of the Biotin Carboxyl Carrier Protein from *E. coli* to the Strep-tactin column. Adding monomeric avidin to the *E. coli* lysate removed this contaminant almost completely from the elution fractions, without interfering with the binding of ArabVDE to the column.

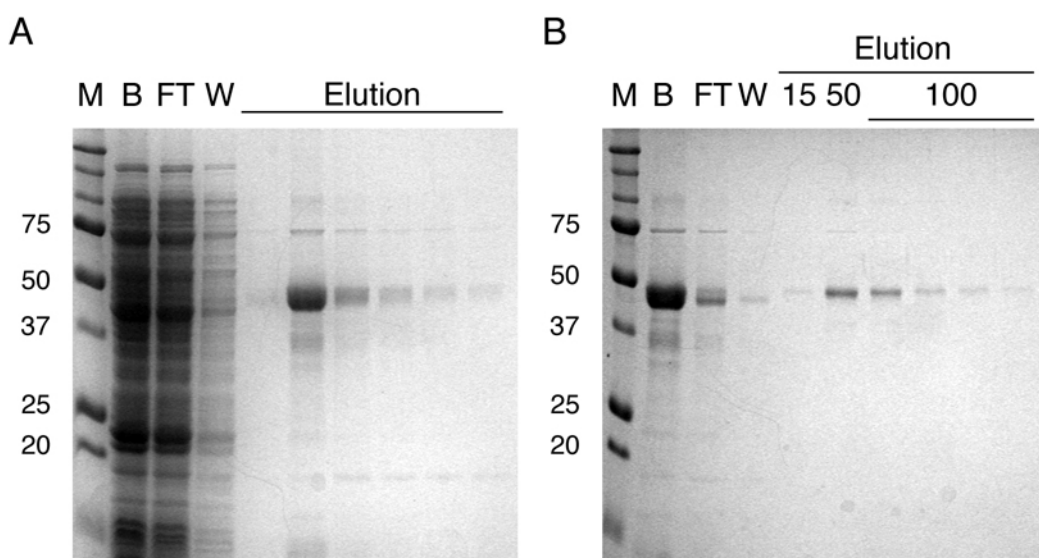


**Figure 5-13 -Purification of VDE expressed in native conditions.**

VDE expressed in soluble form was purified by using two consecutive purification steps by affinity chromatography. (A) SDS-PAGE after the Strep-tag affinity chromatography; (B) SDS-PAGE after the subsequent His-tag affinity chromatography. The complete soluble fraction of the *E. coli* lysate was loaded onto the Strep-tactin column (lane B in figure A). M, molecular weight standards (in kDa); B, samples before chromatography; FT, flow-through; W, wash; 15, 50 and 100, correspond to imidazole concentrations used for elution during the His-tag affinity chromatography.

A second purification step was added to increase the purity of ArabVDE, using the C-terminal His-tag (Figure 5-13 B). Binding to the column material was rather weak. A portion of ArabVDE was eluted either with the flow-through or during the washing step. Nevertheless, the fractions eluted with 50 and 100 mM imidazole contained virtually only ArabVDE.

By the end of the two purification steps, the yield of ArabVDE obtained in soluble form was low. Typically, 0.1 – 0.2 mg of pure protein were obtained from 1 l of *E. coli* culture in TB medium.

Possibly due to the protease inhibitors added to the *E. coli* lysate just after cell breakage, there were no signs of degradation of ArabVDE due to proteolysis.

### 5.1.9 Expression and purification of Thrx-VDE fusion

Soluble expression of ArabVDE was greatly enhanced after fusion with thioredoxin (Thrx). The exact same protocol used to express ArabVDE in soluble

form was applied to the fusion protein. Both constructs with and without the C-terminal His-tag were tested.

The complete soluble fraction of the *E. coli* lysate was incubated with the Ni-affinity gel (Figure 5-14). Binding to the Ni-affinity gel in batch mode was not complete and a substantial fraction of the recombinant protein was eluted from the column in the flow-through. Bound ArabVDE eluted gradually with increasing concentrations of imidazole. A substantial portion of the protein only eluted from the column with 500 mM imidazole, suggesting very strong binding.

There was a very significant increase in the yield of soluble protein obtained when the fusion construct was used. Up to 1.5 mg of purified Thrx-ArabVDE were obtained per liter of *E. coli* culture in TB medium, which represents a ~10 fold increase compared to ArabVDE.

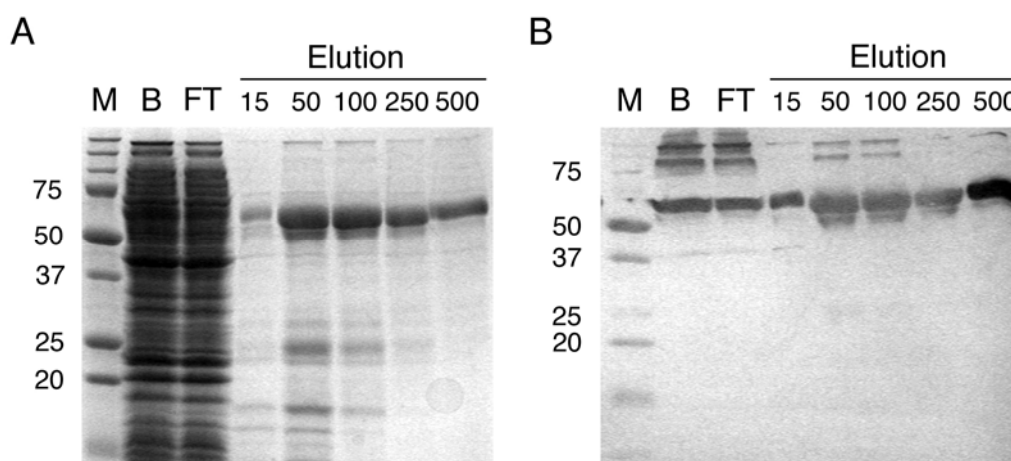


**Figure 5-14 - Expression and purification of Thrx-VDE fusion.**

The Thrx-ArabVDE fusion with a C-terminal His-tag was expressed in *E. coli* Rosetta-gami cells. Cells were broken, ultracentrifuged and the supernatant was loaded onto a Ni-affinity chromatography column. The fusion protein bound strongly to the column material and high concentrations of imidazole were required for complete elution. Fractions from the purification were analysed by (A) SDS-PAGE and (B) Western-blot using an  $\alpha$ -His-tag antibody. M, molecular weight standards (in kDa); B, samples before chromatography; FT, flow-through; 15, 50, 100, 250 and 500 correspond to imidazole concentrations used for elution.

---

### 5.1.10 VDE expression in HEK cells

Dr. Stephen Marino (Dept. of Molecular Membrane Biology, MPI of Biophysics) performed all cell growth and preparation procedures and assisted the author of the present work in performing the transient transfection experiments.

Expression of the eukaryotic enzyme VDE was tested in a eukaryotic expression system. Human Embryonic Kidney (HEK) cells were transiently transfected with a pTriEX6 vector carrying the ArabVDE and ArabVDE-Long constructs. The transfection was chemically promoted using the FuGENE HD Transfection Reagent from Roche.

It was interesting to notice that the same preference of ArabVDE over ArabVDE-Long observed in the bacterial expression systems was also true for the eukaryotic system (Figure 5-15). A larger amount of protein was obtained, as judged from the Western-blot, when the ArabVDE construct was mixed with the highest amount of transfection reagent that was tested. Already 24 hours after transfection a faint band with the correct size for ArabVDE was detected by Western-blotting. An even fainter band was observed with the same DNA/transfection reagent ratio for the ArabVDE-Long construct. For the ArabVDE construct, the condition that yielded a signal after 24 hours showed a stronger signal after 48 hours. The intensity of the ArabVDE-Long band was only marginally higher after 48 hours.

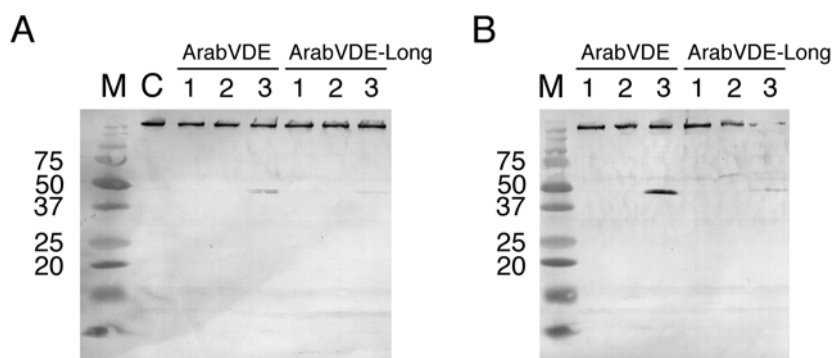


**Figure 5-15 - Expression of VDE in HEK cells.**

Western-blot analysis using an  $\alpha$ -His-tag antibody on HEK cells transiently transfected with the ArabVDE and the ArabVDE-Long constructs in the pTriEx6 vector. Cells were harvested (A) 24 and (B) 48 hours after transfection. M, molecular weight standards (in kDa); C, control experiments with non-transfected cells; 1, 2 and 3 correspond to transfection mixtures containing 2  $\mu$ g of DNA and 3, 4 or 5  $\mu$ l of Fugene HD Transfection Reagent, respectively.

### 5.1.11 Preliminary activity assays

The enzymatic conversion of Vio to Zea can be monitored spectroscopically and used to assess VDE activity (Yamamoto, 1985). The original protocol was downscaled to make use of the 96-well plate reader and some pilot assays were performed.

ArabVDE expressed in Rosetta-gami cells and purified under native conditions was used for these assays. The obtained reaction curves were quite noisy and the reaction seems to have started immediately after addition of the enzyme (Figure 5-16). Some of the initial data points were not recorded for the reactions with higher amounts of ArabVDE. There was nevertheless a clear correlation between the amount of enzyme added to the mixture and the amount of Vio converted to Zea, judging from the final values of  $A_{502}-A_{540}$ .

Due to the large spread of the data points in the experimental curves, statistically sound values for the specific activity of the sample would require a larger number of measurements. However, the main goal of these experiments was to adapt the original protocol to a format with higher-throughput, so that the activity assays can be used to monitor the refolding experiments and the specific activity of the samples purified in native conditions.



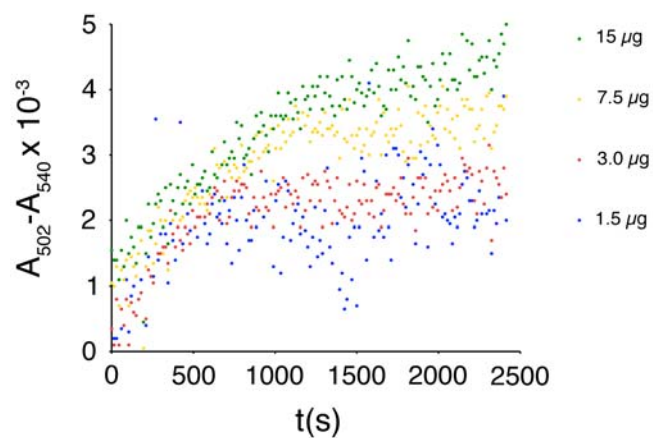


**Figure 5-16 - VDE activity assay.**

$A_{502} - A_{540}$  is proportional to the amount of Vio converted to Zea and increases with time and the amount of ArabVDE added to the reaction mixture.

## 5.2 Discussion

### 5.2.1 VDE production in bacteria

Establishing a protocol for the heterologous expression and purification of VDE is an essential requirement for determining its structure. In addition, active recombinant VDE is undoubtedly a very valuable tool for the study of qE, as it would open the possibility to investigate the dynamics of the Vio by Zea exchange in the LHCs and the qE kinetics in general.

*Arabidopsis* VDE is a difficult target for expression in *E. coli* for two main reasons. First, the coding sequence of this eukaryotic enzyme is suboptimal for bacterial expression. It had in fact already been shown that the addition of the *argU* gene that encodes the *E. coli* arginine AGA tRNA significantly improves the production yield (Hieber et al, 2002). For this reason, the first expression tests were performed with the *E. coli* RosettaBlue strain (Section 5.1.3), which carries an additional plasmid coding rare tRNAs, including the AGA tRNA. The large amounts of inclusion bodies routinely obtained in a variety of expression conditions confirm that this choice of expression strain solved the codon usage problem.

Looking at the VDE gene sequence (Appendix), it is evident that the cysteine-rich N-terminal part of the protein, where the active site is located, constitutes the second and more intricate problem. The exact function of all the 11 cysteines in the first 80 residues is not known and in fact only a structure of VDE can elucidate that. The reversible inhibition by DTT (Bugos & Yamamoto, 1996) suggests that at least part of the residues are involved in the enzyme's fold. Indeed, the increase in soluble protein yield after protein expression in Rosetta-gami cells (which are mutated in both thioredoxin reductase and glutathione reductase genes and also carry the additional plasmid with rare tRNAs) is another clear indication that some of the cysteine residues establish disulphide bridges required for proper folding (Section 5.1.4).

Another increase in the soluble protein yield was achieved by fusing thioredoxin with VDE (Section 5.1.9). However, it is not clear in this case whether that was just a consequence of the extremely high solubility of thioredoxin, which kept the unfolded VDE part of the fusion in solution, or due to a real improvement

---

in VDE folding. Indeed, the combination of thioredoxin fusions and expression in *trxB* mutant cells (like the Rosetta-gami strain used in this work) has been shown to enhance disulphide bond formation in the cytoplasm of *E. coli* (Stewart et al, 1998). The enterokinase cleavage site between the two proteins in the fusion can be used to elucidate which of the two hypotheses is correct.

While no reference to any metal binding has ever been reported, it is plausible that some of the cysteines form a metal-sulphur centre, possibly an iron-sulphur cluster. Iron-sulphur clusters are best known for their role in many oxidation-reduction enzymes such as ferredoxins, hydrogenases, and nitrogenases. Although VDE does not belong to the same category of any of these classes of enzymes, the de-epoxidation reaction does involve the oxidation (removal of one electron and one proton) of ascorbic acid to produce dehydroascorbate. This possible metal binding site or cluster should be taken into consideration for future experiments, in particular while refolding VDE expressed as inclusion bodies.

#### **5.2.1.1 Soluble expression or refolding?**

As happens frequently in bacterial over-expression, the largest fraction of expressed VDE accumulated in the *E. coli* cytoplasm as inclusion bodies. Despite all efforts to lower the expression rate and enhance soluble expression the majority of the protein was found in an insoluble form, in virtually all tested conditions. Purification of VDE under denaturing conditions yielded highly pure protein (Section 5.1.7) and in quantities that were never matched by purification under native conditions.. The question arises as to route should be taken: refolding of unfolded protein expressed as inclusion bodies or optimisation of the soluble expression conditions?

Refolding of VDE has previously been described (Hieber et al, 2002; Morosinotto et al, 2002a). The refolded enzyme was shown to be active, although with much (at least 6 fold) reduced specific activity compared to the native enzyme. The detergent octyl- $\beta$ -D-glucoside is used in the refolding buffer, presumably to protect the hydrophobic cavity in the lipocalin domain of VDE from being exposed to the solvent. Interestingly, the refolding buffer does not contain any reducing or oxidising agent, nor does it include any metal apart from sodium. It seems therefore

very likely that these are suboptimal refolding conditions. Taking the available biochemical data into consideration, a number of experimental parameters may be important when designing new refolding conditions (Table 5-1).

**Table 5-1 - VDE refolding conditions**

Parameter	Options	Rationale
<i>pH</i>	5.5 to 7.5	The enzyme is thought to undergo a large conformational change at low pH, which exposes the catalytic site to the solvent. Possibly, one of the two conformations is favourable for refolding.
<i>Redox agents</i>	TCEP, DTT, mixtures of reduced and oxidised glutathione	Correct folding depends critically on the establishment of disulfide bridges, the number of which is unknown. Tuning the redox properties of the refolding buffer may be critical to improve the refolding yield.
<i>Metals</i>	Iron, zinc, copper, nickel, other?	Although metal binding has never been reported, it is not unreasonable to think that some of the cysteine residues form a metal-sulphur centre.
<i>Substrate</i>	Vio	Binding of Vio to the central hollow of the enzyme could facilitate proper folding.
<i>Additives</i>	Arginine, detergents, PEGs	Most refolding protocols include additives which are frequently hydrophobic compounds. Detergents are often used below the critical micelle concentration.

The refolding success can be most effectively evaluated by the activity assay (Section 5.1.11)(Yamamoto, 1985). Also SEC will give valuable information regarding the conformational homogeneity of the refolded product, which is an essential requirement for crystallisation.

If instead expression of soluble VDE is favoured, another large set of experimental parameters have to be optimised. Several of these have already been tested, including different constructs, medium, temperature, cell density and bacterial strains. Another promising strategy is to target the translated product to the periplasm of the expression host cells. Relative to the cytoplasm, the periplasm has a much more oxidising environment, which could improve disulphide bridge formation.

---

### 5.2.2 VDE production in eukaryotic cells

A common rule of thumb in protein expression is: bacterial protein, bacterial host and eukaryotic protein, eukaryotic host. The problems encountered during the establishment of the bacterial expression system of VDE seem to support this rule. Only one eukaryotic expression system (HEK cells) was tested and the results were somewhat inconclusive. ArabVDE expression was detected 24 hours post-transfection, and increased after 48 hours (Section 5.1.10). Expression of the ArabVDE-Long construct was also detected, but only 48 hours post-transfection. For both constructs expression was only observed for the conditions in which higher amounts of transfection reagent were used. These results can only be considered as preliminary but they are promising. It should be noted that the maintenance of HEK cells is a laborious procedure and large-scale expression in this system is expensive. Further experiments are definitely needed to justify taking this route.

A eukaryotic expression system, either using mammalian, insect or yeast cells, may well be the most straightforward route to obtain the amounts of recombinant VDE required for crystallisation.

## **6 LHC-II CRYSTALLISATION**

Two goals of this doctoral work were to investigate the functional properties of LHC-II in single crystals and to improve the current LHC-II crystal structures. Reproducing previously obtained crystal forms and finding new crystallisation conditions were therefore a priority.

---

## 6.1 Results

### 6.1.1 Reproduction of type-I pea LHC-II crystals

To precisely establish the link between the LHC-II crystal structure and the spectroscopic properties of the complex in the crystalline state, it was necessary to reproduce the crystals from which the structure of pea LHC-II had been determined (Standfuss et al, 2005).

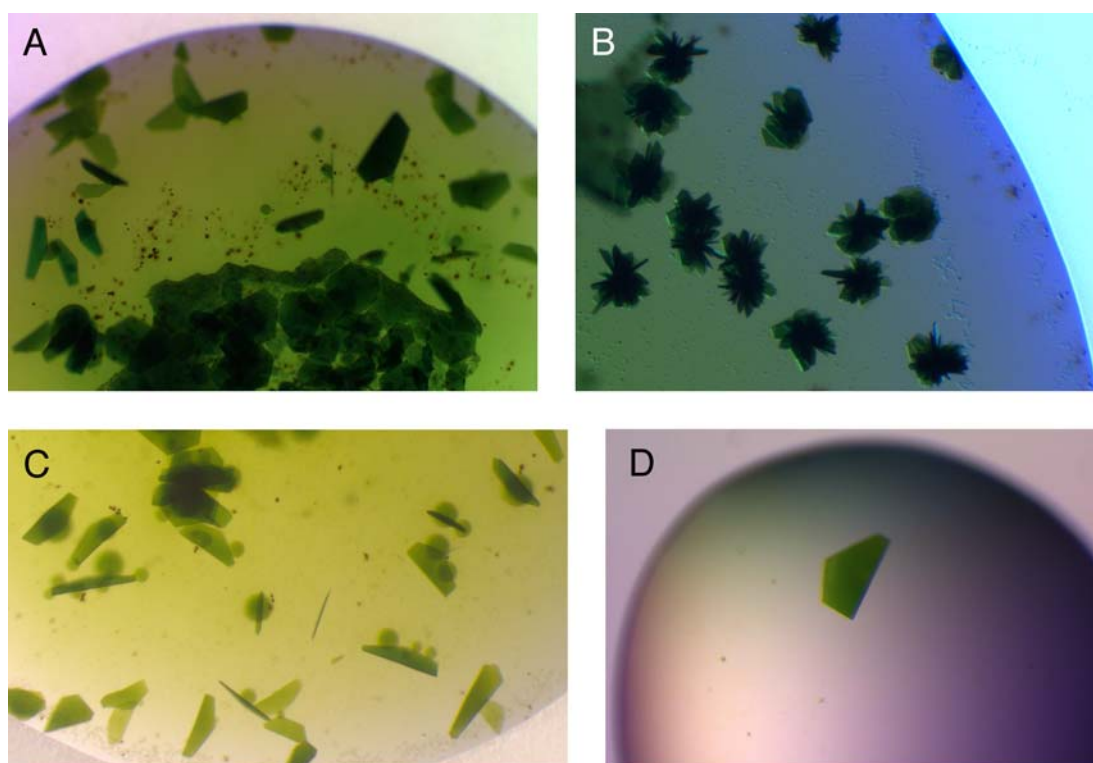


**Figure 6-1 - Type-I pea LHC-II crystals.**

The crystallisation conditions previously established in the lab by Dr. Jörg Standfuss were reproduced (A). (B) Rarely, clusters of crystals were obtained. (C) Very thin plates were also obtained, which were particularly suitable for spectroscopic measurements. (D) A crystal harvested from the crystallisation drop and washed in cryo-protection solution without visible damage.

During this work, a total of ~11500 droplets (160 x 24-well plates, each well with 3 different droplets) were set by hand around these conditions. The success of the crystallisation trials was very dependent on the LHC-II preparation, and the crystals not easily reproducible. Type-I crystals growing from the conditions described in (Standfuss et al, 2005) were not obtained with most pea LHC-II

preparations (Section 4.1.1). A good indication of the crystallisability of a preparation was the extent of precipitation that occurred immediately after setting the crystallisation droplets. Only those preparations from which the droplets remained clear (homogeneously light green) for the first 1 to 2 days eventually yielded crystals. However, the converse was not necessarily true, as clear drops didn't always lead to crystals. Note that these different tendencies to precipitate among different preparations were not correlated with Chl or detergent concentration, as these were screened carefully with all preparations around the same standard concentrations.

Crystallisation was attempted at 4, 12, 15, 18 and 22 °C. The original conditions specified 18 °C, but during this work more crystals were obtained at 15 °C and, especially, 12 °C. In general, higher temperatures lead to precipitation and lower temperatures to extensive phase separation. Also the most successful PEG 350 and glycerol concentrations were slightly lower than in the original crystallisation conditions, the optimal range of both being between 10 and 12 %.

Crystals usually appeared one week after setting the crystallisation plates, and grew for another week. The resulting crystals were in general thinner (up to 15 µm thick) than those used to solve the pea LHC-II structure which measured 400 x 400 x 20 µm (Standfuss et al, 2005) (Figure 6-1).

The cryo-protection solution for these crystals had the same composition as the mother liquor, except that the concentration of both PEG 350 and glycerol were increased to 20 % and NG was added to 0.9%. Consecutive soaks in this cryo-protection solution did not visibly damage the crystals (Figure 6-1 D) and, most importantly for spectroscopic measurements, did not dissolve them.

### **6.1.2 New crystallisation conditions**

Aiming at a pea LHC-II structure at higher resolution, commercial crystallisation screens were used to identify new crystallisation conditions. Due to the almost inevitable thinness of the hexagonal plates that led to the first X-ray structure of pea LHC-II, the main goal was to obtain different crystal forms with a more favourable morphology.

---



LHC-II readily crystallised in a large variety of conditions. Figure 6-2 shows a few examples. In many cases, crystals grew directly on the 96-well plate using the solutions from the commercial screen and without requiring any further optimisation. Among the commercial crystallisation screens tested, the MemStart and MemSys screens from Molecular Dimensions and the MbClass II screen from Qiagen were particularly successful in obtaining crystals. However, with few exceptions, the crystals obtained with these commercial screens were thin hexagonal plates (Figure 6-2 C, D and F for example).

In the 24 well plate format, some other crystallisation conditions yielded octahedral crystals (Figure 6-2 A and B). These conditions had a remarkably simple composition, containing KCl or phosphate salts at relatively low concentrations (25 to 300 mM). None of these crystals diffracted X-rays at a synchrotron source, despite their large size (more than 200  $\mu\text{m}$  across).

More promising conditions were found with a combination of PEG 400 and ammonium sulphate. The initial hit on the commercial screen was composed of 0.1 M HEPES pH 7.5, 2% PEG 400 and 2 M ammonium sulphate. Remarkably, when the initial condition was optimised, a large variety of crystals was obtained (Figure 6-3). The bulk of the crystals were plates, either hexagonal, triangular or a combination of both, similar to a six-pointed star. Some other crystals had a brick-like morphology, but these grew to a relatively small size. Interestingly, some of these brick-shaped crystals grew out of phase separation droplets. The most promising crystals had a rhomboid morphology (Figure 6-3 E). These crystals appeared macroscopically very similar to those obtained in 0.1 M Na chloride, 0.1 M tri-Na citrate, pH 5.6, 30% PEG 400 (Figure 6-2 E), although the chemical composition of the drops was very different.

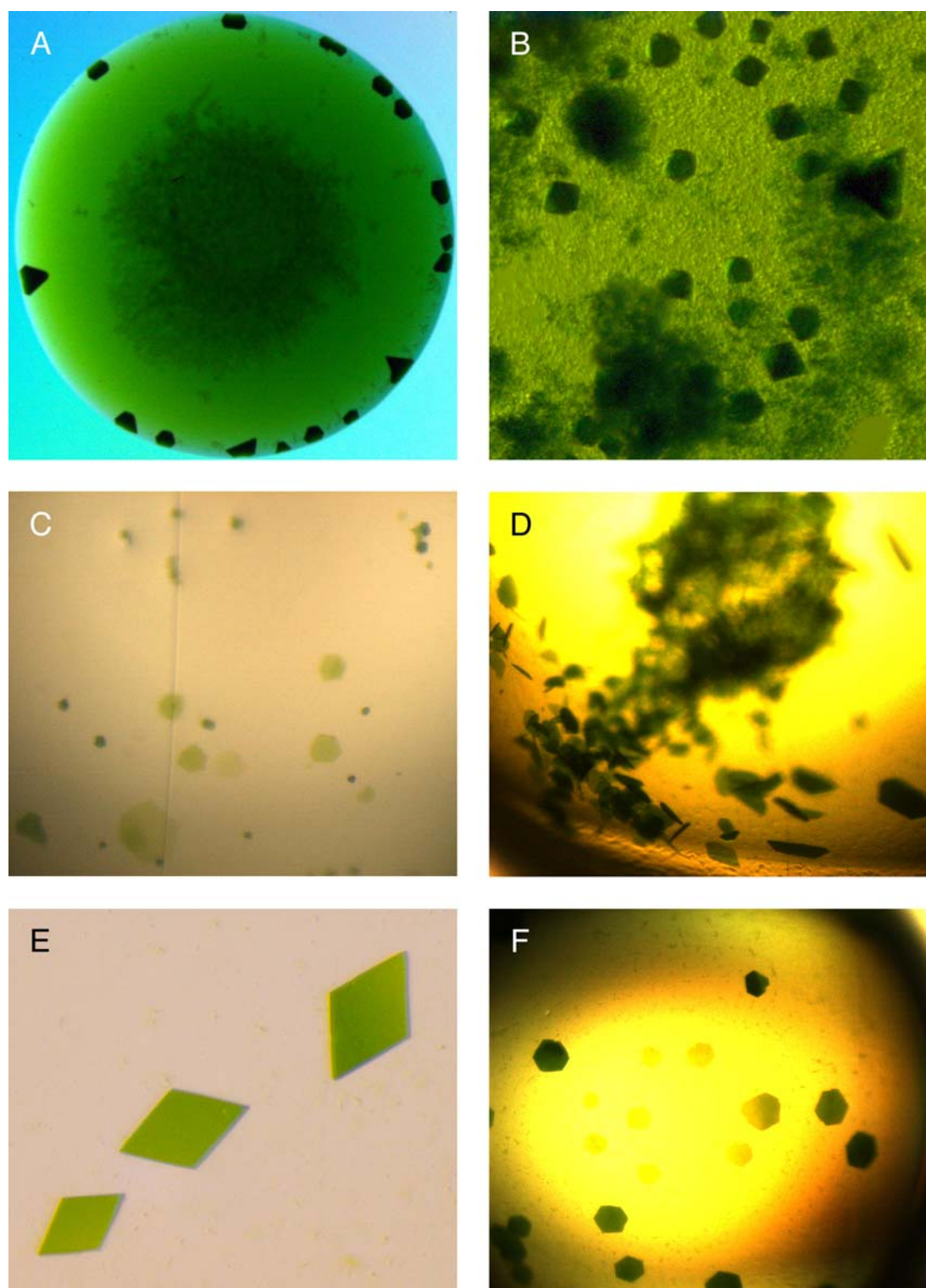


**Figure 6-2 –LHC-II crystals grown from various crystallisation conditions.**

A variety of crystal morphologies was obtained. The conditions in 96-well plates came from commercial screens, while the conditions in 24-well plates were either optimisation of hits from commercial screens or of other conditions described in the literature. (A) 300 mM KCl, 24-well plate; (B) 25 mM Na phosphate, 24-well plate; (C) 0.5 M LiCl, 1.0 M tri-Na citrate, pH 5.6, 96 well plate; (D) 0.1 M KCl, 5% PEG 400, 96 well plate; (E) 0.1 M Na chloride, 0.1 M tri-Na citrate, pH 5.6, 30% PEG 400, 96 well plate; (F) 50 mM Na phosphate, pH 6.7, 5% PEG 4000, 96-well plate.

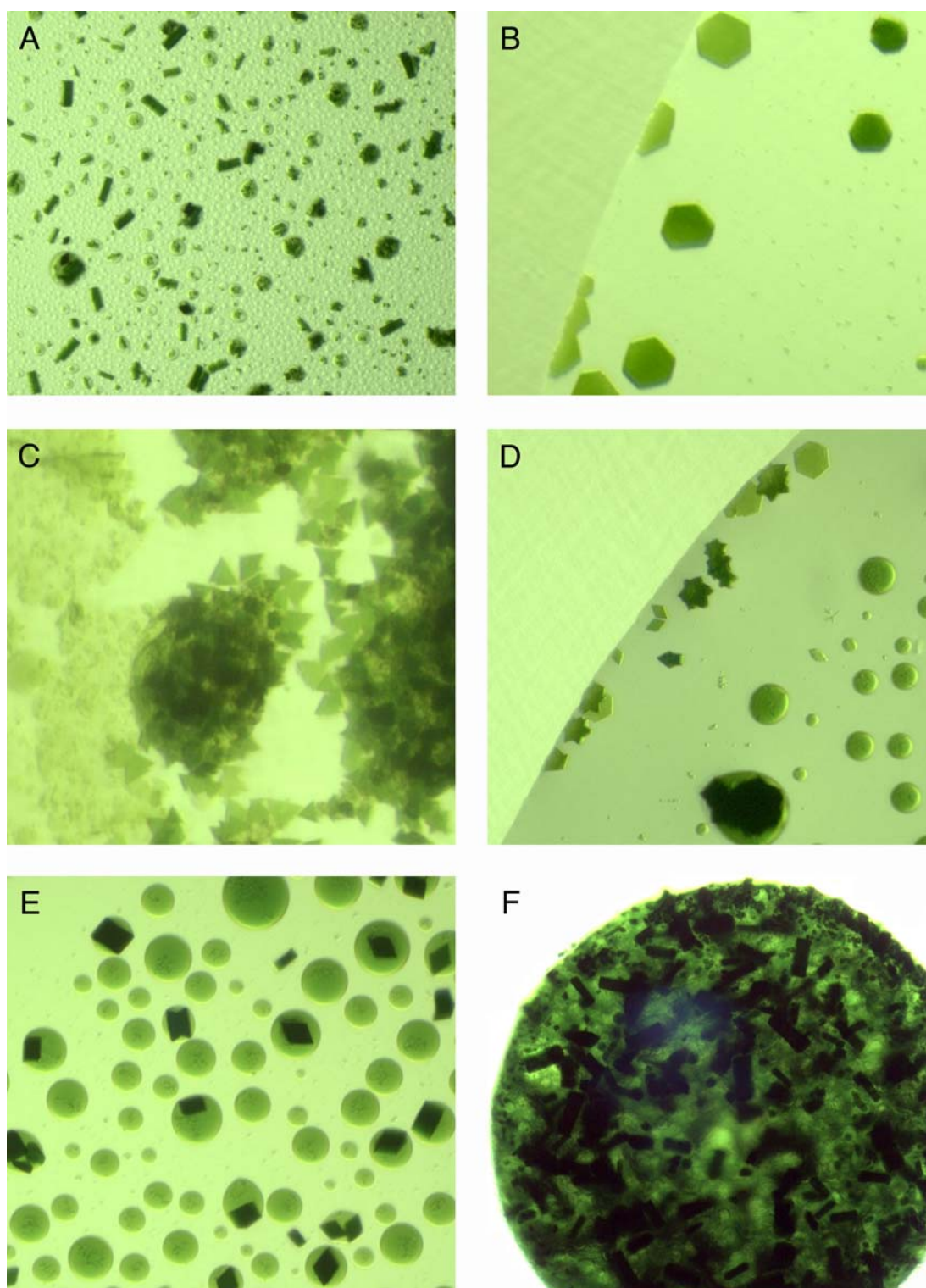


**Figure 6-3 – Different LHC-II crystal morphologies from the same crystallisation conditions.**

A hit from the commercial crystallisation screens (0.1 M HEPES pH 7.5, 2% PEG 400 and 2 M ammonium sulphate) was optimised. All the crystals presented in this panel were obtained in this condition. The variety of crystal morphologies is striking, including (A and F) rectangular bricks, (B) hexagonal plates, (C) triangular plates, (D) Six-pointed star plates and (E) rhomboid bricks. In some cases in (E) and (F) crystals grew out of phase separation droplets. A practical student, Kevin Hall, obtained these crystals.

The first rhomboid crystals that were tested at a synchrotron radiation source (beamline PXII at the SLS) diffracted to almost 4 Å (Figure 6-4). These crystals were obtained in a 96 well plate after 12 days at 8 °C, with minimal optimisation from the hit in the commercial crystallisation screen and a very tentative cryo-protection (increased PEG 400 concentration). A closer inspection of the recorded diffraction verified the presence of two superposed diffraction patterns. There was evidence for radiation damage, as after recording 40 images, the high-resolution reflections did not reach the same ~4 Å limit as at the beginning of data collection. It was not possible to index the reflections from these crystals, most likely due to the multiple diffraction patterns recorded in the images.

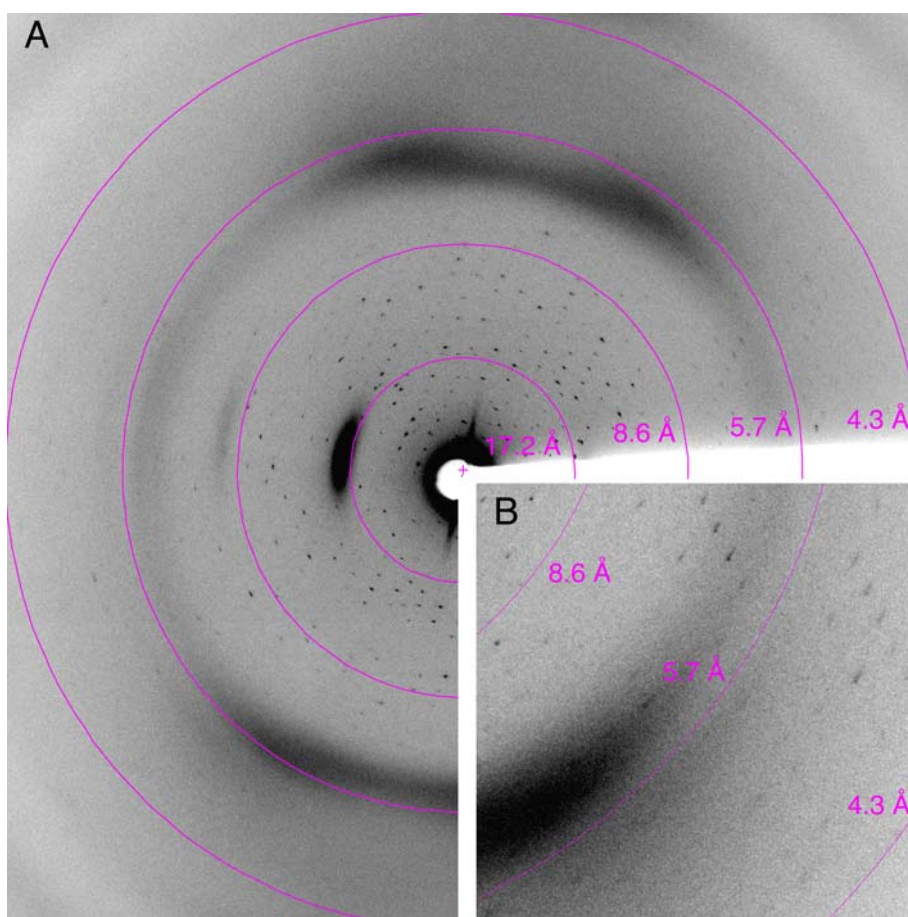


**Figure 6-4 - Diffraction pattern from a rhomboid LHC-II crystal.**

Crystals grown at 8 °C in 0.1 M HEPES pH 7.5, 2% PEG 400 and 2 M ammonium sulphate were tested for X-ray diffraction at the SLS. The crystal used to obtain this diffraction pattern corresponds to one of those presented in Figure 6-3 (E). The reflections of highest resolution are at ~4 Å.

A very similar condition (0.1 M HEPES pH 7.5, 4% PEG 400 and 1.9 M ammonium sulphate) yielded interesting rectangular bricks in a 24 well plate (Figure 6-5). These crystals were not reproducible. In all other plates prepared to reproduce this condition, only extensive phase separation and/or precipitation occurred.

These crystals were also tested for diffraction (Figure 6-6). Already in the initial diffraction tests, the crystals diffracted to almost 2.8 Å. However, these crystals also presented multiple lattices, as indicated by the presence of several (more than 2) superposed diffraction patterns in the diffraction images.

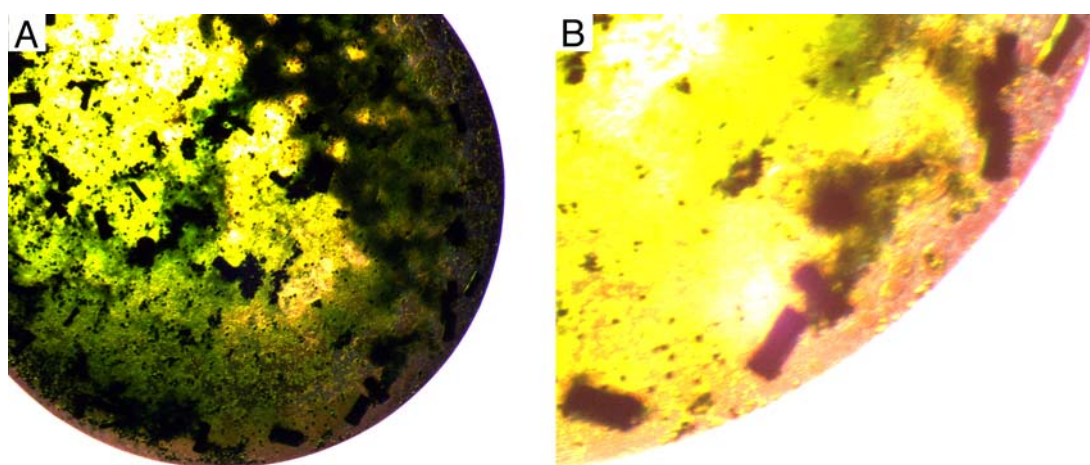


**Figure 6-5 - Brick-shaped LHC-II crystals.**

These crystals were obtained in 24 well plates after fine-tuning the condition that yielded the crystals in Figure 6-3. The mother liquor was composed of 0.1 M HEPES pH 7.5, 4% PEG 400 and 1.9 M ammonium sulphate. These crystals were not reproducible.

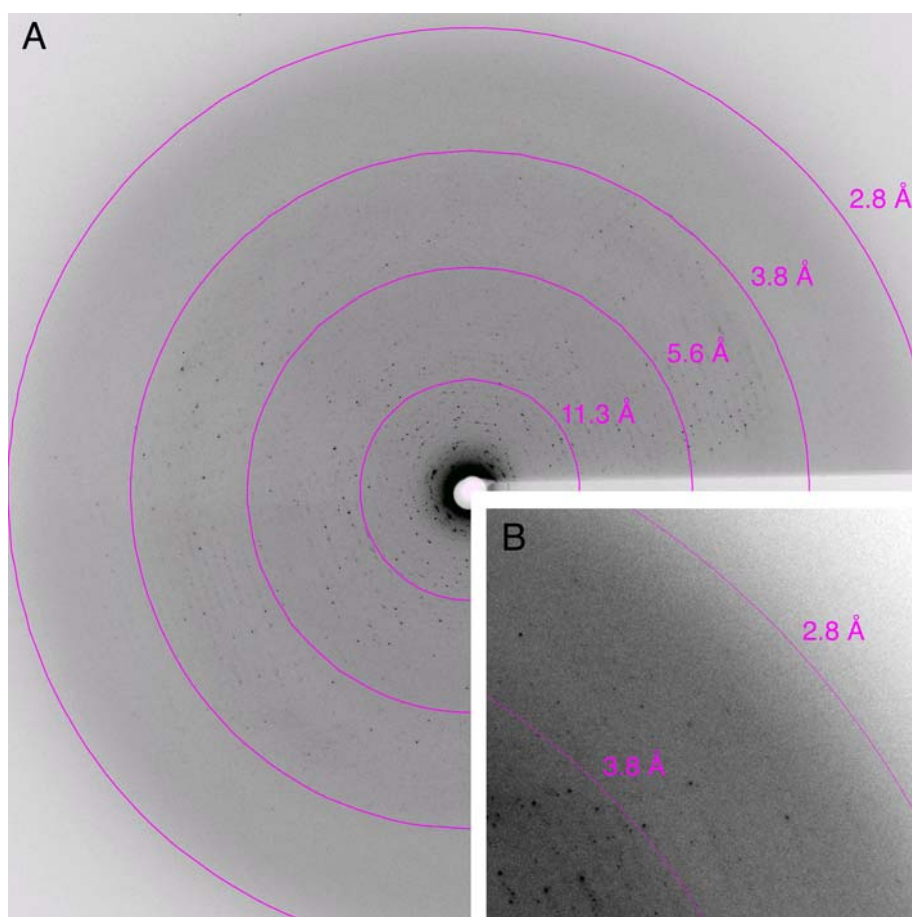


**Figure 6-6 - Diffraction pattern from small brick shaped LHC-II crystals.**

This figure shows a diffraction pattern of crystals presented in Figure 6-5 collected at the SLS. Inspection of the recorded diffraction (A) reveals the presence of multiple crystal lattices, as many diffraction patterns can be seen superposed. Nevertheless, a closer inspection of the high resolution reflections (B) reveals data beyond 3 Å resolution.

### 6.1.3 Freeze-fracture of type-I LHC-II crystals

As the structure of pea LHC-II had been solved (Standfuss et al, 2005), the arrangement of the trimers in the crystal was revealed, showing the stacking of membrane-like two-dimensional crystals. Direct observation of this arrangement was possible by freeze-fracture.

Figure 6-7 shows a well-ordered region of a type-I LHC-II crystal, in which several (at least 6) consecutive layers of two-dimensional crystals can be seen. More importantly, the layers seem to be in register, i.e. stacked in an ordered fashion without noticeable rotation or shift of consecutive layers. The lines that the trimers in the crystal lattice form within each layer were used to evaluate the order of

stacking. In a well-ordered crystal, as in this case, the lines of consecutive layers are parallel.

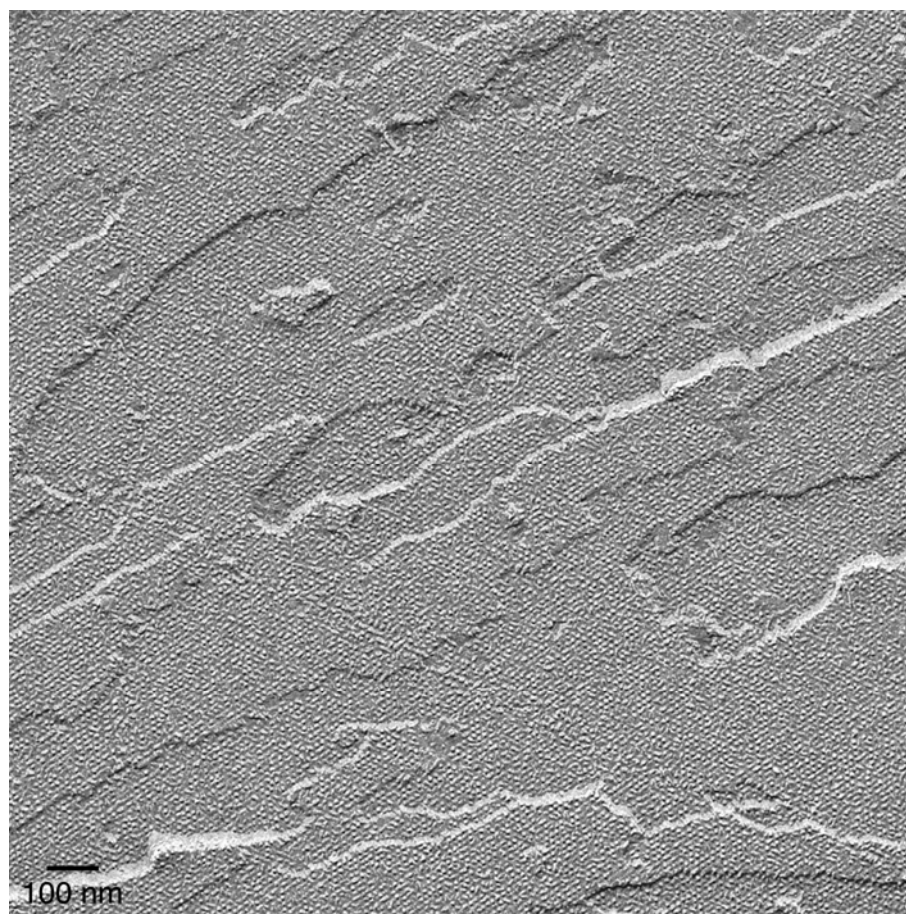


**Figure 6-7 - Freeze-fracture image of a type-I LHC-II crystal.**

Note the stacking of several two-dimensional crystals, with all layers in register.

Many type-I LHC-II crystals have one or more defects in their crystal lattice, and this could also be directly observed by freeze-fracture (Figure 6-8).

The most common problem with the type-I LHC-II crystals is the lack of order in the third dimension, i.e. nonspecific stacking of the two-dimensional crystals. Figure 6-8 A presents a close look at this phenomenon. Large sections of three different crystal layers can be seen out of register. The lines in each of the layers are not parallel to those of the next layer. Figure 6-8 B seems to indicate another problem with the stacking. The amount of staining between the consecutive layers indicated by arrows varies, which implies that the space between the layers also varies slightly.

LHC-II trimers are usually tightly packed within the layers of the type-I crystals. It was therefore surprising to observe a few small regions of the layers that appear to not have trimers (Figure 6-8 C). These gaps in the crystal lattice must be filled with lipid or detergent molecules. Interestingly, these defects in the lattice were observed in a region of the crystal that seems otherwise very well ordered.

The fourth defect in the crystal lattice revealed by freeze-fracture was the lack of planarity of some layers (Figure 6-8 D). In some regions, individual layers appear to be slightly folded, creating a wave effect. This effect seems to be dependent on the age of the crystals, as older crystals tend to show more of this wave-like effect. Surprisingly, crystals that were wavy still diffracted X-rays, even from a home source (not shown). The image additionally shows that the layers are out of register.

---



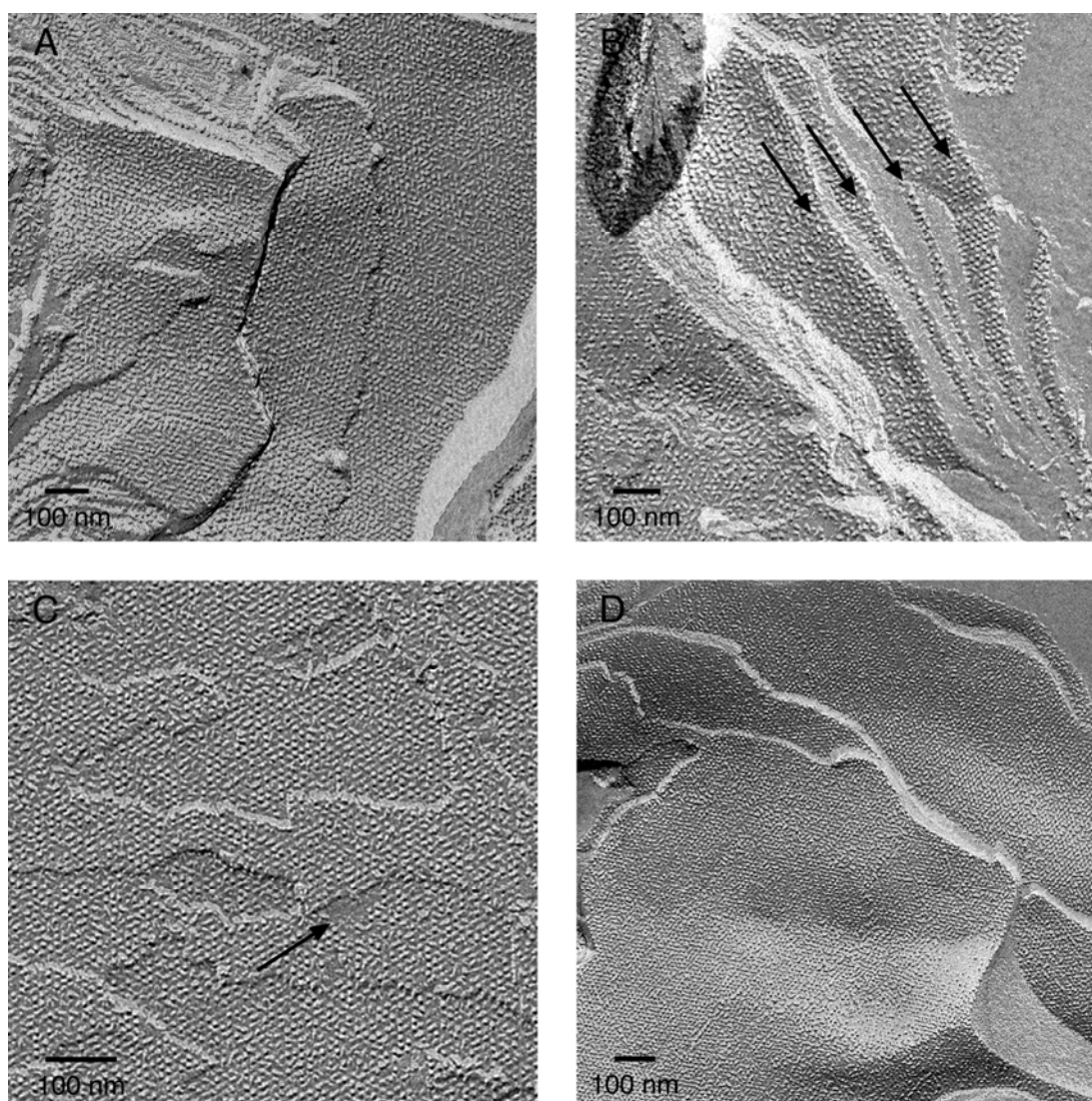


**Figure 6-8 – Defects in the crystal lattice of the type-I LHC-II crystals.**

Freeze-fracture was used to visualise some defects in the crystal lattice of the pea LHC-II crystals. (A) three layers are shown out of register; (B) the spacing between 4 consecutive layers (arrows) varies, as indicated by the different amounts of medium between each two layers; (C) a few small gaps in the crystal lattice were found (one example is indicated by an arrow). These gaps are probably filled with detergent and/or lipid molecules; (D) some layers of older crystals lose their planarity, creating a wave-like effect.

#### **6.1.4 Diffraction of crystals used for spectroscopic measurements**

LHC-II crystals of both type-I (Standfuss et al, 2005) and cubic (Kühlbrandt, 1987) crystal forms were used for spectroscopic measurements (Section 9). It was then interesting to determine if the exposure of the crystal to the bright excitation laser led to crystal damage. Single crystals mounted on the Cryobench system were transferred to liquid nitrogen and mounted afterwards on the beamline BM16 of the ESRF.

Many cubic crystals that were tested did not diffract X-rays at all. However, some other crystals showed weak diffraction, up to 20 Å resolution at best. The scenario was clearly different with the type-I crystals that were used at the Cryobench. Figure 6-9 shows one example. The presented diffraction pattern was collected with the same crystal that was used to generate all the data presented in Figure 9-10 and Table 9-2. This crystal was mounted on the Cryobench for several hours and exposed to the intense laser beam for a total time of about one hour. The high resolution reflections almost reach the 3 Å resolution limit in the initial diffraction images. The diffraction spots were quite well defined. There is therefore no evidence of light radiation damage induced by the excitation laser. In general, the type-I crystals used at the Cryobench had identical X-ray diffraction properties as any other type-I crystal: good diffraction in two dimensions and smeared and weak diffraction in the third dimension. As the crystals used for the spectroscopic studies were rather thin, this poor diffraction in the third dimension was even more pronounced.

---

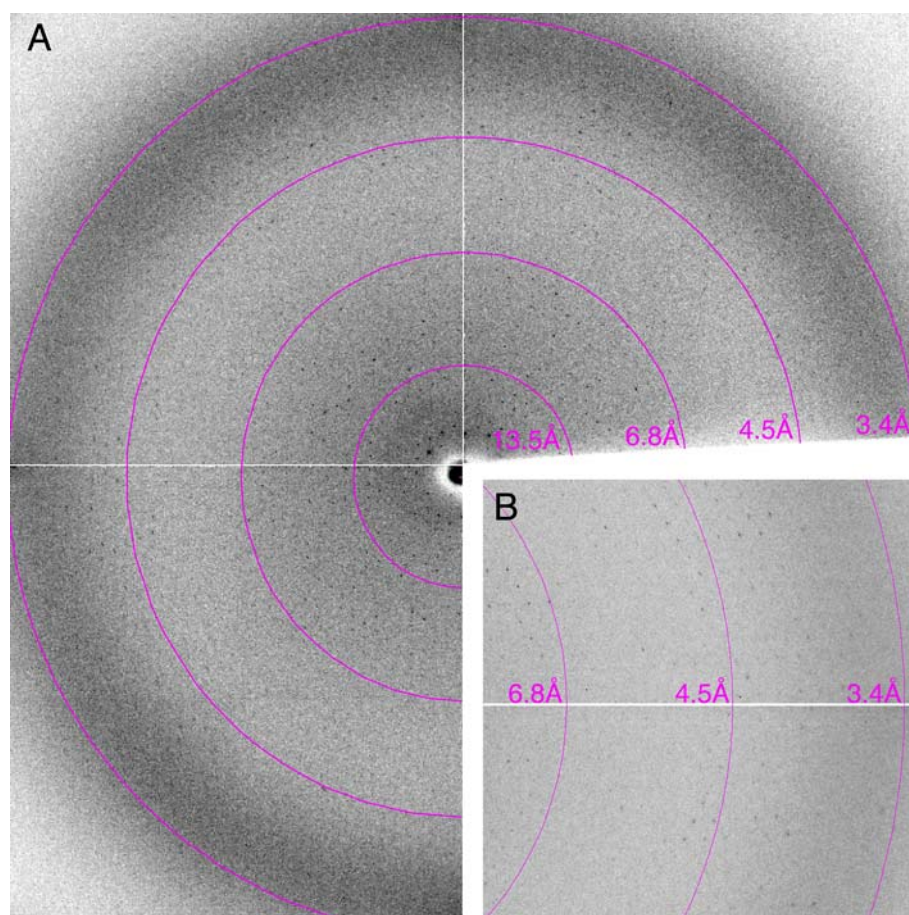


**Figure 6-9 - Diffraction pattern of a type-I LHC-II crystal used for spectroscopic measurements at the Cryobench.**

This figure shows a X-ray diffraction image of the crystal that was used to collect all the data presented in Figure 9-11, revealing reflections with resolution to almost 3 Å.

### 6.1.5 A peculiar diffraction pattern – the diffraction flower

While screening type-I LHC-II crystals at the SLS, a very unusual diffraction pattern from a pea LHC-II hexagonal plate was obtained. The first diffraction images collected already revealed the presence of two lattices. As the crystal was rotated by  $45^\circ$  and  $90^\circ$ , a very curious arrangement of the low-resolution spots was observed. A set of 6 perfect circles defined by reflection spots surrounded the centre of the diffraction image. Each of these small circles had another diffraction spot in the middle. This peculiar diffraction pattern vaguely resembles a sketched flower (Figure 6-10).

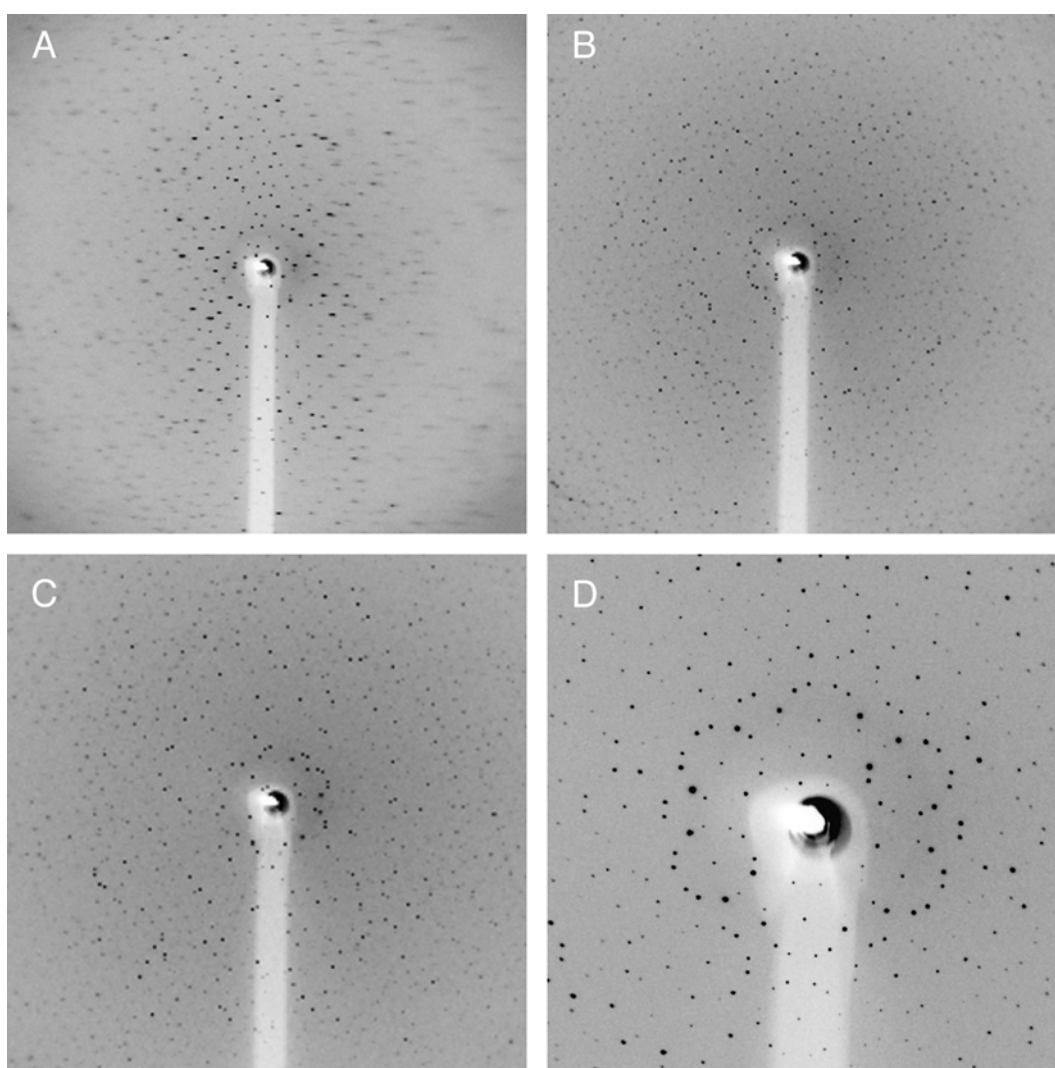


**Figure 6-10 - A peculiar diffraction pattern from a LHC-II crystal.**

(A), (B) and (C) show the diffraction patterns of the crystal at different tilt angles,  $45^\circ$  apart from one another. (D) Close-up on the diffraction pattern shown in (B), revealing the very peculiar arrangement of the of lower resolution reflections, which loosely resemble a sketched flower.

---

## 6.2 Discussion

### 6.2.1 Type-I LHC-II crystals

Reproducing the type-I pea LHC-II crystals from which the structure was solved (Standfuss et al, 2005) was not an easy task. Despite having a well defined set of standard crystallisation conditions in which these crystals usually grow, it was found that many pea LHC-II preparations did not yield crystals, regardless of how wide and fine the standard set of conditions were screened.

Although a proper statistical analysis has not been performed, there was a reproducible infamous seasonal dependence on the success of crystallisation. The most reliable preparations were invariably from plants grown during the summer. The reason for this season dependence is unknown and rather puzzling, as the pea plants were always cultivated in a growth room, completely isolated from the outside. Figure 4-1 shows a SDS-PAGE analysis of several randomly chosen samples prepared throughout this doctoral work. If the seasonal variability is caused by impurities, then they must be present in extremely low concentration, below the sensitivity of the Coomassie and silver staining. Other plausible explanations are that the ratio between the different LHC-II isoforms (Lhcb1-3) or the lipid content of the samples varies on a seasonal basis. During this doctoral work the group of Nathan Nelson published an interesting study on the purification and crystallisation of pea PS-I (Amunts et al, 2005). It was reassuring to read that in their case well diffracting crystals were only obtained during autumn and the beginning of winter.

The type-I crystals obtained were in general thinner than those used to determine the pea LHC-II structure. This turned out to be an accidental advantage, as the prepared crystals were almost exclusively used for spectroscopic studies, for which thinner crystals are actually better suited (Section 9.2.1 below). Another important aspect regarding spectroscopic studies with the type-I crystals was the necessity to ensure that no free pigments were kept in the solution surrounding the crystals. This was achieved by soaking the crystals in pigment-free cryoprotectant droplets, which did not promote any visible damage (Figure 6-1 D).

### 6.2.1.1 Defects in the LHC-II type-I crystal lattice

The type-I (Michel, 1983) pea LHC-II crystals have two common limitations: thinness and disordered stacking of consecutive layers, which in extreme cases can be seen in the light microscope. More often, crystal disorder is observed at the beamline, although sometimes with interesting visual results (Figure 6-10). The “diffraction flower” in Section 6.1.5 is a good example of disordered stacking of crystalline 2D layers. The recorded data most certainly originate from two (or possibly three) crystalline layers that are rotated (as in Figure 6-7 A), so that the corresponding diffraction patterns are equally rotated by the same angle.

Electron microscopy of freeze-fracture replicas uncovered the typical defects in the LHC-II type-I crystals in a very interesting way and also revealed other imperfections that could not be seen by light microscopy or X-ray diffraction (Section 6.1.3). Anisotropic diffraction, manifest in poor diffraction in the z direction, is far from being an exclusive problem of these pea LHC-II crystals. Many other similar type-I crystals of other membrane proteins also suffer from the same problem. Our freeze-fracture study gave some clues regarding possible causes of this problem, namely the variable repeat distance between successive layers (Figure 6-7 B) and bending of the 2D crystal layers (Figure 6-7 D).

### 6.2.2 Improving the LHC-II structure

Structural biology seeks to understand a given biological process by determining and analysing the 3D architecture of the involved macromolecules in ever more detail – the structural biology credo: resolution, resolution, resolution. Our understanding of the LHC-II structure-function relationship exemplifies this very well, as it was built on the back of successive models of increasing resolution. We are now at the point where the 2.5 Å resolution structure (Standfuss et al, 2005) revealed most secrets of the complex, but there remains much more to discover.

More detail requires higher resolution, which by its turn requires better crystals. After two decades of optimisation, it seems difficult to improve the type-I crystals any further. It should not be forgotten that the 2.5 Å dataset that was used to determine the structure was collected from a crystal that was truly exceptional. None of the other >400 crystals tested at the synchrotron, obtained from >100000

---

crystallisation experiments, yielded diffraction data of matching quality (Standfuss, 2004). It seems therefore wiser to search for new crystal forms.

A common strategy for improving crystals of macromolecules of known structure is surface engineering. This is most often done by mutation of surface exposed residues (Derewenda, 2004; Derewenda & Vekilov, 2006). Unfortunately, this is of no avail for LHC-II as it is obviously not possible to mutate the native complex purified from plant leaves. An alternative approach is to perform methylation of exposed lysine residues (Walter et al, 2006). Interestingly, a striking feature of the pea LHC-II structure is a set of three lysines (one per monomer) that protrude from the luminal surface of the complex and make salt bridges to glutamate or aspartate residues of the trimer immediately below in the crystal lattice (Figure 6-11). These are indeed some of the few crystal contacts between successive layers in the type-I crystals.

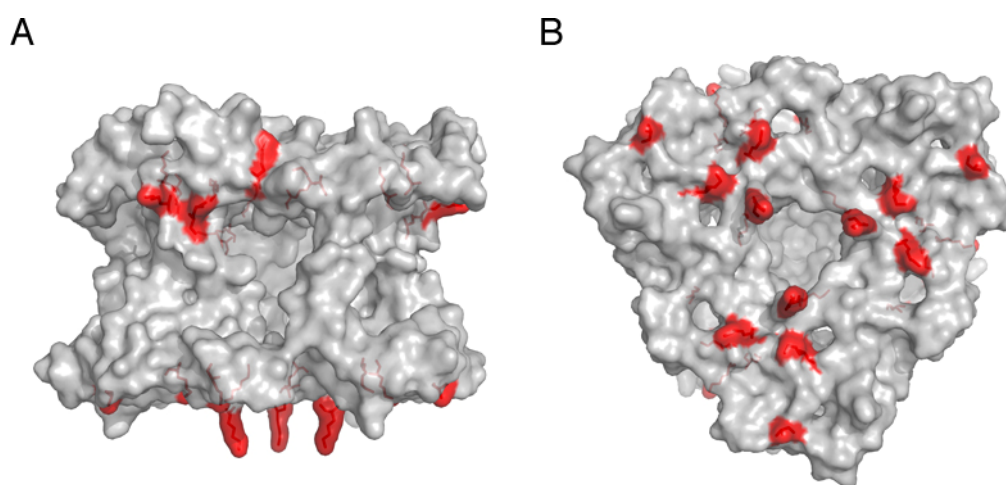


**Figure 6-11 - Exposed lysine residues in the pea LHC-II structure.**

The pea LHC-II protein is shown in surface representation in two orientations. The lysine residues are also shown in stick representation and are coloured in red. A set of three lysine residues in the centre of LHC-II make crystal contacts with the next layer in the type-I crystals.

### 6.2.3 New crystallisation conditions

A less invasive strategy to obtain a different crystal form is to search for new crystallisation conditions. An effort was made to screen a wide range of mother

liquor compositions, using several commercial crystallisation screens. Crystals were obtained in several conditions of these screens (Figure 6-2; Figure 6-3). The LHC-II preference to crystallise as thin plates was clear (Figure 6-2 C, D and F; Figure 6-3 B, C and D). It is very likely that these plates are nothing other than the same type-I crystals of the pea LHC-II structure (Standfuss et al, 2005).

Promising results were obtained with crystallisation conditions rich in ammonium sulphate (Figure 6-3; Figure 6-5). These conditions produced crystals of various shapes, from thin plates to interesting small rectangular and rhomboid bricks. The latter were tested at the synchrotron and despite their small size and tentative cryoprotection diffracted X-rays to better than 3 or 4 Å resolution, respectively. However, the recorded diffraction data revealed that both crystal types were composed of multiple lattices, which made data processing not possible. Reproducibility of these crystals was also problematic, especially because of the various crystal morphologies that were obtained in very similar conditions and in some cases even in the same drop. It is unknown if the different morphologies correspond to the same crystal symmetry.

The recorded data could not be used to determine unambiguously if the rhomboid crystals were in fact a new crystal form or just another morphology of either cubic (Liu et al, 2004) or type-I (Standfuss et al, 2005) crystals. The cubic crystals have very large cell dimensions (approximately 260 x 260 x 660 Å; (Liu et al, 2004)), so that the distances between reflections in the respective diffraction patterns are correspondingly very short. The diffraction patterns recorded from the rhomboid crystals are incompatible with those cell dimensions (Figure 6-4), implying that they are of a different type. Likewise, the LHC-II type-I crystals are usually very thin plates (Kühlbrandt, 1987; Standfuss et al, 2005), which is also at variance with the rhomboid crystals. Although definitive evidence is missing, it seems therefore likely that these crystals are a different crystal form of LHC-II.

---



## **7 LHC-II STRUCTURE ANALYSIS, MODELLING AND CALCULATIONS**

The two available X-ray structures of LHC-II (Liu et al, 2004; Standfuss et al, 2005), solved from very distinct crystal forms, provided an excellent basis for analysing the likelihood of conformational changes within the complex. The type-I packing of the pea LHC-II crystals was also the starting point for modelling the trimer-trimer interaction *in vivo*. Finally, the structural data was used to estimate the energy transfer rates between LHC-II trimers in crystals and *in vivo*.

## 7.1 Results

### 7.1.1 Comparison of LHC-II X-ray structures

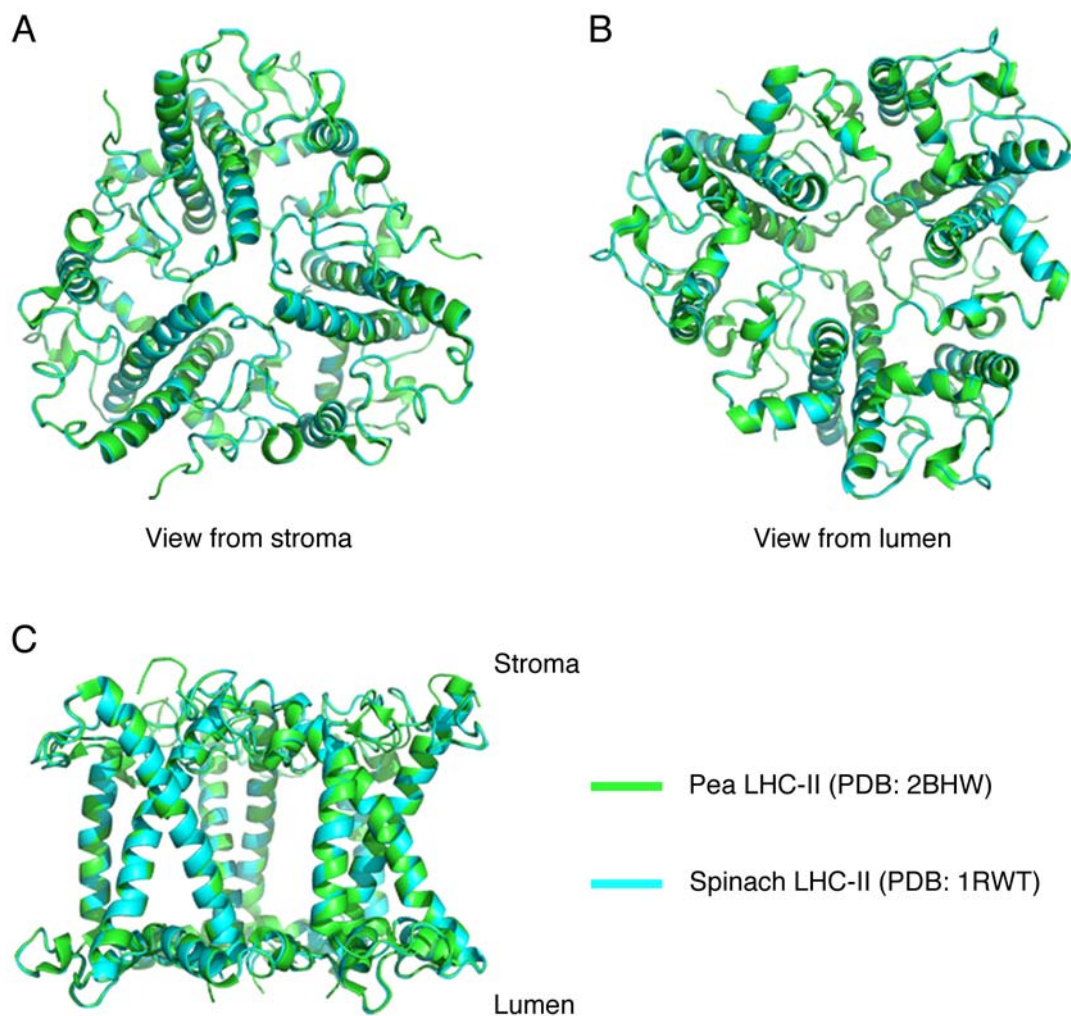
The X-ray structures of pea (Standfuss et al, 2005) PDB code: 2BHW) and spinach (Liu et al, 2004); PDB code: 1RWT) LHC-II were superposed and compared. Superposition of the main chain atoms from residues 20 to 220 of the three monomers reveals an almost perfect overlap, with only minor deviations in small stretches of some loops (Figure 7-1). The rms deviation between all the main chain atoms within this range of the two structures is only 0.35 Å (Table 7-1). This value increases slightly to 0.40 Å when the residue range is extended to residues 14 to 231, at the limit of the residues present in the crystal structures. Remarkably, the largest deviation between two equivalent atoms in the main chain of the two structures is less than 1.2 Å. For comparison, the rms deviation between different LHC-II monomers is 0.05 Å in the pea structure and 0.12 Å in the spinach structure. The maximum deviation between monomers is only 0.11 Å in the pea structure, but goes up to 0.45 Å in the spinach structure, reflecting how tight the non-crystallographic symmetry restraints were applied during refinement.

Figure 7-2 shows the distribution of the rms deviation between the two superposed LHC-II structures within the complex. The main structural features of the LHC-II, comprising in particular the transmembrane helices, are coloured in blue revealing a high degree of similarity between the two structures. On the other hand, the loop regions are in general coloured in red, indicating higher values of rms deviation. Interestingly, the regions where pigments are bound are dark blue, and therefore the most similar.

When the atomic coordinates of only the pigments are superposed, the similarity between the two structures is even higher (Figure 7-3; Table 7-1). Note that the values shown in Table 7-1 were calculated using only atoms of all the Chls of the complex, while Figure 7-3 shows only four selected pairs of Chls and neighbouring carotenoids. Interestingly, the rms deviation and the largest deviation in the Chl atoms are both smaller than those for the polypeptide by a factor of almost 2. The few exceptions to the essentially perfect overlap of pigment atoms are

---

a small deviation in the planarity of Chl 2 and the head groups of the carotenoids. The  $\pi$ -systems of all the carotenoids match exactly.

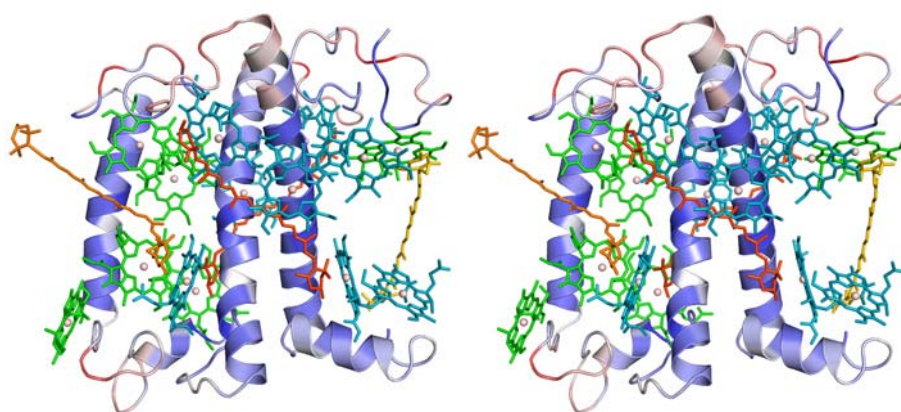


**Figure 7-1 - Superposition of pea and spinach LHC-II polypeptides**

The pea (green) and spinach (blue) LHC-II X-ray structures were superposed, matching their main chain atoms from residues 20 to 220. All non-protein atoms have been removed for clarity.

**Table 7-1 - Superposition of LHC-II X-ray structures**

		rms deviation (Å)	average (Å)	maximum (Å)
<i>Polypeptide</i>				
(14 to 231)	C $\alpha$	0.35	0.30	2.33
	Main chain	0.40	0.31	3.64
(20 to 220)	C $\alpha$	0.34	0.29	1.17
	Main chain	0.35	0.30	1.19
<i>Pigments</i>				
(all Chls)	Mg atoms	0.20	0.18	0.46
	Chlorin rings	0.25	0.23	0.70
<i>Main chain plus pigments</i>				
(14 to 231)	(all Chls)	0.36	0.29	3.64
(20 to 220)	(all Chls)	0.33	0.28	1.21

**Figure 7-2 - Rms deviation between pea and spinach LHC-II structures.**

In this stereo figure, the pea LHC-II polypeptide is shown as a ribbon and coloured according to the rms deviation between the superposed pea and spinach LHC-II backbones. The colour scale goes from blue to white to red, corresponding to increasingly higher rms deviation. The LHC-II pigments are also shown. Cyan, Chl a; green, Chl b; dark orange, lutein; light orange, neoxanthin; yellow, violaxanthin. Chl phytyl chains and lipids have been omitted for clarity.

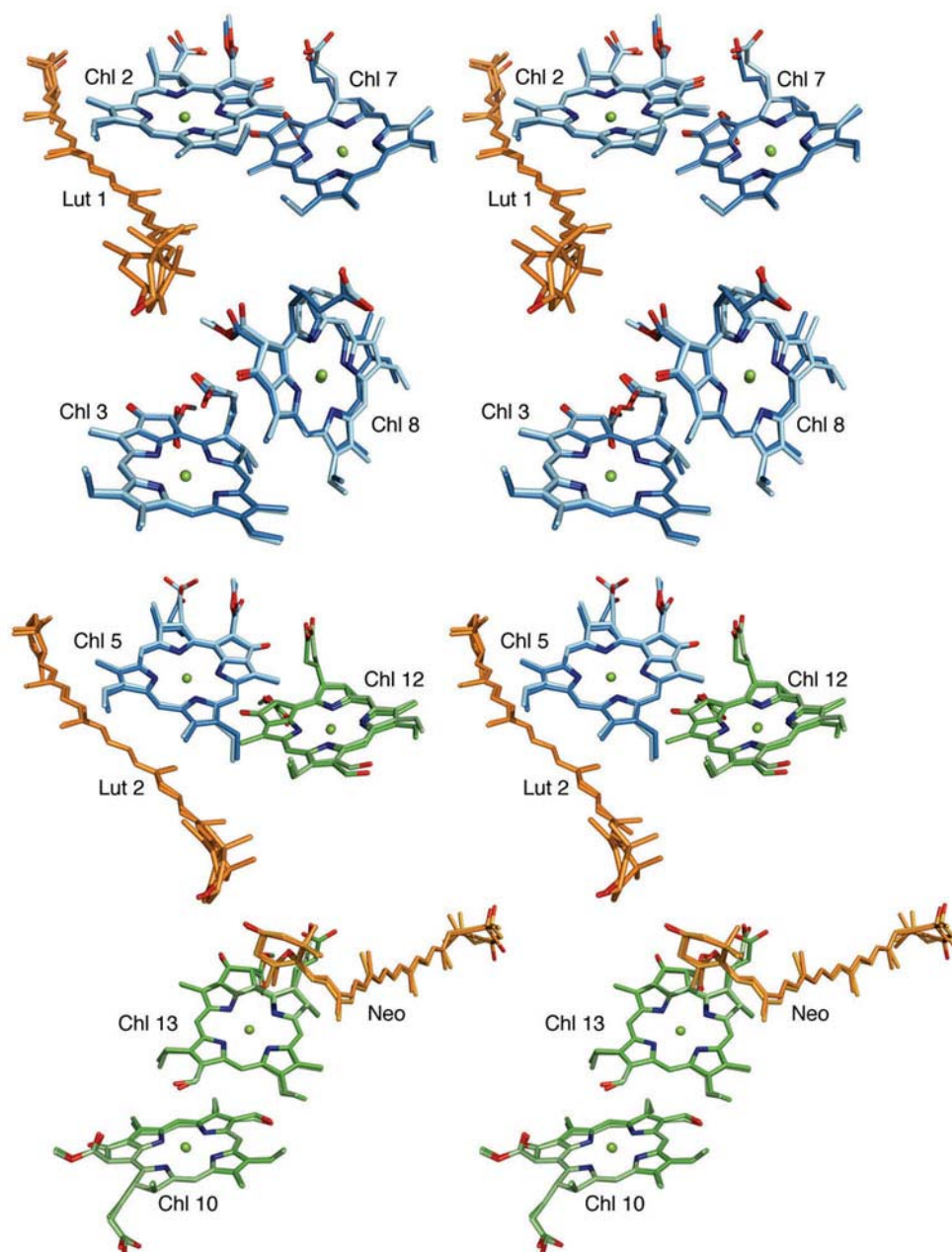


**Figure 7-3 - Superposition of selected pea and spinach LHC-II pigments.**

Stereo diagrams of the four LHC-II Chl pairs in which the  $\pi$ -to- $\pi$  distance is less than 4 Å. Such pairs could potentially form a quenching Chl dimer. The stereo diagrams show these four Chl pairs and closest carotenoids in the spinach (lighter colours) and the pea (darker colours) LHC-II structures. Phytol chains were omitted for clarity. Cyan, Chl *a*; green Chl *b*; orange, lutein and neoxanthin.

### 7.1.2 Crystallographic B-factor analysis

The crystallographic B-factor distribution within the structures of pea and spinach LHC-II was also mapped. In Figure 7-4 the two structures are depicted according to a colour code reflecting the crystallographic B-factor of each atom. Although the B-factor values of individual atoms in the two structures vary within a similar ~100-fold range of magnitude, the distribution in the pea LHC-II structure seems to have a higher variability than in the spinach structure. In the latter case, the increase or decrease of the B-factors in neighbouring regions of the complex appears to be more gradual, reflecting that the B-factor variation was more tightly restrained during refinement of the spinach LHC-II structure. However, the same general trend is observed in the two structures, in which higher B-factors are associated with the luminal and stromal surfaces of the complex. The low B-factor regions map in the core of the complex, where the transmembrane helices are located.

A striking observation in the B-factor distribution of the spinach LHC-II structure is the increase in B-factor value in the Neo molecules that protrude into the lipidic phase of the membrane (central position in Figure 7-4), with a smooth gradient from the interior of the complex (lower B-factors) to the opposite end of the carotenoid (high B-factors). When only the carotenoids are plotted (Figure 7-5) it can be seen that the same gradient is present in the Neo of pea LHC-II. The other 3 carotenoids in LHC-II have similar, low B-factors.

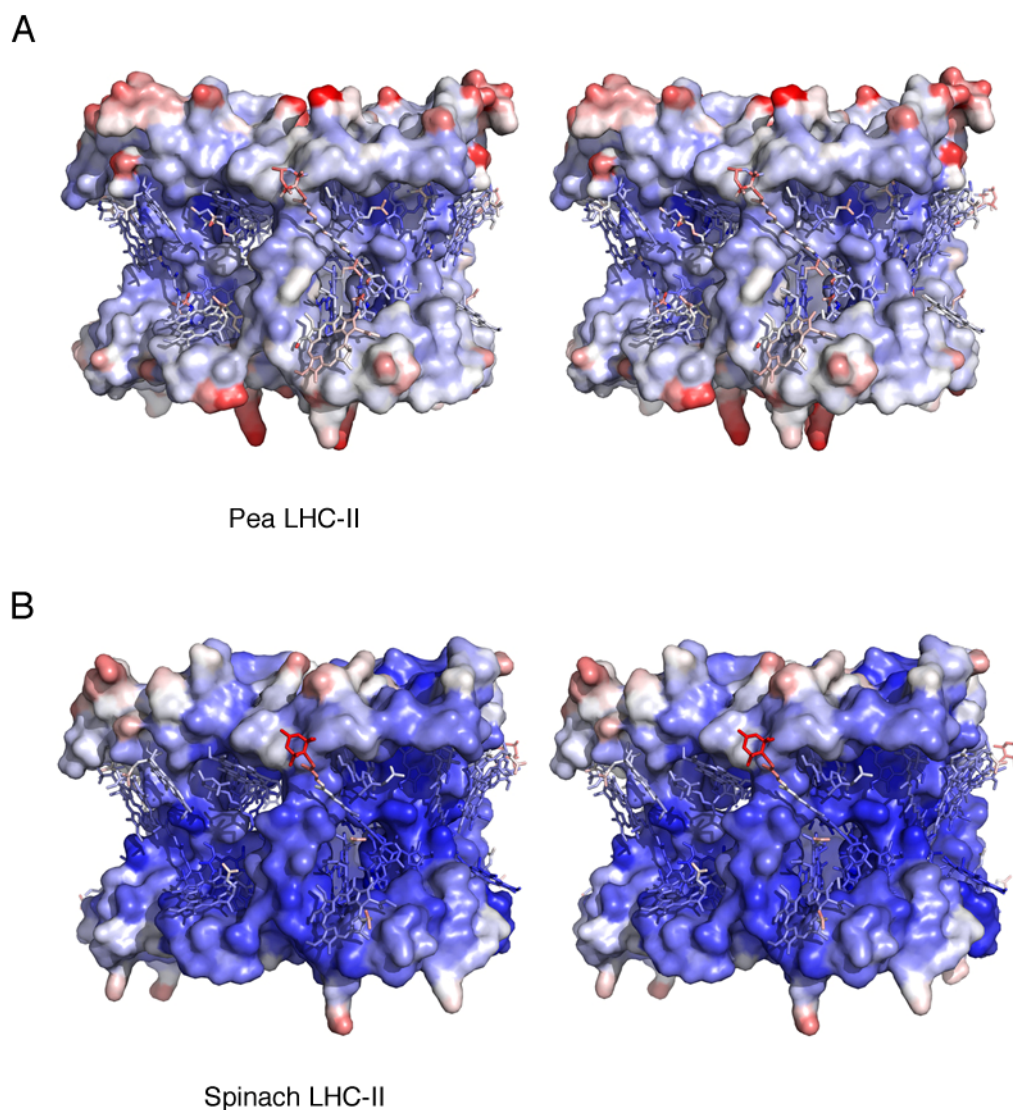


**Figure 7-4 - B-factor distribution in the pea and spinach LHC-II structures.**

Stereo diagrams of the B-factor distribution in the structure of pea (A; PDB code 2BHW) and spinach (B; PDB code 1RWT) LHC-II. The colour gradient from blue to white, to red represents increasing B-factor values. The protein is shown in surface representation and the pigments in stick representation. Detergent, lipids and phytol chains were omitted for clarity.

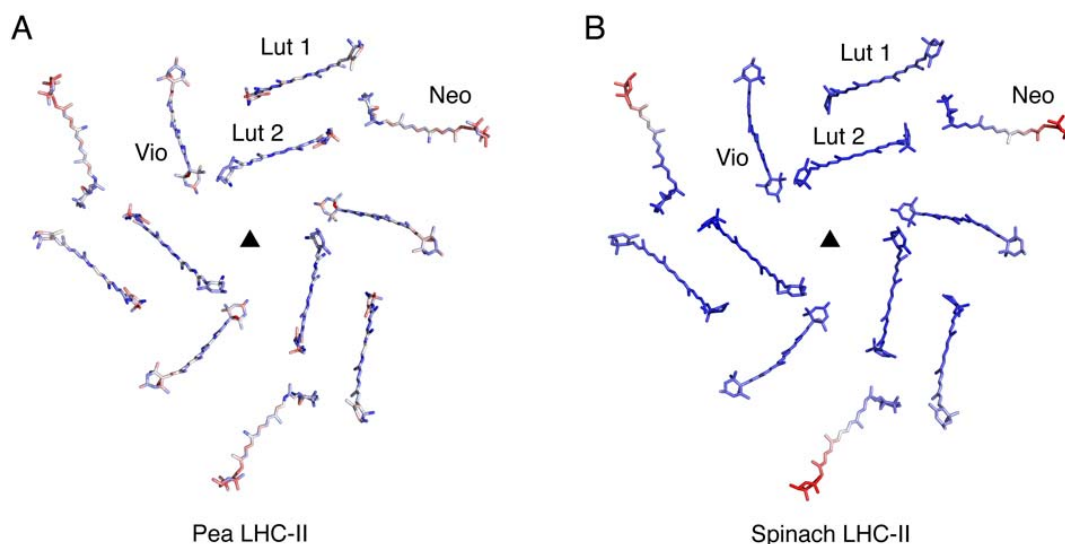


**Figure 7-5 - B-factor distribution in the pea and spinach LHC-II carotenoids**

The carotenoids in the pea and spinach LHC-II X-ray structures are shown in stick representation and coloured according to the B-factors of the individual atoms. The colour gradient from blue, to white, to red corresponds to increasing B-factor values. The pigments in one monomer of each trimer are labelled and the approximate position of the 3-fold symmetry axis in the trimer is indicated with a triangle.

### 7.1.3 Interaction between LHC-II trimers in crystals and *in vivo*

In the context of energy transfer between LHC-II trimers and aggregation quenching of LHC-II fluorescence, it is essential to assess the molecular contacts between interacting trimers. It was then necessary to create a model of interacting trimers in crystals and *in vivo*. The symmetry in the crystal packing dictates these contacts between neighbouring trimers in the pea and spinach LHC-II crystals (Figure 6-7; Figure 7-6). The distance between the Mg atoms of the two closest Chls of neighbouring trimers is 17.6 Å in the pea LHC-II crystals and 12.3 Å in the spinach crystals. Likewise, the distance between the  $\pi$ -systems of these Chls is 14.8 Å in the pea LHC-II crystals but decreases to 3.9 Å in the spinach crystals.

An interesting feature of the type-I packing of the pea LHC-II crystals is that the trimers in each layer of the crystal are lying in a flat “thylakoid-like” membrane (Figure 6-7; Figure 7-6). The trimers are however in an up-and-down (anti-parallel) relative orientation to one another, while they are all in the same orientation *in vivo* in the thylakoid membrane. The trimer-trimer interaction *in vivo* was modelled by rotating one trimer in the pair by 180° so that both complexes have the same



parallel orientation. The model was further refined so that clashes between trimers were avoided (see Section 3.8.2 for details). From these simple models, it can be estimated that closest possible Mg-Mg distance between Chls of neighbouring trimers in thylakoids is 13.5 Å, and that the closest distance between  $\pi$ -systems is about 9.4 Å.

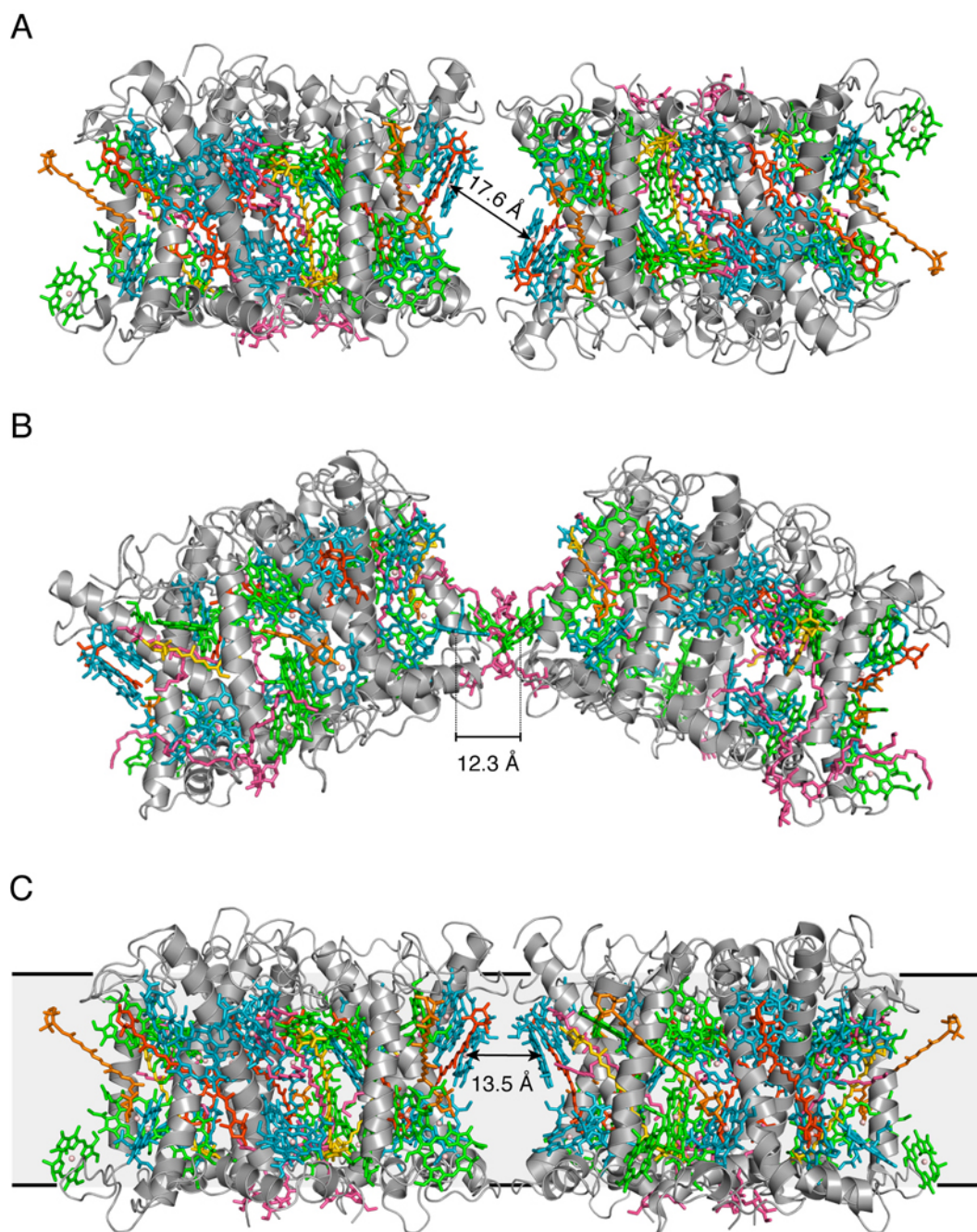


**Figure 7-6 - Interactions between neighbouring LHC-II trimers.**

(A) In the membrane-like, type-I crystals of pea LHC-II, neighbouring trimers are symmetrically related within each crystalline layer in an up and down manner. (B) In the vesicular crystals from spinach LHC-II, the interacting trimers are oriented in the same direction, but on an angle; (C) Model for trimer-trimer interaction *in vivo* within the thylakoid membrane. The centre-to-centre distance between the closest Chls in neighbouring trimers are shown. Grey, polypeptide; cyan, Chl *a*; green, Chl *b*; dark orange, lutein; light orange, neoxanthin; yellow, violaxanthin; pink, lipids.

### 7.1.4 Coupling strength

The coupling strength ( $V$ ) between Chls of neighbouring trimers in crystals and *in vivo* was estimated using the model by van Amerongen & van Grondelle (van Amerongen & van Grondelle, 2001) and the atomic coordinates of the crystal structures and the model presented in the previous section. The obtained values are summarised in Table 7-2.

**Table 7-2 - Coupling strength ( $V$ ) between LHC-II trimers in crystals and *in vivo***

		Mg to Mg (Å)	$\kappa$	$V$ (cm <sup>-1</sup> )
<i>Pea LHC-II crystals</i> <sup>a</sup>				
<i>(Chl 2 – Chl 2')</i>	Set 1	17.6	0.658	10.8
	Set 2	17.5	0.629	10.6
	Set 3	17.6	0.660	10.8
	Average	17.6	0.649	10.7
<i>Spinach LHC-II crystals</i> <sup>b</sup>				
<i>(Chl 8 – Chl 14')</i>	Set 1	12.3	1.513	61.7
	Set 2	12.4	1.537	60.5
	Set 3	12.4	1.425	55.6
	Set 4	12.3	1.505	60.6
	Set 5	12.2	1.500	61.2
	Average	12.3	1.496	59.9
<i>In vivo</i>				
<i>(Chl 2 – Chl 2')</i>		13.4	-0.303	-11.4

<sup>a</sup> – Each LHC-II trimer interacts with 3 other trimers within each layer of the type-I pea LHC-II crystals. The interaction between the one trimer with each of its 3 neighbours was used, labelled as set 1, 2 and 3.

<sup>b</sup> – There are 10 different monomers in the asymmetric unit of the spinach LHC-II crystals, generating a total of 5 different trimer-trimer contacts. Each of these was used, labelled as set 1, 2, 3, 4 and 5.

### 7.1.5 Förster energy transfer rates

The same structural information used to estimate the coupling strength between Chls of neighbouring trimers was used to estimate the Förster energy transfer rates between them, according to the same authors (van Amerongen & van Grondelle, 2001). Table 7-3 summarises the obtained results.

**Table 7-3 - Förster energy transfer rates ( $K$ ) in crystals and *in vivo***

		Mg to Mg (Å)	$\kappa$	$K$ (ns <sup>-1</sup> )
<i>Pea LHC-II crystals</i> <sup>a</sup>				
<i>(Chl 2 – Chl 2')</i>	Set 1	17.6	0.658	80.7
	Set 2	17.5	0.629	77.3
	Set 3	17.6	0.660	81.1
	Average	17.6	0.649	79.7
<i>Spinach LHC-II crystals</i> <sup>b</sup>				
<i>(Chl 8 – Chl 14')</i>	Set 1	12.3	1.513	1127.4
	Set 2	12.4	1.537	1084.9
	Set 3	12.4	1.425	915.4
	Set 4	12.3	1.505	1086.5
	Set 5	12.2	1.500	1109.9
	Average	12.3	1.496	1064.8
<i>In vivo</i>				
<i>((Chl 2 – Chl 2'))</i>		13.4	-0.303	88.6

<sup>a</sup> – Each LHC-II trimer interacts with 3 other trimers within each layer of the type-I pea LHC-II crystals. The interaction between the one trimer with each of its 3 neighbours was used, labelled as set 1, 2 and 3.

<sup>b</sup> – There are 10 different monomers in the asymmetric unit of the spinach LHC-II crystals, generating a total of 5 different trimer-trimer contacts. Each of these was used, labelled as set 1, 2, 3, 4 and 5.

## 7.2 Discussion

### 7.2.1 The two X-ray structures of LHC-II are identical within error

In recent years, the structure of LHC-II has come to focus due to the role of the complex in the qE component of NPQ. Under qE conditions, the antennae of PS-II switch to a quenched state and excess excitation energy is safely dissipated as heat (Table 1-2). Although a conformational change in LHC-II has long been postulated as the cause for the switch of the complex to the quenched state (Horton et al, 1991; Horton et al, 2005), conclusive evidence that it actually occurs is still missing. The X-ray structures of spinach and pea LHC-II were determined independently from very distinct crystal forms, grown either at pH 5.4 (Standfuss et al, 2005) or 7.5 (Liu et al, 2004). If the complex were to undergo a conformational change, particularly as the result of a pH change, this would have to be visible in the X-ray structures and significant differences in the arrangement of the LHC-II pigments would be expected.

This is however not the case (Section 7.1.1). Figure 7-2 shows the distribution of the rms deviation between the two superposed LHC-II polypeptides. The main structural features of LHC-II, in particular the transmembrane helices, reveal a high degree of similarity between the two structures. In particular, the pigment binding regions are the most similar. The only significant rms deviations are found in the surface loop regions of the polypeptide. When the atomic coordinates of the pigment are compared, the rms differences are smaller by a factor of almost 2 compared to the polypeptide main chain (Table 7-1). The rms deviation between the coordinates of the chlorin rings in the two X-ray structures (Figure 7-3) is remarkably small for two medium-resolution structures of complexes from two different species, crystallised in two completely different crystal forms produced in completely different crystallisation conditions. This indicates that the pigment structure in LHC-II is even more highly conserved than that of the polypeptide, no doubt because the exact distances and mutual arrangement between Chls on the one hand, and between Chls and carotenoids on the other, are vital for its proper function, a definitive reason for assuming that no flexibility of the complex can be allowed.

### 7.2.2 With one exception, the LHC-II pigments are rigid

A small, but interesting difference between the two X-ray structures is related to the hydrogen bonding of the formyl group of Chl 14. In the spinach crystal structure, the formyl group of Chl 14 makes a polar contact with an acyl group of the DGDG molecule that mediates the inter-trimer contacts in the icosahedral vesicles. In the pea structure this DGDG is absent, and the only hydrogen bond to the Chl 14 formyl group is to the backbone nitrogen of Ser123, which is also present in the spinach structure. The location of DGDG in the spinach structure is closely linked to the extreme curvature of the proteoliposome vesicles, so that this polar contact between Chl 14 and DGDG is very unlikely to occur *in vivo* in the thylakoid membrane. Indeed, it has been suggested that an extra hydrogen bond to a Chl *b* formyl group is present in the cubic crystal form compared to trimers in detergent solution (Pascal et al, 2005), and this evidently is it. The same 1639 cm<sup>-1</sup> band in the resonance Raman spectrum attributed to the stretching mode of a Chl *b* formyl group had previously been observed in aggregated LHC-II but not in solubilised trimers (Ruban et al, 1995b). This could indicate that the icosahedral vesicles are also present in aggregated trimers and, indeed, this has been observed (Prof. W. Kühlbrandt, personal communication; Figure 7-7).

---

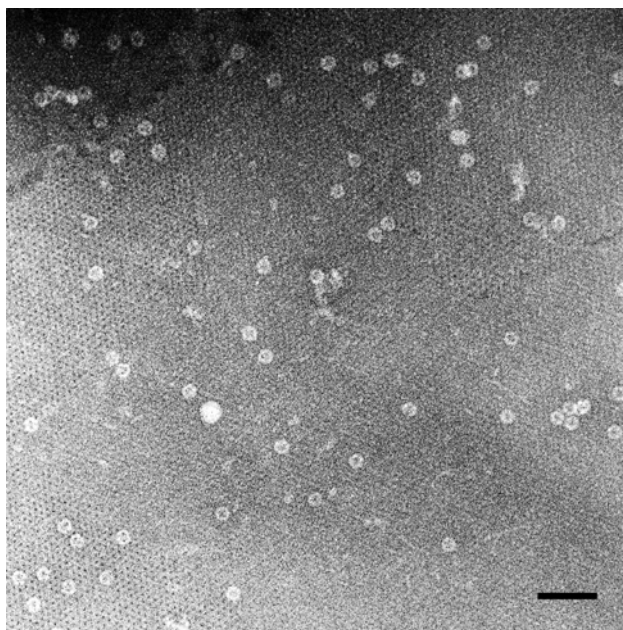


**Figure 7-7 - Icosahedral vesicles in LHC-II preparations.**

The same icosahedral vesicles that build the cubic spinach crystals (Liu et al, 2004) form spontaneously during 2D crystallisation experiments and can be observed by electron microscopy. Scale bar: 100 nm. Figure from Prof. W. Kühlbrandt.

Apart from the rms deviation between two independently determined experimental structures, another measure of the internal flexibility of a protein is the crystallographic temperature factor (B-factor). This parameter describes by how much individual atoms, or groups of atoms, oscillate around their mean position in a protein structure. Looking at the X-ray structures of the pea and spinach LHC-II colour-coded for the B-factor (Figure 7-4), it is immediately obvious that the distribution is uneven. The surface loops and residues exposed on the stromal and luminal side of the complex have moderate B-factors and are thus more flexible than the central region of the complex, which is characterized by low B-factors and is hence the most rigid part of the structure. This region comprises the hydrophobic core of the monomer, with its central motif of the coiled helix pair, the two luteins in their binding pockets and the chlorin head groups of all Chls, as well as the third trans-membrane helix. The striking exception in this central region of the complex is the part of the Neo that protrudes by  $\sim 9$  Å from the trimer surface into the lipid bilayer. When only the carotenoids are considered (Figure 7-5), it is clear that the protruding half of Neo stands out by its high temperature factors, whereas the two luteins in the centre of the monomer, and the violaxanthin at the monomer interface have low B-factors. Like the Chl chlorins, they are thus rigid and unlikely

to undergo conformational changes. The only light-absorbing part of an LHC-II pigment that has any inherently flexibility is the protruding half of the Neo molecule. The Neo conformation is therefore likely to be sensitive to contacts between LHC-II trimers in aggregates, crystals or in the thylakoid membrane. This would account for any twist observed by Resonance Raman spectroscopy, which would thus be a diagnostic of close intermolecular contacts.

The observation of two main LHC-II populations with different fluorescence lifetimes in detergent solution was taken as evidence for two conformations (quenched or unquenched) that were supposed to be in equilibrium (Moya et al, 2001; van Oort et al, 2007b). A variety of experimental procedures have been used to shift this equilibrium towards the quenched conformation: incorporation into liposomes (Moya et al, 2001), high pressure (van Oort et al, 2007b), detergent removal from gel-immobilised complexes (Illoaia et al, 2008) and precipitation (Ruban et al, 2007; van Oort et al, 2007a). Evidently, detergent removal or precipitation results in quenched aggregates. Aggregates are also a likely side product when LHC-II is reconstituted into liposomes. Finally, under extreme pressure non-physiological contacts between LHC-II trimers that form quenching centres are likely to occur. The observed differences between the two alleged conformations were attributed to changes in the Neo conformation and an additional hydrogen bond of the formyl group of at least one Chl *b*. Although Neo is not required for quenching, a change in its conformational has been correlated with the extent of qE *in vivo* (Ruban et al, 2007). However, both effects can be fully explained by parts of pigments exposed on the exterior surface of the complex, i.e. Neo and Chl 14, and thus do not signify an internal rearrangement.

A conformational switch in the central region of LHC-II, which harbours the pigments that have been implicated in NPQ (Pascal et al, 2005; Ruban et al, 2007), seems unlikely. This region is packed particularly tightly, and this would effectively prevent any movement without disruption of the entire complex, including the opening of the interlocking salt bridges that hold helices 1 and 4 together. Indeed it looks as if the whole interior of LHC-II is designed to prevent such movements, which would make sense in a complex whose proper function depends on the precise distance and alignment of the light-harvesting pigments. A

---



sliding mechanism by which the distance between Lut and Chls varies gradually in response to photosynthetic activity, as recently proposed (Ruban et al, 2007), can be excluded. Such a movement would only be possible if the corresponding part of the complex were flexible, and this would certainly be reflected in the crystallographic B-factors.

Although a structure of any of the minor LHCs is still missing, the remarkable sequence conservation with the Lhc family leads to the conclusion that the rigidity of the LHC-II pigment structure is a hallmark of the entire family, not a peculiarity of the major complex. Apart from the fact that so far there is no hard, structural evidence for any conformational change in the LHCs' interior, such a switch would be potentially counterproductive and dangerous if it were ever to occur spontaneously. It would only take a very small change in the distance between two pigments in the LHCs to convert these complexes from light-harvesters and energy-transmitters to energy sinks that would switch the entire PS-II supercomplex to an unproductive state. Ensuring that the pigment structure in all the LHCs is rigid is the only way to guarantee an efficient photosynthetic apparatus.

### **7.2.3 Energy transfer between LHC-II trimers**

The conclusion of Pascal et al (Pascal et al, 2005) that LHC-II in crystals of the spinach complex is quenched rests partly on the assumption that the crystalline trimers are functionally separate. If that were the case, a large majority of the trimers in the crystals would have to be in a quenched state to account for the drastic reduction in fluorescence lifetime observed by FLIM. If, on the contrary, efficient energy transfer would occur between trimers in the crystal lattice, it would then be possible that only a few efficiently quenched trimers acting as energy sinks dissipate the excitation energy of a large domain within the crystal. The fluorescence decays would then be primarily dependent on the distance between quenching centres and the energy transfer rates between trimers. The calculations presented in Sections 7.1.4 and 7.1.5 clearly show that the latter hypothesis is correct. Trimers in both crystal forms are excitonically coupled and, in the case of the proteoliposome crystals, even more strongly than they would be in thylakoids, so that excitation energy is rapidly exchanged between them.

## **8 LHC-II SPECTROSCOPY IN SOLUTION**

The general theme of the spectroscopic studies carried out in this work concerned the mechanisms of fluorescence quenching in LHC-II, aiming at the elucidation of the likely related mechanisms of excess excitation energy dissipation *in vivo* under high light conditions (NPQ).

The mechanism of LHC-II aggregation quenching and the influence of substituting Vio by Zea on LHC-II function were investigated in solubilised LHC-II by a wide range of spectroscopic techniques.

Spectroscopic studies of LHC-II in single crystals have very special experimental requirements. For this reason, the results obtained with LHC-II in solution and in single crystals are presented separately.

## 8.1 Results

### 8.1.1 Fluorescence spectrum of native LHC-II in solution

Emission fluorescence spectra of native pea LHC-II in solution were recorded at low (100 K) and room temperature on the Cryobench (Section 3.11) using a 400 nm laser for excitation, at two different Chl concentrations. The corresponding spectra show clear differences at both temperatures (Figure 8-1). Note that the high Chl concentration sample is slightly less concentrated in the low temperature measurements. This was due to the necessity of adding a cryoprotective agent (glycerol) to the samples at low temperature in order to prevent ice formation. At lower Chl concentrations, the LHC-II fluorescence emission spectrum shows a maximum at 680 nm, independent of the temperature. The emission peak is wider at room temperature. The full width at half maximum of the emission peak is 19 nm at room temperature, but only 11 nm at 100 K. The emission maximum was red-shifted with increasing Chl concentration due to self-absorption. It is unlikely that the more pronounced red-shift of the emission peak observed at 100 K is a direct consequence of the temperature. It most likely reflects different extents of self-absorption due to different geometries of the experiments.

Apart from the red-shift of the emission maximum, the emission spectra at low and high Chl concentration are very similar at room temperature. However, at low temperature the structure of the emission spectra varied with the Chl concentration; the emissions around 700, 710 and 740 nm are clearly enhanced at high Chl concentration.

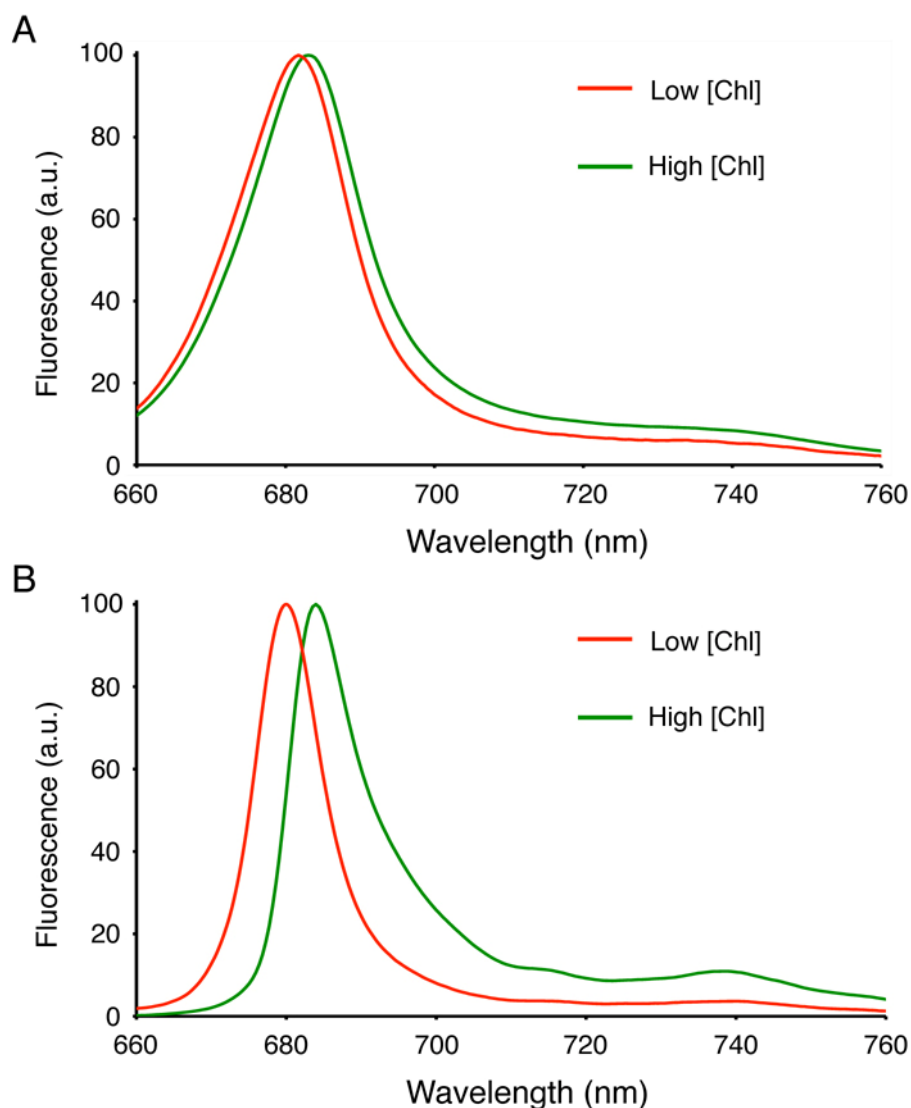


**Figure 8-1 - Fluorescence spectra of solubilised native LHC-II.**

The emission spectra were recorded at the Cryobench at (A) room or (B) low (100 K) temperature. Samples were prepared at low (0.05 mg/ml; red) or high (5.38 mg/ml at room temperature and 3.50 mg/ml at low temperature; green) Chl concentration. The emission maximum is red-shifted by 1.5 or 4 nm on the sample with high Chl concentration at room or low temperature, respectively. The excitation wavelength was set to 440 nm in all experiments. All spectra were normalised to 100 at the maximum emission.

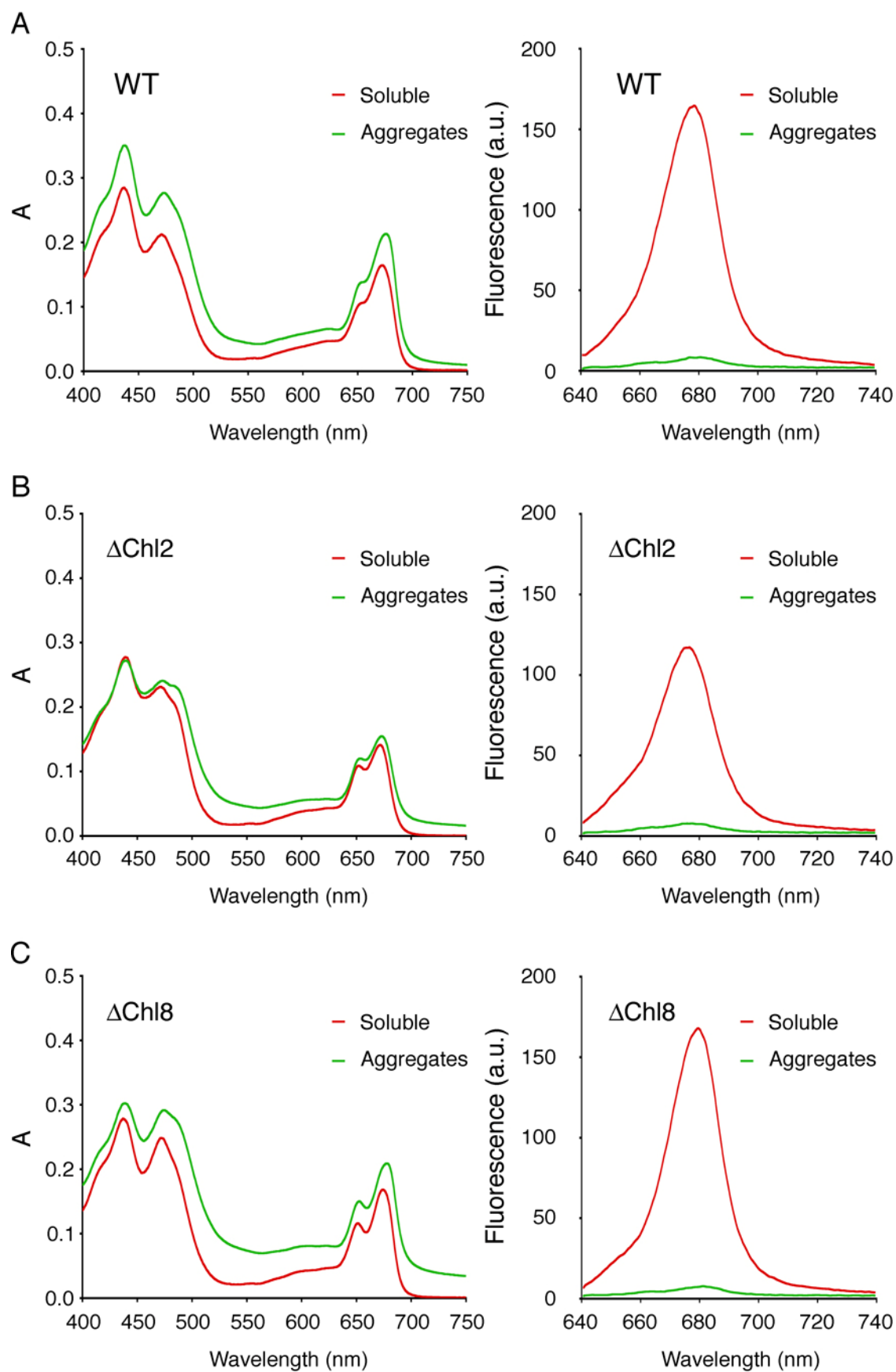
### 8.1.2 Aggregation quenching in LHC-II mutants

Fluorescence quenching in LHC-II aggregates is thought to involve a Chl dimer within the LHC-II monomer (Pascal et al, 2005). Four Chl pairs can be identified within each LHC-II monomer such that the  $\pi$ - $\pi$  distance between the paired pigments is less than 4 Å (Table 8-1). Among the LHC-II mutants that were refolded (Section 4.1.5), one can find at least one mutant for each of these Chl

pairs. WT LHC-II and the  $\Delta$ Chl 2,  $\Delta$ Chl 8,  $\Delta$ Chl 12 and  $\Delta$ Chl 13 mutants were refolded and the monomeric band from the sucrose gradient separation was harvested. Samples were diluted to  $A_{440} \sim 0.3$  and their absorption and fluorescence emission spectra were recorded (Figure 8-2). The same dilution procedure was then repeated with the same dilution factor, with detergent-free buffer to generate aggregates of all variants. The absorption spectra of all variants show some differences between the soluble and aggregated states. At least some of these differences are due to scattering, which is evidently higher for aggregated samples. Nevertheless, the  $Q_y$  band of Chl *a* is red-shifted by 4 nm in aggregates of all variants except  $\Delta$ Chl 2, in which the shift is only 2 nm. Differences in the Soret region and the  $Q_y$  band of Chl *b* are less pronounced, with the difference in the peak position for solubilised or aggregated samples being within 1 nm. Coupling between pigments of closely interacting trimers in the aggregated samples, which do not occur in solubilised complexes, may explain the observed spectral shifts. While the differences in the absorption spectra with the aggregation state were subtle, drastic differences were observed in the fluorescence emission spectra. Strikingly, for all the variants the amplitude of the emission peak decreased by almost 2 orders of magnitude upon aggregation. The Chl *a* cluster comprising Chl 7 and Chl 2 is known to be the final emitter of LHC-II fluorescence. Consistently, the emission maximum of the  $\Delta$ Chl 2 mutant in the soluble state was blue-shifted, with a difference of  $\sim 2$  nm compared to the WT. The same blue-shift was observed in the aggregated state.

**Table 8-1 - Chl pairs in LHC-II and respective mutants**

Chl pairs	$\pi$ - $\pi$ distance	Mg-Mg distance <sup>1</sup>	Mutant
Chl 2/Chl 7	3.8 Å	9.8 Å	N183A ( $\Delta$ Chl 2)
Chl 3/Chl 8	3.9 Å	9.4 Å	H212A ( $\Delta$ Chl 8)
Chl 5/Chl 12	3.9 Å	9.8 Å	E139A ( $\Delta$ Chl 12)
Chl 10/Chl 13	3.7 Å	9.5 Å	Q131A ( $\Delta$ Chl 13)



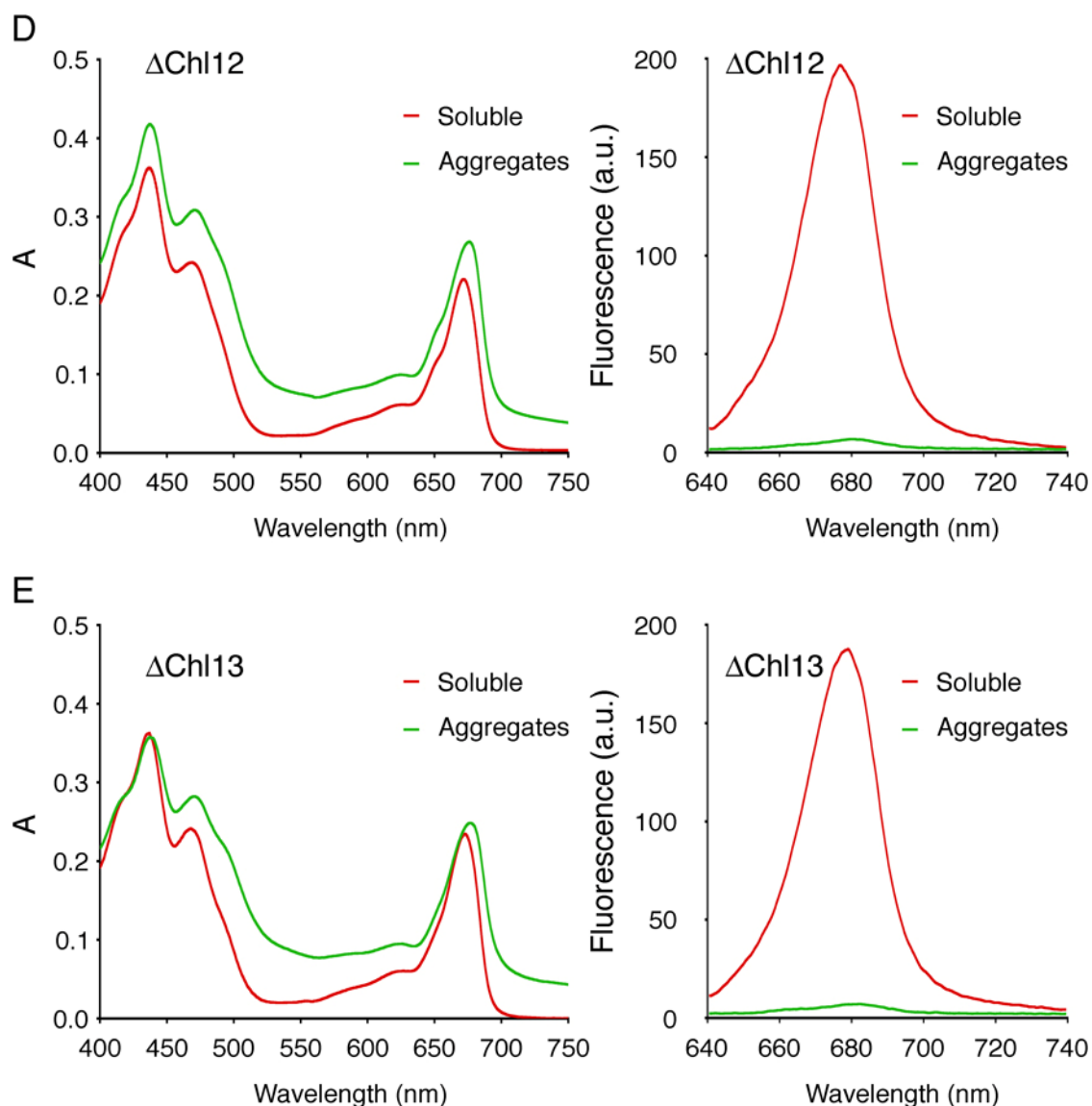


**Figure 8-2 - Absorption and fluorescence spectra of refolded LHC-II variants.**

Absorption (left) and fluorescence emission (right) spectra of monomeric refolded LHC-II variants were measured at room temperature. Samples collected from the sucrose gradients were first diluted in buffer with detergent to  $A_{440} \sim 0.3$ . The same dilution was then applied to these samples in detergent-free buffer to generate the aggregated form. The amplitude of the emission spectrum in the aggregated state is almost 2 orders of magnitude smaller than that of the solubilised samples in all variants.

### 8.1.3 Ultrafast transient absorption spectroscopy

The author of the present work prepared the samples used to obtain the results presented in this section. S. Amarie, Institute of Physical and Theoretical Chemistry, JW Goethe University, performed all the spectroscopic measurements.

Ultrafast transient absorption spectroscopy was used to investigate the influence of the Vio by Zea substitution on the lifetime of the Chl excited state in LHC-II. A laser pulse at 660 nm excited the  $Q_y$  band of Chl *a*. The Chl excited state absorption was monitored between 800 and 1050 nm. The same measurements were repeated for Vio-LHC-II or Zea-LHC-II that had been isolated from pea thylakoids. To obtain the Zea-LHC-II samples, thylakoid membranes were incubated at low pH in the presence of ascorbate to trigger the xanthophyll cycle *in vitro*. Figure 8-3 shows the transient absorption kinetics at 904 nm for the two samples. Global fitting analysis indicated two main decays: one very fast ( $\sim 10$  ps) and the other very slow (1.5 ns), which fell beyond the time scale of the experiment. The observed kinetics were identical for Vio- and Zea-LHC-II.

Carotenoid radical cations ( $\text{Car}^{+\cdot}$ ) were experimentally generated in LHC-II by resonant two colour 2 photon ionisation (R2C2PI). Excited Chls and  $\text{Car}^{+\cdot}$  have overlapping transient absorption spectra in the near infrared region. The transient absorption spectrum in that region after R2C2PI reflects not only the transient absorption spectrum from the generated  $\text{Car}^{+\cdot}$  but also from excited Chls. It was therefore necessary to determine the transient absorption spectrum of the excited Chls by pump-probe and then determine the difference transient absorption spectrum (R2C2PI minus pump-probe) to reveal the structure of the  $\text{Car}^{+\cdot}$  transient absorption spectrum. Figure 8-4 shows such difference spectra for Vio- and Zea-LHC-II, revealing the transient absorption spectra of all generated  $\text{Car}^{+\cdot}$ . The same figure shows the difference between these two spectra. A negative peak centred at 909 nm and a positive peak centred at 983 nm can be identified in this difference spectrum. These peaks reveal transient absorption from  $\text{Vio}^{+\cdot}$  and  $\text{Zea}^{+\cdot}$ , respectively.

---



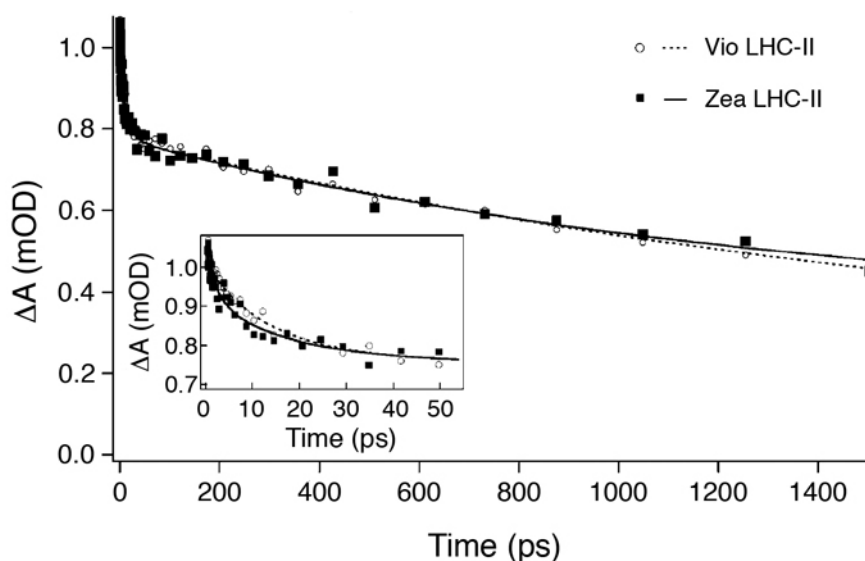


**Figure 8-3 - Transient absorption kinetics of the Chl excited state in LHC-II.**

Transient absorption at 904 nm for Vio-LHC-II (open circles) and Zea-LHC-II (filled squares) after Chl excitation by a 660 nm laser pulse. The lines represent the fit curve obtained by global fitting routine. Adapted from (Amarie et al, 2007).

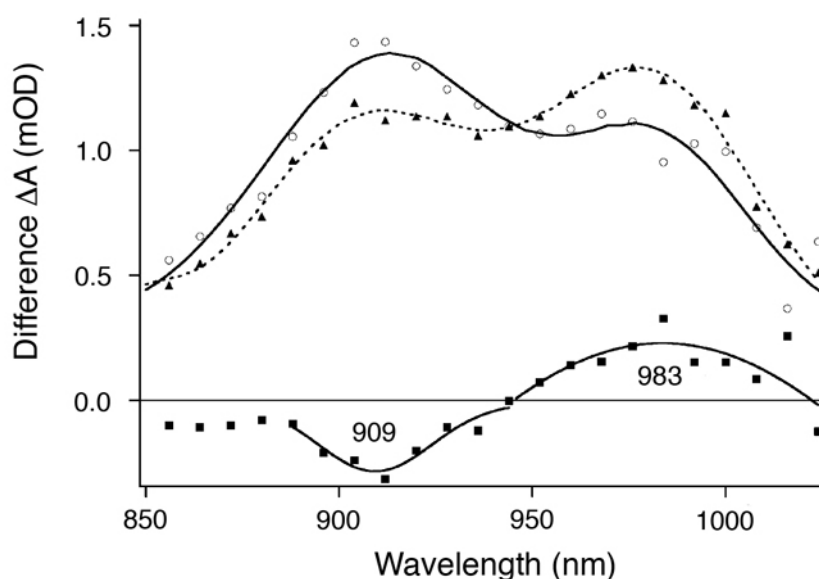


**Figure 8-4 – Difference transient absorption spectrum between R2C2PI and pump-probe in LHC-II.**

Difference transient absorption spectra between R2C2PI and PP revealing all  $\text{Car}^{\bullet+}$  in Vio-LHC-II (open circles) and Zea-LHC-II (filled triangles). The lines correspond to Gaussian fits of the data points. The difference between Vio- and Zea-LHC-II (squares) and respective Gaussian fits with extremes at 909 and 983 nm reflects the  $\text{Vio}^{\bullet+}$  and  $\text{Zea}^{\bullet+}$ . Adapted from (Amarie et al, 2007).

### 8.1.3.1 Two-photon excitation spectroscopy

The author of the present work prepared the samples for the results presented in this section. S. Bode and C. Quentmeier, Institute for Physical and Theoretical Chemistry, Braunschweig University, performed all the spectroscopic measurements.

Two-photon excitation was used to investigate the coupling between Car  $S_1$  states and Chls ( $\Phi_{\text{coupling}}$ ) in native and refolded Vio- and Zea-LHC-II. The pigment composition of the samples used in these studies is presented in Table 4-2 and Table 4-3. Compared to Vio-LHC-II ( $\Phi_{\text{coupling}}$  normalised to 1 for both native and refolded samples), Zea-LHC-II showed  $\Phi_{\text{coupling}} = 0.945 \pm 0.010$  or  $\Phi_{\text{coupling}} = 0.971 \pm 0.023$  for native or refolded complexes, respectively (Figure 8-5; Table 8-2). This is a small (although statistically significant) reduction in the Car  $S_1$  to Chl energy transfer efficiency, which is not proportional to the amount of Zea present in the Zea-LHC-II samples. To further investigate the differences between Vio- and Zea-LHC-II, the Chl fluorescence lifetime was measured for the native samples. The small decrease observed in  $\Phi_{\text{coupling}}$  was not correlated with a decrease in the Chl fluorescence lifetime ( $\tau$ ). The obtained values of  $\tau$  (3.81 ns  $\pm$  0.01 for Vio-LHC-II or 3.77 ns  $\pm$  0.03 for Zea-LHC-II) are identical within experimental error.

---

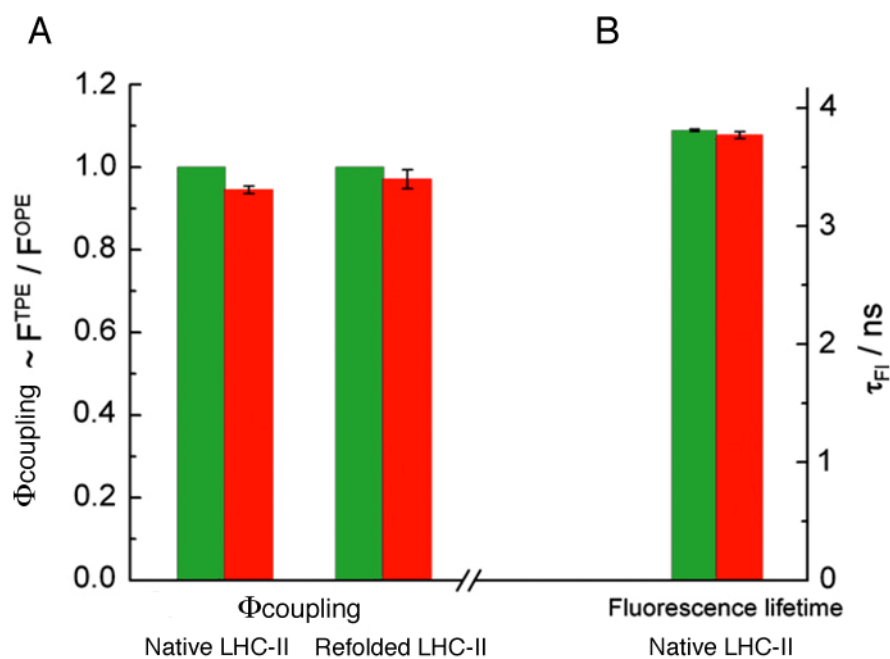


**Figure 8-5 –Relative Car  $S_1$  to Chl energy transfer efficiency ( $\Phi$ ) and Chl fluorescence lifetime ( $\tau$ ) in LHC-II.**

(A)  $\Phi_{\text{coupling}}$ , a measure of the Car to Chl energy transfer efficiency, for isolated (left) or refolded (right) preparations of Vio-LHC-II (green) or Zea-LHC-II (red); (B) Fluorescence lifetime of isolated native LHC II samples used in the left part of (A). Adapted from (Bode et al, 2008).

**Table 8-2 – Relative Car  $S_1$  to Chl energy transfer efficiency ( $\Phi$ ) and Chl fluorescence lifetime ( $\tau$ ) in native or refolded LHC-II**

	$\Phi_{\text{transfer}}$	(sd)	$\tau$ (ns)	(sd)
<i>Native</i>				
Vio-LHC-II	1	-	3.81	0.01
Zea-LHC-II	0.945	0.010	3.77	0.03
<i>Refolded</i>				
Vio-LHC-II	1	-		
Zea-LHC-II	0.971	0.023		

## 8.2 Discussion

### 8.2.1 Quenching does not require a specific Chl pair, Vio or Neo

LHC-II variants were used (Section 8.1.2) to target the pigments that had been reported to have a direct role in qE (Pascal et al, 2005). These included all possible Chl pairs that could hypothetically form quenching dimers (Figure 7-3). All the studied mutants were quenched in the aggregate state, indistinguishably from the WT (Figure 8-6). In this way 8 out of the 14 Chls were excluded from the quenching mechanism, as each makes a Chl pair with another, and therefore, if one Chl of the pair was removed and there was no difference to WT, that pair is not a quenching Chl dimer, and therefore the other Chl of the pair is also not required. Of the 6 Chls that are left, 3 are Chl *b* which cannot be part of a quenching centre, because the energy transfer from Chl *a* to Chl *b* would be faster than the quenching event. The remaining 3 Chls *a* are relatively isolated and so it is difficult to see how they can be part of a quenching centre without a major rearrangement of the LHC-II structure to move them closer to another pigment.

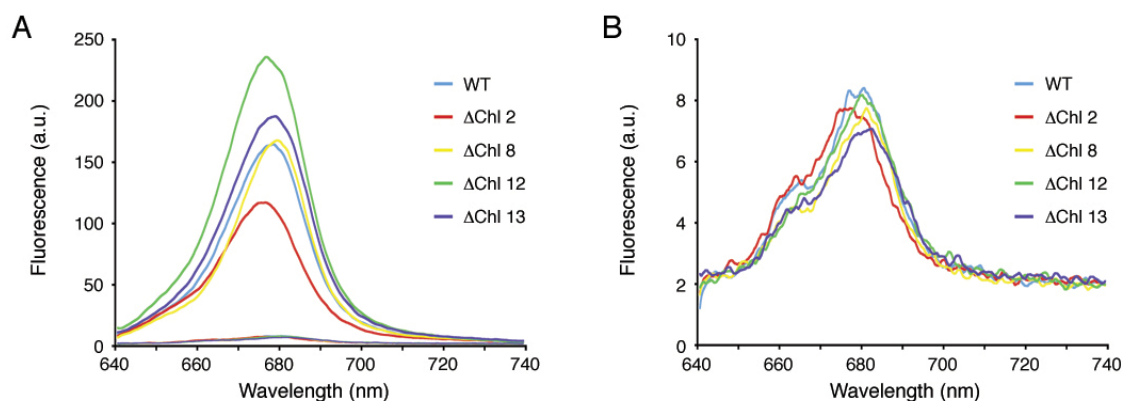


**Figure 8-6 - Aggregation quenching of LHC-II mutants.**

Room temperature fluorescence emission spectra of refolded LHC-II mutants each lacking a specific Chl binding site (same data as in Figure 8-2) and refolded wild-type complex. (A) Refolded complexes in detergent solution (solid lines) and in the aggregated state on the same scale (dashed lines, at the bottom). The spectra of individual Chl variants have not been normalized. (B) Same spectra of refolded complexes in the aggregated state as in (A) on an enlarged scale.

Several of the studied variants (WT, Chl 2, Chl 8 and Chl 13) had very reduced Vio content, which on average corresponded to roughly 1 Vio molecule per 8 to 10 LHC-II monomers (Table 4-4). This comes as no surprise, because Vio is known to be the LHC-II Car with the lowest affinity, due to its very peripheral position in the LHC-II monomer. It is however relevant that aggregation quenching is not at all correlated with the Vio content. For all variants, including those that on average had Vio in less than 10% of the monomers, the fluorescence yield dropped by more than one order of magnitude. It can thus be safely concluded that Vio is also not required for aggregation quenching.

In addition to Tyr122, the chlorine rings of Chl 6 and Chl 13 line the Neo binding site and the epoxy group of Neo makes a polar contact with the keto group of the Chl 13 phytyl chain. As a result, disruption of Chl 13 binding site by mutation will necessarily affect Neo binding, and this was indeed verified by the HPLC analysis of the Chl 13 mutant, which showed that this mutant had only trace amounts of bound Neo (Table 4-4). Studying this mutant is particularly relevant because twisting of the Neo conformation has been correlated with fluorescence quenching in LHC-II aggregates and crystals (Pascal et al, 2005), as well as with qE *in vivo* (Ruban et al, 2007). The fluorescence spectra of aggregated LHC-II mutants (Figure 8-6) clearly show that aggregation quenching is as effective for the Chl 13 mutant as is for WT. The conclusion that neither a particular Chl pair nor Vio is required for LHC-II aggregation quenching can thus be extended to Neo, which is therefore also not involved in the quenching mechanism.

### **8.2.2 Zea binding to LHC-II is not sufficient for efficient quenching**

A complete explanation of the mechanisms governing NPQ requires elucidation of the role played by the exchange of Vio by Zea in the LHCs, but so far a conclusive model is still missing. One line of thought argues that Zea plays an indirect role in the quenching mechanisms, acting as an allosteric effector that shifts the equilibrium between the active and the quenched conformation of the LHCs towards the dissipative state (Dall'Osto et al, 2005; Crouchman et al, 2006; Perez-Bueno et al, 2008). The conformational switch hypothesis has already been discussed and shown to be very unlikely, but it is nevertheless important to note that the reduction in Car S<sub>1</sub>-Chl energy transfer efficiency in Zea-LHC-II (3 to 5%),

observed by two-photon excitation spectroscopy, was not proportional to the fraction of native (14%) and refolded (36%) LHC-II binding Zea (Section 8.1.3.1). If Zea binding to LHC-II were to function as an allosteric effector, the resulting switch to the quenched conformation would be necessarily translated into a much larger change in the Car  $S_1$ -Chl coupling, as a result of the change in the pigment structure.

The other line of thought implicates Zea directly in the quenching mechanism. One of the first explanations put forward was the so-called gear-shift model (Frank et al, 1994). Presumably, the  $S_1$  state of Zea, but not of Vio, has a lower energy level than the  $Q_y$  state of the neighbouring Chls, allowing excitation energy transfer from the Chls to the Zea but not to Vio. The excited Zea would then rapidly decay to the ground state, dissipating the excitation energy as heat by internal conversion. This model predicts that Zea-LHC-II has a lower fluorescence quantum yield and lifetime than Vio-LHC-II. To verify this hypothesis experimentally, a spectroscopic comparison between Zea-LHC-II and Vio-LHC-II was performed (Sections 8.1.3; Section 8.1.3.1). It was found that Zea binding to LHC-II induces only a very small reduction of the Chl excited state lifetime, as determined by both transient absorption and time-resolved fluorescence spectroscopy. These results are in agreement with another spectroscopic study in which a 11% reduction of LHC-II quantum yield was observed when Zea was bound to the complex (Avenson et al, 2008b) and with recent calculations, which indicate that the difference between the excited state energies of Vio and Zea in LHC-II are in fact too small to account for effective dissipation of excess excitation energy via excitation energy transfer (Dreuw & Wormit, 2008).

Calculations (Dreuw et al, 2003; Dreuw et al, 2005) and ultra-fast spectroscopy on thylakoid membranes from different *Arabidopsis* mutants (Holt et al, 2005) established an alternative link between Zea and qE. It was found that under qE conditions a Zea radical cation is formed, supporting previous suggestions that Chl de-excitation can be brought about via a charge transfer state of a Zea-Chl heterodimer. The exact origin of this transient form of Zea implicated in quenching is however unclear. In agreement with others (Avenson et al, 2008b), the results presented in Section 8.1.3 show that Zea binding to LHC-II is not sufficient to

---

generate the Zea radical cation upon Chl excitation., implying that the Zea radical cation mechanism of quenching either takes place in another LHC or requires additional components that have not been included in our experiments. Other effects such as pH sensing by PsbS are likely to play a role.

### **8.2.3 Zea radical cation in LHC-II**

The Zea radical cation generated by R2P2CI in isolated Zea-LHC-II had an absorption peak centred at 983 nm, i.e. ~20 nm blue-shifted compared to the Car radical cation found in thylakoid membranes under qE conditions (Holt et al, 2005). Another spectroscopic signature of qE in leaves and intact thylakoids is a rise in absorption at 535 nm, which has been attributed to a red-shift of Zea (sometimes referred to as “Zea-activation”) (Ruban et al, 2002). The positions of the carotenoid absorption bands are known to be dependent on the polarizability of the solvent (Amarie et al, 2007). The changes in the photophysical properties of Zea during qE may therefore reflect binding to PsbS, which would provide a more polar environment than the lipid phase of the membrane.

## 9 LHC-II SINGLE CRYSTAL SPECTROSCOPY

The functional state of pea LHC-II in single crystals was investigated by steady-state and time-resolved spectroscopy. Measurements were performed under a variety of experimental conditions. Different geometries of the experiments, crystal forms and temperatures were used to investigate the functional properties of crystalline LHC-II (Figure 9-1). In parallel, experiments with solubilised complexes and aggregates at different concentrations were performed to assist the interpretation of the results. All the results presented in this section were obtained at the Cryobench of the ESRF, Grenoble. The contribution of Dr. A. Royant (Institute of Structural Biology Jean-Pierre Ebel and ESRF, Grenoble) was essential for obtaining the results presented here.

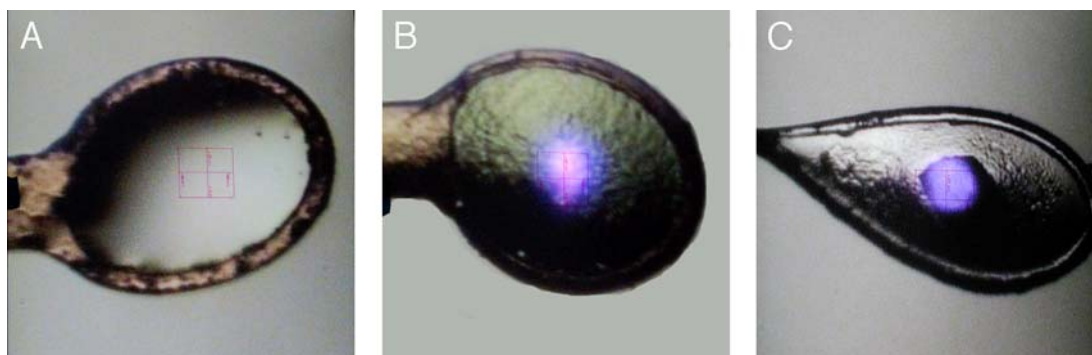


**Figure 9-1 – Different types of samples used for low temperature spectroscopic measurements at the Cryobench.**

Absorption and fluorescence measurements were performed at 100 K with LHC-II solutions at (A) low and (B) high Chl concentration and (C) LHC-II crystals. The blue-violet spot in the middle of the sample is the focussed laser beam used for Chl excitation.



## 9.1 Results

### 9.1.1 Absorption spectra of LHC-II crystals

Measuring the absorption spectrum of a sample as optically dense as an LHC-II crystal is not straightforward (Figure 9-2). Nevertheless, it was possible to record absorption spectra of type-I pea LHC-II crystals at 100 K. The recorded spectra lacked fine structure, especially in the Chl Soret region that overlaps with the visible absorption bands of the carotenoids. On the other hand, although also lacking fine structure, the absorption spectra in the  $Q_y$  region revealed a sharp edge between  $\sim 680$  and  $\sim 690$  nm. This implies that LHC-II crystals absorb virtually all photons in the visible range up to  $\sim 690$  nm, and are transparent at longer wavelengths. The lack of defined peaks in the absorption spectra was due to a sensitivity limitation, i.e. to the very small number of photons transmitted through the crystals.

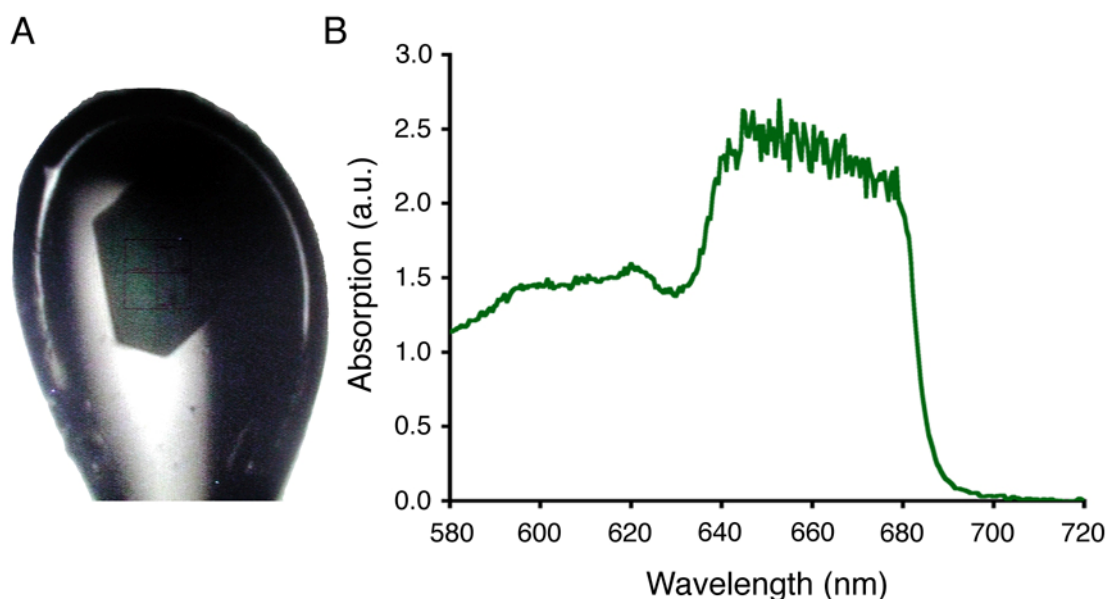


**Figure 9-2 – Low temperature absorption spectrum of a type-I LHC-II crystal in the  $Q_y$  region.**

(A) Picture of the crystal used to record the absorption spectrum. (A) Absorption spectrum recorded at 100 K. There is a sharp drop in absorbance between 680 and 690 nm, so that the LHC-II crystals absorb virtually all the visible light at wavelengths shorter than  $\sim 690$  nm.

### 9.1.2 Emission spectra of LHC-II crystals

The key spectroscopic signature of energy-transmitting LHC-II *in vitro* is its strong fluorescence peak centred at 680 nm. The appearance of an additional band centred at 700 nm at low temperature (100 K) has been correlated with fluorescence quenching in the complex. The emission spectra of single LHC-II crystals therefore give direct insight into the functional state of the complex in the crystalline state. Emission spectra of LHC-II in two distinct crystal forms at low temperature: type-I hexagonal plates (Standfuss et al, 2005) and cubic octahedral (Kühlbrandt, 1987) were recorded (Figure 9-3). About 10 crystals of each form were measured. In both crystal forms, LHC-II fluoresces with an emission maximum at roughly 680 nm, with some small variation towards the red on the exact position of this band. This peak was however always within 2 to 3 nm of the expected 680 nm peak. Another major fluorescence band detected with both crystal forms was centred at 700 nm. The position of this band did not vary in the same manner as the 680 nm band. The ratio between the intensities of the bands at 680 and 700 nm varied widely from crystal to crystal and within each crystal depending on the positioning of the excitation laser. The spectra presented in Figure 9-3 are therefore typical examples obtained from each of the two crystal forms. Fluorescence at 680 nm was observed with all crystals. A third, weak and very broad band centred at 740 nm was also observed in both crystal forms.

---

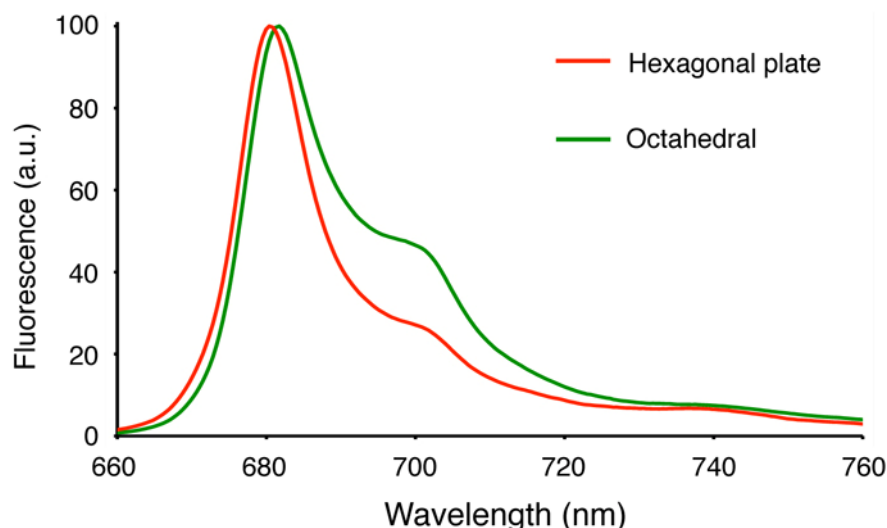


**Figure 9-3 - Emission spectra of LHC-II crystals.**

The emission spectra of LHC-II in two crystal forms were recorded at 100 K. Red, spectrum from a hexagonal plate with a type-I crystal packing; green, spectrum from an octahedral crystal with a cubic crystal lattice. Both spectra were normalised to 100 at the emission maximum.

### 9.1.3 Geometry dependence of LHC-II crystal emission spectra

The apparent variability of the LHC-II emission spectra in single crystals was investigated by changing the geometry of the experiment. The exact orientation of the crystal was tuned by rotation and translation in the x, y and z directions. In addition, the detection position was alternatively set at  $90^\circ$  or  $270^\circ$  from the axis defined by the excitation laser (Figure 3-6). Figure 9-4 and Figure 9-5 show the variation of the emission spectrum as the crystal of each form rotated through a complete  $360^\circ$  cycle. The changes in the region between 680 and 700 nm with each rotation are striking, showing that the position of the emission maximum varies dramatically with rotation. In fact, not only the position and intensity of individual bands but also the total emission intensity varied with the rotation angle. Specifically regarding the 680 nm band, the signature of LHC-II fluorescence, the intensity varied from being the main emission peak to being completely absent from the spectrum ( $135^\circ$  and  $270^\circ$  for the type-I crystal, for example; Figure 9-4). While the intensity of the 700 nm emission band also changed considerably, its position was fixed throughout the revolution in both crystal forms.

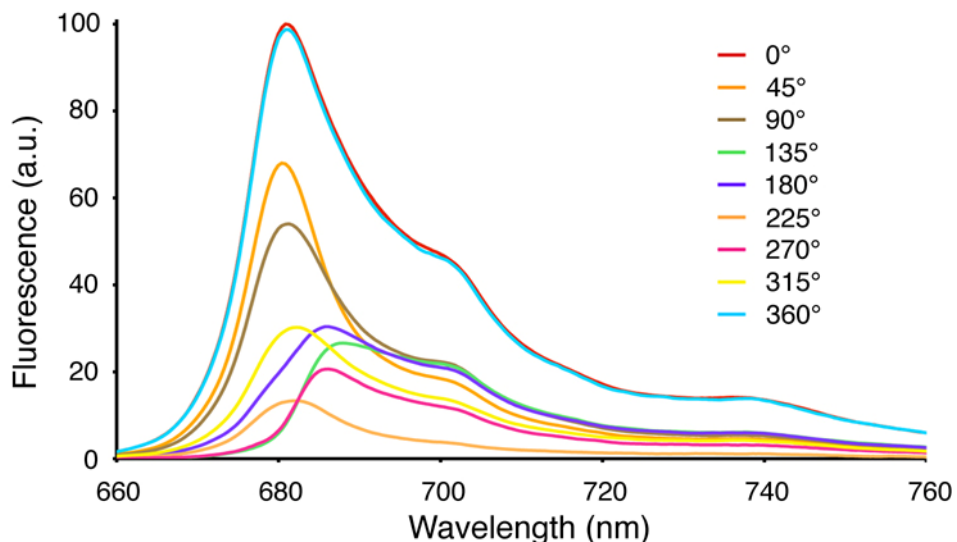


**Figure 9-4 - Emission spectra of a type-I LHC-II crystal at different tilt angles.**

Variability of the fluorescence emission spectrum of a type-I LHC-II crystal as the crystal is rotated. The crystal was mounted on a goniometer head (Figure 3-4) and each spectrum was recorded upon a 45° rotation. After a full rotation of the goniometer head, the final spectrum superposes almost perfectly with the initial spectrum.

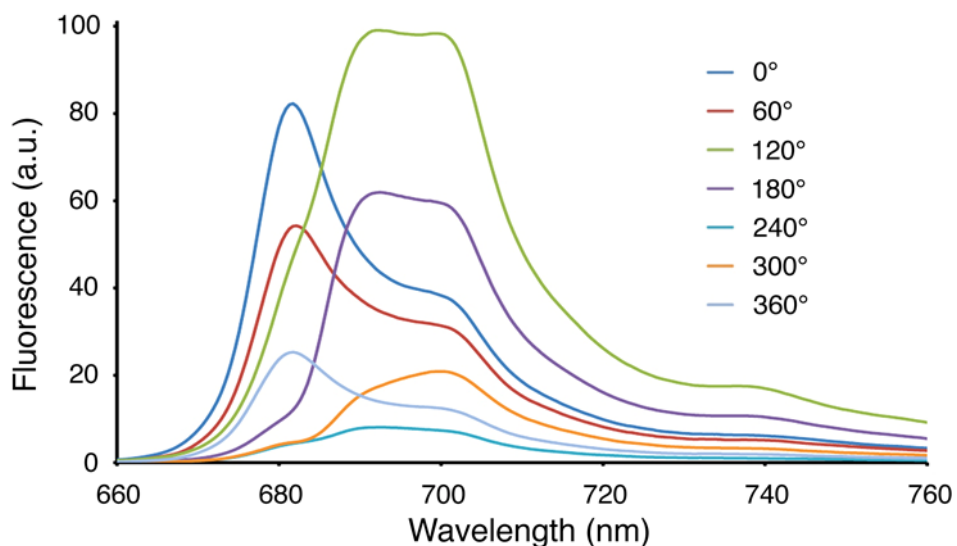


**Figure 9-5 - Emission spectra of a cubic LHC-II crystal at different tilt angles.**

Variability of the fluorescence emission spectrum of a cubic LHC-II crystal as the crystal is rotated. The crystal was mounted on a goniometer head (Figure 3-4) and each spectrum was recorded upon a 60° rotation.

While the spectra of the type-I crystal overlap almost perfectly at  $0^\circ$  and  $360^\circ$ , the corresponding spectra for the cubic crystal look dissimilar. However, when the two spectra are normalised (Figure 9-6) it becomes clear that their overall structure is identical and that the differences observed in Figure 9-5 correspond almost exclusively to the different intensities of the bands, most likely due to a small movement of the crystal upon the  $360^\circ$  rotation.

Another set of fluorescence measurements was performed in which the position of the excitation spot on the crystals was changed by translation and the emitted light was detected at  $90^\circ$  or  $270^\circ$  (Figure 3-6). With the beam focused on the crystal surface, the fluorescence recorded on the same side ( $90^\circ$  position), showed a strong peak at 680 nm (Figure 9-7 A). When the detector was placed on the opposite side ( $270^\circ$  position), emission at 680 nm was weak or absent (Figure 9-7 A), and the broad 700 nm band was observed instead. The converse effect was observed when the laser was focussed to the crystal interior, which was nearer to its opposite surface of the crystal due to its thinness (Figure 9-7 B). The 680 nm band was thus the main emission peak at shorter distances between the excitation spot and the detection objective, and was virtually absent as this distance increased.

In sum, all the geometric parameters that were analysed (crystal orientation, position of the excitation spot within the crystal and detection geometry) had a major effect on the emission spectra of the LHC-II crystals, and were particularly critical for the intensity of the main emission band at 680 nm.

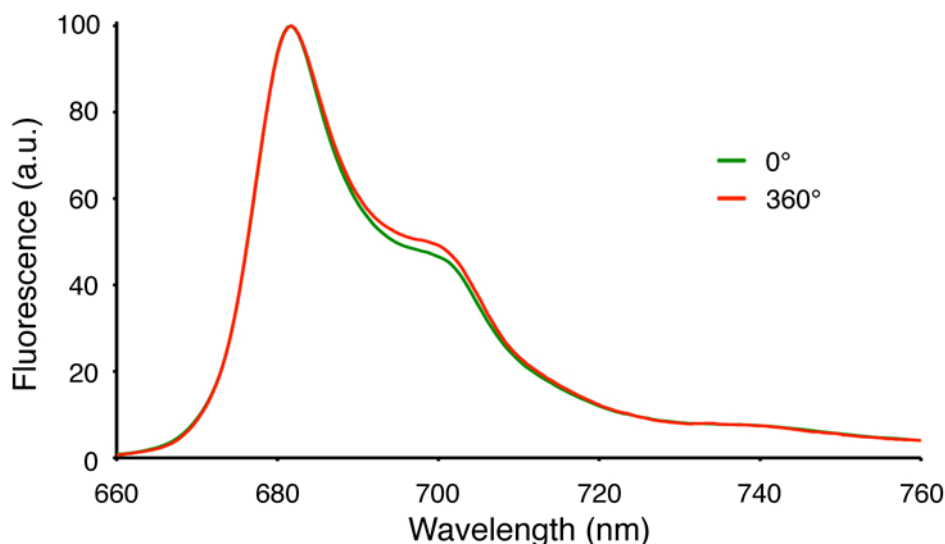


**Figure 9-6 – Normalised emission spectrum of a cubic LHC-II crystal at 0° and 360°.**

The spectra at 0° (green) and 360° (red) from Figure 9-5 were normalised so that their maximum intensity is the same.

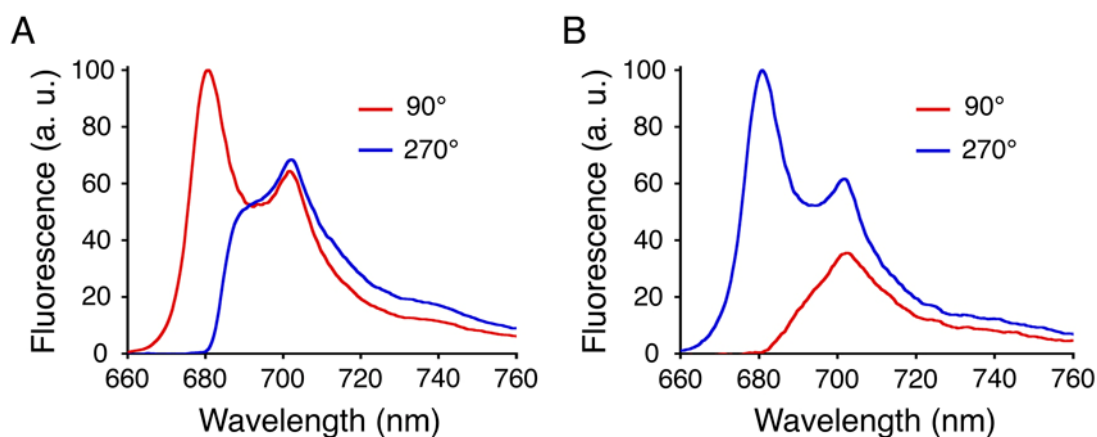


**Figure 9-7 - Emission spectra of a type-I LHC-II crystal in different geometries.**

The geometry of the fluorescence measurements at the Cryobench could be adjusted not only by rotation of the crystal but also by translating the position of the laser spot within the crystal. In (A) the laser spot was focused at the crystal surface closest to the objective used for detection at 90° (Figure 3-6). In (B) the laser spot was moved inside the crystal, placing it essentially at the opposite surface due to the thinness of the crystal and closer to the objective used for detection at 270°. The emission at 680 nm is predominant when the laser spot is closer to the detection objective (detection at 90° in (A) and at 270° in (B)) and virtually absent in the complementary geometry (detection at 270° in (A) and at 90° in (B)).

### 9.1.4 Temperature dependence of LHC-II crystal emission spectra

The emission spectrum of LHC-II aggregates at low temperature is characterised by the appearance of a band at 700 nm. This band is essentially absent or not detectable at room temperature. All the emission spectra of LHC-II crystals presented so far were recorded at 100 K, and all presented the same band at 700 nm. A single type-I LHC-II crystal in a small droplet of mother liquor was mounted on the Cryobench as described in Figure 3-5 and its emission spectrum at room temperature was recorded. Emission at 700 nm appears much weaker in these conditions compared to the low-temperature measurements (see for example Figure 9-4 and Figure 9-7). The emission maximum from the 5 measured crystals was always between 683 and 684 nm, thus also slightly red-shifted from the characteristic position at 680 nm, as observed at low temperature. Curiously, emission from LHC-II crystals at low temperature starts around 660 nm and stops around 760 nm, while at room temperature emission starts already around 630 nm and decreases to baseline levels at 780 nm. The spectra were in general much more noisy than those recorded at low temperature. Due to the extreme sensitivity of the fluorescence emission with the geometry of the experiments, a quantitative analysis of quantum yield has not been performed and is indeed very difficult. Nevertheless, the fluorescence intensity in the 680 nm peak in the emission spectra of LHC-II crystals at room temperature was consistently reduced compared to 100 K, in otherwise identical experimental conditions, suggesting a clear reduction in quantum yield.

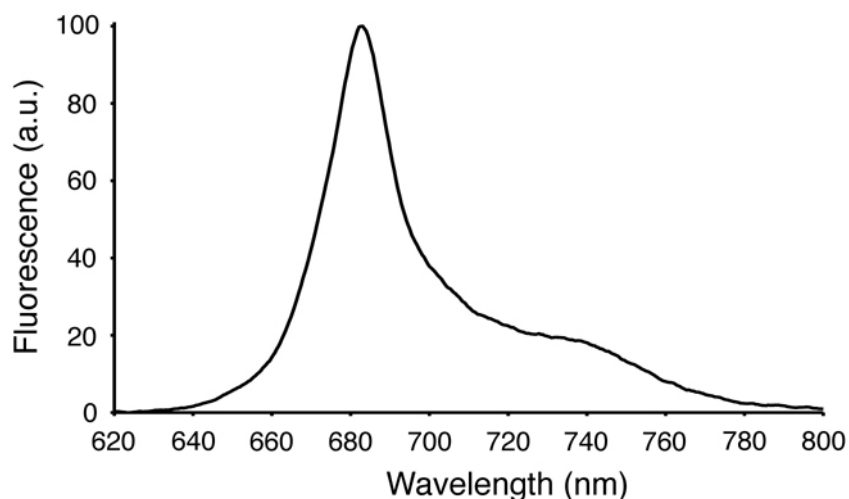


**Figure 9-8 – Room temperature emission spectrum of a type-I LHC-II crystal.**

The emission spectrum of a type-I LHC-II crystal at room temperature was recorded using the apparatus shown in Figure 3-5. The emission maximum is red-shifted by  $\sim 3$  nm from the characteristic peak in solution at 680 nm.

### 9.1.5 Fluorescence lifetimes at low temperature

A detailed investigation of the fluorescence lifetimes of LHC-II in solution, aggregates and single crystals at 100 K was carried out using time-correlated single photon counting (TCSPC). Histograms were recorded from photons in the entire range of the fluorescence emission spectrum or from individual bands using 10 nm width filters. Figure 9-9 shows the experimental TCSPC histograms and their respective fits. Table 9-1 summarises the lifetimes and amplitudes of the decays components derived from data fitting, as well as the average lifetime for all measurements.

From a first look at the TCSPC histograms, it is evident that LHC-II in solution has much longer fluorescence lifetimes than in either aggregates or crystals. This is true for the total emission and for the individual bands at 680 and 700 nm. The average fluorescence lifetime for LHC-II in solution in these three spectral ranges was always close to  $\sim 5.2$  ns and the decay was also always bi-exponential. There was only a small variation in the lifetime of these two components (roughly 3.0 and 5.5 ns) and the amplitude (roughly 0.2 and 0.8, respectively) throughout all the measurements.

Another major difference between LHC-II in solution and in aggregates or crystals is that the fluorescence decay could be fit in the first case with just two

---



decay components, as evaluated by the  $\chi^2$  analysis, while three components were necessary to achieve a satisfactory fit in the latter cases. The presence of additional components in aggregates and crystals cannot be excluded, as data fitting was restricted to three decay components.

While the histograms recorded with LHC-II in solution are clearly distinct, the data from aggregates and crystals share more similarities. This is particularly true for the histograms recorded using the total fluorescence emission. The lifetime and amplitude of the two shortest components are almost identical. Only the longest decay component shows a significant difference, being more than 0.5 ns longer in LHC-II crystals than in aggregates. Even so, the average fluorescence lifetime for crystals is also 0.5 ns longer than in aggregates.

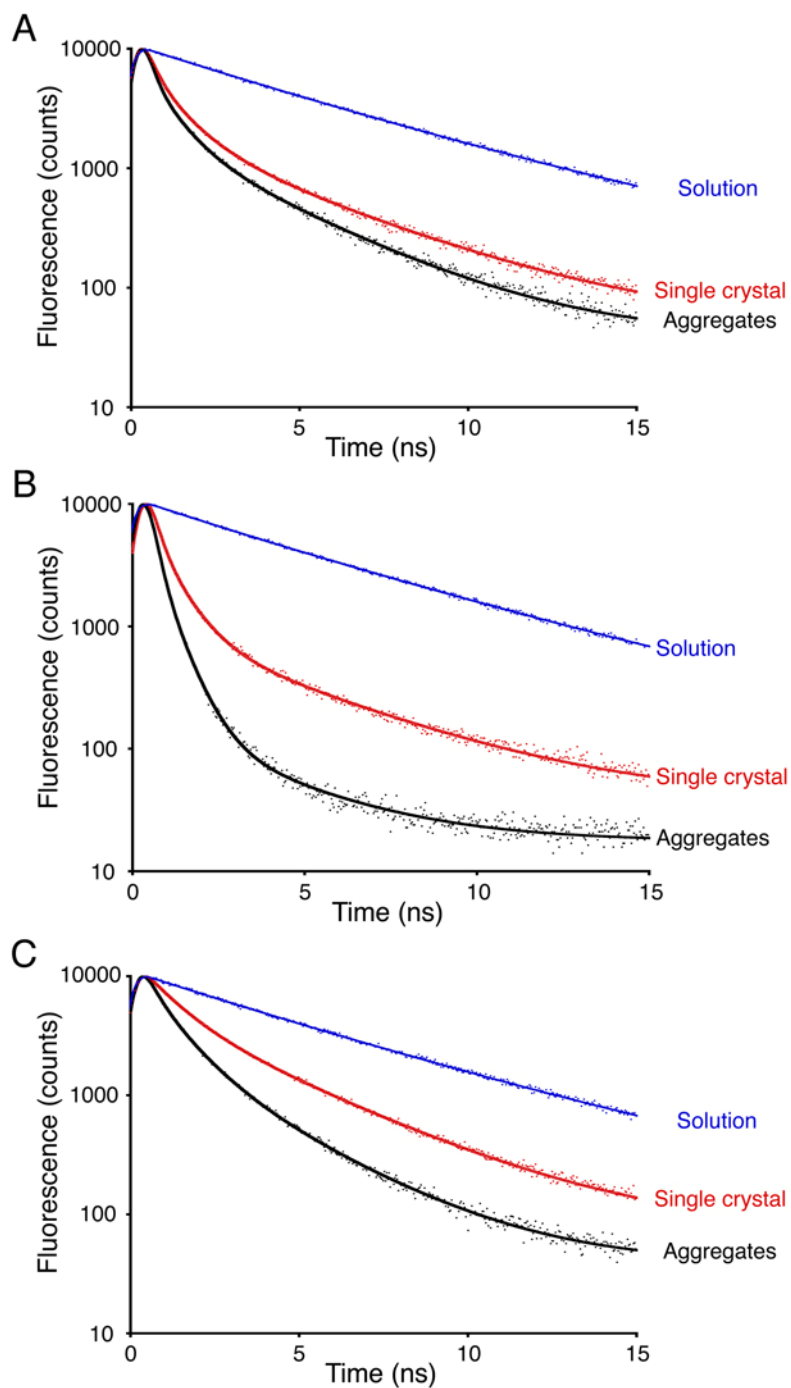


**Figure 9-9 - TCSPC histograms of the fluorescence decay of LHC-II in solution, crystals and aggregates**

Fluorescence lifetimes of LHC-II in different aggregation states at 100 K were analysed by TCSPC. (A) Decay of the total fluorescence emission; (B) decay of the 680 nm fluorescence band; (C) decay of the 700 nm fluorescence band. To record the data in (B) and (C) band-pass filters were used. LHC-II in solution was at a concentration of 0.01 mg (Chl)/ml. One single type-I crystal was used to generate the data presented here. The experimental data are shown as dots and the fitted curves as lines.

Table 9-1 - Low temperature LHC-II fluorescence lifetimes

	[Chl] (mg/ml)	$\tau_1$ (ns)	$a_1$	$f_1$	$\tau_2$ (ns)	$a_2$	$f_2$	$\tau_3$ (ns)	$a_3$	$f_3$	$\langle\tau\rangle$ (ns)
<i>Total emission</i>											
	0.01	2.89	0.22	0.13	5.57	0.78	0.87	-	-	-	5.22
	~150	0.27	0.65	0.24	0.90	0.27	0.34	3.78	0.08	0.43	1.98
	n.a.	0.23	0.77	0.36	0.85	0.17	0.29	3.16	0.06	0.35	1.43
<i>680 nm band</i>											
	0.01	2.73	0.22	0.12	5.53	0.78	0.88	-	-	-	5.19
	~150	0.24	0.78	0.43	0.76	0.20	0.34	4.05	0.03	0.23	1.31
	n.a.	0.19	0.88	0.69	0.56	0.12	0.27	2.94	<0.01	0.03	0.39
<i>700 nm band</i>											
	0.01	3.04	0.26	0.16	5.54	0.74	0.84	-	-	-	5.14
	~150	0.43	0.21	0.05	1.24	0.50	0.35	3.62	0.29	0.60	2.63
	n.a.	0.30	0.44	0.15	0.92	0.43	0.45	2.68	0.13	0.40	1.52

The differences between aggregates and crystals became clearer when individual bands were analysed. The average lifetime of the 700 nm band is more than 1 ns longer in crystals (2.63 ns) than in aggregates (1.52 ns), and is more than three times longer in the case of the 680 nm band (1.31 and 0.39 ns, respectively). This is mostly due to the fact that the longest decay components in LHC-II aggregates are roughly 1 ns shorter than in crystals, and their amplitude is in comparison systematically much smaller. Note that the difference in lifetime between LHC-II in solution and in aggregates or crystals is larger for the particularly interesting 680 nm band.

### **9.1.6 Fluorescence lifetimes at room temperature**

Analysis of the LHC-II fluorescence lifetime in single crystals at room temperature was severely hampered by drift of the crystals in the mother liquor droplet. Small changes in the position of the crystal relative to the laser spot resulted in a large increase or decrease in the photon count, which made data fitting problematic. The few successful measurements revealed that the average LHC-II fluorescence lifetime for total emission dropped to  $\sim 1$  ns at room temperature. Only type-I crystals were measured at room temperature.

The increased temperature also reduced the average fluorescence lifetime of LHC-II in aggregates and solution, by roughly 1 ns in both cases.

### **9.1.7 Wavelength-dependence of LHC-II fluorescence lifetimes**

Approximated decay associated spectra (described in Section 3.11.3) were obtained using 10 nm wide band pass filters, covering the spectral range of the LHC-II crystal emission at low temperature. TCSPC histograms were recorded with a set of 9 filters centred at every 10 nm from 670 to 750 nm and then analysed using a three-decay component model (Figure 9-10; Table 9-2). The type-I LHC-II crystal was oriented for the measurement so that both bands at 680 and 700 nm had similar intensities. The three decay components derived from the data fitting had relatively constant lifetimes throughout the entire spectral range (Figure 9-10 B), and are therefore referred to as short (average lifetime of  $0.31 \pm 0.06$  ns), medium (average lifetime of  $1.01 \pm 0.19$  ns) and long component (average lifetime of  $3.93 \pm 0.26$  ns).

---

The lifetime of the shortest decay component was in general close to 0.30 ns, i.e. close to the time resolution of the measurements. Interestingly, this decay component provides the biggest contribution to the emission of the 680 nm band. From 700 nm onwards, towards the red, its contribution became very small. The medium lifetime component contributed more or less equally to the emission in the entire spectral range, with the exception of the band at 690 nm where this component had the largest contribution. Concomitantly, the long component provided most photons in the red region of the spectrum, starting at 700 nm. The corresponding approximated decay associated spectrum has an almost perfect peak at 700 nm, with a depression on the 690 nm band.

Two distinct regions can be distinguished in the analysis of the wavelength-dependence of the average fluorescence lifetime of the LHC-II crystal. The first region, between 670 and 690 nm, has shorter average lifetimes, in the order of 1.3 ns. The second region, ranging from 690 nm to the red-end of the emission spectrum, has much longer average fluorescence lifetimes, always above 2 ns and with a maximum of almost 3 ns at 710 nm. This increase of the average lifetime correlates with the small increase of the fluorescence lifetime of the short and medium decay components.

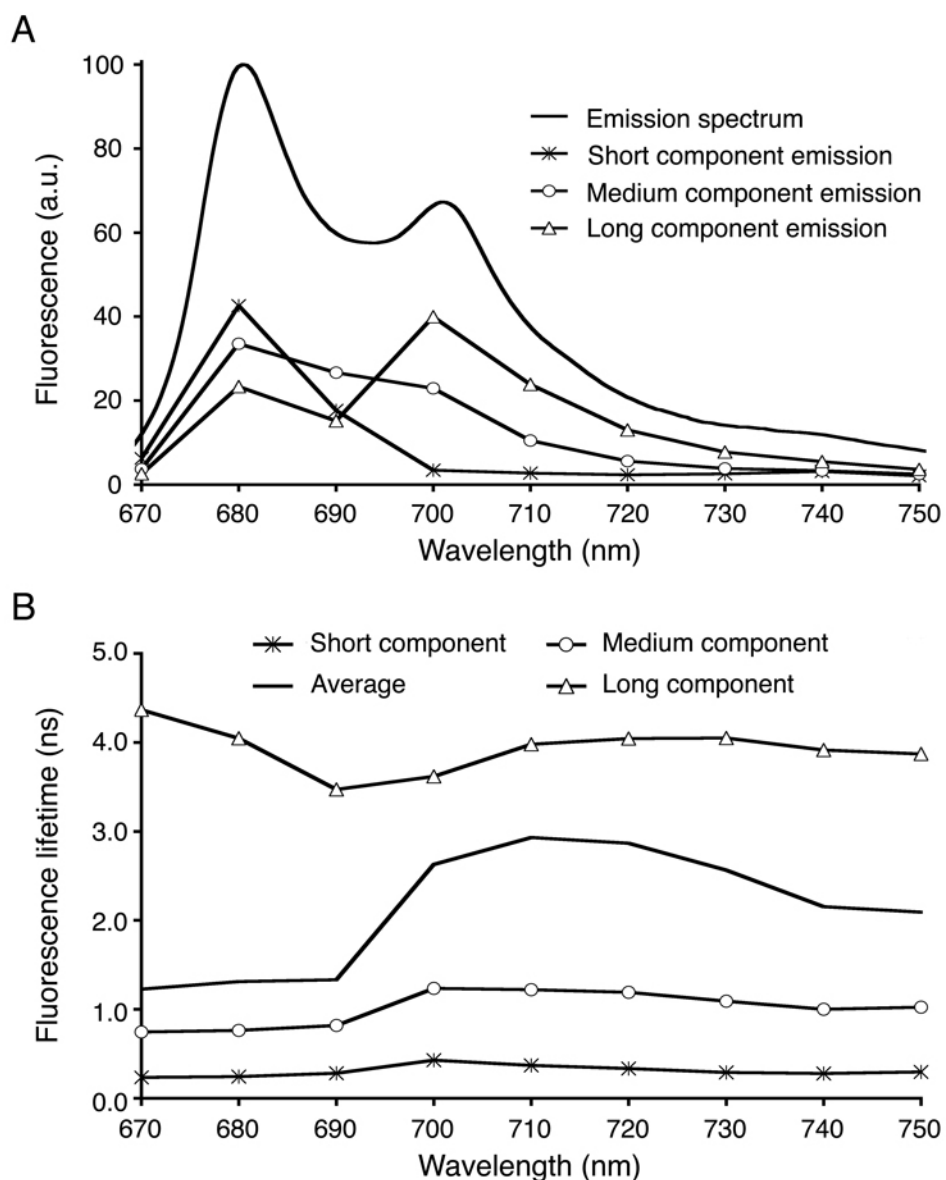


**Figure 9-10 - Wavelength dependence of the LHC-II fluorescence decay components in crystals at low temperature.**

TCSPC histograms were recorded using band-pass filters centred at every 10 nm from 670 to 750 nm. Approximated decay associated spectra were determined decomposing the fluorescence decay recorded with each of the filters into 3 components, termed short, medium and long. (A) Total emission spectrum and relative emission of the 3 components used to fit the fluorescence decay. (B) Wavelength dependence of average and component lifetimes.

**Table 9-2 - Wavelength dependence of the LHC-II fluorescence decay components in crystals at low temperature**

Wavelength	Short			Medium			Long			$\tau_{av}$ (ns)	$\chi^2$
	$\tau$ (ns)	$\alpha$	f	$\tau$ (ns)	$\alpha$	f	$\tau$ (ns)	$\alpha$	f		
All	0.27	0.65	0.24	0.90	0.27	0.34	3.78	0.08	0.43	1.98	1.30
670	0.23	0.83	0.50	0.75	0.15	0.30	4.37	0.02	0.20	1.23	1.26
680	0.24	0.78	0.43	0.76	0.20	0.34	4.05	0.03	0.23	1.31	1.27
690	0.28	0.63	0.30	0.82	0.33	0.45	3.47	0.04	0.25	1.33	1.40
700	0.43	0.21	0.05	1.24	0.50	0.35	3.62	0.29	0.60	2.63	1.27
710	0.37	0.34	0.07	1.22	0.39	0.28	3.98	0.27	0.64	2.93	1.19
720	0.33	0.47	0.11	1.19	0.31	0.27	4.04	0.21	0.62	2.87	1.23
730	0.29	0.62	0.18	1.09	0.25	0.27	4.05	0.13	0.55	2.57	1.20
740	0.28	0.70	0.26	1.00	0.21	0.28	3.92	0.09	0.46	2.15	1.24
750	0.30	0.68	0.26	1.03	0.23	0.30	3.87	0.09	0.44	2.09	1.24

### 9.1.8 Concentration-dependence of LHC-II fluorescence decay in solution

The first obvious difference between LHC-II in solution and crystals is local concentration. Trying to verify the hypothesis that LHC-II fluorescence lifetimes are directly influenced by concentration, at least above a certain high concentration, a set of experiments was carried out in which the Chl concentration in the measured samples was progressively increased. To facilitate the connection between these measurements and the crystal data, all experiments were performed at 100 K. For this reason, glycerol was used a cryo-protectant to avoid vitreous ice formation in the samples, which interferes with the measurements. All measurements were performed with the same LHC-II preparation.

Judging from the  $\chi^2$  analysis, the LHC-II fluorescence decay in dilute detergent solution can be described as virtually mono-exponential (with a lifetime of approximately 5 ns). However, beyond a critical Chl concentration ( $\sim 3$  mg/ml) an additional decay component with a shorter lifetime ( $\tau < 3.5$  ns) is required to fit to fluorescence decay data. Figure 9-11 shows the amplitude (a) of that second

component as a function of the Chl concentration. The amplitude of this additional component increases with Chl concentration, with an exponential rise above the critical concentration of 3 mg/ml.

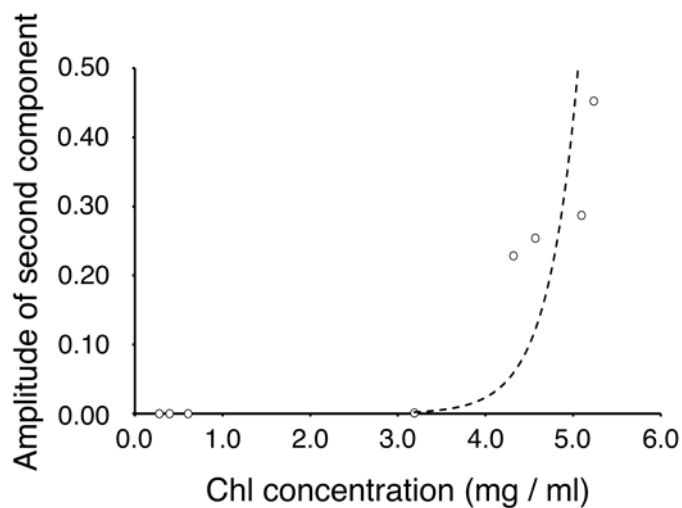


**Figure 9-11 - Concentration dependence of the relative amplitude of a second lifetime component in solubilised LHC-II at low temperature.**

Concentration dependence of the relative amplitude (a) of a second component with the Chl concentration. The fitted curved is given by the equation:  $a = 2E-07e^{2.9009[Chl]}$ .



## 9.2 Discussion

### 9.2.1 Self-absorption distorts emission spectra of LHC-II crystals

Previous studies of crystalline LHC-II found either that the crystals did not emit at 680 nm (Pascal et al, 2005), or that the 680 nm emission depended on crystal age (Yan et al, 2007). From this it was concluded either that the crystalline complex was quenched, and that therefore the structure was that of an energy-dissipating state of LHC-II (Pascal et al, 2005), or that the complex changed from an unquenched to a quenched state in the course of a year, as a consequence of gradual crystal dehydration (Yan et al, 2007). However, all of the ~20 crystals examined in this work emitted strong 680 nm fluorescence in some orientations. Any of the published crystal spectra could be reproduced with virtually any crystal of LHC-II (Figure 9-12), simply by changing the geometry of the experiment, either rotating the crystal around an axis perpendicular to the incident light (Figure 9-4; Figure 9-5) or changing the position of the laser within the crystal by translation (Figure 9-7). Polarization effects as an explanation of the orientation dependence of the crystal spectra can be excluded, as an earlier study revealed only minor linear dichroism in LHC-II crystals as a function of crystal tilt (Kühlbrandt et al, 1988). It appears that both of the previous studies (Pascal et al, 2005; Yan et al, 2007) examined each crystal in only one orientation and thus failed to notice the strong orientation dependence of the fluorescence signal. The orientation dependence is clearly due to self-absorption, as the optically dense crystals self-absorb 680 nm light almost completely (Figure 9-13). This is not surprising, given that the Chl concentration in single crystals is 150 mg/ml, roughly 30 times higher than the most concentrated LHC-II solutions, which look virtually black to the eye.

The 680 nm fluorescence is evident in orientations where the emitted radiation travels only a short distance through the crystal. This is the case when the exciting laser is focussed on the crystal surface, and fluorescence is recorded on the same side (Figure 9-14). In the opposite direction, only the longer-wave 700 nm radiation is detected, which is hardly absorbed by LHC-II, and thus can traverse longer distances through the crystals. At intermediate orientations, a mixture of both spectra is obtained. The relative intensity of the 700 nm band will clearly depend on the thickness of the individual crystal, as the 680 nm light re-absorbed by

the crystal volume on the far side of the focal spot (Figure 9-14) will give rise to non-directional 700 nm fluorescence, and this will contribute to the spectrum even when the recorded 680 nm emission is at its maximum. Accordingly, the fluorescence spectra of extremely thin single crystals of LHC-II should resemble those of the complex in detergent solution quite closely.

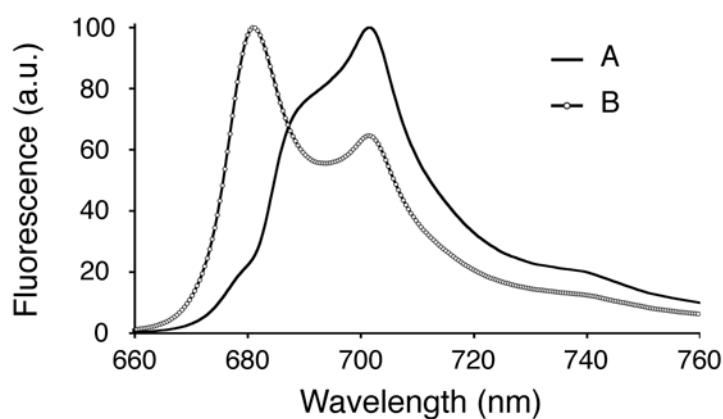


**Figure 9-12 - Low-temperature fluorescence spectra of a single crystal of pea LHC-II in two different orientations.**

By changing the position of the laser spot within the crystal, the spectrum changes from a broad band at 700 nm with very little emission at 680 nm (A), to a spectrum showing an emission peak at 680 nm characteristic of unquenched LHC-II, with a second band at 700 nm (B). (A) is very similar to previously published crystal spectra (Pascal et al, 2005; Yan et al, 2007).

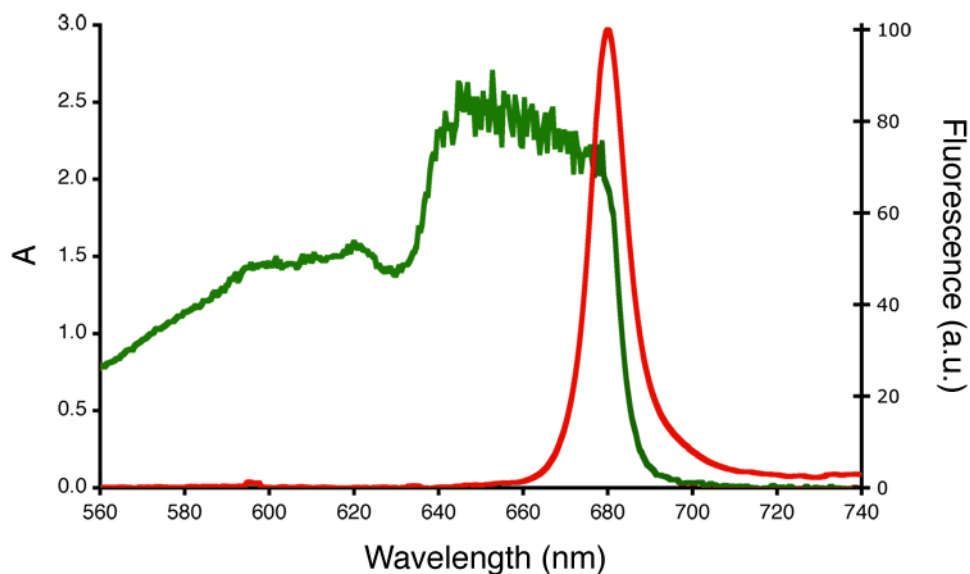


**Figure 9-13 – Low temperature LHC-II absorption and fluorescence emission spectra.**

The low temperature absorption spectrum (green; y axis on the left) of LHC-II in single crystals has a sharp edge between 680 and 690 nm, so that the crystals absorb all visible light before the edge and are virtually transparent thereafter. The low temperature emission spectrum (red; y axis on the right) of LHC-II in solution has a single peak centred at 680 nm, coinciding with the sharp edge on the absorption spectrum.

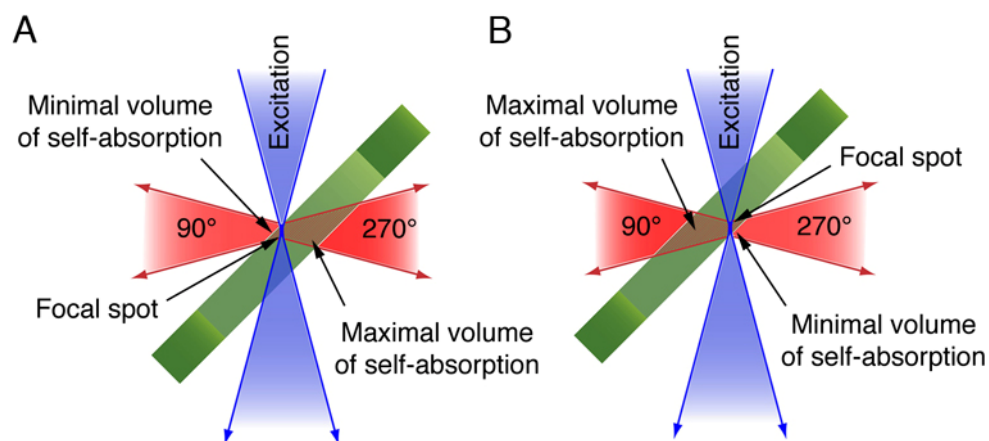


**Figure 9-14 - Self-absorption of LHC-II fluorescence in single crystals.**

The variability of the LHC-II fluorescence emission spectra in single crystals can be explained by orientation-dependent self-absorption. The position where the excitation beam hits the crystal and the geometry of the emission detection will dictate the amount to spectral distortion that is observed. (A) and (B) explain the variability of the spectra presented in Figure 9-7 A and B, respectively.

### 9.2.2 Low-temperature 700 nm fluorescence

The broad emission band centred at 700 nm is often considered to be a low-temperature signature of fluorescence quenching in LHC-II (Ruban et al, 1995a; Vasil'ev et al, 1997; Pascal et al, 2005; Yan et al, 2007). However, low temperature emission at 700 nm is also observed in the detergent-solubilised complex, as shown by the 700 nm shoulder of the 680 nm emission peak in Figure 8-1, and in published spectra of LHC-II in detergent solution (Ruban et al, 1995a; Moya et al, 2001; Palacios et al, 2002). The contribution of this shoulder to the spectrum clearly depends on the LHC-II concentration, which determines how much of the 680 nm emission is re-absorbed. In dilute solutions, where self-absorption is negligible, the 700 nm emission is almost completely eclipsed by the bright 680 nm band, whereas it becomes more and more visible with increasing concentration and progressive self-absorption of the 680 nm band. Self-absorption is particularly strong in LHC-II crystals, but it is also apparent in the precipitated complex. With increasing optical pathlengths, the 680 nm emission of LHC-II aggregates is progressively removed, until virtually only the 700 nm band remains (Vasil'ev et al, 1997). The 700 nm low-temperature emission of LHC-II therefore appears not to be directly associated with fluorescence quenching. It is always present, and merely becomes more prominent, or even dominant, at the high local concentrations of LHC-II that have been used to study quenching *in vitro* or *in vivo*, due to self-absorption of the main 680 nm emission.

This opens the question of where in the complex the 700 nm band originates, and why it is not observed at room temperature. From a close examination of the Chl positions in the LHC-II structure and their associated energy levels, it seems likely that this band is due to fluorescence from uncoupled Chl states at low temperature, arising from the structural relaxation of a Chl *a* pair in the excited state within the complex. A likely candidate would be the Chl 2 / Chl 7 pair. Preliminary calculations indicate that relaxation of this pair would yield an energy gain of 0.03 eV, resulting in a Stokes shift from 680 to 703 nm, close to the observed 700 nm (Prof. A. Dreuw, personal communication). As the difference in energy levels between the initial excited state and the structurally relaxed excited state is small, the thermal energy at room temperature is sufficient to overcome this minimal energy barrier. With decreasing temperature, the

---

structurally relaxed state becomes more populated and therefore emission at 700 nm is enhanced. Obviously, these Chl states, which are populated only at unphysiologically low temperatures, will not affect energy transfer in the temperature range where LHC-II normally functions in plants.

Fluorescence measurements at low temperature with the LHC-II mutant that lacks Chl 2 aggregates could verify this hypothesis experimentally. If indeed the 700 nm peak originates from the Chl 2 / Chl 7 pair, it should not be present in the low temperature emission spectrum of Chl 2 mutant aggregates.

### 9.2.3 Fluorescence lifetimes in crystals, aggregates and solutions

Apart from the red shift of the fluorescence maximum, earlier assertions that the crystal structure shows the quenched state (Pascal et al, 2005; Yan et al, 2007) were based on the ~1 ns average lifetime of the fluorescence emitted by spinach LHC-II crystals.

A detailed investigation of the fluorescence lifetimes of LHC-II in single crystals, aggregates and detergent solution was carried out by time-correlated single-photon counting (TCSPC), using the same experimental device for all measurements. Single crystals at 100 K indicated two main emitting species at 680 and 700 nm with average fluorescence lifetimes of 1.31 and 2.63 ns, respectively (Figure 9-10; Table 9-2). The average fluorescence lifetime of the total emission was 1.98 ns. Under the same conditions, the average total fluorescence lifetime of LHC-II aggregates was 1.43 ns, but only 0.39 ns for the main 680 nm emission band (Table 9-1), close to the time resolution limit of our apparatus. The total emission from a frozen drop of dilute LHC-II solution at 100 K indicated two decay components (Figure 9-9; Table 9-1), with an average lifetime of 5.22 ns, which is in agreement with the literature (Palacios et al, 2002) and validates the accuracy of our measurements.

The total emission fluorescence decay of LHC-II crystals and aggregates at low temperature appear overall similar (Figure 9-9). This is largely due to the 700 nm region where lifetimes are long, and which is hardly affected by quenching or self-absorption. There is however a very clear difference in the average lifetime of the critical 680 nm emission, which is much longer than expected for a quenched

state in crystalline LHC-II, but consistent with literature values for LHC-II aggregates (Mullineaux et al, 1993; Vasil'ev et al, 1997), suggesting that at least some of the quenching mechanisms occurring in aggregates are also occurring in crystals.

At room temperature the average fluorescence lifetime of crystals dropped to  $\sim 1$  ns, in good agreement with fluorescence lifetime imaging of a spinach LHC-II crystal (Pascal et al, 2005). For comparison, these single crystal lifetimes are on average 5 to 10 times longer than those reported recently for quenched aggregates (van Oort et al, 2007a).

#### **9.2.4 Crystal structures show the active, energy-transmitting state**

One of the most interesting questions associated with the structure of LHC-II is whether it represents the energy-transmitting, unquenched or a hypothetical, energy-dissipating state of the complex. The two available X-ray structures (Liu et al, 2004; Standfuss et al, 2005) are identical within experimental error (Section 7.1.1; Section 7.2.1), and thus both show the same state of the complex. The structure is therefore either that of unquenched LHC-II, or it is that of a quenched state. The possibility that it may represent an average of quenched and unquenched states can be ruled out for two reasons: First, careful inspection of electron densities did not suggest significant contributions from alternate conformations. Second, the two X-ray structures (Liu et al, 2004; Standfuss et al, 2005) show LHC-II from two different plant species, determined from two entirely different crystal forms grown under dissimilar conditions. If the crystals were to consist of a mixture of two different hypothetical conformations, the proportions of these conformations would have to be the same in both forms, which is unlikely.

If the structure is not the average of two states, every LHC-II trimer on the crystal lattice has the same conformation. If the structure were to show the quenched state of the complex, as claimed by Pascal et al (Pascal et al, 2005), each and every trimer in the crystals would have to be quenched. The pigment conformations in the three monomers are identical in both crystal forms, so that every monomer would contain a quenching centre, and therefore there would be three such centres per trimer. Energy transfer paths to the quenching centres would

---

---

then be extremely short, in the range of 1-3 ns at most. The corresponding fluorescence decay times would then be extremely fast, close to the 35 ps of the excitation energy equilibration time (van Oort et al, 2007a), which is dictated by the intramolecular energy transfer rates in LHC-II (Novoderezhkin et al, 2005). In this situation the crystals should emit virtually no 680 nm fluorescence. However, the crystals do show strong fluorescence at 680 nm, if self-absorption is avoided, and for this reason alone the structure cannot be that of quenched LHC-II.

A detailed analysis of the low temperature fluorescence lifetimes of LHC-II aggregates (Mullineaux et al, 1993) indicated main components with lifetimes of 120 and 360 ps, and minor contributions with longer lifetimes of ~1.1 and 3.6 ns. Our measurements revealed that the long lifetime components are significantly stronger in single LHC-II crystals than in aggregates (Table 9-1), especially for the main 680 nm band. Although components shorter than ~0.23 ns are not resolved by our apparatus, the substantial contribution of the >3.5 ns components confirms the conclusion that the LHC-II trimers in the single crystals are unquenched and that the structures from them determined show the complex in the active, energy-transmitting state.

## **10 GENERAL DISCUSSION**



---

## 10.1 Implications for the mechanism of LHC-II aggregation quenching

The spectroscopic similarities between LHC-II aggregation quenching and the qE component of NPQ are intriguing. Perhaps not less intriguing is the fact that the very structurally uncharacterised (and possibly uncharacterisable) LHC-II aggregates have been exhaustively investigated in recent years with ever more sophisticated spectroscopic techniques (Ide et al, 1987; Ruban & Horton, 1992; Mullineaux et al, 1993; Ruban et al, 1995a; Vasil'ev et al, 1997; Barzda et al, 2001a; Kirchhoff et al, 2003; Lambrev et al, 2007; Ruban et al, 2007; van Oort et al, 2007a). This is only possible due to the large abundance of LHC-II and the simplicity of producing precipitates. What remains unclear is if LHC-II aggregation quenching and qE are indeed related.

It should be mentioned that aggregation quenching is far from being an exclusive property of LHC-II. Highly quenched precipitates of IsiA (Ihalainen et al, 2005), a cyanobacterial light-harvesting complex that is mainly produced under iron deficiency conditions and has a very different structure from LHC-II, and all three minor LHCs (Wilk, 2006) have been described. In the present work, it was shown that virtually any refolded LHC-II complexes, regardless of their pigment composition, are quenched when aggregated. The only pigments that have not been verified if required for aggregation quenching were the two Luts, which are indispensable for obtaining stable complexes. It seems then logical that precipitates of any LHC will be quenched, with the only requirement being that at least one Chl in the complex is exposed, allowing for coupling between pigments of interaction complexes in the precipitate.

### 10.1.1 Proposed mechanism of LHC-II aggregation quenching

A model for LHC-II aggregation quenching mechanism *in vitro* is proposed. The very short lifetimes of LHC-II aggregates are attributed to the formation of quenching centres through random, tight interaction of pigments exposed on the outer perimeter of the LHC-II trimer, or by van der Waals contact with contaminating free pigments (Figure 10-1) or other impurities. Such interactions

would create energy sinks on the exterior surface of the complex capable of effectively annihilating excitation energy (Beddard et al, 1976; Dreuw et al, 2003; van Oort et al, 2007a). In detergent solution, the probability of creating similar quenching interactions depends on the LHC-II concentration, and this was indeed verified by the correlated increase of short-lived populations and concentration (Section 9.1.8).

The proposed model explains the pronounced local heterogeneity in lifetimes of LHC-II aggregates ranging from 0.5 to 3 ns, as measured by fluorescence lifetime imaging (Barzda et al, 2001a). Regions with short lifetimes have a higher density of randomly generated, quenching pigment pairs than those with longer lifetimes. The lifetimes of the latter areas actually resemble those of LHC-II crystals, which is not unexpected, considering that the aggregates are partly microcrystalline. If all trimers in the aggregates were quenched, one would not expect any such heterogeneity. This model also explains the variability in the overall fluorescence lifetimes of LHC-II aggregates reported, which varied significantly depending on the detergent from which they were precipitated (Vasil'ev et al, 1997), most likely due to different proportions of microcrystalline or amorphous components. Again, if the aggregated trimers were all quenched, there should be no such detergent dependence. Furthermore, this model explains the increased heterogeneity in fluorescence lifetimes of aggregates of LHC-II monomers, as compared to aggregates of trimers (van Oort et al, 2007a). Several more Chls are exposed on the periphery of LHC-II monomers than in trimers. Also, monomer solutions inevitably contain more free pigment, giving rise to more and different quenching centres upon aggregation. Finally, this notion is consistent with an earlier study (Ruban et al, 1995a), which found that the drop in fluorescence yield upon LHC-II aggregation is reversed at 4 K. At very low temperature, the absorbed energy is thus lost as fluorescence before it can be transmitted to any quenching centres, which suggests that they must be physically distant from the emitting pigments. If they were in the same monomer, quenching should be effective even at 4 K.

Randomly generated quenching centres on the periphery of aggregated LHC-II trimers fully and effortlessly accounts for all four of the above effects, and

---

consequently there is no need to assume a rearrangement of the pigment structure within the complex for the effective dissipation of excitation energy in aggregates and, more importantly, in the PS-II antenna.

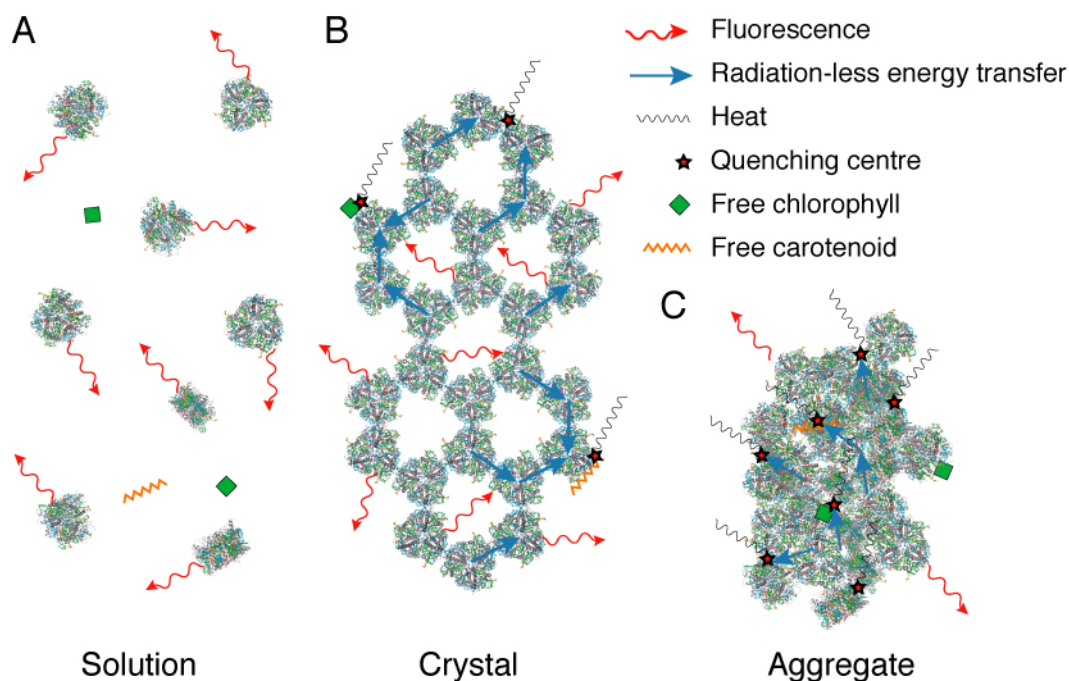


**Figure 10-1 - Energy transfer and dissipation by LHC-II *in vitro*.**

(A) Solubilized LHC-II trimers in detergent solution are functionally independent and re-emit absorbed light as fluorescence. (B) LHC-II crystals show similar fluorescence, although its intensity and spectral range is modified by re-absorption. Conceivably, occasional tight interaction of LHC-II trimers with one another, e.g. at grain boundaries, or with contaminating free pigments, can generate quenching centres, to which the energy flows via the excitonically coupled complexes. (C) Randomly compacted trimers in LHC-II aggregates generate a high density of quenching centres, resulting in reduced lifetimes and conversion of the absorbed energy into heat.

## 10.2 Implications for the mechanism of qE

### 10.2.1 Crystalline LHC-II resembles the complex in thylakoids

In many ways, the environment of LHC-II in 2D or 3D crystals comes close to that in the thylakoid membrane. All crystals of LHC-II are either grown from preparations containing about 30 lipids per trimer (Nussberger et al, 1993) or lipids are added (Liu et al, 2004). In all known crystal forms of the complex, the trimers are thus likely to be surrounded by thylakoid lipids. Furthermore, the distance between trimers on the crystal lattice is very similar to their mean distance in grana membranes, which is estimated to be ~10 nm. Inter-trimer contacts in LHC-II crystals are close enough to allow rapid energy transfer, but not so close as to give rise to quenching Chl dimers at the interface, except perhaps at grain boundaries. LHC-II in single crystals thus resembles its state in the thylakoid membrane more closely than either that in dilute solution, or that in precipitates *in vitro*. The spectroscopic properties of LHC-II in single crystals can therefore be taken to be similar to those of the complex in the thylakoid membrane.

Another close-to-native state of the complex is that of LHC-II trimers reconstituted into proteoliposomes (Moya et al, 2001). Interestingly, the emission and lifetimes of trimers reconstituted at high lipid/protein ratios, where they would be far apart in the lipid bilayer, seem to resemble those of dilute solutions, with a gradual transition from the dilute state to that in the more tightly packed membranes. A hypothetical switch upon transition from the detergent-solubilized to the membrane-inserted state can be ruled out, as it would affect all complexes equally at any lipid/protein ratio. Membrane insertion itself therefore does not convert the complex from the unquenched state in detergent solution to a quenched state, as has been postulated (Moya et al, 2001). Proteoliposomes reconstituted with a low lipid/protein ratio and hence a comparatively high protein density would resemble reaction centre-free grana thylakoids quite closely, except that the orientation of the LHC-II trimers with respect to the lipid bilayer is random *in vitro*. In terms of low-temperature emission spectra as well as wavelength dependence of fluorescence lifetimes, these reconstituted membranes are strikingly similar to single crystals, suggesting that the complex is in the same state in both.

---

The observed geometry dependence of the LHC-II crystal fluorescence emission is in many respects equivalent to that found in plant leaves (Louis et al, 2006; Buschmann, 2007). Although the origin of the various fluorescence bands is necessarily different in LHC-II crystals and leaves, there is pronounced extinction of the most blue-shifted bands around 680 nm when the emitted photons travel through the thickness of the leaf, exactly as in LHC-II crystals. All known light-harvesting complexes of PS-II, including CP24, CP26 and CP29, which together with LHC-II account for the bulk of Chl in chloroplasts, fluoresce maximally at 680 nm in detergent solution (Henrysson et al, 1989; Pagano et al, 1998; Croce et al, 2002), with an average lifetime of ~4 ns at room temperature (Moya et al, 2001), very similar to LHC-II. Similarly long fluorescence lifetimes have not been reported for leaves (Schmuck & Moya, 1994; Moise & Moya, 2004) or isolated chloroplasts (Haehnel et al, 1982; Reisberg et al, 1982; Roelofs et al, 1992; Gilmore et al, 1995), because *in vivo* no unconnected LHCs exist, and the excitation energy will inevitably be channelled towards a photochemical or a non-photochemical energy sink, i.e. a reaction centre or an unproductive, dissipating quenching centre.

### 10.2.2 Structure of Zea-bound LHC-II

One of the original goals of this doctoral work was to determine the structure of the Zea-bound state of LHC-II. However, none of the experimental strategies developed yielded Zea-LHC-II samples suitable for crystallisation. As discussed above (Section 4.2.2), LHC-II isolated from the *Arabidopsis* mutant *npq2* was unstable and had an artificial pigment composition. The two other experimental strategies invariably produced samples that were mixtures of Vio-LHC-II and Zea-LHC-II, which is likewise undesirable for crystallisation. However, the spectroscopic comparison between these two states of LHC-II clearly showed that they are identical (Section 8.2.2). This implies that Zea binding is not sufficient for efficient quenching, either by directly forming a quenching centre with a Chl or inducing a hypothetical rearrangement of the pigment structure in the LHC-II trimer. The importance of obtaining a Zea-LHC-II structure is then put in question. Due to the peripheral position of the Vio binding pocket, it is very unlikely that Zea binding induces substantial changes in the LHC-II structure. None of the Vio epoxy groups is involved in important contacts with other pigments or amino acids in the trimer. As the head groups of Zea make part of its

conjugated  $\pi$ -system, they will necessarily adopt a slightly different geometry as compared to the head groups of Vio. Looking at the structure of LHC-II it seems likely that the spacious Vio binding pocket easily adapts to the more rigid structure of Zea, requiring at most only small rearrangements, either by keeping the head groups in the same position and slightly rotating the conjugated chain or vice-versa.

### 10.2.3 qE is independent from Zea binding to the L2 site

A recent study gave new insights on the Car radical cation quenching mechanism (Ahn et al, 2008). It was suggested that a conformational change brings Zea bound to the L2 site of the minor LHCs closer together to a Chl, so that the created Chl-Zea heterodimer dissipates excitation energy via a charge-transfer state that leads to Zea radical cation formation. Although it has been repeatedly assumed that the L2 site may be occupied by Vio in the minor LHCs (see (Schmid, 2008; Jahns et al, 2009) for reviews), this is both unproven and difficult to prove. L2 is exclusively occupied by Lut in LHC-II, and the high sequence conservation of the Lut binding pockets (Figure 1-4; Figure 10-2) suggests that, on the contrary, *in vivo* both sites are occupied by Lut in all LHCs.

Looking at the structure of the LHC-II monomer (Figure 10-2), it is difficult to envisage how carotenoids in the L1 or L2 binding pockets can be exchanged on a fast timescale, without virtually complete disassembly and reassembly of the whole complex. In order to partition from LHC-II into the lipid phase of the membrane, Lut 1 would have to extract itself from behind the tightly bound chlorin ring of Chl 2, while Lut 2 would have to pass the chlorin rings of both Chl 5 and Chl 10, not to mention the phytol chains of several other Chls. Both replacements would require the breaking of at least 4 hydrogen bonds, which is energetically highly unfavourable in a membrane environment. The binding pockets of Chl 2 and Chl 5 are located in regions of extreme sequence conservation that are also the most tightly packed, rigid part of the LHC-II monomer, and the same Chl / Car arrangement is to be expected in the minor LHCs. When native complexes were used instead to demonstrate Car<sup>•+</sup> formation in the minor LHCs (Avenson et al, 2008b), the Zea enriched samples were purified from the *Arabidopsis* mutant *npq2*, which lacks both Neo and Vio (Section 4.1.4.1; Section 4.2.1.1)(Niyogi et al, 1998); these isolated complexes therefore inevitably had a non-WT pigment composition.

---

For all these reasons, the Car<sup>++</sup> mechanism of qE proposed by Fleming, Bassi and co-workers is far from certain.

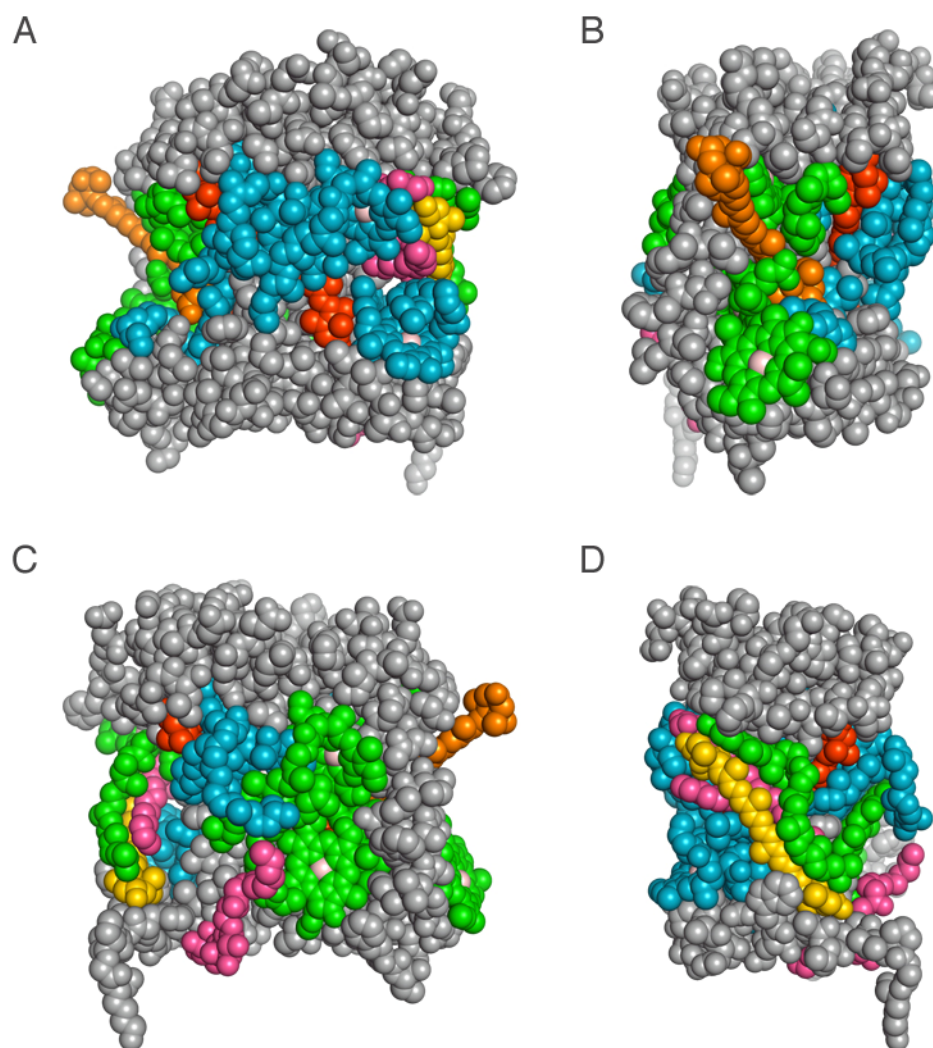


**Figure 10-2 – Accessibility of the lutein binding sites in the LHC-II monomer.**

Accessibility of the L1 and L2 binding sites in the LHC-II monomer shown in four different orientations, rotated by 90° relative to one another. The two luteins (dark orange) are deeply buried in the complex, so that exchange of a carotenoid bound to either site would require disassembly of the complex. Colour coding as in Figure 1-8.

#### 10.2.4 Proposed mechanism of qE

As the simple substitution of Vio by Zea in the complex does not bring about energy dissipation and a conformational switch in the rigid LHC-II is not possible, the controlled interaction of pigment-protein complexes in the membrane appears to be the most probable mechanism for qE. The likely interaction partner with the

LHC-II or the minor LHCs is the PsbS protein, which is required for qE in *Arabidopsis thaliana* (Li et al, 2000), and has been shown to interact with LHC-II and CP29 *in vivo* (Teardo et al, 2007). PsbS is a dimer at neutral pH that dissociates into monomers at low pH, where qE occurs (Bergantino et al, 2003), probably in response to the protonation of lumenally exposed glutamates (Li et al, 2004). Low pH also triggers the conversion of Vio into Zea in the xanthophyll cycle (Yamamoto, 1985). The PsbS protein seems to be stable in the absence of pigments (Funk et al, 1995; Dominici et al, 2002; Bonente et al, 2008), although it has been reported to bind Zea *in vitro* (Aspinall-O'Dea et al, 2002), which has however been challenged (Bonente et al, 2008). Pigment binding by PsbS thus appears to be transient, and may occur only under qE conditions.

Based on these considerations a simple, although speculative, feedback mechanism for qE in thylakoid membranes is proposed, based on the mechanism previously suggested by Szabo et al (Szabo et al, 2005) (Figure 10-3). When the lumenal pH drops as a result of high photosynthetic activity, Vio is converted into Zea, which partitions into the lipid phase of the membrane. At the same time, PsbS monomerizes. Presumably the dimer-to-monomer transition uncovers the Zea binding site on the hydrophobic surface of PsbS. Presumably, Zea binds in a position where, upon interaction with LHC-II or one of the minor LHCs, it is brought into van der Waals contact with a pigment exposed on the hydrophobic, membrane-embedded surface of the complex, most likely Chl 2 (or its equivalent in the minor LHCs), which is thought to be the terminal emitter in the antenna. This specific interaction would form the quenching Zea-Chl heterodimer that has been observed by femtosecond time-resolved spectroscopy of thylakoid membranes and has the very short 0.1 to 1 ps relaxation time expected of an efficient quencher (Holt et al, 2005). At lower light levels, the lumenal pH rises, PsbS dimerizes, the released Zea is converted back into Vio, and the system reverts to normal photosynthetic activity (Figure 10-3). In LHC-II aggregates, the tight interaction of LHC-II trimers with one another or with pigment impurities mimics this NPQ, although it is then significantly slower. Neither quenching process requires a conformational change within LHC-II.

---



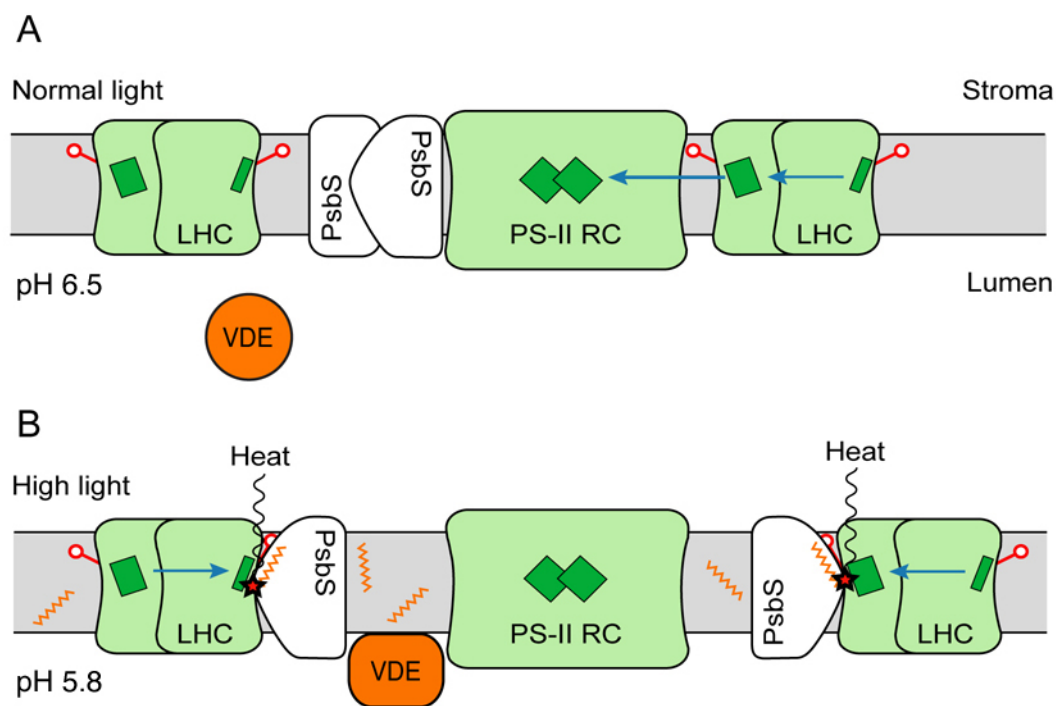


**Figure 10-3 - Proposed model for qE in thylakoids.**

LHCs normally transmit the absorbed excitation energy to the reaction centres of photosystem II (PSI-II RC). Under high-light conditions, Vio is converted into Zea in the xanthophyll cycle. Zea is proposed to bind to PsbS, which monomerizes as the pH in the thylakoid lumen drops (pH values according to (Kramer et al, 1999)). Upon interaction with LHC, a Zea/Chl heterodimer is created which converts excess excitation energy into heat. Green rectangles, representative Chls; orange, Zea; red, flexible part of Neo; blue arrows, radiation-less energy transfer; stars, quenching centres.

### 10.3 Experiment proposal

An experimental system is suggested to verify the proposed model for qE. The basic idea is to produce thylakoid-like liposomes in which all LHCs are reconstituted together with PsbS and VDE is added to the solution in the outside of the liposomes (Figure 10-4). An increase in  $\Delta\text{pH}$ , which is the trigger for qE *in vivo*, could be induced by acidification of the solution, which would promote attachment of VDE to the liposomes, subsequent conversion of Vio in the lipidic phase into Zea and PsbS monomerization. Tuning the pH on the outside of the liposomes would therefore mimic low and high light conditions. The effect of  $\Delta\text{pH}$ , Zea incorporation and interaction with PsbS on the LHCs should be investigated spectroscopically. The lifetime of the Chls excited state, which can be measured by time-resolved fluorescence or transient-absorption spectroscopy, would indicate the extent of quenching. On the other hand, near-infrared transient-absorption kinetics would give insights into the actual quenching mechanism.

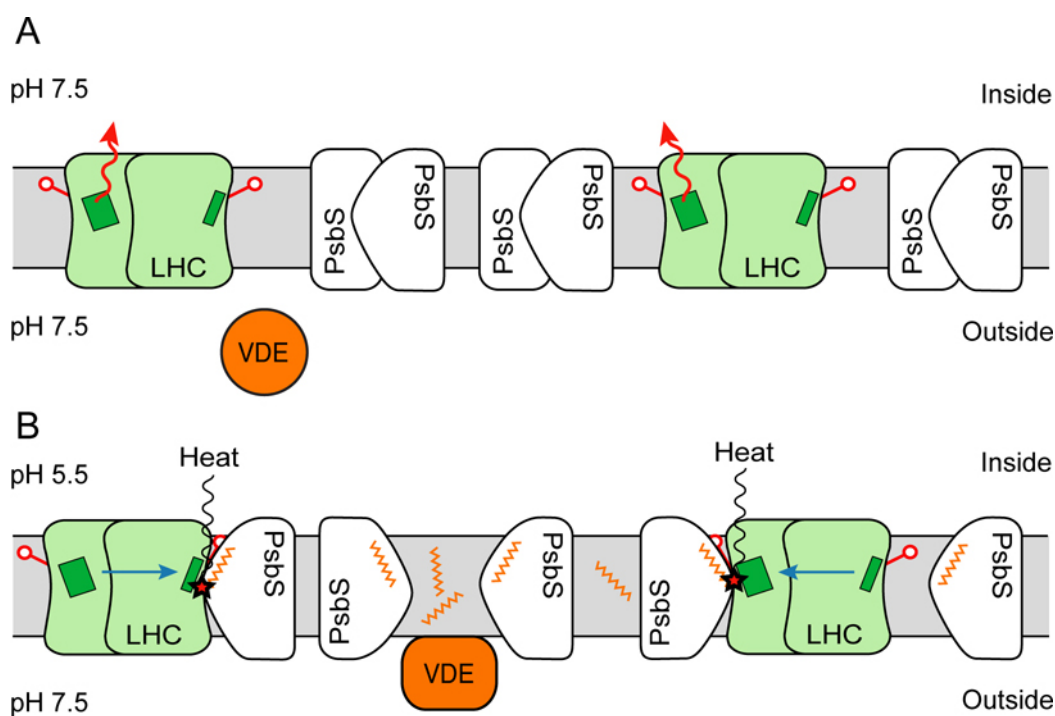


**Figure 10-4 – Proposed experimental system.**

Individual LHCs are reconstituted together with PsbS into thylakoid-like liposomes. VDE is added to the system on the outside of the liposomes. By changing the pH of the buffer, normal and high-light conditions are mimicked.

## 10.4 Concluding remarks and outlook

As this doctoral work comes to an end, the mechanism of qE in higher plants is still unresolved. It is fascinating to realise that despite the enormous body of research devoted to this question, the current models of qE are not only quite diverse but also contradictory to one another. More experiments and especially more advanced biochemistry are needed and many of the open questions will only be answered after determining the PsbS structure and improving the current models of the PS-II supercomplex.

Photosynthesis and NPQ research is traditionally dominated by spectroscopic methods, but it is my strong belief that structural biology will finally solve the qE enigma.

## REFERENCES

- Adamska I (1997) ELIPs - Light-induced stress proteins. *Physiologia Plantarum* **100**(4): 794-805
- Ahn TK, Avenson TJ, Ballottari M, Cheng Y-C, Niyogi KK, Bassi R, Fleming GR (2008) Architecture of a Charge-Transfer State Regulating Light Harvesting in a Plant Antenna Protein. *Science* **320**(5877): 794-797
- Allen JF (1992) Protein phosphorylation in regulation of photosynthesis. *Biochim Biophys Acta* **1098**(3): 275-335
- Allen JF, Bennett J, Steinback KE, Arntzen CJ (1981) Chloroplast protein phosphorylation couples plastoquinone redox state to distribution of excitation energy between photosystems. *Nature* **291**(5810): 25-29
- Allen JF, Forsberg J (2001) Molecular recognition in thylakoid structure and function. *Trends Plant Sci* **6**(7): 317-326
- Amarie S, Standfuss J, Barros T, Kühlbrandt W, Dreuw A, Wachtveitl J (2007) Carotenoid Radical Cations as a Probe for the Molecular Mechanism of Nonphotochemical Quenching in Oxygenic Photosynthesis. *J Phys Chem B* **111**(13): 3481-3487
- Amunts A, Ben-Shem A, Nelson N (2005) Solving the structure of plant photosystem I-biochemistry is vital. *Photochem Photobiol Sci* **4**(12): 1011-1015
- Amunts A, Drory O, Nelson N (2007) The structure of a plant photosystem I supercomplex at 3.4 Å resolution. *Nature* **447**(7140): 58-63
- Andersson J, Wentworth M, Walters RG, Howard CA, Ruban AV, Horton P, Jansson S (2003) Absence of the Lhcb1 and Lhcb2 proteins of the light-harvesting complex of photosystem II - effects on photosynthesis, grana stacking and fitness. *Plant J* **35**(3): 350-361
- Aslanidis C, de Jong PJ (1990) Ligation-independent cloning of PCR products (LIC-PCR). *Nucl Acids Res* **18**(20): 6069-6074
- Aspinall-O'Dea M, Wentworth M, Pascal A, Robert B, Ruban A, Horton P (2002) In vitro reconstitution of the activated zeaxanthin state associated with energy dissipation in plants. *Proc Natl Acad Sci U S A* **99**(25): 16331-16335
- Avenson TJ, Ahn TK, Niyogi KK, Ballottari M, Bassi R, Fleming GR (2008a) Lutein can act as a switchable charge-transfer quencher in the CP26 light-harvesting complex. *J Biol Chem*
- Avenson TJ, Ahn TK, Zigmantas D, Niyogi KK, Li Z, Ballottari M, Bassi R, Fleming GR (2008b) Zeaxanthin Radical Cation Formation in Minor Light-harvesting Complexes of Higher Plant Antenna. *J Biol Chem* **283**(6): 3550-3558
-

- 
- Barber J (1980) Membrane surface charges and potentials in relation to photosynthesis. *Biochim Biophys Acta* **594**(4): 253-308
- Barker A, Manning PA (1997) VlpA of *Vibrio cholerae* O1: the first bacterial member of the alpha 2-microglobulin lipocalin superfamily. *Microbiology* **143** ( Pt 6): 1805-1813
- Barzda V, de Grauw CJ, Vroom J, Kleima FJ, van Grondelle R, van Amerongen H, Gerritsen HC (2001a) Fluorescence lifetime heterogeneity in aggregates of LHCII revealed by time-resolved microscopy. *Biophys J* **81**(1): 538-546
- Barzda V, Gulbinas V, Kananavicius R, Cervinskis V, van Amerongen H, van Grondelle R, Valkunas L (2001b) Singlet-singlet annihilation kinetics in aggregates and trimers of LHCII. *Biophys J* **80**(5): 2409-2421
- Bassham JA, Benson AA, Calvin M (1950) The path of carbon in photosynthesis. *J Biol Chem* **185**(2): 781-787
- Bassi R, Croce R, Cugini D, Sandona D (1999) Mutational analysis of a higher plant antenna protein provides identification of chromophores bound into multiple sites. *Proc Natl Acad Sci U S A* **96**(18): 10056-10061
- Beddard GS, Carlin SE, Porter G (1976) Concentration quenching of chlorophyll fluorescence in bilayer lipid vesicles and liposomes. *Chemical Physics Letters* **43**(1): 27-32
- Beddard GS, Porter G (1976) Concentration quenching in chlorophyll. *Nature* **260**(5549): 366-367
- Bellaïfio S, Barneche F, Peltier G, Rochaix JD (2005) State transitions and light adaptation require chloroplast thylakoid protein kinase STN7. *Nature* **433**(7028): 892-895
- Bennett J (1977) Phosphorylation of chloroplast membrane polypeptides. *Nature* **269**(5626): 344-346
- Bennett J (1979) Chloroplast phosphoproteins. The protein kinase of thylakoid membranes is light-dependent. *FEBS Lett* **103**(2): 342-344
- Bennett J, Steinback KE, Arntzen CJ (1980) Chloroplast phosphoproteins: regulation of excitation energy transfer by phosphorylation of thylakoid membrane polypeptides. *Proc Natl Acad Sci U S A* **77**(9): 5253-5257
- Bergantino E, Segalla A, Brunetta A, Teardo E, Rigoni F, Giacometti GM, Szabo I (2003) Light- and pH-dependent structural changes in the PsbS subunit of photosystem II. *Proc Natl Acad Sci U S A* **100**(25): 15265-15270
- Berglund GI, Carlsson GH, Smith AT, Szoke H, Henriksen A, Hajdu J (2002) The catalytic pathway of horseradish peroxidase at high resolution. *Nature* **417**(6887): 463-468

## References

---

- Bode S, Quentmeier CC, Liao P-N, Barros T, Walla PJ (2008) Xanthophyll-cycle dependence of the energy transfer between carotenoid dark states and chlorophylls in NPQ mutants of living plants and in LHC II. *Chemical Physics Letters* **450**(4-6): 379-385
- Boekema EJ, Hankamer B, Bald D, Kruij J, Nield J, Boonstra AF, Barber J, Rogner M (1995) Supramolecular structure of the photosystem II complex from green plants and cyanobacteria. *Proc Natl Acad Sci U S A* **92**(1): 175-179
- Boekema EJ, van Roon H, Calkoen F, Bassi R, Dekker JP (1999) Multiple types of association of photosystem II and its light-harvesting antenna in partially solubilized photosystem II membranes. *Biochemistry* **38**(8): 2233-2239
- Bonente G, Howes BD, Caffarri S, Smulevich G, Bassi R (2008) Interactions between the Photosystem II Subunit PsbS and Xanthophylls Studied in Vivo and in Vitro. *J Biol Chem* **283**(13): 8434-8445
- Booth PJ, Paulsen H (1996) Assembly of light-harvesting chlorophyll a/b complex in vitro. Time-resolved fluorescence measurements. *Biochemistry* **35**(16): 5103-5108
- Bourgeois D, Royant A (2005) Advances in kinetic protein crystallography. *Curr Opin Struct Biol* **15**(5): 538-547
- Bradford MM (1976) A rapid and sensitive method for the quantitation of microgram quantities of protein utilizing the principle of protein-dye binding. *Analytical Biochemistry* **72**(1-2): 248-254
- Bricker T (1990) The structure and function of CPa-1 and CPa-2 in Photosystem II. *Photosynthesis Research* **24**(1): 1-13
- Brogliè R, Bellemare G, Bartlett SG, Chua NH, Cashmore AR (1981) Cloned DNA sequences complementary to mRNAs encoding precursors to the small subunit of ribulose-1,5-bisphosphate carboxylase and a chlorophyll a/b binding polypeptide. *Proc Natl Acad Sci U S A* **78**(12): 7304-7308
- Brunisholz RA, Zuber H (1992) Structure, function and organization of antenna polypeptides and antenna complexes from the three families of Rhodospirillaceae. *J Photochem Photobiol B* **15**(1-2): 113-140
- Bugos RC, Yamamoto HY (1996) Molecular cloning of violaxanthin de-epoxidase from romaine lettuce and expression in *Escherichia coli*. *Proc Natl Acad Sci U S A* **93**(13): 6320-6325
- Burke JJ, Ditto CL, Arntzen CJ (1978) Involvement of the light-harvesting complex in cation regulation of excitation energy distribution in chloroplasts. *Archives of Biochemistry and Biophysics* **187**(1): 252-263
- Buschmann C (2007) Variability and application of the chlorophyll fluorescence emission ratio red/far-red of leaves. *Photosynthesis Research* **92**(2): 261-271
-

- 
- Butler PJ, Kühlbrandt W (1988) Determination of the aggregate size in detergent solution of the light-harvesting chlorophyll a/b-protein complex from chloroplast membranes. *Proc Natl Acad Sci U S A* **85**(11): 3797-3801
- Camm EL, Green BR (2004) How the Chlorophyll-Proteins got their Names. *Photosynth Res* **80**(1-3): 189-196
- Castelletti S, Morosinotto T, Robert B, Caffarri S, Bassi R, Croce R (2003) Recombinant Lhca2 and Lhca3 subunits of the photosystem I antenna system. *Biochemistry* **42**(14): 4226-4234
- Cherezov V, Clogston J, Papiz MZ, Caffrey M (2006) Room to move: crystallizing membrane proteins in swollen lipidic mesophases. *J Mol Biol* **357**(5): 1605-1618
- Cline K (1986) Import of proteins into chloroplasts. Membrane integration of a thylakoid precursor protein reconstituted in chloroplast lysates. *J Biol Chem* **261**(31): 14804-14810
- Cogdell RJ, Gall A, Kohler J (2006) The architecture and function of the light-harvesting apparatus of purple bacteria: from single molecules to in vivo membranes. *Q Rev Biophys* **39**(3): 227-324
- Collaborative (1994) The CCP4 suite: programs for protein crystallography. *Acta Crystallographica Section D* **50**(5): 760-763
- Corbet D, Schweikardt T, Paulsen H, Schmid VH (2007) Amino acids in the second transmembrane helix of the Lhca4 subunit are important for formation of stable heterodimeric light-harvesting complex LHCI-730. *J Mol Biol* **370**(1): 170-182
- Coruzzi G, Broglie R, Cashmore A, Chua NH (1983) Nucleotide sequences of two pea cDNA clones encoding the small subunit of ribulose 1,5-bisphosphate carboxylase and the major chlorophyll a/b-binding thylakoid polypeptide. *J Biol Chem* **258**(3): 1399-1402
- Crimi M, Dorra D, Bosinger CS, Giuffra E, Holzwarth AR, Bassi R (2001) Time-resolved fluorescence analysis of the recombinant photosystem II antenna complex CP29. Effects of zeaxanthin, pH and phosphorylation. *Eur J Biochem* **268**(2): 260-267
- Croce R, Canino G, Ros F, Bassi R (2002) Chromophore organization in the higher-plant photosystem II antenna protein CP26. *Biochemistry* **41**(23): 7334-7343
- Croce R, Morosinotto T, Ihalainen JA, Chojnicka A, Breton J, Dekker JP, van Grondelle R, Bassi R (2004) Origin of the 701-nm fluorescence emission of the Lhca2 subunit of higher plant photosystem I. *J Biol Chem* **279**(47): 48543-48549
- Crouchman S, Ruban A, Horton P (2006) PsbS enhances nonphotochemical fluorescence quenching in the absence of zeaxanthin. *FEBS Lett* **580**(8): 2053-2058

## References

---

- Dall'Osto L, Caffarri S, Bassi R (2005) A mechanism of nonphotochemical energy dissipation, independent from PsbS, revealed by a conformational change in the antenna protein CP26. *Plant Cell* **17**(4): 1217-1232
- Dall'Osto L, Cazzaniga S, North H, Marion-Poll A, Bassi R (2007) The Arabidopsis aba4-1 mutant reveals a specific function for neoxanthin in protection against photooxidative stress. *Plant Cell* **19**(3): 1048-1064
- Das D, Krishna SS, McMullan D, Miller MD, Xu Q, Abdubek P, Acosta C, Astakhova T, Axelrod HL, Burra P, Carlton D, Hsiu-Ju Chiu, Thomas Clayton, Deller MC, Duan L, Elias Y, Elsliger M-A, Ernst D, Feuerhelm J, Grzechnik A, Grzechnik SK, Hale J, Han GW, Jaroszewski L, Jin KK, Klock HE, Knuth MW, Kozbial P, Kumar A, Marciano D, Morse AT, Murphy KD, Nigoghossian E, Okach L, Oommachen S, Paulsen J, Reyes R, Rife CL, Sefcovic N, Tien H, Trame CB, Trout CV, Bedem Hvd, Weekes D, White A, Hodgson KO, Wooley J, Deacon AM, Godzik A, Lesley SA, Wilson IA (2009) Crystal structure of the Fic (Filamentation induced by cAMP) family protein SO4266 (gi|24375750) from *Shewanella oneidensis* MR-1 at 1.6  $\approx$  resolution. *Proteins: Structure, Function, and Bioinformatics* **75**(1): 264-271
- Day DA, Ryrie IJ, Fuad N (1984) Investigations of the role of the main light-harvesting chlorophyll-protein complex in thylakoid membranes. Reconstitution of depleted membranes from intermittent-light-grown plants with the isolated complex. *J Cell Biol* **98**(1): 163-172
- De la Mora-Rey T, Wilmot CM (2007) Synergy within structural biology of single crystal optical spectroscopy and X-ray crystallography. *Current Opinion in Structural Biology* **17**(5): 580-586
- Dekker JP, Boekema EJ (2005) Supramolecular organization of thylakoid membrane proteins in green plants. *Biochim Biophys Acta* **1706**(1-2): 12-39
- Dekker JP, van Roon H, Boekema EJ (1999) Heptameric association of light-harvesting complex II trimers in partially solubilized photosystem II membranes. *FEBS Lett* **449**(2-3): 211-214
- Demmig B, Winter K, Kruger A, Czygan FC (1987) Photoinhibition and Zeaxanthin Formation in Intact Leaves : A Possible Role of the Xanthophyll Cycle in the Dissipation of Excess Light Energy. *Plant Physiol* **84**(2): 218-224
- Derewenda ZS (2004) Rational protein crystallization by mutational surface engineering. *Structure* **12**(4): 529-535
- Derewenda ZS, Vekilov PG (2006) Entropy and surface engineering in protein crystallization. *Acta Crystallogr D Biol Crystallogr* **62**(Pt 1): 116-124
- Diretto G, Tavazza R, Welsch R, Pizzichini D, Mourgues F, Papacchioli V, Beyer P, Giuliano G (2006) Metabolic engineering of potato tuber carotenoids through tuber-specific silencing of lycopene epsilon cyclase. *BMC Plant Biol* **6**: 13
- Dominici P, Caffarri S, Armenante F, Ceoldo S, Crimi M, Bassi R (2002) Biochemical properties of the PsbS subunit of photosystem II either purified from chloroplast or recombinant. *J Biol Chem* **277**(25): 22750-22758
-



- 
- Dreuw A, Fleming GR, Head-Gordon M (2003) Chlorophyll fluorescence quenching by xanthophylls. *Physical Chemistry Chemical Physics* **5**(15): 3247-3256
- Dreuw A, Fleming GR, Head-Gordon M (2005) Role of electron-transfer quenching of chlorophyll fluorescence by carotenoids in non-photochemical quenching of green plants. *Biochem Soc Trans* **33**(Pt 4): 858-862
- Dreuw A, Wormit M (2008) Simple replacement of violaxanthin by zeaxanthin in LHC-II does not cause chlorophyll fluorescence quenching. *Journal of Inorganic Biochemistry* **102**(3): 458-465
- Duckham SC, Linforth RST, Taylor IB (1991) Abscisic-acid-deficient mutants at the *aba* gene locus of *Arabidopsis thaliana* are impaired in the epoxidation of zeaxanthin. *Plant, Cell and Environment* **14**(6): 601-606
- Edgar RC (2004) MUSCLE: multiple sequence alignment with high accuracy and high throughput. *Nucl Acids Res* **32**(5): 1792-1797
- Edman K, Nollert P, Royant A, Belrhali H, Pebay-Peyroula E, Hajdu J, Neutze R, Landau EM (1999) High-resolution X-ray structure of an early intermediate in the bacteriorhodopsin photocycle. *Nature* **401**(6755): 822-826
- Emsley P, Cowtan K (2004) Coot: model-building tools for molecular graphics. *Acta Crystallographica Section D* **60**(12 Part 1): 2126-2132
- Faham S, Watanabe A, Besserer GM, Cascio D, Specht A, Hirayama BA, Wright EM, Abramson J (2008) The crystal structure of a sodium galactose transporter reveals mechanistic insights into Na<sup>+</sup>/sugar symport. *Science* **321**(5890): 810-814
- Fenna RE, Matthews BW (1975) Chlorophyll arrangement in a bacteriochlorophyll protein from *Chlorobium limicola*. *Nature* **258**(5536): 573-577
- Ferreira KN, Iverson TM, Maghlaoui K, Barber J, Iwata S (2004) Architecture of the photosynthetic oxygen-evolving center. *Science* **303**(5665): 1831-1838
- Fling SP, Gregerson DS (1986) Peptide and protein molecular weight determination by electrophoresis using a high-molarity tris buffer system without urea. *Analytical Biochemistry* **155**(1): 83-88
- Flower DR (1996) The lipocalin protein family: structure and function. *Biochem J* **318** ( Pt 1): 1-14
- Frank HA, Cua A, Chynwat V, Young A, Gosztola D, Wasielewski MR (1994) Photophysics of the Carotenoids Associated with the Xanthophyll Cycle in Photosynthesis. *Photosynthesis Research* **41**(3): 389-395

## References

---

- Funk C, Adamska I, Green BR, Andersson B, Renger G (1995) The nuclear-encoded chlorophyll-binding photosystem II-S protein is stable in the absence of pigments. *J Biol Chem* **270**(50): 30141-30147
- Gilmore AM, Hazlett TL, Govindjee (1995) Xanthophyll Cycle-Dependent Quenching of Photosystem II Chlorophyll a Fluorescence: Formation of a Quenching Complex with a Short Fluorescence Lifetime. *Proceedings of the National Academy of Sciences* **92**(6): 2273-2277
- Gilmore AM, Yamamoto HY (1991) Resolution of lutein and zeaxanthin using a non-encapped, lightly carbon-loaded C18 high-performance liquid chromatographic column. *Journal of Chromatography A* **543**: 137-145
- Gilmore AM, Yamamoto HY (1992) Dark Induction of Zeaxanthin-Dependent Nonphotochemical Fluorescence Quenching Mediated by ATP. *Proceedings of the National Academy of Sciences* **89**(5): 1899-1903
- Giuffra E, Cugini D, Croce R, Bassi R (1996) Reconstitution and pigment-binding properties of recombinant CP29. *Eur J Biochem* **238**(1): 112-120
- Green BR, Kühlbrandt W (1995) Sequence conservation of light-harvesting and stress-response proteins in relation to the three-dimensional molecular structure of LHCII. *Photosynthesis Research* **44**(1): 139-148
- Green RR, Pichersky E (1994) Hypothesis for the evolution of three-helix Chl a/b and Chl a/c light-harvesting antenna proteins from two-helix and four-helix ancestors. *Photosynthesis Research* **39**(2): 149-162
- Greene LH, Chrysina ED, Irons LI, Papageorgiou AC, Acharya KR, Brew K (2001) Role of conserved residues in structure and stability: tryptophans of human serum retinol-binding protein, a model for the lipocalin superfamily. *Protein Sci* **10**(11): 2301-2316
- Grigorieff N, Ceska TA, Downing KH, Baldwin JM, Henderson R (1996) Electron-crystallographic refinement of the structure of bacteriorhodopsin. *J Mol Biol* **259**(3): 393-421
- Grotz B, Molnar P, Stransky H, Hager A (1999) Substrate specificity and functional aspects of violaxanthin-de-epoxidase, an enzyme of the xanthophyll cycle. *J Plant Physiol* **154**(4): 437-446
- Haehnel W, Nairn JA, Reisberg P, Sauer K (1982) Picosecond Fluorescence Kinetics and Energy-Transfer in Chloroplasts and Algae. *Biochimica Et Biophysica Acta* **680**(2): 161-173
- Hajdu J, Neutze R, Sjogren T, Edman K, Szoke A, Wilmouth RC, Wilmot CM (2000) Analyzing protein functions in four dimensions. *Nat Struct Biol* **7**(11): 1006-1012
- Hanahan D (1983) Studies on transformation of *Escherichia coli* with plasmids. *Journal of Molecular Biology* **166**(4): 557-580
-

- Haripal PK, Raval HK, Raval MK, Rawal RM, Biswal B, Biswal UC (2006) Three-dimensional model of zeaxanthin binding PsbS protein associated with nonphotochemical quenching of excess quanta of light energy absorbed by the photosynthetic apparatus. *J Mol Model* **12**(6): 847-853
- Haun RS, Serventi IM, Moss J (1992) Rapid, Reliable Ligation-Independent Cloning of Pcr Products Using Modified Plasmid Vectors. *Biotechniques* **13**(4): 515-518
- Henderson R, Baldwin JM, Downing KH, Lepault J, Zemlin F (1986) Structure of purple membrane from halobacterium halobium: recording, measurement and evaluation of electron micrographs at 3.5 Å resolution. *Ultramicroscopy* **19**(2): 147-178
- Henrysson T, Schroder WP, Spangfort M, Akerlund HE (1989) Isolation and Characterization of the Chlorophyll-a/B Protein Complex Cp29 from Spinach. *Biochimica Et Biophysica Acta* **977**(3): 301-308
- Hieber D, Bugos R, Verhoeven A, Yamamoto H (2002) Overexpression of violaxanthin de-epoxidase: properties of C-terminal deletions on activity and pH-dependent lipid binding. *Planta* **214**(3): 476-483
- Himmelbach A, Yang Y, Grill E (2003) Relay and control of abscisic acid signaling. *Curr Opin Plant Biol* **6**(5): 470-479
- Hobe S, Forster R, Klingler J, Paulsen H (1995) N-proximal sequence motif in light-harvesting chlorophyll a/b-binding protein is essential for the trimerization of light-harvesting chlorophyll a/b complex. *Biochemistry* **34**(32): 10224-10228
- Hobe S, Prytulla S, Kühlbrandt W, Paulsen H (1994) Trimerization and crystallization of reconstituted light-harvesting chlorophyll a/b complex. *Embo J* **13**(15): 3423-3429
- Hoffman NE, Pichersky E, Malik VS, Castresana C, Ko K, Darr SC, Cashmore AR (1987) A cDNA clone encoding a photosystem I protein with homology to photosystem II chlorophyll a/b-binding polypeptides. *Proceedings of the National Academy of Sciences of the United States of America* **84**(24): 8844-8848
- Holt NE, Zigmantas D, Valkunas L, Li XP, Niyogi KK, Fleming GR (2005) Carotenoid cation formation and the regulation of photosynthetic light harvesting. *Science* **307**(5708): 433-436
- Horn R, Grundmann G, Paulsen H (2007) Consecutive binding of chlorophylls a and b during the assembly in vitro of light-harvesting chlorophyll-a/b protein (LHCIIb). *J Mol Biol* **366**(3): 1045-1054
- Horton P, Ruban AV, Rees D, Pascal AA, Noctor G, Young AJ (1991) Control of the light-harvesting function of chloroplast membranes by aggregation of the LHCII chlorophyll-protein complex. *FEBS Lett* **292**(1-2): 1-4
- Horton P, Ruban AV, Wentworth M (2000) Allosteric regulation of the light-harvesting system of photosystem II. *Philos Trans R Soc Lond B Biol Sci* **355**(1402): 1361-1370

## References

---

- Horton P, Wentworth M, Ruban A (2005) Control of the light harvesting function of chloroplast membranes: the LHCII-aggregation model for non-photochemical quenching. *FEBS Lett* **579**(20): 4201-4206
- Ide JP, Klug DR, Kühlbrandt W, Giorgi LB, Porter G (1987) The State of Detergent Solubilized Light-Harvesting Chlorophyll-a/B Protein Complex as Monitored by Picosecond Time-Resolved Fluorescence and Circular-Dichroism. *Biochimica Et Biophysica Acta* **893**(2): 349-364
- Ihalainen JA, D'Haene S, Yeremenko N, van Roon H, Arteni AA, Boekema EJ, van Grondelle R, Matthijs HC, Dekker JP (2005) Aggregates of the chlorophyll-binding protein IsiA (CP43') dissipate energy in cyanobacteria. *Biochemistry* **44**(32): 10846-10853
- Ilioaia C, Johnson MP, Horton P, Ruban AV (2008) Induction of efficient energy dissipation in the isolated light-harvesting complex of Photosystem II in the absence of protein aggregation. *J Biol Chem* **283**(43): 29505-29512
- Jabłoński A (1935) Über den Mechanismus der Photolumineszenz von Farbstoffphosphoren. *Zeitschrift für Physik A Hadrons and Nuclei* **94**(1): 38-46
- Jahns P, Latowski D, Strzalka K (2009) Mechanism and regulation of the violaxanthin cycle: The role of antenna proteins and membrane lipids. *Biochim Biophys Acta* **1787**(1): 3-14
- Jansson S (1994) The light-harvesting chlorophyll a/b-binding proteins. *Biochimica et Biophysica Acta (BBA) - Bioenergetics* **1184**(1): 1-19
- Jansson S (1999) A guide to the Lhc genes and their relatives in *Arabidopsis*. *Trends Plant Sci* **4**(6): 236-240
- Jansson S, Pichersky E, Bassi R, Green B, Ikeuchi M, Melis A, Simpson D, Spangfort M, Staehelin L, Thornber J (1992) A nomenclature for the genes encoding the chlorophyll a/b-binding proteins of higher plants. *Plant Molecular Biology Reporter* **10**(3): 242-253
- Jansson S, Stefansson H, Nyström U, Gustafsson P, Albertsson P-Å (1997) Antenna protein composition of PS I and PS II in thylakoid sub-domains. *Biochimica et Biophysica Acta (BBA) - Bioenergetics* **1320**(3): 297-309
- Kabsch W (1993) Automatic Processing of Rotation Diffraction Data from Crystals of Initially Unknown Symmetry and Cell Constants. *J Appl Crystallogr* **26**: 795-800
- Katona G, Carpentier P, Niviere V, Amara P, Adam V, Ohana J, Tsanov N, Bourgeois D (2007) Raman-assisted crystallography reveals end-on peroxide intermediates in a nonheme iron enzyme. *Science* **316**(5823): 449-453
- Kim S, Sandusky P, Bowlby NR, Aebersold R, Green BR, Vlahakis S, Yocum CF, Pichersky E (1992) Characterization of a spinach psbS cDNA encoding the 22 kDa protein of photosystem II. *FEBS Lett* **314**(1): 67-71
-

- 
- Kirchhoff H, Hinz HJ, Rosgen J (2003) Aggregation and fluorescence quenching of chlorophyll a of the light-harvesting complex II from spinach in vitro. *Biochim Biophys Acta* **1606**(1-3): 105-116
- Koornneef M, Jorna ML, Brinkhorst-van der Swan DLC, Karszen CM (1982) The isolation of abscisic acid (ABA) deficient mutants by selection of induced revertants in non-germinating gibberellin sensitive lines of *Arabidopsis thaliana* (L.) Heynh. *TAG Theoretical and Applied Genetics* **61**(4): 385-393
- Kramer DM, Sacksteder CA, Cruz JA (1999) How acidic is the lumen? *Photosynthesis Research* **60**(2-3): 151-163
- Krissinel E, Henrick K (2004) Secondary-structure matching (SSM), a new tool for fast protein structure alignment in three dimensions. *Acta Crystallogr Sect D-Biol Crystallogr* **60**: 2256-2268
- Kühlbrandt W (1984) Three-dimensional structure of the light-harvesting chlorophyll a/b-protein complex. *Nature* **307**(5950): 478-480
- Kühlbrandt W (1987) Three-dimensional crystals of the light-harvesting chlorophyll a/b protein complex from pea chloroplasts. *J Mol Biol* **194**(4): 757-762
- Kühlbrandt W, Becker A, Mäntele W (1988) Chlorophyll dichroism of three-dimensional crystals of the light-harvesting chlorophyll a/b-protein complex. *FEBS Letters* **226**(2): 275-279
- Kühlbrandt W, Thaler T, Wehrli E (1983) The structure of membrane crystals of the light-harvesting chlorophyll a/b protein complex. *J Cell Biol* **96**(5): 1414-1424
- Kühlbrandt W, Wang DN (1991) Three-dimensional structure of plant light-harvesting complex determined by electron crystallography. *Nature* **350**(6314): 130-134
- Kühlbrandt W, Wang DN, Fujiyoshi Y (1994) Atomic model of plant light-harvesting complex by electron crystallography. *Nature* **367**(6464): 614-621
- Külheim C, Ågren J, Jansson S (2002) Rapid regulation of light harvesting and plant fitness in the field. *Science* **297**: 91-93
- Kung SD, Thornber JP, Wildman SG (1972) Nuclear DNA codes for the photosystem II chlorophyll-protein of chloroplast membranes. *FEBS Lett* **24**(2): 185-188
- Kuttkat A, Hartmann A, Hobe S, Paulsen H (1996) The C-terminal domain of light-harvesting chlorophyll-a/b-binding protein is involved in the stabilisation of trimeric light-harvesting complex. *Eur J Biochem* **242**(2): 288-292
- La Roche J, van der Staay GW, Partensky F, Ducret A, Aebersold R, Li R, Golden SS, Hiller RG, Wrench PM, Larkum AW, Green BR (1996) Independent evolution of the prochlorophyte and green plant chlorophyll a/b light-harvesting proteins. *Proc Natl Acad Sci U S A* **93**(26): 15244-15248

## References

---

- Laemmli UK (1970) Cleavage of Structural Proteins during the Assembly of the Head of Bacteriophage T4. *Nature* **227**(5259): 680-685
- Lakowicz JR (2006) *Principles of Fluorescence Spectroscopy*, 3 edn. New York: Springer.
- Lambrev PH, Varkonyi Z, Krumova S, Kovacs L, Miloslavina Y, Holzwarth AR, Garab G (2007) Importance of trimer-trimer interactions for the native state of the plant light-harvesting complex II. *Biochimica et Biophysica Acta (BBA) - Bioenergetics* **1767**(6): 847-853
- Leslie AGW (1992) Recent changes to the MOSFLM package for processing film and image plate data. In *Joint CCP4 + ESF-EAMCB Newsletter on Protein Crystallography* Vol. 26.
- Li X-P, Phippard A, Pasari J, Niyogi KK (2002) Structure-function analysis of photosystem II subunit S (PsbS) *in vivo*. *Functional Plant Biology* **29**(10): 1131-1139
- Li XP, Bjorkman O, Shih C, Grossman AR, Rosenquist M, Jansson S, Niyogi KK (2000) A pigment-binding protein essential for regulation of photosynthetic light harvesting. *Nature* **403**(6768): 391-395
- Li XP, Gilmore AM, Caffarri S, Bassi R, Golan T, Kramer D, Niyogi KK (2004) Regulation of photosynthetic light harvesting involves intrathylakoid lumen pH sensing by the PsbS protein. *J Biol Chem* **279**(22): 22866-22874
- Lichtenthaler HK (1987) Chlorophylls and Carotenoids - Pigments of Photosynthetic Biomembranes. *Method Enzymol* **148**: 350-382
- Liu Z, Yan H, Wang K, Kuang T, Zhang J, Gui L, An X, Chang W (2004) Crystal structure of spinach major light-harvesting complex at 2.72 Å resolution. *Nature* **428**(6980): 287-292
- Lokstein H, Tian L, Polle JrEW, DellaPenna D (2002) Xanthophyll biosynthetic mutants of *Arabidopsis thaliana*: altered nonphotochemical quenching of chlorophyll fluorescence is due to changes in Photosystem II antenna size and stability. *Biochimica et Biophysica Acta (BBA) - Bioenergetics* **1553**(3): 309-319
- Loll B, Kern J, Saenger W, Zouni A, Biesiadka J (2005) Towards complete cofactor arrangement in the 3.0 Å resolution structure of photosystem II. *Nature* **438**(7070): 1040-1044
- Louis J, Cerovic ZG, Moya I (2006) Quantitative study of fluorescence excitation and emission spectra of bean leaves. *Journal of Photochemistry and Photobiology B: Biology* **85**(1): 65-71
- Lyon MK, Miller KR (1985) Crystallization of the light-harvesting chlorophyll a/b complex within thylakoid membranes. *J Cell Biol* **100**(4): 1139-1147
- McDermott G, Prince SM, Freer AA, Hawthornthwaite-Lawless AM, Papiz MZ, Cogdell RJ, Isaacs NW (1995) Crystal structure of an integral membrane light-harvesting complex from photosynthetic bacteria. *Nature* **374**(6522): 517-521
-

- 
- McDonnell A, Staehelin LA (1980) Adhesion between liposomes mediated by the chlorophyll a/b light-harvesting complex isolated from chloroplast membranes. *J Cell Biol* **84**(1): 40-56
- Meyer G, Kloppstech K (1984) A rapidly light-induced chloroplast protein with a high turnover coded for by pea nuclear DNA. *Eur J Biochem* **138**(1): 201-207
- Michel H (1983) Crystallization of membrane proteins. *Trends in Biochemical Sciences* **8**(2): 56-59
- Moise N, Moya I (2004) Correlation between lifetime heterogeneity and kinetics heterogeneity during chlorophyll fluorescence induction in leaves: 2. Multi-frequency phase and modulation analysis evidences a loosely connected PSII pigment-protein complex. *Biochim Biophys Acta* **1657**(1): 47-60
- Morosinotto T, Baronio R, Bassi R (2002a) Dynamics of chromophore binding to Lhc proteins in vivo and in vitro during operation of the xanthophyll cycle. *J Biol Chem* **277**(40): 36913-36920
- Morosinotto T, Castelletti S, Breton J, Bassi R, Croce R (2002b) Mutation analysis of Lhca1 antenna complex. Low energy absorption forms originate from pigment-pigment interactions. *J Biol Chem* **277**(39): 36253-36261
- Moukhametzianov R, Klare JP, Efremov R, Baeken C, Goppner A, Labahn J, Engelhard M, Buldt G, Gordeliy VI (2006) Development of the signal in sensory rhodopsin and its transfer to the cognate transducer. *Nature* **440**(7080): 115-119
- Moya I, Silvestri M, Vallon O, Cinque G, Bassi R (2001) Time-resolved fluorescence analysis of the photosystem II antenna proteins in detergent micelles and liposomes. *Biochemistry* **40**(42): 12552-12561
- Mozzo M, Morosinotto T, Bassi R, Croce R (2006) Probing the structure of Lhca3 by mutation analysis. *Biochim Biophys Acta* **1757**(12): 1607-1613
- Müller P, Li X-P, Niyogi KK (2001) Non-Photochemical Quenching. A Response to Excess Light Energy. *Plant Physiol* **125**(4): 1558-1566
- Mullet JE (1983) The amino acid sequence of the polypeptide segment which regulates membrane adhesion (grana stacking) in chloroplasts. *J Biol Chem* **258**(16): 9941-9948
- Mullet JE, Arntzen CJ (1980) Simulation of grana stacking in a model membrane system. Mediation by a purified light-harvesting pigment-protein complex from chloroplasts. *Biochim Biophys Acta* **589**(1): 100-117
- Mullineaux CW, Pascal AA, Horton P, Holzwarth AR (1993) Excitation-energy quenching in aggregates of the LHC II chlorophyll-protein complex: a time-resolved fluorescence study. *Biochimica et Biophysica Acta (BBA) - Bioenergetics* **1141**(1): 23-28

## References

---

- Mullis K, Faloona F, Scharf S, Saiki R, Horn G, Erlich H (1986) Specific Enzymatic Amplification of DNA In vitro - the Polymerase Chain-Reaction. *Cold Spring Harbor Symp Quant Biol* **51**: 263-273
- Murata K, Mitsuoka K, Hirai T, Walz T, Agre P, Heymann JB, Engel A, Fujiyoshi Y (2000) Structural determinants of water permeation through aquaporin-1. *Nature* **407**(6804): 599-605
- Murray JW, Duncan J, Barber J (2006) CP43-like chlorophyll binding proteins: structural and evolutionary implications. *Trends Plant Sci* **11**(3): 152-158
- Nambara E, Marion-Poll A (2005) Abscisic acid biosynthesis and catabolism. *Annual Review of Plant Biology* **56**(1): 165-185
- Nelson N, Ben-Shem A (2004) The complex architecture of oxygenic photosynthesis. *Nat Rev Mol Cell Biol* **5**(12): 971-982
- Nesterenko MV, Tilley M, Upton SJ (1994) A simple modification of Blum's silver stain method allows for 30 minute detection of proteins in polyacrylamide gels. *Journal of Biochemical and Biophysical Methods* **28**(3): 239-242
- Niyogi KK, Grossman AR, Bjorkman O (1998) Arabidopsis mutants define a central role for the xanthophyll cycle in the regulation of photosynthetic energy conversion. *Plant Cell* **10**(7): 1121-1134
- Novoderezhkin VI, Palacios MA, van Amerongen H, van Grondelle R (2005) Excitation Dynamics in the LHCII Complex of Higher Plants: Modeling Based on the 2.72 Å Crystal Structure. *J Phys Chem B Condens Matter Mater Surf Interfaces Biophys* **109**(20): 10493-10504
- Nussberger S, Dorr K, Wang DN, Kuhlbrandt W (1993) Lipid-protein interactions in crystals of plant light-harvesting complex. *J Mol Biol* **234**(2): 347-356
- Ogawa T, Obata F, Shibata K (1966) Two pigment proteins in spinach chloroplasts. *Biochim Biophys Acta* **112**(2): 223-234
- Pagano A, Cinque G, Bassi R (1998) In vitro reconstitution of the recombinant photosystem II light-harvesting complex CP24 and its spectroscopic characterization. *J Biol Chem* **273**(27): 17154-17165
- Palacios MA, de Weerd FL, Ihalainen JA, van Grondelle R, van Amerongen H (2002) Superradiance and Exciton (De)localization in Light-Harvesting Complex II from Green Plants? *J Phys Chem B* **106**(22): 5782-5787
- Palacios MA, Standfuss J, Vengris M, van Oort BF, van Stokkum IH, Kuhlbrandt W, van Amerongen H, van Grondelle R (2006) A comparison of the three isoforms of the light-harvesting complex II using transient absorption and time-resolved fluorescence measurements. *Photosynth Res*
- Pascal AA, Liu Z, Broess K, van Oort B, van Amerongen H, Wang C, Horton P, Robert B, Chang W, Ruban A (2005) Molecular basis of photoprotection and control of photosynthetic light-harvesting. *Nature* **436**(7047): 134-137
-



- 
- Paulsen H, Finkenzeller B, Kuhlein N (1993) Pigments induce folding of light-harvesting chlorophyll a/b-binding protein. *Eur J Biochem* **215**(3): 809-816
- Paulsen H, Rümmler U, Rüdiger W (1990) Reconstitution of pigment-containing complexes from light-harvesting chlorophyll a/b-binding protein overexpressed in *Escherichia coli*. *Planta* **181**(2): 204-211
- Perez-Bueno ML, Johnson MP, Zia A, Ruban AV, Horton P (2008) The Lhcb protein and xanthophyll composition of the light harvesting antenna controls the DeltapH-dependency of non-photochemical quenching in *Arabidopsis thaliana*. *FEBS Lett* **582**(10): 1477-1482
- Perozzo MA, Ward KB, Thompson RB, Ward WW (1988) X-ray diffraction and time-resolved fluorescence analyses of *Aequorea* green fluorescent protein crystals. *J Biol Chem* **263**(16): 7713-7716
- Peter GF, Thornber JP (1991) Biochemical composition and organization of higher plant photosystem II light-harvesting pigment-proteins. *J Biol Chem* **266**(25): 16745-16754
- Plumley FG, Schmidt GW (1987) Reconstitution of chlorophyll a/b light-harvesting complexes: Xanthophyll-dependent assembly and energy transfer. *Proc Natl Acad Sci U S A* **84**(1): 146-150
- Pogson BJ, Niyogi KK, Bjorkman O, DellaPenna D (1998) Altered xanthophyll compositions adversely affect chlorophyll accumulation and nonphotochemical quenching in *Arabidopsis* mutants. *Proc Natl Acad Sci U S A* **95**(22): 13324-13329
- Polivka T, Sundstrom V (2004) Ultrafast Dynamics of Carotenoid Excited States&#x2212;From Solution to Natural and Artificial Systems. *Chemical Reviews* **104**(4): 2021-2072
- Porra RJ, Thompson WA, Kriedemann PE (1989) Determination of accurate extinction coefficients and simultaneous equations for assaying chlorophylls a and b extracted with four different solvents: verification of the concentration of chlorophyll standards by atomic absorption spectroscopy. *Biochimica et Biophysica Acta (BBA) - Bioenergetics* **975**(3): 384-394
- Reisberg P, Nairn JA, Sauert K (1982) Picosecond fluorescence kinetics in spinach chloroplasts at low temperature. *Photochemistry and Photobiology* **36**(6): 657-661
- Remelli R, Varotto C, Sandona D, Croce R, Bassi R (1999) Chlorophyll binding to monomeric light-harvesting complex. A mutation analysis of chromophore-binding residues. *J Biol Chem* **274**(47): 33510-33521
- Rock CD, Zeevaart JA (1991) The aba mutant of *Arabidopsis thaliana* is impaired in epoxy-carotenoid biosynthesis. *Proceedings of the National Academy of Sciences of the United States of America* **88**(17): 7496-7499
- Roelofs TA, Lee CH, Holzwarth AR (1992) Global Target Analysis of Picosecond Chlorophyll Fluorescence Kinetics from Pea-Chloroplasts - a New Approach to the Characterization of the

## References

---

- Primary Processes in Photosystem-II Alpha-Units and Beta-Units. *Biophysical Journal* **61**(5): 1147-1163
- Rogl H, Kosemund K, Kühlbrandt W, Collinson I (1998) Refolding of Escherichia coli produced membrane protein inclusion bodies immobilised by nickel chelating chromatography. *FEBS Lett* **432**(1-2): 21-26
- Rogl H, Kühlbrandt W (1999) Mutant trimers of light-harvesting complex II exhibit altered pigment content and spectroscopic features. *Biochemistry* **38**(49): 16214-16222
- Rogl H, Schodel R, Lokstein H, Kühlbrandt W, Schubert A (2002) Assignment of spectral substructures to pigment-binding sites in higher plant light-harvesting complex LHC-II. *Biochemistry* **41**(7): 2281-2287
- Ros F, Bassi R, Paulsen H (1998) Pigment-binding properties of the recombinant photosystem II subunit CP26 reconstituted in vitro. *Eur J Biochem* **253**(3): 653-658
- Royant A, Carpentier P, Ohana J, McGeehan J, Paetzold B, Noirclerc-Savoie M, Vernede X, Adam V, Bourgeois D (2007) Advances in spectroscopic methods for biological crystals. 1. Fluorescence lifetime measurements. *J Appl Crystallogr* **40**(6): 1105-1112
- Royant A, Edman K, Ursby T, Pebay-Peyroula E, Landau EM, Neutze R (2000) Helix deformation is coupled to vectorial proton transport in the photocycle of bacteriorhodopsin. *Nature* **406**(6796): 645-648
- Ruban A, Horton P (1994) Spectroscopy of non-photochemical and photochemical quenching of chlorophyll fluorescence in leaves; evidence for a role of the light harvesting complex of Photosystem II in the regulation of energy dissipation. *Photosynthesis Research* **40**(2): 181-190
- Ruban AV, Berera R, Iliaia C, van Stokkum IH, Kennis JT, Pascal AA, van Amerongen H, Robert B, Horton P, van Grondelle R (2007) Identification of a mechanism of photoprotective energy dissipation in higher plants. *Nature* **450**(7169): 575-578
- Ruban AV, Dekker JP, Horton P, Grondelle RVAN (1995a) Temperature dependence of chlorophyll fluorescence from light-harvesting complex II of higher plants. *Photochemistry and Photobiology* **61**(2): 216-221
- Ruban AV, Horton P (1992) Mechanism of  $[\Delta]pH$ -dependent dissipation of absorbed excitation energy by photosynthetic membranes. I. Spectroscopic analysis of isolated light-harvesting complexes. *Biochimica et Biophysica Acta (BBA) - Bioenergetics* **1102**(1): 30-38
- Ruban AV, Horton P, Robert B (1995b) Resonance Raman spectroscopy of the photosystem II light-harvesting complex of green plants: a comparison of trimeric and aggregated states. *Biochemistry* **34**(7): 2333-2337
-

- 
- Ruban AV, Lee PJ, Wentworth M, Young AJ, Horton P (1999) Determination of the stoichiometry and strength of binding of xanthophylls to the photosystem II light harvesting complexes. *J Biol Chem* **274**(15): 10458-10465
- Ruban AV, Pascal AA, Robert B, Horton P (2002) Activation of zeaxanthin is an obligatory event in the regulation of photosynthetic light harvesting. *J Biol Chem* **277**(10): 7785-7789
- Ruban AV, Rees D, Noctor GD, Young A, Horton P (1991) Long-wavelength chlorophyll species are associated with amplification of high-energy-state excitation quenching in higher plants. *Biochimica et Biophysica Acta (BBA) - Bioenergetics* **1059**(3): 355-360
- Ruban AV, Wentworth M, Yakushevskaya AE, Andersson J, Lee PJ, Keegstra W, Dekker JP, Boekema EJ, Jansson S, Horton P (2003) Plants lacking the main light-harvesting complex retain photosystem II macro-organization. *Nature* **421**(6923): 648-652
- Ryrie IJ, Fuad N (1982) Membrane adhesion in reconstituted proteoliposomes containing the light-harvesting chlorophyll a/b-protein complex: the role of charged surface groups. *Arch Biochem Biophys* **214**(2): 475-488
- Samsonoff WA, MacColl R (2001) Biliproteins and phycobilisomes from cyanobacteria and red algae at the extremes of habitat. *Arch Microbiol* **176**(6): 400-405
- Sass HJ, Buldt G, Gessenich R, Hehn D, Neff D, Schlesinger R, Berendzen J, Ormos P (2000) Structural alterations for proton translocation in the M state of wild-type bacteriorhodopsin. *Nature* **406**(6796): 649-653
- Schmid V (2008) Light-harvesting complexes of vascular plants. *Cellular and Molecular Life Sciences (CMLS)* **65**(22): 3619-3639
- Schmid VH, Cammarata KV, Bruns BU, Schmidt GW (1997) In vitro reconstitution of the photosystem I light-harvesting complex LHCI-730: heterodimerization is required for antenna pigment organization. *Proc Natl Acad Sci U S A* **94**(14): 7667-7672
- Schmuck G, Moya I (1994) Time-Resolved Chlorophyll Fluorescence-Spectra of Intact Leaves. *Remote Sensing of Environment* **47**(1): 72-76
- Schuenemann D, Gupta S, Persello-Cartieaux F, Klimyuk VI, Jones JD, Nussaume L, Hoffman NE (1998) A novel signal recognition particle targets light-harvesting proteins to the thylakoid membranes. *Proc Natl Acad Sci U S A* **95**(17): 10312-10316
- Standfuss J (2004) Struktur und Funktion des LHC-II - Röntgenkristallographische Strukturaufklärung und funktionelle Charakterisierung der drei Isoformen. PhD Thesis, JW-Goethe University, Frankfurt am Main
- Standfuss J, Kühlbrandt W (2004) The three isoforms of the light-harvesting complex II: spectroscopic features, trimer formation, and functional roles. *J Biol Chem* **279**(35): 36884-36891
-

## References

---

- Standfuss J, Terwisscha van Scheltinga AC, Lamborghini M, Kühlbrandt W (2005) Mechanisms of photoprotection and nonphotochemical quenching in pea light-harvesting complex at 2.5 Å resolution. *Embo J* **24**(5): 919-928
- Stengel KF, Holdermann I, Cain P, Robinson C, Wild K, Sinning I (2008) Structural basis for specific substrate recognition by the chloroplast signal recognition particle protein cpSRP43. *Science* **321**(5886): 253-256
- Stewart EJ, Aslund F, Beckwith J (1998) Disulfide bond formation in the Escherichia coli cytoplasm: an in vivo role reversal for the thioredoxins. *EMBO J* **17**(19): 5543-5550
- Storf S, Jansson S, Schmid VH (2005) Pigment binding, fluorescence properties, and oligomerization behavior of Lhca5, a novel light-harvesting protein. *J Biol Chem* **280**(7): 5163-5168
- Straus NA (1994) Iron Deprivation: Physiology and Gene Regulation. In *The Molecular Biology of Cyanobacteria*, Bryant DA (ed), 25, pp 731-750. Kluwer Academic Publishers
- Studier FW (2005) Protein production by auto-induction in high-density shaking cultures. *Protein Expression and Purification* **41**(1): 207-234
- Szabo I, Bergantino E, Giacometti GM (2005) Light and oxygenic photosynthesis: energy dissipation as a protection mechanism against photo-oxidation. *EMBO Rep* **6**(7): 629-634
- Tanford C (1962) Contribution of Hydrophobic Interactions to the Stability of the Globular Conformation of Proteins. *Journal of the American Chemical Society* **84**(22): 4240-4247
- Tardy F, Havaux M (1996) Photosynthesis, chlorophyll fluorescence, light-harvesting system and photoinhibition resistance of a zeaxanthin-accumulating mutant of Arabidopsis thaliana. *J Photochem Photobiol B* **34**(1): 87-94
- Tavan P, Schulten K (1987) Electronic excitations in finite and infinite polyenes. *Phys Rev B Condens Matter* **36**(8): 4337-4358
- Teardo E, de Laureto PP, Bergantino E, Dalla Vecchia F, Rigoni F, Szabo I, Giacometti GM (2007) Evidences for interaction of PsbS with photosynthetic complexes in maize thylakoids. *Biochim Biophys Acta* **1767**(6): 703-711
- Thornber JP (1995) Thirty years of fun with antenna pigment-proteins and photochemical reaction centers: A tribute to the people who have influenced my career. *Photosynthesis Research* **44**(1): 3-22
- Thornber JP, Gregory RP, Smith CA, Bailey JL (1967) Studies on the nature of the chloroplast lamella. I. Preparation and some properties of two chlorophyll-protein complexes. *Biochemistry* **6**(2): 391-396
- Thornber JP, Highkin HR (1974) Composition of the photosynthetic apparatus of normal barley leaves and a mutant lacking chlorophyll b. *Eur J Biochem* **41**(1): 109-116
-

- 
- Tocquin P, Corbesier L, Havelange A, Pieltain A, Kurtem E, Bernier G, Perilleux C (2003) A novel high efficiency, low maintenance, hydroponic system for synchronous growth and flowering of *Arabidopsis thaliana*. *BMC Plant Biology* **3**(1): 2
- Trémolières A, Dubacq JP, Ambard-Bretteville F, RÈmy R (1981) Lipid composition of chlorophyll-protein complexes: Specific enrichment in trans-hexadecenoic acid of an oligomeric form of light-harvesting chlorophyll a/b protein. *FEBS Letters* **130**(1): 27-31
- van Amerongen H, van Grondelle R (2001) Understanding the Energy Transfer Function of LHCII, the Major Light-Harvesting Complex of Green Plants. *J Phys Chem B* **105**(3): 604-617
- van Grondelle R, Novoderezhkin VI (2006) Energy transfer in photosynthesis: experimental insights and quantitative models. *Phys Chem Chem Phys* **8**(7): 793-807
- van Oort B, van Hoek A, Ruban AV, van Amerongen H (2007a) Aggregation of light-harvesting complex II leads to formation of efficient excitation energy traps in monomeric and trimeric complexes. *FEBS Lett* **581**(18): 3528-3532
- van Oort B, van Hoek A, Ruban AV, van Amerongen H (2007b) Equilibrium between quenched and nonquenched conformations of the major plant light-harvesting complex studied with high-pressure time-resolved fluorescence. *J Phys Chem B* **111**(26): 7631-7637
- Vasil'ev S, Irrgang KD, Schrotter T, Bergmann A, Eichler HJ, Renger G (1997) Quenching of chlorophyll a fluorescence in the aggregates of LHCII: steady state fluorescence and picosecond relaxation kinetics. *Biochemistry* **36**(24): 7503-7512
- Walter TS, Meier C, Assenberg R, Au KF, Ren J, Verma A, Nettleship JE, Owens RJ, Stuart DI, Grimes JM (2006) Lysine methylation as a routine rescue strategy for protein crystallization. *Structure* **14**(11): 1617-1622
- Wang DN, Kühlbrandt W (1992) Three-dimensional electron diffraction of plant light-harvesting complex. *Biophys J* **61**(2): 287-297
- Wedel N, Klein R, Ljungberg U, Andersson B, Herrmann RG (1992) The single-copy gene psbS codes for a phylogenetically intriguing 22 kDa polypeptide of photosystem II. *FEBS Lett* **314**(1): 61-66
- Wentworth M, Ruban AV, Horton P (2000) Chlorophyll fluorescence quenching in isolated light harvesting complexes induced by zeaxanthin. *FEBS Lett* **471**(1): 71-74
- Wilk L (2006) Structure and Function of Plants' Minor Light-Harvesting Complexes. Diploma Thesis, JW-Goethe University, Frankfurt am Main
- Wollman FA (2001) State transitions reveal the dynamics and flexibility of the photosynthetic apparatus. *EMBO J* **20**(14): 3623-3630

## References

---

Yamamoto HY (1985) Xanthophyll cycles. In *Methods in Enzymology* Vol. Volume 110, pp 303-312. Academic Press

Yamamoto HY, Nakayama TOM, Chichester CO (1962) Studies on the light and dark interconversions of leaf xanthophylls. *Archives of Biochemistry and Biophysics* **97**(1): 168-173

Yamashita A, Singh SK, Kawate T, Jin Y, Gouaux E (2005) Crystal structure of a bacterial homologue of Na<sup>+</sup>/Cl<sup>-</sup>-dependent neurotransmitter transporters. *Nature* **437**(7056): 215-223

Yan H, Zhang P, Wang C, Liu Z, Chang W (2007) Two lutein molecules in LHCII have different conformations and functions: Insights into the molecular mechanism of thermal dissipation in plants. *Biochemical and Biophysical Research Communications* **355**(2): 457-463

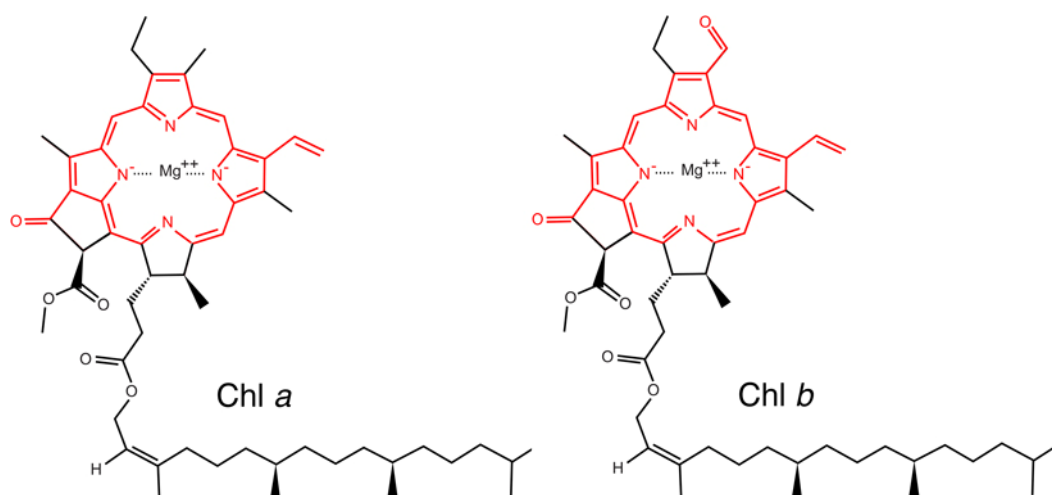
Yano J, Kern J, Sauer K, Latimer MJ, Pushkar Y, Biesiadka J, Loll B, Saenger W, Messinger J, Zouni A, Yachandra VK (2006) Where water is oxidized to dioxygen: structure of the photosynthetic Mn<sub>4</sub>Ca cluster. *Science* **314**(5800): 821-825

Zhu X-G, Long SP, Ort DR (2008) What is the maximum efficiency with which photosynthesis can convert solar energy into biomass? *Current Opinion in Biotechnology* **19**(2): 153-159

---

# APPENDIX

## Chlorophylls



## *Arabidopsis thaliana* VDE cDNA translation product

```

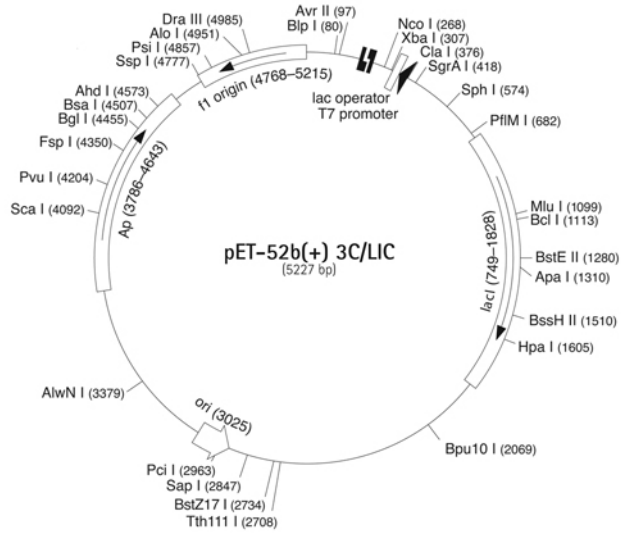
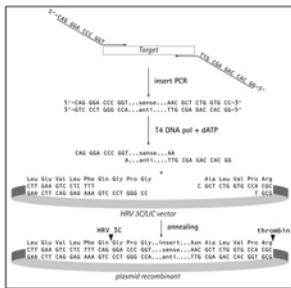
1 MAVATHCFTS PCHDRIRFFS SDDGIGRLGI TRKRINGTFL LKILPPIQSA
51 DLRTTGGRSS RPLSAFRSGF SKGIFDIVPL PSKNELKELT APLLLKLVGV
101 LACAFLIVPS ADAVDALKTC ACLKGCRIE LAKCIANPAC AANVACLQTC
151 NNRPDETECQ IKCGDLFENS VVDEFNECAV SRKKCVPRKS DLGEFPAPDP
201 SVLVQNFNIS DFNGKWIYTS GLNPTFDAFD CQLHEFHTEG DNKLVGNISW
251 RIKTLDSGFF TRSAVQKFVQ DPNQPGVLYN HDNEYLHYQD DWYILSSKIE
301 NKPEDYIFVY YRGRNDAWDG YGGAVVYTRS SVLPNSIPE LEKAAKSISR
351 DFSTFIRTDN TCGPEPALVE RIEKTVEEGE RIIVKEVEEI EEEVEKEVEK
401 VGRTEMTLFQ RLAEGFNELK QDEENFVREL SKEEMFLDE IKMEASEVEK
451 LFGKALPIRK VR*

```

Vectors

pET-52b(+)<sup>3C</sup>/LIC Vector

	Cat No.
pET-52b(+) <sup>3C</sup> /LIC Vector Kit	71571-3
<b>pET-52b(+)<sup>3C</sup>/LIC sequence landmarks</b>	
T7 promoter	342-358
T7 transcription start	341
Strep•Tag II coding sequence	239-262
His•Tag coding sequence	109-139
T7 terminator	26-73
lacI coding sequence	749-1828
pBR322 ori	3025
bla (Amp <sup>r</sup> )	3786-4643
f1 origin	4768-5215



```

pET Upstream Primer #59214-3
SgrA I #59214-3
T7 Promoter Primer #69348-3
T7 promoter
lac operator
Strep•Tag II
HRV 3C
3C/LIC Cloning Site
thrombin I
His•Tag
T7 terminator
T7 Terminator Primer #69337-3

TGCCGCGGATGATCGCGCCACGATCGCTCCGGCTAGAGGATCGAGATCGATCTCGATCCCGCAAATTAATACGACTCACTATAGGGGAATTGTGAGC
ACC GCGGCCACTACGGCCGGTGCTACGCGAGCCGCTCTCCTAGCTAGCTAGAGCTAGGGCGCTTAATTAATGCTGAGTGATATCCCTTAACACTCG

lac operator Xba I rbs Nco I
GGATAACAATTCCTCTAGAATAAATTTGTTTAACTTAAAGAGATATACCATGCGAAGCTGGAGCCACCCGAGTTGCAAAAGGGTGCACCTGGA
CCATTGTTAAGGGGAGATCTTATAAACAATAAGAAATCTTCTCTATATGGTACCGTTCGACCTGGTGGGCGTCAAGCTTTCCACGTGAAC

HRV 3C I thrombin I His•Tag
ValLeuPheGlnGlyProGly AlaLeuValProArgGlySerSerAlaHisHisHisHis
AGTCCTTT CGCTGCTGGCCACGCGTAGTTCCGCTCATCACCAAT
TCAGGAAAGTCCTGGGCC TGCCCATCAAGCGGAGTAGTGGTGTA

His•Tag
HisHisHisHisHisHisHisEnd
CATCACCATCACCACTAATAAAGTGGCTGCTGCCACCGCTGAGCAATAACTAGCATAACCCCTTGGGGCCTTAACGGGCTTGGAGGGGTTTTT
GTAGTGGTAGTGGTGGTAAATGGATCCGACGAGGTTGGGACTCGTTATGATCGTATTGGGGAAACCCGGAGATTTGCCAGAACTCCCAAAA

T7 Terminator Primer #69337-3
    
```

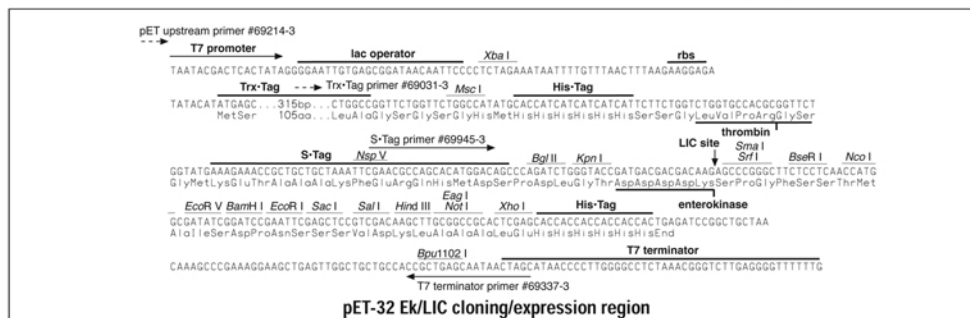
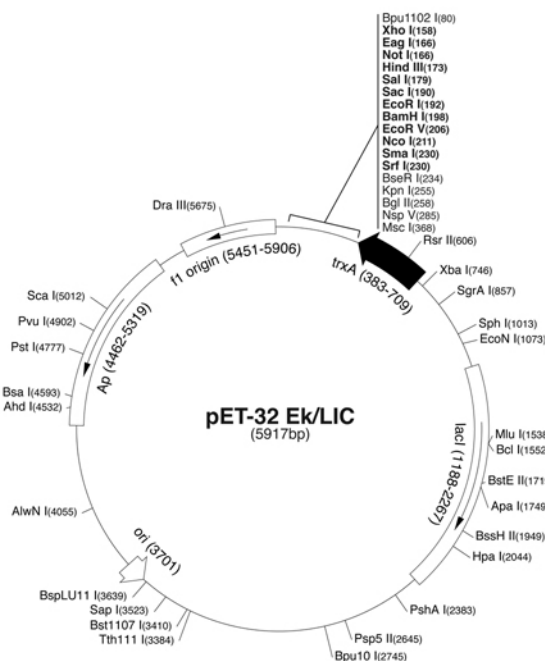
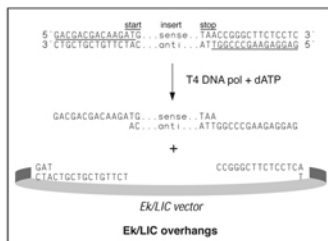
pET-52b(+)<sup>3C</sup>/LIC cloning/expression region



### pET-32 Ek/LIC Vector

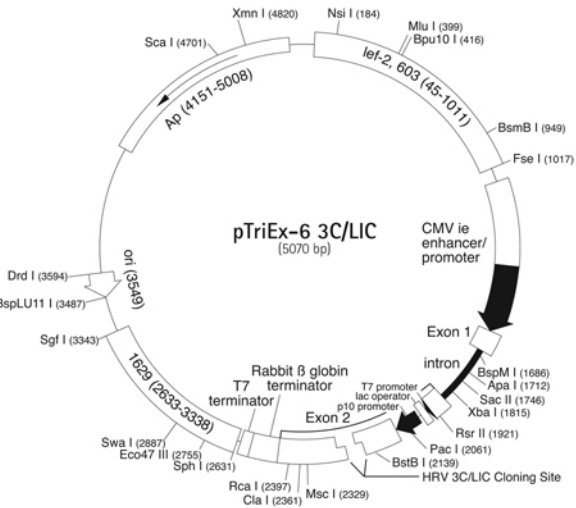
**pET-32 Ek/LIC sequence landmarks**

T7 promoter	781-797
T7 transcription start	780
Trx•Tag coding sequence	383-709
His•Tag coding sequence	344-361
S•Tag coding sequence	266-310
Multiple cloning sites ( <i>BseR</i> I - <i>Xho</i> I)	158-224
His•Tag coding sequence	140-157
T7 terminator	26-72
<i>lacI</i> coding sequence	1188-2267
pBR322 origin	3701
<i>bla</i> coding sequence	4462-5319
<i>f1</i> origin	5451-5906



**pTriEx-6 3C/LIC Vector**

	Cat No.
pTriEx-6 3C/LIC Vector Kit	71576-3
<b>pTriEx-6 3C/LIC sequence landmarks</b>	
CMV ie enhancer/promoter	1021–1597
Vertebrate transcription start	1598
T7 promoter	1931–1947
T7 transcription start	1948
lac operator	1952–1972
p10 promoter region	1986–2099
p10 transcription start	2030–2031
Strep*Tag II coding sequence	2123–2146
His*Tag coding sequence	2246–2275
Rabbit globin terminator	2363–2569
bla (Amp <sup>R</sup> )	4151–5008
pUC ori	3549



**CMV immediate early enhancer/promoter region**

**TATA box** 5' Cap

TGTACGGTGGGAGGCTATATAAGCAGACGCTGTTTAGTGAACCTCAGATCAGTAGATGCTTTATGCGGTAGTTCACAGTAAATTCGAACGCC

Exon 1 TrExUP primer #70846-3

**Intron**

AGTCTCGAACTTAACGTGCGAAGTGTGCTGAGGCACCTGGGCAGGT...T60 bp...AGCTCCTGGCAAGCTGCTGTTATTGTGCTCATCA

Exon 1 Exon 2

**Exon 2**

TTTTGGCAAGAATTGGATCGGACCGAAATTAATACGACTCACTATAGGGGAATGTGAGCGGATAACAATTCCTCCGGAGTAAATCGGGACCTTAAT

**T7 promoter** **lac operator** **p10 promoter region**

CAACCCCAACAAATATATTAGTTAAATAAGAATTATTATCAAACTATTGTATATAAATAACTATACGTAAATTTACATTTTACAATCA

**p10 promoter region** **p10 mRNA initiation** **Pac I**

**Exon 2** **3C/LIC Cloning Site**

**Kozak consensus** **Strep\*Tag II** **BstB I** **HRV 3C**

**rbs** MetAlaSerTrpSerHisProGlnPheGluLysGlyAlaLeuGluValLeuPheGlnGlyProGly

AAGGAGATATACCATGGCAGCTGGAGCCACCCGAGTTCGAAAAGGGTGCACTTGAAGTCCTCT

TTCTCTATATGGTACCGTTCGACCTCGGTGGGCGTCAAGCTTTTCCACGTGAACCTCAGGAGAAAGTCCCTGGGCC

**3C/LIC Cloning Site** **thrombin I** **His\*Tag** **Dra III**

AlaLeuValProArgGlySerSerAlaHisHisHisHisHisHisHisHisHisHisEnd Bsu36 I

CGCTCTGGTGCACCGCGGTAGTTCGCCATCACCACCATCACCATCACCACTAAGTGATTAACCTCAGGTGCAGGC

TGCCCATCAAGCGAGTAGTGTGAGTAGTGTGATGTTTACTAATTTGGAGTCCACGTCCG

**Exon 2**

TGCCTATCAGAAAGTTGGGCTGCTGTGCCAATGCCCTGGCTCAGAAATACCACAGATCGATCTTTTCCCTGCCCAGAAATATGGGGACATCAT

**Exon 2** **polyA signal** **TriExDOWN primer #70847-3**

BspH I SAAGCCCTTGAGCATCTGACTCTGGCTAATAAGGGAAATTTATTTTCATTGCAATAGTGTGGAAATTTTGTGTCTCACTCGGAAGGACATAT

**Exon 2**

**pTriEx-6 3C/LIC cloning/expression region**

---

## MyPlot script

A script was written to facilitate the visualisation of data files from the Cryobench, including absorption and fluorescence spectra and TCSPC histograms.

```
#!/bin/bash
fname=$2

source ~/.profile

if [ ! -r $fname ]; then
    echo "Cannot read $fname"
    exit
fi

if [ ${fname##*.} = "Scope" ]; then
    spec $fname > tmp_spec

elif [ ${fname##*.} = "Absorbance" ]; then
    spec $fname > tmp_spec

elif [ ${fname##*.} = "tcs" ]; then
    hist $fname > tmp_hist
fi

if [ ${fname##*.} = "Scope" ]; then
    gnuplot - <<EOF

    set title '$2'

    set xrange [600:800]

    set xtics 600,20

    plot 'tmp_spec'

EOF
```

## Appendix

---

```
elif [ ${fname##*.} = "Absorbance" ]; then
    gnuplot - <<EOF
    set title '$2'
    set xrange [400:750]
    plot 'tmp_spec'
EOF
```

```
elif [ ${fname##*.} = "tcs" ]; then
    gnuplot - <<EOF
    set title '$2'
    set xrange [2700:3500]
    plot 'tmp_hist'
EOF
```

```
else
    echo "Unknown type: $fname"
fi
```

```
if [ ${fname##*.} = "Scope" ]; then
    rm tmp_spec
```

```
elif [ ${fname##*.} = "Absorbance" ]; then
    rm tmp_spec
```

```
elif [ ${fname##*.} = "tcs" ]; then
    rm tmp_hist
fi
```

This script was converted to a MacOS X application using Platypus (<http://www.sveinbjorn.org/platypus>).

---

## ACKNOWLEDGEMENTS

First and foremost, I would like to thank Prof. Werner Kühlbrandt. It didn't take me long to realise that doing my PhD on LHC-II in his lab was nothing less than a privilege, and I honestly hope that I have fulfilled his expectations. I am honoured by the trust and freedom he always gave me, which allowed me to shape my PhD as I found it best. Sometimes I felt that I never had a supervisor, but I definitely had an outstanding mentor.

I wish to thank Prof. Bernd Ludwig for accepting me as his student at the Johann Wolfgang Goethe University and for the nice words of support and advice.

It is essentially impossible for me to imagine how my PhD would have been if Laura Wilk had decided to make her Diploma somewhere else. I believe that Laura and I complement each other in the lab and most of what I accomplished is also due to her. With time, Laura became not only my favourite colleague, who I could always trust and was always there when I needed something, but also my closest friend. Laura is also highly acknowledged for the German version of the summary of this thesis.

Much of what I presented in this thesis was came from all I inherited from Dr. Jörg Standfuss. I honestly think that Jörg and I made an excellent team and I want to sincerely thank him for making my first times in the department such a wonderful experience.

During my PhD I had the opportunity of working together with a number of excellent collaborators. Among them, I should highlight Dr. Antoine Royant and Prof. Andreas Dreuw. Antoine showed me what genuine scientific interest, hard work and patience is and also how two people can collaborate seamlessly from two far corners of this planet. Andreas was essential for teaching me all I know about fluorescence quenching, excited states and so many other physical chemistry concepts. Andreas was always there to bounce ideas; I quickly found how precious that is. A special word also to Prof. Joseph Wachtveitl and Sergiu Amarie in Frankfurt and Prof. Peter Jomo Walla, Stefan Bode and Claudia Quentmeier in

## Acknowledgements

---

Braunschweig for our fruitful collaborations. I thank Prof. Alfred Holzwarth for many enlightening discussions.

Many results I presented in this thesis could not be achieved without the dedication of Heidi Betz. Heidi has “green fingers” and she crystallises LHC-II like no one else. When the samples refused to crystallise, Heidi just smiled and prepared another tray. I am in debt to her for all the help she gave me.

The work with *Arabidopsis* plants presented in this thesis was only possible with the help from Britta Grosardt at the MPI of Plant Breeding in Cologne, Holger Schranz and Fausto at the Johann Wolfgang Goethe University in Frankfurt and Johan Zeelen in our department. Among many other things, Johan helped me with the plant growth in hydroponic medium.

I remember the day I first met Anke Terwisscha van Scheltinga and Remco Wouts, in the coffee room of the Janos Hajdu lab in Uppsala. Thank you Anke for showing me the pictures of the MPIbp building. In a way, this thesis started on that day. I very much enjoyed all the opportunities we had to work together; they were just too few. Thank you Remco for your help and for catalysing my Mac addiction.

My very sincere gratitude to Monika Hobrack for all her help during my PhD. Monika is always willing to help and makes the life of everyone in the department so much easier.

Paolo Lastrico is highly acknowledge for advice and help with some of the figures presented in this thesis.

The little I know about electron microscopy came from Deryck Mills, Janet Vonck and Winfried Haase. I honestly admire Deryck for his patience and his skill for maintaining the entire EM facility at such a superb standard.

I believed that the biggest strength of a lab is the people who work in it and the knowledge that they share and discuss. My almost four years in Werner’s department only confirmed my belief. I am very thankful to all the people in the department who taught me some much and made me a better and more skilled scientist. I should nevertheless highlight Sabrina Schulze, Dr. Özkan Yildiz, Stefan

---

Köster and Dr. Vinoth Kumar who probably answered most of my famous “potentially stupid questions” and PD Dr. Götz Hofhaus with whom I had so many wonderful discussions.

A very special thanks to Dr. Stephen Marino for the critical reading of this thesis, the numerous discussions on various topics of science and the great time we had together outside the borders of the institute.

I wish to thank Nora Bluhme for continuing the VDE project and for coping with my lack of time and attention during the beginning of her Diploma work.

The Cluster of Excellence Frankfurt and especially Fundação para a Ciência e a Tecnologia are highly acknowledged for generous financial support.

My time as a PhD student was probably the richest I had so far and I owe that mostly to you, Susanne. Thank you so much for being there for me.

Last, but my no means less importantly, I would like to thank all my family and in particular my parents for the continuous support and encouragement.

## CURRICULUM VITAE



Tiago Ferreira de Barros

Born 22.04.1982 in Porto, Portugal

### EDUCATION AND TRAINING

06/2005 – 12/2008	PhD student in the MPI of Biophysics and JW Goethe University, Frankfurt, Germany
11/2004 – 05/2005	Research fellow at the IBMC, Porto, Portugal
03/2004 – 08 /2004	Training at the Molecular Biophysics department of the Biomedical Centre, Uppsala University, Sweden
09/2003 – 02/2004	Training at the Molecular Structure group of the IBMC, Porto University, Portugal
10/2000 – 09/2004	<i>Licenciatura</i> in Biochemistry, Biophysics core area, Porto University, Portugal

### AWARDS AND FELLOWSHIPS

09/2008	Research grant from the Cluster of Excellence Frankfurt
05/2006	“Eng. Antonio de Almeida” award, Porto University
01/2005	PhD Fellowship from Fundação para a Ciência e a Tecnologia
11/2003	“Professor Doutor Fernando Serrão” award, Porto University

---



---

**PUBLICATIONS**

**Barros T**, Kühlbrandt W (2009) Crystallisation, structure and function of plant Light-Harvesting complex II. *Submitted*

Amarie S, Wilk L, **Barros T**, Kühlbrandt W, Dreuw A, Wachtveitl J (2009) Properties of Zeaxanthin and its Radical Cation Bound to the Minor Light-Harvesting Complexes CP24, CP26 and CP29. *Biochem Biophys Acta – Bioenergetics*, *in press*

Bode S, Quentmeier CC, Liao PN, Hafi N, **Barros T**, Wilk L, Bittner F, Walla PJ (2009) Evidence for excitonic carotenoid dark state - chlorophyll interactions regulating plant photosynthesis. *Submitted*

**Barros T**, Royant A, Standfuss J, Dreuw A, Kuhlbrandt W (2009) Crystal structure of plant light-harvesting complex shows the active, energy-transmitting state. *EMBO J* **28**: 298 - 306

Bode S, Quentmeier CC, Liao P-N, **Barros T**, Walla PJ (2008) Xanthophyll-cycle dependence of the energy transfer between carotenoid dark states and chlorophylls in NPQ mutants of living plants and in LHC II. *Chemical Physics Letters* **450**(4-6): 379-385

Amarie S, Standfuss J, **Barros T**, Kühlbrandt W, Dreuw A, Wachtveitl J (2007) Carotenoid Radical Cations as a Probe for the Molecular Mechanism of Nonphotochemical Quenching in Oxygenic Photosynthesis. *J Phys Chem B* **111**(13): 3481-3487

Fernandes PA, Cruz AIS, Maia ARR, Almeida AAS, da Silva AMN, Silva BFB, Ribeiro CMS, Ribeiro CFB, Cunha EMS, Maia F, Tedim JAC, Ferreira J, Gomes LC, Matos LRC, Cruz L, Pinto M, da Encarnacao MAR, Teixeira P, Seixas R, da Quinta R, Gomes SS, Patricio SG, Martins SDS, **Barros TF**, Selao T, Pande V, Ramos MJ (2004) Design of 2-cyclopentenone derivatives with enhanced NF-kappa B: DNA binding inhibitory properties. *Theochem-J Mol Struct* **685**(1-3): 73-82

Fernandes PA, Maia ARR, Almeida AAS, Silva BFB, Ribeiro CMS, Ribeiro CFB, Ribeiro DSM, Fonseca DAP, Henriques ES, Cunha EMS, Maia F, Pereira JAA, Pacheco JPG, Ferreira J, Matos LRC, Pinto M, Borges MCS, Magalhaes P, Teixeira P, Veloso P, Ferreira RJF, Gomes SS, **Barros TF**, Selao T, Pande V, Fernandes V, Ramos MJ (2005) New designs for inhibitors of the NF-kappa B: DNA binding. *Theor Chem Acc* **113**(4): 197-204